Stability Analysis and Neuro-control of Nonlinear Systems: a Dynamic Pole Motion Approach

A Thesis Submitted

to the College of Graduate and Postdoctoral Studies

in Partial Fulfillment of the Requirements

for the Degree of Master of Science

in the Department of Mechanical Engineering

University of Saskatchewan

by

Mohammad Hasan Majumdar

Saskatoon, Saskatchewan, Canada

© Copyright Mohammad Hasan Majumdar, December 2018. All rights reserved

Permission to Use

In presenting this thesis in partial fulfillment of the requirements for a Postgraduate degree from the University of Saskatchewan, it is agreed that the Libraries of this University may make it freely available for inspection. Permission for copying of this thesis in any manner, in whole or in part, for scholarly purposes may be granted by the professors who supervised this thesis work or, in their absence, by the Head of the Department of Mechanical Engineering or the Dean of the College of Graduate Studies and Research at the University of Saskatchewan. Any copying, publication, or use of this thesis, or parts thereof, for financial gain without the written permission of the author is strictly prohibited. Proper recognition shall be given to the author and to the University of Saskatchewan in any scholarly use which may be made of any material in this thesis.

Request for permission to copy or to make any other use of the material in this thesis in whole or in part should be addressed to:

Head of the Department of Mechanical Engineering
57 Campus Drive
University of Saskatchewan
Saskatoon, Saskatchewan, Canada
S7N 5A9

OR

Dean
College of Graduate and Postdoctoral Studies
University of Saskatchewan
116 Thorvaldson Building, 110 Science Place
Saskatoon, Saskatchewan, Canada
S7N 5C9

Abstract

In a linear time-invariant system, the parameters are constant thereby poles are static. However, in a linear time-varying system since the parameters are a function of time, therefore, the poles are not static rather dynamic. Similarly, the parameters of a nonlinear system are a function of system states, and that makes nonlinear system poles dynamic in the complex plane. The location of nonlinear system poles are a function of system states explicitly and time implicitly. Performance characteristics of a dynamic system, e.g., stability conditions and the quality of response depend on the location of dynamic poles in the complex plane.

In this thesis, a dynamic pole motion in the complex g −plane based approach is established to enhance the performance characteristics of a nonlinear dynamic system. g −plane is a three-dimensional complex plane.

The stability approach, initiated by Sahu et al. (2013), was an exertion of the dynamic Routh's stability criterion by constructing a dynamic Routh's array to examine the absolute stability of a nonlinear system in time domain. This thesis extends the work to investigate the relative stability as well as stability in the frequency domain with the introduction of the dynamic Nyquist and Bode plots. A dynamic Nyquist criterion together with the concept of the dynamic pole motion is developed. The locations of the dynamic poles are executed by drawing a dynamic root locus from the dynamic characteristic equation of a nonlinear system.

The quality of the response of a nonlinear dynamic system is enhanced by using a dynamic pole motion based neuro-controller, introduced by Song et al. (2011). In this thesis, we give a more comprehensive descriptions of the neuro-controller design techniques and illustrate the neuro-controller design approach with the help of several nonlinear dynamic system examples. The controller parameters are a function of the error, and continually relocate the dynamic poles in the complex g −plane to assure a higher bandwidth and lower damping for larger errors and lower bandwidth and larger damping for smaller errors. Finally, the theoretical concepts are further corroborated by simulation results.

Acknowledgments

I want to express my most profound appreciation and gratitude to my supervisors, Prof. Madan M. Gupta and Prof. WJ (Chris) Zhang, whose encouragement, guidance and support throughout my study program enabled me continuously to reach my research goals. Their expertise and enthusiasm inspired me to explore every challenge in my research. I am grateful.

I also like to extend my appreciation to the members of my Advisory Committee, Prof. Reza Fotouhi, and Asst. Prof. Travis Wiens, for their examination and advice in my research program.

I thank my parents for the endless love and support they provide through my entire life.

I express my appreciation to my friend Ramesh Ramanujam who made my days memorable at the University of Saskatchewan.

Finally, I gratefully acknowledge Government of Saskatchewan and the University of Saskatchewan for their financial support of my studies through the Saskatchewan Innovation and Opportunity Scholarship.

Dedications

To my parents

and

To Late Professor Lotfi A. Zadeh, the father of fuzzy logic

Table of Contents

Permission to Use…….. i

Abstract ……..... ii

Acknowledgments ……. iii

Dedications…….. iv

Table of Contents……... v

List of Figures……. viii

List of Tables…….. xx

Chapter 1: Neuro-Control Systems: an Introduction……. 1

1.1 Previous Research……..... 2

1.2 Motivations……... 4

1.3 Objectives……. 5

1.4 Thesis Organization…….. 6

Chapter 2: g −Plane Characteristics of a Nonlinear Dynamic System…… 9

2.1 Mathematical Representation of a Dynamic System…… 9

2.2 g −Transfer Matrix…….. 12

2.2.1 Complex g −plane…… 14

2.2.2 Dynamic Poles and Zeros……. 15

2.3 Dynamic Root Locus…… 16

2.4 Illustrative Numerical Examples…….. 17

Example 2.1…… 17

Example 2.2…… 19

Example 2.3…… 22

Example 2.4……..... 23

Example 2.5…… 27

2.5 Summary……... 30

Chapter 3: Nonlinear Systems Stability Analysis Using the Dynamic Routh's Criterion and the Development of Dynamic Nyquist Criterion…….. 31

3.1 Dynamic Routh's Stability Criterion……... 32

3.2 Illustrative Numerical Examples…….. 34

Example 3.1…… 34

Example 3.2…… 42

Example 3.3.. …… 51

Example 3.4…… 54

Example 3.5…… 58

Example 3.6…… 59

3.3 Development of the dynamic Nyquist Stability Criterion…… 62

Example 3.7…… 65

3.4 Summary……..... 74

Chapter 4: The Design of a Neuro-controller using g −Plane Approach…… 76

4.1 Neuro-controller Concept……. 76

4.2 Neuro-controller Design Criteria……. 78

4.3 Controller Design…….. 82

4.3.1 Design of Position Feedback $K_p(e,t)$ and Velocity Feedback $K_v(e,t)$ …….. 82

4.3.2 Neuro-controller Parameters Design K_{pf}, K_{vf}, α and β……... 84

4.4 Illustrative Numerical Examples…….. 85

Example 4.1…… 85

Example 4.2…… 91

Example 4.3…… 101

Example 4.4…… 109

4.5 Summary……..... 117

Chapter 5: Concluding Remarks and Future Work……... 118

5.1 Overview and Conclusions…… 118

5.2 Future Works…… 123

Appendix A: Verification of Examples…… 125

Appendix B: Linearization vs. Dynamic Pole Motion Approach…….. 157

Appendix C: Details of the Simulink Models…….. 165

References……... 172

List of Figures

Figure 1.1	Biological Control Loop.	5
Figure 2.1	An equivalent block diagram of the state-space representation, $\dot{\mathbf{x}}(t) = \mathbf{A}(\mathbf{x}, t)\mathbf{x} + \mathbf{B}(t)\mathbf{u}(t),\ \mathbf{y}(t) = \mathbf{C}(\mathbf{x}, t)\mathbf{x} + \mathbf{D}(t)\mathbf{u}(t)$.	11
Figure 2.2	Three-dimensional complex g −plane, $g(t) = \sigma(t) + j\omega(t)$. The horizontal axis represents the real part $\sigma(t)$, the vertical axis represents the imaginary part $j\omega(t)$. The third axis can be either error $e(t)$, system states $\mathbf{x}$, or time t.	15
Figure 2.3	Block diagram representation of the state-space model of the nonlinear system, $\ddot{x} - \dot{x}^3 + x^2 = u(t)$.	18
Figure 2.4	An equivalent block diagram of the nonlinear dynamic system, $\dot{x_1} = -2x_1,\ \dot{x_2} = 2{x_2}^2 x_1 + 2x_2, y = x_1$.	20
Figure 2.5	Three-dimensional dynamic root locus of the dynamic characteristic equation, $g^2 + 2({x_2}^2 - 2)\ = 0$. The third axis represents the system state x_2.	21
Figure 2.6	A two-dimensional projection of a three-dimensional dynamic root locus of the characteristic equation $g^2 + 2({x_2}^2 - 2)\ = 0$. The horizontal axis is the real axis $\boldsymbol{\sigma}(\boldsymbol{t})$, the vertical axis is the imaginary axis $\boldsymbol{j\omega}(\boldsymbol{t})$, and the third axis represents the system state x_2.	21
Figure 2.7	Three-dimensional dynamic root locus of the nonlinear dynamic system represented by state-equations, $\dot{x_1} = -6x_1 + 2x_2,\ \dot{x_2} = 2x_1 - 6x_2 - 2{x_2}^3$. The third axis represents the system state x_2.	23
Figure 2.8	An equivalent block diagram of the simplified model of a single link manipulator with a flexible joint system presented by Eq. 2.30	24
Figure 2.9	Three-dimensional dynamic root locus of the nonlinear system defined by Eq. 2.30. The third axis is presenting the system state x_3.	26

Figure 2.10	A two-dimensional projection of a three-dimensional dynamic root locus of the nonlinear system defined by Eq. 2.30. The horizontal axis is the real axis $\boldsymbol{\sigma(t)}$, the vertical axis is the imaginary axis $\boldsymbol{j\omega(t)}$, and the third axis represents the system state x_3.	26
Figure 2.11	An equivalent block diagram of the nonlinear dynamic system defined by Eq. 2.34.	28
Figure 2.12	Dynamic root locus of the nonlinear system defined by Eq. 2.34 for the increased value of the system state x_1 from zero to infinity. The third axis is representing x_1.	29
Figure 2.13	A two-dimensional projection of the three-dimensional dynamic root locus of the nonlinear system defined by Eq. 2.34. The horizontal axis is the real axis $\boldsymbol{\sigma(t)}$, the vertical axis is the imaginary axis $\boldsymbol{j\omega(t)}$, and the third axis is representing the system state x_1.	29
Figure 3.1	The definition of stability region in the complex g −plane, $g(t) = \sigma(t) + j\omega(t)$.	32
Figure 3.2	Graphical representation of the stability region of the dynamic characteristic equation, $g^2 + (1 - {x_1}^2)g + 1 = 0$.	37
Figure 3.3	Dynamic root locus of the characteristic equation, $g^2 + (1 - {x_1}^2)g + 1 = 0$. The horizontal axis is the real axis, the vertical axis is the imaginary axis, and the third axis is representing system state x_1.	38
Figure 3.4	An inverse relation between system state x_1 and the dynamic damping ratio $\xi(t)$ of the nonlinear system $\ddot{x} + (1 - x^2)\dot{x} + x = u(t)$.	39
Figure 3.5	Dynamic Bode plot, a three-dimensional Bode plot of the second-order nonlinear system $\ddot{x} + (1 - x^2)\dot{x} + x = u(t)$. The third axis represents the system state x_1.	40
Figure 3.6	Magnitude and phase frequency response of the nonlinear system, $\ddot{x} + (1 - x^2)\dot{x} + x = u(t)$ for the various values of the system state x_1.	41

Figure 3.7	Graphical representation of the stability region of the dynamic characteristic equation $g^2 + ({x_1}^2 - 1)g + 1 = 0$.	44
Figure 3.8	Dynamic root locus of the dynamic characteristic equation, $g^2 + ({x_1}^2 - 1)g + 1 = 0$. The third axis is representing the system state x_1.	45
Figure 3.9	Dynamic Bode plot, a three-dimensional bode plot of the nonlinear system $\ddot{x} + (x^2 - 1)\dot{x} + x = u(t)$. The third axis represents the system state x_1.	46
Figure 3.10	Magnitude and phase frequency response of the nonlinear system $\ddot{x} + (x^2 - 1)\dot{x} + x = u(t)$ for the various values of the system state x_1.	47
Figure 3.11	The phase portrait of the nonlinear time-variant dynamic system, $\ddot{x} + (x^2 - 1)\dot{x} + x = 0$.	49
Figure 3.12	Effect of changing the values of K_p of the oscillatory dynamic system $\ddot{x} + (x^2 - \alpha)\dot{x} + K_p x = 0$ with an initial condition $(x_1, x_2) = (0.5,1)$. α is kept constant $\alpha = 1$.	50
Figure 3.13	Effect of changing the values of α of the oscillatory dynamic system $\ddot{x} + (x^2 - \alpha)\dot{x} + K_p x = 0$ with an initial condition $(x_1, x_2) = (0.5,1)$. K_p is kept constant, $K_p = 1$.	50
Figure 3.14	A three-dimensional sketch of the dynamic root locus of the characteristic equation $g^2 + 0.6g + (3 + x_1) = 0$. The third axis represents system state x_1. Left-half side (LHS) is a stable region, and the right-half side (RHS) is an unstable region.	53
Figure 3.15	A two-dimensional projection of the three-dimensional dynamic root locus of the characteristic equation $g^2 + 0.6g + (3 + x_1) = 0$. The horizontal axis is the real axis, the vertical axis is the imaginary axis, and the third axis represents system state x_1. Left-half side (LHS) is a stable region, and right-half side (RHS) is an unstable region.	53
Figure 3.16	The block diagram representation of the second-order nonlinear system,	54

$\dot{x_1} = \mu x_1^2 x_2 - x_2 sin x_1, \dot{x_2} = -x_1 - \mu x_1^2 x_2 + x_2.$

Figure 3.17 A two-dimensional plot of the dynamic root contour of the dynamic characteristic equation $g^2 + (\mu x_1^2 - 1)g + (\mu x_1^2 - sin x_1) = 0$ for three different values of μ: $\mu = 1, \mu = 2, \mu = 3$. The horizontal axis represents the real axis, the vertical axis represents the imaginary axis, and the third axis represents the system state x_1. 56

Figure 3.18 A three-dimensional sketch of dynamic root contour plot of the characteristic equation $g^2 + (\mu x_1^2 - 1)g + (\mu x_1^2 - sin x_1) = 0$ for three different values of μ: $\mu = 1, \mu = 2, \mu = 3$. The third axis represents the system state x_1. 57

Figure 3.19 The dynamic Root locus of the first-order time-varying dynamic system $\dot{x_1} = (4t \sin t - 2t)x_1$. The third axis is representing time t. 60

Figure 3.20 The stable and unstable region of the time-varying linear system $\dot{x_1} = (4t \sin t - 2t)x_1$. A $-ve$ value of $(4t \sin t - 2t)$ defines stability, and a $+ve$ value of $(4t \sin t - 2t)$ defines instability situation. 60

Figure 3.21 System response for the initial condition $x_1 = 1$ of the first-order time-varying linear system $\dot{x_1} = (4t \sin t - 2t)x_1$. The response has two unstable peaks between $0.53s < t < 2.62s$ and $6.81s < t < 8.90s$. 61

Figure 3.22 (a) Dynamic pole-zero configuration of $\mathbf{L}(g)$ and an arbitrary g −plane trajectory Γ_g. (b) $\mathbf{L}(g)$ −plane locus, Γ, which corresponds to the Γ_g locus of (a) through one to one mapping. 63

Figure 3.23 A three-dimensional dynamic root locus of the nonlinear system $\dddot{x} + 6\ddot{x} + 11\dot{x} + (6 + x)x = u(t)$. The dynamic poles are on the left-hand side of the complex g −plane for $x_1 < 60$. For $x_1 = 60$, the dynamic conjugate poles are on the $j\omega(t)$ −axis. The dynamic conjugate poles are on the right-hand side of the complex g −plane for $x_1 > 60$. 67

Figure 3.24 A two-dimensional projection of the three-dimensional dynamic root locus Figure 3.23. The location of the dynamic poles changes with the increased value of x_1. For instance, (a) when $x_1 = 25$, poles are at -5.03 and $-4.08 \pm j2.43$, (b) when $x_1 = 60$, poles are at -6.0, and $\pm j3.31$, 68

(c) when $x_1 = 100$, poles are at -6.7, and $0.35 \pm j3.95$.

Figure 3.25 The dynamic Nyquist plot of the system defined by Eq. (3.42) for three different values of the system state, (a) $x_1 = 25$, (b) $x_1 = 60$ and (c) $x_1 = 100$. The dotted arrowhead indicates the direction of the increased value of system state x_1. 70

Figure 3.26 A magnified sketch of the dynamic Nyquist plot, Figure 3.25, for three different values of system state (a) $x_1 = 25$, (b) $x_1 = 60$ and (c) $x_1 = 100$. 71

Figure 3.27 The step response of the nonlinear system defined by Eq. (3.42) at three different values of the system state, (a) $x_1 = 25$, (b) $x_1 = 60$ and (c) $x_1 = 100$. 71

Figure 3.28 The dynamic magnitude and phase frequency response of the nonlinear system defined by Eq. (3.42) for three different values of the system state, (a) $x_1 = 25$, (b) $x_1 = 60$ and (c) $x_1 = 100$. 72

Figure 3.29 A magnified sketch of The dynamic magnitude and phase frequency response, Figure 3.28, for three different values of the system state, (a) $x_1 = 25$, (b) $x_1 = 60$ and (c) $x_1 = 100$, to show the dynamic gain margin and dynamic phase margin. 73

Figure 4.1 System responses to a unit step input with two different pole locations: (i) underdamped situation ($\xi < 1$) and (ii) overdamped situation ($\xi > 1$). Initially, for large error the desired response curve follows an underdamped curve and then settle down to a steady-state value for decreasing errors, i.e., following the overdamped curve. The desired response curve is a marriage between an underdamped and an overdamped response curve. 77

Figure 4.2 The proposed neuro-controller. $x_2 = \dot{x_1}$. $K_p(e,t)$ and $K_v(e,t)$ are defined according to the design criteria I and II. 80

Figure 4.3 The dynamic pole motion (DPM) concept explanation. Section 1, 2, 3 shows the dynamic pole locations in the complex g −plane in (a), and correspondent response is shown in (b). 80

Figure 4.4	Step responses of a typical second-order system with a neuro-controller for the variation of K_p and K_v, one at a time.	81
Figure 4.5	Effect of the variation of α and β on the function $K_p(e,t)$ and $K_v(e,t)$, respectively.	83
Figure 4.6	The neuro-controlled response of the system $\ddot{x} + 2\dot{x} + 6x = 6u(t)$ to a unit step input. Rise time $T_r = 0.11$s and settling time $T_s = 0.63$s. Neuro-controller parameters are $K_{pf} = 40$, $K_{vf} = 6.5$, $\alpha = 18$ and $\beta = 12$. Blue dotted line is the uncontrolled response of the system.	87
Figure 4.7	Dynamic pole motion of the system $\ddot{x} + 2\dot{x} + 6x = 6u(t)$ with neuro-controller in the complex g −plane for a decreasing error $e(t)$. Dynamic poles are located at $-1.0 \pm j27.6$ and $-4.2 \pm j5.28$ for $t = 0$s and $t = 5$s, respectively.	88
Figure 4.8	A graphical representation of natural frequency $\omega_n(t)$ vs. damping ratio $\xi(t)$ with the increase of time t and decrease of error $e(t)$ of the system $\ddot{x} + 2\dot{x} + 6x = 6u(t)$ with a neuro-controller.	89
Figure 4.9	Natural frequency $\omega_n(t)$ and damping ratio $\xi(t)$ at various time t and locations of a unit step response of the system $\ddot{x} + 2\dot{x} + 6x = 6u(t)$.	91
Figure 4.10	Block diagram representation of the state-space model of the nonlinear dynamic system $\ddot{x} + (1 - x^2)\dot{x} + x = u(t)$.	92
Figure 4.11	Dynamic root locus of the dynamic characteristic equation, $g^2 + (1 - {x_1}^2)g + 1 = 0$ as system state x_1 is varied from zero to infinity.	93
Figure 4.12	Neuro-controlled response of the system $\ddot{x} + (1 - x^2)\dot{x} + x = u(t)$ to a unit step input. Rise time $T_r = 0.19$s and settling time $T_s = 0.49$s. Neuro-controller parameters are $K_{pf} = 24$, $K_{vf} = 12$, $\alpha = 150$ and $\beta = 40$. The green dotted line is the system error $e(t)$.	94
Figure 4.13	Dynamic pole motion of the system $\ddot{x} + (1 - x^2)\dot{x} + x = u(t)$ with a	95

neuro-controller in the complex g −plane for a decreasing error $e(t)$. For $t = 0$s the dynamic poles are located at $-0.5 \pm j13.2$. When $t = 3$s the dynamic poles move to $-10.65 + j0.0$ and $-2.34 + j0.0$, respectively.

Figure 4.14 The neuro-controller parameters vs error $e(t)$. (i) The position feedback $K_p(e,t)$ vs. error $e(t)$ and (ii) velocity feedback $K_v(e,t)$ vs. error $e(t)$. 96

Figure 4.15 The dynamic damping ratio $\xi(t)$ vs error $e(t)$ and time t of the neuro-controlled system $\ddot{x} + (1 - x^2)\dot{x} + x = u(t)$. 97

Figure 4.16 The relationship between the maximum magnitude of the frequency response curve $M_p(t)$ and dynamic damping ratio $\xi(t)$. 98

Figure 4.17 The variation of the dynamic bandwidth $\omega_{BW}(t)$ of the overall neuro-controlled system at each time interval. 99

Figure 4.18 Block diagram representation of the state-space model of the nonlinear system,
$\dot{x_1} = x_2 - ax_1(x_1^2 + x_2^2)$, $\dot{x_2} = -x_1 - ax_2(x_1^2 + x_2^2)$, $y = x_1$. 102

Figure 4.19 The neuro-controlled response of the system defined by Eq. 4.18 to a unit step input. Rise time $T_r = 0.13$s and settling time $T_s = 0.29$s. Neuro-controller parameters are $K_{pf} = 85$, $K_{vf} = 23$, $\alpha = 50$ and $\beta = 5$. The green dotted line is the system error $e(t)$. 103

Figure 4.20 Natural frequency $\omega_n(t)$ and damping ratio $\xi(t)$ at various time t and locations of a unit step response of the system defined by Eq. 4.18. 103

Figure 4.21 The dynamic pole motion of the neuro-controlled system defined by Eq. 4.18 on the three-dimensional complex g −plane. At $t = 0$s dynamic poles are at $-0.07 \pm j11.6$ and at t=2s poles are at $-18.3 + j0.0$ and $-4.69 + j0.0$. 104

Figure 4.22 A graphical representation of the natural frequency $\omega_n(t)$ vs. damping ratio $\xi(t)$ with the increase of time t of the system defined by Eq. 4.18 with a neuro-controller. 105

Figure 4.23	The neuro-controller parameters vs error $e(t)$. (i) The position feedback $K_p(e,t)$ vs. error $e(t)$ and (ii) velocity feedback $K_v(e,t)$ vs. error $e(t)$.	106
Figure 4.24	The variation of the bandwidth $\omega_{BW}(t)$ of the overall neuro-controlled system defined by Eq. 4.18 at each time interval.	107
Figure 4.25	The neuro-controlled response for a periodic input reference $u(t) = \sin\frac{t}{2} + \frac{1}{2}\sin 2t$ of the nonlinear system defined by Eq. 4.18.	108
Figure 4.26	The block diagram representation of the state-space model of the nonlinear dynamic system defined by Eq. 4.23.	109
Figure 4.27	The neuro-controlled response of the system defined by Eq. 4.23 to a unit step input. Rise time $T_r = 0.19$s and settling time $T_s = 0.49$s. Neuro-controller parameters are $K_{pf} = 650$, $K_{vf} = 250$, $K_{af} = 25$, $\alpha = 18$, $\beta = 12$ and $\gamma = 1$. The green dotted line is the system error $e(t)$.	111
Figure 4.28	The dynamic pole movement of the neuro-controlled system defined by Eq. 4.23 in the complex g −plane. At $t = 0$s dynamic poles are at $-0.5 \pm j13.2$ and the steady-state dynamic poles are at $-10.65 + j0.0$ and $-2.34 + j0.0$.	112
Figure 4.29	A two-dimensional projection of the Figure 4.28. At $t = 0$s dynamic poles are at $-0.5 \pm j13.2$ and the steady-state dynamic poles are at $-10.65 + j0.0$ and $-2.34 + j0.0$.	112
Figure 4.30	The neuro-controller parameters vs error $e(t)$. (i) The position feedback $K_p(e,t)$ vs. error $e(t)$ and (ii) velocity feedback $K_v(e,t)$ vs. error $e(t)$.	113
Figure 4.31	A graphical representation of the natural frequency $\omega_n(t)$ vs. damping ratio $\xi(t)$ with the increase of time t of the system defined by Eq. 4.23 with a neuro-controller.	114
Figure 4.32	The dynamic damping ratio $\xi(t)$ vs. error $e(t)$ and time t of the neuro-controlled system defined by Eq. 4.23.	114
Figure 4.33	The variation of the dynamic bandwidth $\omega_{BW}(t)$ of the overall system at each time interval of the neuro-controlled system Eq. 4.23.	115

Figure 4.34	The neuro-controlled response for a periodic input reference $u(t) = \sin\frac{t}{2} + \frac{1}{2}\sin\frac{3}{4}t + \frac{1}{2}\sin t$ of the nonlinear system defined by Eq. 4.23.	116
Figure A.1	Simulink model of the nonlinear system Eq. (A.3) with a step input $u(t) = +50$.	127
Figure A.2	Overdamped response of the nonlinear system for a step input $u(t) = +50$.	127
Figure A.3	A three-dimensional plot of the location of poles in the complex plane of the nonlinear system for step input $u(t) = +50$.	129
Figure A.4	A two-dimensional projection of the three-dimensional dynamic root locus plot Figure A.3.	130
Figure A.5	Simulink model of the nonlinear system Eq. (A.3) with a step input $u(t) = +200$.	131
Figure A.6	Underdamped response of the nonlinear system for a step input $u(t) = +200$.	131
Figure A.7	A three-dimensional plot of the location of poles in the complex plane of the nonlinear system for step input $u(t) = +200$.	132
Figure A.8	A two-dimensional projection of the three-dimensional root locus Figure A.7.	132
Figure A.9	Simulink model of the nonlinear system Eq. with step input $u(t) = -50$.	133
Figure A.10	Unstable response of the nonlinear system for a step input $u(t) = -50$.	134
Figure A.11	A three-dimensional plot of the location of poles in the complex plane of the nonlinear system for step input $u(t) = -50$.	134
Figure A12	A two-dimensional projection of the three-dimensional root locus Figure A.11.	135
Figure A.13	Simulink model of the nonlinear system Eq. (A.3) with an input $u(t) = 75\sin t$.	136

Figure A.14 Stable response of the nonlinear system for an input $u(t) = 75 \sin t$. 136

Figure A.15 The location of poles vs. time $t(s)$ in the complex plane of the nonlinear system for an input $u(t) = 75 \sin t$. 137

Figure A.16 The location of poles vs. system state x_1 in the complex plane of the nonlinear system for an input $u(t) = 75 \sin t$. 138

Figure A.17 A two-dimensional projection of the three-dimensional dynamic root locus Figures A.15 and A.16. 138

Figure A.18 Simulink model of the nonlinear system Eq. (A.3) with an input $u(t) = 10 \sin t$. 139

Figure A.19 Stable response of the nonlinear system Eq. (A.3) for an input $u(t) = 10 \sin t$. 140

Figure A.20 The location of poles vs. time $t(s)$ in the complex plane of the nonlinear system for an input $u(t) = 10 \sin t$. 140

Figure A.21 The location of poles vs. system state x_1 in the complex plane of the nonlinear system for an input $u(t) = 10 \sin t$. 141

Figure A.22 A two-dimensional projection of the three-dimensional dynamic root locus Figures A.20 and A.21. 141

Figure A.23 Simulink model of the nonlinear system Eq. (A.3) with an input $u(t) = 75\sin 0.8t$. 142

Figure A.24 Unstable response of the nonlinear system Eq. (A.3) for an input $u(t) = 75\sin 0.8t$. 143

Figure A.25 The location of poles vs. time $t(s)$ in the complex plane of the nonlinear system for an input $u(t) = 75 \sin 0.8t$. 143

Figure A.26 The location of poles vs. system state x_1 in the complex plane of the nonlinear system for an input $u(t) = 75 \sin 0.8t$. 144

Figure A.27 A two-dimensional projection of a three-dimensional dynamic root locus plots Figures A.25 and A.26. 144

Figure A.28 A three-dimensional dynamic root locus of the characteristic equation $g^2 + 8g + (12 + x_1) = 0$ varying the system state x_1 from 0~3.274. 148

Figure A.29 A two-dimensional projection of a three-dimensional dynamic root locus plot Figure A.28 varying the system state x_1 from 0~3.274. 148

Figure A.30 A three-dimensional dynamic root locus of the characteristic equation $g^2 + 8g + (12 + x_1) = 0$ varying System state x_1 from 0~9.362. 149

Figure A.31 A two-dimensional projection of a three-dimensional dynamic root locus Figure A.30. 150

Figure A.32 A three-dimensional dynamic root locus of the dynamic characteristic equation $g^2 + 8g + (12 + x_1) = 0$ varying the system state x_1 from -400~0. 151

Figure A.33 A two-dimensional projection of the three-dimensional dynamic root locus Figure A.32. 151

Figure A.34 A three-dimensional dynamic root locus of the dynamic characteristic equation $g^2 + 8g + (12 + x_1) = 0$ varying the system state x_1 from $-9.9\sim +4.42$. 152

Figure A.35 A two-dimensional projection of the three-dimensional dynamic root locus Figure A.33. 153

Figure A.36 A three-dimensional dynamic root locus of the dynamic characteristic equation $g^2 + 8g + (12 + x_1) = 0$ varying the system state x_1 from $-0.766\sim +0.712$. 154

Figure A.37 A two-dimensional projection of the three-dimensional dynamic root locus Figure A.35. 155

Figure A.38 A three-dimensional dynamic root locus of the dynamic characteristic equation $g^2 + 8g + (12 + x_1) = 0$ varying the system state x_1 from $-20\sim +4.47$. 156

Figure B.1 Simulink model of the nonlinear system Eq. (B.2) and its linearized model Eq. (B.3) at the operating point $u(t)$=+50. 160

Figure B.2	The output of the nonlinear system Eq. (B.2) and its linearized model Eq. (B.3) at the operating point $u(t)$ = +50.	161
Figure B.3	The pole locations of the nonlinear system Eq. (B.2) and its linearized model Eq. (B.3) at the operating point $u(t)$ = +50.	162
Figure B.4	The output of the nonlinear system Eq. (B.2) and its linearized model Eq. (B.3) with a step input $u(t)$ = +50.5.	162
Figure B.5	The output of the nonlinear system Eq. (B.2) and its linearized model Eq. (B.3) with a step input $u(t)$ = −50.	163
Figure B.6	The dynamic pole locations of the nonlinear system Eq. (B.2), and its linearized model Eq. (B.3) for a step input $u(t)$ = −50.	164
Figure C.1	Simulink model of example 4.1	167
Figure C.2	Simulink model of example 4.2	168
Figure C.3	Simulink model of example 4.3	169
Figure C.4	Simulink model of example 4.4	170

List of Tables

Table 3.1	Dynamic Routh's Array.	33
Table 4.1	Various types of possible functions and their graphical representations for the position feedback $K_p(e,t)$ and velocity feedback $K_v(e,t)$ of a neuro-controller.	83

Chapter 1
Neuro-Control Systems: an Introduction

Controlling a system is becoming a more and more integral part of our daily life with the advancement of engineering and technology. In fact, from missile guidance to household gadgets, heating water to human-made manufacturing machines, and so on, the omnipotent application of automatic control is found almost everywhere. Besides, motivations from biological systems to ensure the concurrence of human and human-built structures with nature were growing since the ancient history. The portrayal of human calibers to dominant over situations through robust cognition (i.e., thinking, learning, adaption, and perception) has been a desire of control engineers to apply on machines for many years [1].

Nonlinearity is an undeniable phenomenon in physical dynamic systems to be controlled [2]. Nonlinearities come inherently with the structure of a system and its motion. The example of the nonlinear systems is biological, structural, socio-economic systems and so forth. Controlling a nonlinear dynamic system to get its desired response and the stability of the system along with its controller is getting one of the highest fields of interest from engineers and scientists.

However, most physical systems can be modeled mathematically with the help of a system of nonlinear equations that include algebraic, differential, integral and functional terms [3]. Stability analysis of this system of equation sometimes becomes cumbersome and complicated. On the other hand, stability analysis of a linear dynamic system is comparatively easy, and standard tools are available to analyze the stability region of a linear dynamic system. Most nonlinear systems can be approximated to a linear system close to some operating points [2]. Stability analysis of this approximate linear system of a nonlinear system using the linear stability theorem is sometimes gruesome and often dangerous because stability beyond those operating points cannot be guaranteed.

A mathematical model of any dynamic physical system, through proper treatment, is nothing but an arithmetic combination of poles and zeros. The characteristics of a dynamic system such as transient response and steady-state response depend on the location of poles and zeros in the complex plane [4, 5]. Location of poles and zeros may be fixed (e.g., a linear time-invariant system with unit gain), changes with the change of system gains (e.g., a linear time-invariant system with variable gain), or with the change of system states and time (e.g., nonlinear, and/or time-variant system). In other words, poles can be static or dynamic. Dynamic poles change their location in the complex plane with the change of time and/or system parameters [6]. Stability and the performance of a nonlinear and/or time-variant dynamic system depend on the location and movement of dynamic poles in the complex plane [6].

In this thesis, the dynamic Routh's stability criterion, an approach to account for the stability of any nonlinear and/or time-varying dynamic system based on the dynamic pole motion in a complex plane, is presented. A dynamic Nyquist stability criterion is also developed to analyze the stability in the frequency domain. The location of dynamic poles in the complex plane is calculated using the dynamic Routh's array. This thesis also introduces several tools for analyzing and examining the behavior of a nonlinear dynamic system, including g −transfer matrix, dynamic root locus and root contour, and dynamic Nyquist and Bode plots. Dynamic pole movement is also used to design a neuro-controller which is an error based adaptive controller. The neuro-controller controls the pole locations as a function of error by adjusting the controller parameters in a systematic way to get the best system response by the continuous rectification of the overall plant dynamics.

1.1 Previous Research

Over the decades, a great effort has been taken on the stability analysis and the controller design of a dynamic system. The concept of poles and zeros, in the complex s −plane, is the fundamental to analysis the stability and design of the controller for a linear and time-invariant system [4, 5]. The linear and time-invariant plant dynamic behavior depends on the location of poles, for instance, a stable under-damped system has left-half complex poles in the complex s −plane, whereas a stable over-damped system has real left-half poles [4, 5]. The study of a

linear system is mature enough with many analyzing tools available, e.g., root locus, Bode plot, Routh-Hurwitz stability criterion, etc. On the other hand, many of these tools are not applicable to the nonlinear dynamic systems. The first attempt to extend the Routh's stability criterion for the nonlinear time-varying dynamic systems was dynamic Routh's criterion, developed in [6]. Although they successfully implemented the concept of dynamic pole motion in the complex g −plane to analyze the stability conditions of a nonlinear dynamic system, it was limited to the absolute stability of a nonlinear system in time domain. Besides, a dynamic pole motion-based adaptive neuro-controller for the desired response of a nonlinear system was initiated in [7, 8, 9, 10, 11].

The equilibrium of a conservative mechanical system based on the theory of minimum potential energy with the absence of external forces is a pioneer work on the stability analysis, carried out by Lagrange in 1788. The most famous and general method of determining the stability of nonlinear and/or time-varying systems is the direct method of Lyapunov's, conducted in 1892. Lyapunov's work on defining the stability based on Lagrange's principle for the establishment of equilibrium is one of the most crucial events in the field of dynamic system stability [12]. Despite its vast usefulness, the mathematical counterpart of defining the energy like 'Lyapunov's function' from a purely mathematical form of the nonlinear dynamic system for stability analysis sometimes becomes cumbersome and requires considerable perception and expertise [13]. To eliminate much of the supposition with Lyapunov's method, Ingwerson [13] included an intermediate condition to the original stability criterion based upon an integration of matrices which solves the linearization problem exactly.

Popov's criterion for defining the bounded input and bounded output (BIBO) stability of a nonlinear system with single nonlinearity has received massive attention in the early seventies [14]. Lagrange stability of a nonlinear, memoryless, single-valued and single instantaneous system, confined within a gain, can be identified sufficiently using Popov's stability criterion [14]. Popov's criterion can be used satisfactorily to investigate the stochastic stability of a nonlinear system in large, with probability one, and exponential *p*-stability [6, 15].

Stability analysis of uncertain control systems with separable nonlinearities using the describing function (DF) method and Bode envelope of linear uncertain transfer functions have gained popularity and is covered in many texts [16]. The stability of a class of nonlinear systems with real parametric uncertainties and norm-bounded perturbations are studied in [17]. Impram and Munro [17] made a combination of the small gain theorem (SGT) with the fundamental concept of circular arithmetic to analyze the robust stability of the systems with separable nonlinearities. Detailed treatments can be found in [18, 19, 20]. The translation of the origin of the local exponential stability of a no-triangular nonlinear system to global exponential stability based on the Hurwitz nature of the Jacobian at the origin is studied in [21].

Stability analysis of a nonlinear systems having fractional-order dynamics is proven theoretically by using Gronwall-Bellman lemma and fractional calculus in [22]. A simple criterion is then derived based on the theory to design a controller for stabilizing original nonlinear, fractional-order systems [22, 23]. Linear matrix inequities (LMIs) technique is extended to analyze the stability and performance of nonlinear systems by use of the sum of squares (SOS) programming [24, 25]. An algorithm is developed using SOS programming to find the global contraction matric of an autonomous nonlinear system. Contraction analysis, a stability theory for nonlinear systems where stability is defined between two arbitrary trajectories, is then carried out to find the maximum allowable uncertainty of the system [24].

1.2 Motivations

The most wondrous carbon-based biological computer, the human brain, which controls all the actions, is made of billions of individual nerve cells called neurons, and neurons are the powerhouses for executing all the complex biological algorithms in the brain [1].

Neuro means ‘learn plus adaptation.’ Human neurons learn from the situation and adapt the brain dynamics to accomplish the task assigned to it. The biological motivation of a neuro-controller comes from the biological control scheme of the human brain for accomplishing a task by controlling human hands and legs.

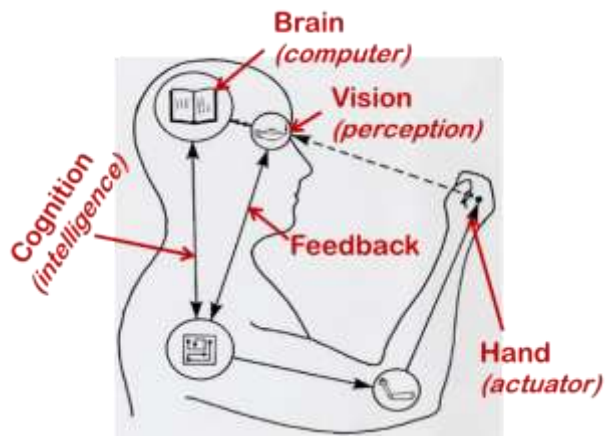

Figure 1.1: Biological Control Loop.

The control action of the neuron-made human brain is a closed-loop control action. Hands and legs are actuators, vision and cognition are sensors, and brain acts as a controller. Brain varies its control output to control hands and legs, continuously, taking the sensor feedback from vision and cognition. For example, walking on the street, the human brain changes its output to adjust the walking speed. If the target is far away, the brain controls actuators, i.e., hand and leg to increase the walking speed. On the other hand, if the target is close, the brain changes its output to decrease the walking speed. The brain takes the position and velocity feedback of the body via sensor action, through vision and cognition, to change its control action.

An error based neuro-controller is designed, in this thesis, to control the complex dynamic systems where the controller learns from error and adapts its parameters as a function of the system error yielding the response very fast without overshoot.

1.3 Objectives

The overall objective of this thesis is to extend a dynamic pole motion in the complex g −plane based stability analysis, dynamic Routh's stability criterion presented in [6], to study the relative stability, and frequency domain characteristics by developing a dynamic Nyquist criterion along with its application in the analysis of nonlinear systems. The concepts will be

applied to the design of a neuro-controller to achieve a very fast response with zero overshoot, original work is done in [7], along with several nonlinear examples. A neuro-controller continuously adjusts its dynamics and relocates the overall system dynamic poles in the complex g −plane as a function of the system error.

The overall objective can be broken down to the following specific objectives:

1. To develop a general state-space representation of a dynamic system, the introduction of g operator and the complex g −plane to establish the input-output relationship regarding g −transfer matrix, and the derivation of the dynamic characteristic equation to locate the dynamic poles in the complex g −plane. The effects of the changing values of the system parameters, e.g., gain, system states $\mathbf{x}$ and time t, on the location of dynamic poles in the complex g −plane are also need to be examined. The sketching procedure of the dynamic root locus and dynamic root contour will be discussed.
2. To develop a theory for stability analysis based on dynamic pole locations in the complex g −plane in the frequency domain, the dynamic Nyquist criterion, to characterize different perspectives of system behaviors with a commencement to dynamic Nyquist and Bode plots. A phase plane analysis will be studied applying the dynamic Routh's criterion to determine the stability region. A study to present the interrelationship between the dynamic root locus, and the dynamic Nyquist and Bode plots will be discussed.
3. To design an error-based adaptive neuro-controller based on dynamic pole movement in the complex g −plane in such a way that dynamic pole moves as a function of system error to get a very fast response with zero overshoot. The stability of the proposed neuro-controlled system needs to be verified according to the dynamic Routh's stability criterion.

All the simulation works presented in this thesis are performed by using the software packages MATLAB r2016a, and SIMULINK v8.7.

1.4 Thesis Organization

The rest of the thesis is organized as follows. Some basic mathematical concepts regarding nonlinear systems are introduced in Chapter 2. A general state-space representation is presented to address the dynamic systems, i.e., linear, nonlinear and/or time-variant systems. The g operator along with the complex g −plane is introduced in this chapter to establish the input-output relationship by establishing a g −transfer matrix and finding out the dynamic characteristic equations to locate the dynamic poles in the complex g −plane. Dynamic root locus, the movement of dynamic poles with the variation of system parameters, e.g., system states and time and its sketching procedure, is also presented. Several numerical examples to explain the dynamic root locus techniques are given at the end of Chapter 2.

The dynamic pole location based stability analysis in the complex g −plane, dynamic Routh's stability criterion is discussed in Chapter 3. The dynamic pole locations in the complex g −plane are determined from the dynamic Routh's array. The dynamic Nyquist criterion is developed to analyze a nonlinear system frequency domain characteristics and relative stability. Dynamic Nyquist and Bode plots are also introduced in this chapter. The dynamic Routh's criterion is also applied to do a phase plane analysis to find out the stability region. Several numerical examples including nonlinear systems and their stability results according to the dynamic Routh's stability criterion are illustrated. An interrelationship between the dynamic root locus and the dynamic Nyquist and Bode plots is also presented.

The design criteria for the neuro-controllers are devoted to Chapter 4. A neuro-controller adjusts the overall system dynamics by continuously changing its parameters as a function of the system error to ensure a very fast response with zero overshoot. Various possible functions along with their graphical correspondence representations are also given in this chapter. Several numerical examples were chosen from the literature, and the neuro-controller parameters are designed to work on these examples at the end of the chapter. The stability analysis of the neuro-controlled systems for these exemplary systems are carried out by using the dynamic Routh's stability criterion, as discussed in Chapter 3.

Finally, the summary of the thesis by discussing the main contributions with some future research issues are recapitulated in Chapter 5. The verification of the examples presented in this thesis are given in Appendix A, a comparison between linearization and dynamic pole motion approach on nonlinear system performance is given on Appendix B, and the details of the Simulink models of the examples in Chapter 4 are shown in Appendix C.

Chapter 2

g −Plane Characteristics of a Nonlinear Dynamic System

This chapter gives some preliminary discussions of a dynamic system representation to facilitate the understanding of a new method for representing the stability of a nonlinear dynamic system (in Chapter 3) and of a new methodology for designing a neuro-controller to control the response (in Chapter 4).

The achievements of this chapter lies in the construction of a g −transfer matrix of a nonlinear dynamic system and as well as, the derivation of the dynamic characteristic equation from it. The definition and the sketching procedure of the dynamic root locus are also illustrated. Several numerical examples have been undertaken to illustrate the concepts.

2.1 Mathematical Representation of a Dynamic System

A linear, nonlinear, time-variant, or time-invariant dynamic system can be modeled by a finite number of coupled first-order ordinary differential equations [2, 26],

$$\begin{aligned}
\dot{x_1} &= f_1(x_1, \cdots, x_n, t, u_1, \cdots, u_m), \quad && x_1(0) \\
\dot{x_2} &= f_2(x_1, \cdots, x_n, t, u_1, \cdots, u_m), \quad && x_2(0) \\
&\vdots && \vdots \\
\dot{x_i} &= f_i(x_1, \cdots, x_n, t, u_1, \cdots, u_m), \quad && x_i(0) \\
&\vdots && \vdots \\
\dot{x_n} &= f_n(x_1, \cdots, x_n, t, u_1, \cdots, u_m), \quad && x_n(0)
\end{aligned} \tag{2.1}$$

where x_i, $i \in [1, n]$, is the state variable of the system and $\dot{x_i}$ is the time derivative of x_i. u_i, $i \in [1, m]$, is the control input. $x_i(0)$, $i \in [1, n]$, is the initial condition.

We can represent this system of first-order differential equations, Eq. (2.1) to a n −dimentional first-order vector differential equation [2, 26],

$$\dot{\mathbf{x}} = \mathbf{f}(\mathbf{x}, t, \mathbf{u}) \in \Re^n, \quad \mathbf{x}(0) \tag{2.2}$$

where

$$\mathbf{x} = \begin{vmatrix} x_1 \\ x_2 \\ \vdots \\ x_i \\ \vdots \\ x_n \end{vmatrix} \in \Re^n, \ \mathbf{u} = \begin{vmatrix} u_1 \\ u_2 \\ \vdots \\ u_i \\ \vdots \\ u_m \end{vmatrix} \in \Re^m, \mathbf{f}(\mathbf{x}, t, \mathbf{u}) = \begin{vmatrix} f_1(\mathbf{x}, t, \mathbf{u}) \\ f_2(\mathbf{x}, t, \mathbf{u}) \\ \vdots \\ f_i(\mathbf{x}, t, \mathbf{u}) \\ \vdots \\ f_n(\mathbf{x}, t, \mathbf{u}) \end{vmatrix} \in \Re^n, \mathbf{x}(0) = \begin{vmatrix} x_1(0) \\ x_2(0) \\ \vdots \\ x_i(0) \\ \vdots \\ x_n(0) \end{vmatrix} \in \Re^n.$$

$\mathbf{f}(\cdot)$ is a continuously differentiable nonlinear function. The output vector is defined as [2, 26],

$$\mathbf{y} = \mathbf{h}(\mathbf{x}, t, \mathbf{u}) \tag{2.3}$$

where

$$\mathbf{y} = \begin{vmatrix} y_1 \\ y_2 \\ \vdots \\ y_i \\ \vdots \\ y_p \end{vmatrix} \in \Re^p, \mathbf{h}(\mathbf{x}, t, \mathbf{u}) = \begin{vmatrix} h_1(\mathbf{x}, t, \mathbf{u}) \\ h_2(\mathbf{x}, t, \mathbf{u}) \\ \vdots \\ h_i(\mathbf{x}, t, \mathbf{u}) \\ \vdots \\ h_p(\mathbf{x}, t, \mathbf{u}) \end{vmatrix} \in \Re^p$$

$\mathbf{h}(\cdot)$ is a continuously differentiable nonlinear function. Equations (2.2) and (2.3) together refer to a state-space model of the dynamic system.

The state and output equations for nonlinear systems, as given in Eq. (2.2) and (2.3), can also be represented in the following state-space form [6],

$$\begin{aligned} \dot{\mathbf{x}}(t) &= \mathbf{A}(\mathbf{x}, t)\mathbf{x}(t) + \mathbf{B}(t)\mathbf{u}(t) \ , \quad \mathbf{x}(\mathbf{0}) \\ \mathbf{y}(t) &= \mathbf{C}(\mathbf{x}, t)\mathbf{x}(t) + \mathbf{D}(t)\mathbf{u}(t) \end{aligned} \tag{2.4}$$

where $\mathbf{A}(\mathbf{x},t) = [a_{ij}(\mathbf{x},t)] \in \Re^{n\times n}$ is the system matrix of the nonlinear system. Each element of the matrix $\mathbf{A}(\mathbf{x},t)$ can be a function of states $\mathbf{x}$ and/or time t. System states $\mathbf{x}$ are a function of input $\mathbf{u}(t)$ in both amplitude and frequency. $\mathbf{B}(t) \in \Re^{n\times m}$ is the input matrix, where $m \leq n$. The elements of $\mathbf{B}(t)$ can be a constant or a function of time t. $\mathbf{C}(\mathbf{x},t) \in \Re^{l\times p}$ is the output matrix, where $1 \leq l \leq p$. $\mathbf{D}(t) \in \Re^{l\times m}$ is the feed-forward matrix. The state-space representation of Eq. (2.4) is shown graphically in Figure 2.1.

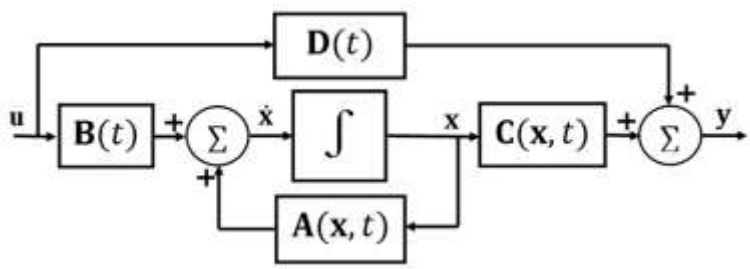

Figure 2.1. An equivalent block diagram of the state-space representation,
$\dot{\mathbf{x}}(t) = \mathbf{A}(\mathbf{x},t)\mathbf{x} + \mathbf{B}(t)\mathbf{u}(t),\ \mathbf{y}(t) = \mathbf{C}(\mathbf{x},t)\mathbf{x} + \mathbf{D}(t)\mathbf{u}(t).$

However, in a linear system, the system matrix $\mathbf{A}(\mathbf{x},t)$ and the output matrix $\mathbf{C}(\mathbf{x},t)$ are independent of system states $\mathbf{x}$. The state and output equations of a linear dynamic system [4],

$$\begin{aligned} \dot{\mathbf{x}} &= \mathbf{A}(t)\mathbf{x} + \mathbf{B}(t)\mathbf{u}, \quad \mathbf{x}(\mathbf{0}) \\ \mathbf{y} &= \mathbf{C}(t)\mathbf{x} + \mathbf{D}(t)\mathbf{u} \end{aligned} \tag{2.5}$$

where $\mathbf{A}(t) \in \Re^{n\times n}$ is the system matrix of a linear system. Elements of the matrix $\mathbf{A}(t)$ are a constant or a function of time t. $\mathbf{B}(t) \in \Re^{n\times m}$ is the input matrix, where $m \leq n$. $\mathbf{C}(t) \in \Re^{l\times p}$ is the output matrix, where $1 \leq l \leq p$. $\mathbf{D}(t) \in \Re^{l\times m}$ is the feed-forward matrix.

It can be noted that Eq. (2.4) defines a general state-space representation of any dynamic system either linear or nonlinear, time-variant or time-invariant. A quantitative comparison

between Eq. (2.4) and (2.5) gives a certain ideology that the state-space representation of a linear system is a subset of the general state-space representation.

2.2 g −Transfer Matrix

The system states $\mathbf{x}$ of a dynamic system are implicitly time t dependent. Unlike the linear time-invariant system, a nonlinear system may change explicitly with the change of system states $\mathbf{x}$ while implicitly with time t. This changing behavior of a nonlinear system with system states $\mathbf{x}$ and time t causes to change the location of poles and zeros in the complex pole-zero plane [6]. Thus, it becomes an obvious practice to relate this dynamic nature of poles and zeros movement with system states $\mathbf{x}$ or time t in the complex pole-zero plane.

Let us consider g is a differential operator, $\frac{d}{dt}$. Introducing g operator to the state-space equation, Eq. (2.4), we can write,

$$\begin{aligned} g\mathbf{x}(t) &= \mathbf{A}(\mathbf{x},t)\mathbf{x}(t) + \mathbf{B}(t)\mathbf{u}(t) \\ \mathbf{y}(t) &= \mathbf{C}(\mathbf{x},t)\mathbf{x}(t) + \mathbf{D}(t)\mathbf{u}(t) \end{aligned} \tag{2.6}$$

Rearranging Eq. (2.6), we get,

$$\big(g\mathbf{I} - \mathbf{A}(\mathbf{x},t)\big)\mathbf{x}(t) = \mathbf{B}(t)\mathbf{u}(t) \tag{2.7}$$

where $\mathbf{I}$ is a $n \times n$ identity matrix. Pre-multiplying both sides of Eq. 2.7 with $(g\mathbf{I} - \mathbf{A}(\mathbf{x},t))^{-1}$ leads to,

$$\mathbf{x}(t) = \big(g\mathbf{I} - \mathbf{A}(\mathbf{x},t)\big)^{-1}\mathbf{B}(t)\mathbf{u}(t) \tag{2.8}$$

where $(g\mathbf{I} - \mathbf{A}(\mathbf{x},t))$ is invertible. Substituting the value of $\mathbf{x}(t)$ from Eq. (2.8) to $\mathbf{y}(t) = \mathbf{C}(\mathbf{x},t)\mathbf{x}(t) + \mathbf{D}(t)\mathbf{u}(t)$, we obtain,

$$\mathbf{y}(t) = \left[\mathbf{C}(\mathbf{x},t)\left(g\mathbf{I} - \mathbf{A}(\mathbf{x},t)\right)^{-1}\mathbf{B}(t) + \mathbf{D}(t)\right]\mathbf{u}(t) \tag{2.9}$$

where $\left[\mathbf{C}(\mathbf{x},t)\left(g\mathbf{I} - \mathbf{A}(\mathbf{x},t)\right)^{-1}\mathbf{B}(t) + \mathbf{D}(t)\right]$ is the g −transfer matrix and it relates the output vector $\mathbf{y}(t)$ to the input vector $\mathbf{u}(t)$. Expanding Eq. (2.9),

$$\mathbf{y}(t) = \left[\mathbf{C}(\mathbf{x},t)\frac{\mathbf{adj}\left(g\mathbf{I} - \mathbf{A}(\mathbf{x},t)\right)}{\mathbf{det}\left(g\mathbf{I} - \mathbf{A}(\mathbf{x},t)\right)}\mathbf{B}(t) + \mathbf{D}(t)\right]\mathbf{u}(t) \tag{2.10}$$

or,

$$\mathbf{y}(t) = \left[\frac{\mathbf{C}(\mathbf{x},t)\mathbf{adj}\left(g\mathbf{I} - \mathbf{A}(\mathbf{x},t)\right)\mathbf{B}(t) + \mathbf{det}\left(g\mathbf{I} - \mathbf{A}(\mathbf{x},t)\right)\mathbf{D}(t)}{\mathbf{det}\left(g\mathbf{I} - \mathbf{A}(\mathbf{x},t)\right)}\right]\mathbf{u}(t) \tag{2.11}$$

where $\mathbf{det}(g\mathbf{I} - \mathbf{A}(\mathbf{x},t)) \neq 0$. $\mathbf{adj}$ and $\mathbf{det}$ stands for the adjoint and determinant of a matrix, respectively. The elements of the adjoint matrix $\mathbf{adj}(g\mathbf{I} - \mathbf{A}(\mathbf{x},t))$ are either constant or a function of g. The numerator of Eq. (2.10) gives the location of the **zeros**, if any, in the complex pole-zero plane. $\mathbf{det}(g\mathbf{I} - \mathbf{A}(\mathbf{x},t))$ is a scalar function of g, and the location of **poles** in the complex pole-zero plane depends on the solution of the equation, $\mathbf{det}(g\mathbf{I} - \mathbf{A}(\mathbf{x},t)) = 0$ for g. The dynamic characteristic equation is thus defined by

$$\mathbf{det}(g\mathbf{I} - \mathbf{A}(\mathbf{x},t)) = 0 \tag{2.12}$$

where $\mathbf{I}$ is a $n \times n$ identity matrix. Elements of $n \times n$ system matrix $\mathbf{A}$ ($\mathbf{A}_{ii}$, where $i = 1,2,\cdots,n$) contains all the states $\mathbf{x}$ and time t dependent nonlinear terms. Solving Eq. (2.12) for g gives the roots of the dynamic characteristic equation, which are also the poles of the nonlinear system represented by Eq. (2.4).

A care must be taken that $s \triangleq \frac{d}{dt}$ is a differential operator widely used to characterize linear time-invariant systems [4, 5], whereas the time-varying differential operator g is equally applicable to linear, nonlinear, time-variant or time-invariant dynamic systems. In other words, s operator is a subset of g operator.

2.2.1 Complex g −plane

A complex number has a real and an imaginary part. Similarly, a complex variable also has a real and an imaginary part [5]. The real and imaginary parts of a complex variable can be a function of system states $\mathbf{x}$ and/or time t. If $g[\mathbf{x}, t]$ denotes a time t and a state $\mathbf{x}$ dependent complex variable, then

$$g[\mathbf{x}, t] = \sigma[\mathbf{x}, t] + j\omega[\mathbf{x}, t] \tag{2.13}$$

where $\sigma[\mathbf{x}, t]$ and $\omega[\mathbf{x}, t]$ are the time and state-dependent real and imaginary parts, respectively. Note that system states $\mathbf{x}$ are implicitly time t dependent. We can reduce Eq. (2.13) to a simpler form [6],

$$g(t) = \sigma(t) + j\omega(t) \tag{2.14}$$

where $g(t)$ is a differential operator, $\frac{d}{dt}$. $g(t)$, $\sigma(t)$ and $\omega(t)$ are explicitly state $\mathbf{x}$ and implicitly time t dependent. $g(t)$ gives time-varying roots of the dynamic characteristic equation represented by Eq. (2.12). The magnitude and angle of $g(t)$ at a particular time t_c is given by $\sqrt{\sigma_x^2(t_c) + \omega_y^2(t_c)}$ and $\tan^{-1}\left[\sigma_x(t_c)/\omega_y(t_c)\right]$, respectively.

A nonlinear system dynamics can be examined graphically by plotting their poles and zeros in the complex g −plane. g −plane is a three-dimensional complex pole-zero plane, where the horizontal axis represents the real part $\sigma(t)$ of the complex variable $g(t)$, the vertical axis represents the imaginary part $\omega(t)$ of the complex variable $g(t)$, and the third axis of g −plane represents the pole-zero movement to the system error $e(t)$, system states $\mathbf{x}$, or time t. The graphical representation of the complex g −plane is shown in Figure 2.2 [6].

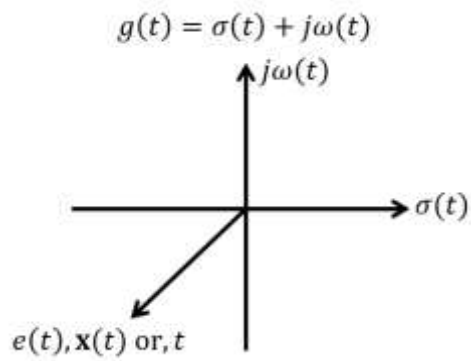

Figure 2.2. Three-dimensional complex g −plane, $g(t) = \sigma(t) + j\omega(t)$. The horizontal axis represents the real part $\sigma(t)$, the vertical axis represents the imaginary part $j\omega(t)$. The third axis can be either error $e(t)$, system states **x**, or time t.

Note that poles and zeros in the g −plane are not static rather dynamic [6]. Similar to the g operator, the g −plane is applicable to a linear, nonlinear, time-invariant, and time-variant dynamic system.

2.2.2 Dynamic Poles and Zeros

The dynamic characteristic equation, Eq. (2.12), can also be described by [6],

$$a_n g^n + a_{n-1} g^{n-1} + \cdots + a_1 g + a_0 = 0 \tag{2.15}$$

where $a_i = a_i(\mathbf{x}, t)$, $i = 0,1,2,3, \ldots, n$, is the coefficient of g^i and a function the states **x** and time t. The roots of the dynamic characteristic equation, Eq. (2.15), are a function of states **x** and moves in the complex g −plane with the change of states **x** and time t [6]. As mentioned before, the roots of the dynamic characteristic equation are poles of the nonlinear dynamic system, so the poles of the system, Eq. (2.4), also moves with the change of system states **x** and time t. This moving behavior of the nonlinear system poles in the complex g −plane with the change of the system states **x** or time t is called **dynamic poles** [6].

Similarly, the elements of the numerator of Eq. (2.10) and (2.11) $\mathbf{C}(t)[\mathbf{adj}\left(g\mathbf{I}-\mathbf{A}(\mathbf{x},t)\right)]\mathbf{B}(t)+\mathbf{D}(t)\,[\mathbf{det}(g\mathbf{I}-\mathbf{A}(\mathbf{x},t))]$ can be a constant or a function of states $\mathbf{x}$ and time t. $\mathbf{det}\,[\,\mathbf{C}(\mathbf{x},t)[\mathbf{adj}\left(g\mathbf{I}-\mathbf{A}(\mathbf{x},t)\right)]\mathbf{B}(t)+\mathbf{D}(t)\,[\mathbf{det}(g\mathbf{I}-\mathbf{A}(\mathbf{x},t))]]=0$ gives the location of the zeros in the complex g −plane. These zeros are a constant or change their location in the complex g −plane with the change of system states $\mathbf{x}$ or time t. This changing behavior of the nonlinear system zeros in the complex g −plane is called **dynamic zeros**.

2.3 Dynamic Root Locus

Root locus is a graphical representation of the paths of the closed-loop poles of a linear time-invariant system with the variation of system parameters (e.g., gain) from zero to infinity and it is a tool for analyzing the performance of a dynamic system [4]. The root locus technique has been extended for the nonlinear and/or time-varying dynamic systems and has given a name **dynamic root locus** in the complex g −plane.

Definition I: Dynamic root locus is the graphical representation of the path of the dynamic poles of a nonlinear and/or time-variant system, as the parameters of the system are varied, respectively, from zero to infinity. Although the parameters can be any other variable of the system, in most cases the system states $\mathbf{x}$ and time t are the common system parameters.

Rearranging the dynamic characteristic equation, Eq. (2.15),

$$1+K(\mathbf{x},t)\frac{\left(g+z_1(\mathbf{x},t)\right)\left(g+z_2(\mathbf{x},t)\right)\cdots\left(g+z_m(\mathbf{x},t)\right)}{(g+p_1(\mathbf{x},t))(g+p_1(\mathbf{x},t))\cdots(g+p_n(\mathbf{x},t))}=0 \tag{2.16}$$

$(g+p_i(\mathbf{x},t))$, $i=1,2,\ldots.,n$, gives the locations of dynamic poles in the complex g −plane and $(g+z_k(\mathbf{x},t))$, $k=0,1,2,\ldots,m$, gives the locations of dynamic zeros. $K(\mathbf{x},t)$ is the system state $\mathbf{x}$ and time t dependent dynamic gain and determines the path of dynamic roots in the complex g −plane.

It is possible that a nonlinear system dynamics involves more than one parameter to be varied. The dynamic root locus for a nonlinear and/or time-variant system with multiple parameters to be varied, respectively, from zero to infinity is called **dynamic root contour**, is an extension of the root contour plots of a linear time-invariant system [5].

2.4 Illustrative Numerical Examples

In this section, several examples of nonlinear dynamic systems are taken to illustrate the g −plane characteristics. The nature of a dynamic system can be described qualitatively regarding its dominant parameters. For instance, the dynamics of a typical second-order system is,

$$\ddot{x} + k_v\dot{x} + k_p x = u(t) \tag{2.17}$$

where $k_p = {\omega_n}^2$ is the position feedback and determines the bandwidth of the system. $k_v = 2\boldsymbol{\xi}\omega_n$ is the velocity feedback and determines the damping ratio. For a linear system, k_p and k_v are a constant but for a nonlinear system; they can be a constant or a function of states **x** and/or time t.

Example 2.1:

Consider a nonlinear time-invariant second-order differential equation with a nonlinear damping and nonlinear spring, represented by

$$\ddot{x} - \dot{x}^3 + x^2 = u(t) \tag{2.18}$$

This system can be represented by the state-space model, i.e.,

$$\begin{aligned} \dot{x_1} &= x_2 \\ \dot{x_2} &= -x_1x_1 + {x_2}^2x_2 + u(t) \end{aligned} \tag{2.19}$$

where $x_1 = x$ and $x_2 = \dot{x}$ are the states of the system. The position feedback k_p and velocity feedback k_v are given by x_1 and $-{x_2}^2$, respectively. The output is given by

$$y = x_1 \tag{2.20}$$

Equations **(**2.19) and (2.20) can also be represented by

$$\begin{aligned} \dot{\mathbf{x}}(t) &= \mathbf{A}(\mathbf{x}, t)\mathbf{x}(t) + \mathbf{B}(t)\mathbf{u}(t) \\ \mathbf{y}(t) &= \mathbf{C}(\mathbf{x}, t)\mathbf{x}(t) \end{aligned} \tag{2.21}$$

where

$\mathbf{x} \in \Re^n$: the state vector,

$\dot{\mathbf{x}} \in \Re^n$: the derivation of the state vector $\mathbf{x}$ to time t,

$\mathbf{y} \in \Re^p$: the output vector, and

$\mathbf{u} \in \Re^m$: the control input.

System matrix $\mathbf{A}(\mathbf{x}, t) = \begin{vmatrix} 0 & 1 \\ -x_1 & {x_2}^2 \end{vmatrix}$.

Input matrix $\mathbf{B}(t) = \begin{vmatrix} 0 \\ 1 \end{vmatrix}$.

Output matrix $\mathbf{C}(\mathbf{x}, t) = |1 \quad 0|$.

The equivalent block diagram is shown in Figure 2.3.

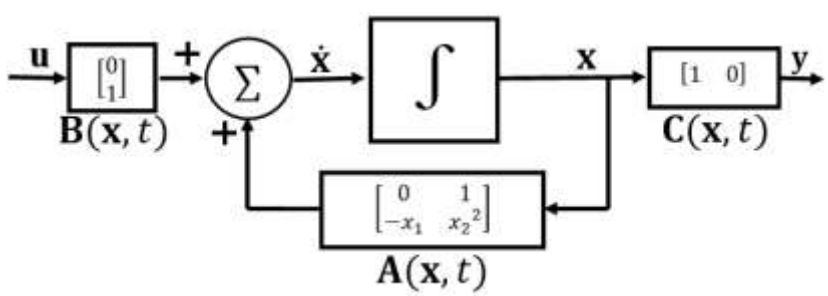

Figure 2.3. Block diagram representation of the state-space model of the nonlinear system, $\ddot{x} - \dot{x}^3 + x^2 = u(t)$.

Invertible matrix $(g\mathbf{I} - \mathbf{A}(\mathbf{x}, t)) = \begin{bmatrix} g & -1 \\ x_1 & g - {x_2}^2 \end{bmatrix}$. So the dynamic characteristic equation $\mathbf{det}(g\mathbf{I} - \mathbf{A}(\mathbf{x}, t)) = 0$ of the nonlinear time-invariant system, Eq. (2.18), is given by

$$g^2 - {x_2}^2 g + x_1 = 0 \tag{2.22}$$

The roots of the dynamic characteristic equation, Eq. (2.22), are,

$$g_{1,2} = \frac{{x_2}^2 \pm \sqrt{{x_2}^4 - 4x_1}}{2} \tag{2.23}$$

From Eq. (2.23) we conclude that the system has a conjugate dynamic pole and these dynamic poles are a function of system states x_1 and x_2. x_1 and x_2 are a function of input signal $\mathbf{u}(t)$ and the initial conditions. The dynamic poles $g_{1,2}$ are real or complex depending on the values of x_1 and x_2.

Example 2.2:

Consider a second-order nonlinear differential equation,

$$\begin{aligned} \dot{x_1} &= -2x_1 \\ \dot{x_2} &= 2{x_2}^2 x_1 + 2x_2 + u(t) \end{aligned} \tag{2.24}$$

and the output,

$$y = x_1$$

where $x_1 = x$ and $x_2 = \dot{x}$ are the states of the dynamic system. The system matrix $\mathbf{A}(\mathbf{x}, t) = \begin{bmatrix} -2 & 0 \\ 2{x_2}^2 & 2 \end{bmatrix}$. An equivalent block diagram of the nonlinear system is,

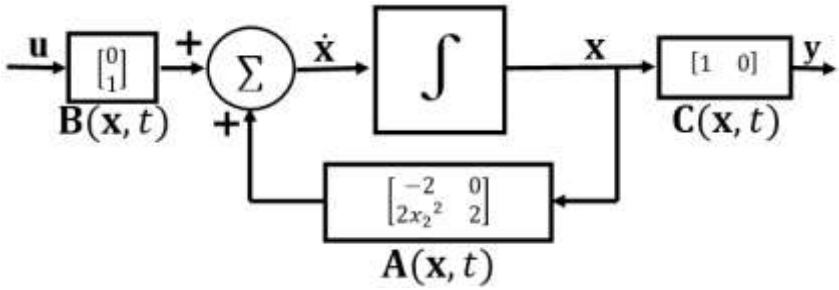

Figure 2.4. An equivalent block diagram of the nonlinear dynamic system,

$$\dot{x_1} = -2x_1,\ \dot{x_2} = 2{x_2}^2 x_1 + 2x_2,\ y = x_1.$$

The dynamic characteristic equation $\mathbf{det}(g\mathbf{I} - \mathbf{A}(\mathbf{x}, t)) = 0$ of the nonlinear time-invariant system Eq. (2.24) is,

$$g^2 + 2({x_2}^2 - 2) = 0 \tag{2.25}$$

The roots of this dynamic characteristic equation, Eq. (2.25), are a function of the system states x_2 explicitly and time t implicitly. Rearranging Eq. (2.25),

$$1 + \frac{2{x_2}^2}{g^2 - 4} = 0 \tag{2.26}$$

From Eq. (2.26), the nonlinear system has a conjugate dynamic pole in the complex g −plane. When $x_2 = 0$, dynamic poles are located at ± 2. With the change of the value of system state x_2, the conjugate dynamic poles change their location in the complex g −plane because of the presence of a nonlinear spring $({x_2}^2 - 2)$ in the dynamic characteristic equation, Eq. (2.25). For instance, the conjugate dynamic poles are located at $\pm j6.78$ for $x_2 = 5$. A three-dimensional sketch of the dynamic root locus of the nonlinear system, Eq. (2.24), varying system state x_2 is shown in Figure 2.5. Arrowhead indicates the direction of the increased value of x_2.

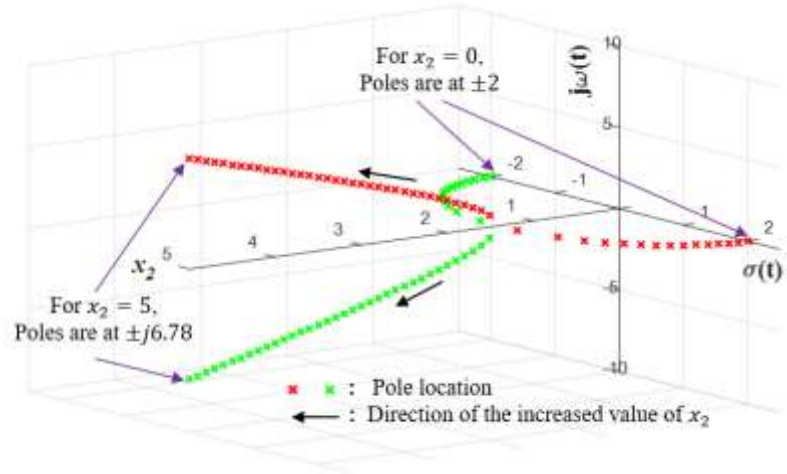

Figure 2.5. Three-dimensional dynamic root locus of the dynamic characteristic equation, $g^2 + 2({x_2}^2 - 2) = 0$. The third axis represents the system state x_2.

A two-dimensional projection of the three-dimensional dynamic root locus plot, Figure 2.4, is shown in Figure 2.6.

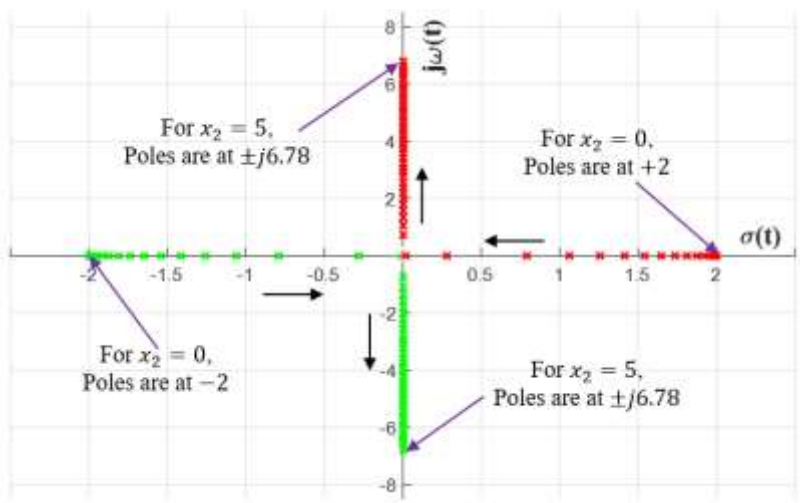

Figure 2.6. A two-dimensional projection of a three-dimensional dynamic root locus of the characteristic equation $g^2 + 2({x_2}^2 - 2) = 0$. The horizontal axis is the real axis $\boldsymbol{\sigma(t)}$, the vertical axis is the imaginary axis $\boldsymbol{j\omega(t)}$, and the third axis represents the system state x_2.

From Figure 2.5 and 2.6, for a small value of x_2 both dynamic poles are on the real axis, one is on the left-half side, and another is on the right-half side of the complex g −plane. As x_2 increases from a value of zero, both dynamics poles move towards each other creating a break-away point at (0,0,1.41). If x_2 increases above the value of 1.41, both dynamic poles leave the real axis creating a 90^0 angles with the imaginary axis. These poles stay on the imaginary axis for $x_2 > 1.41$.

Example 2.3:

A second-order nonlinear dynamic system,

$$\begin{aligned} \dot{x_1} &= -6x_1 + 2x_2 \\ \dot{x_2} &= 2x_1 - (6 + 2{x_2}^2)x_2 \end{aligned} \tag{2.27}$$

where $x_1 = x$ and $x_2 = \dot{x}$ are the states of the system. The system matrix $\mathbf{A}(\mathbf{x}, t) = \begin{vmatrix} -6 & 2 \\ 2 & -(6 + 2{x_2}^2) \end{vmatrix}$.

The dynamic characteristic equation $\mathbf{det}(g\mathbf{I} - \mathbf{A}(\mathbf{x}, t)) = 0$ of the nonlinear time-invariant system Eq. (2.27) is,

$$g^2 + 2(6 + {x_2}^2)g + (32 + 12{x_2}^2) = 0 \tag{2.28}$$

Nonlinearity arises in this dynamic characteristic equation because of the presence of two nonlinear terms, nonlinear spring $32 + 12{x_2}^2$, and nonlinear damping $6 + {x_2}^2$. Nonlinearity, as well as dynamic pole locations in the complex g −plane, depend on the value of system state x_2. Rearranging Eq. (2.28),

$$1 + \frac{2{x_2}^2(g + 6)}{g^2 + 12g + 32} = 0 \tag{2.29}$$

Figure 2.7 plots a three-dimensional representation of the dynamic root locus of the dynamic characteristic equation, Eq. (2.29), in the complex g −plane. The third axis is describing x_2. From the dynamic characteristic equation, Eq. (2.28) and (2.29), the system has a conjugate dynamic pole located at -8 and -4, and a dynamic zero located at -6. As x_2 increases, one of the dynamic poles moves towards the zero, and another moves to infinity. For example, at $x_2 = 5$ dynamic poles are located at -56.08 and -5.92. The arrowhead indicates the direction of the increased value of x_2.

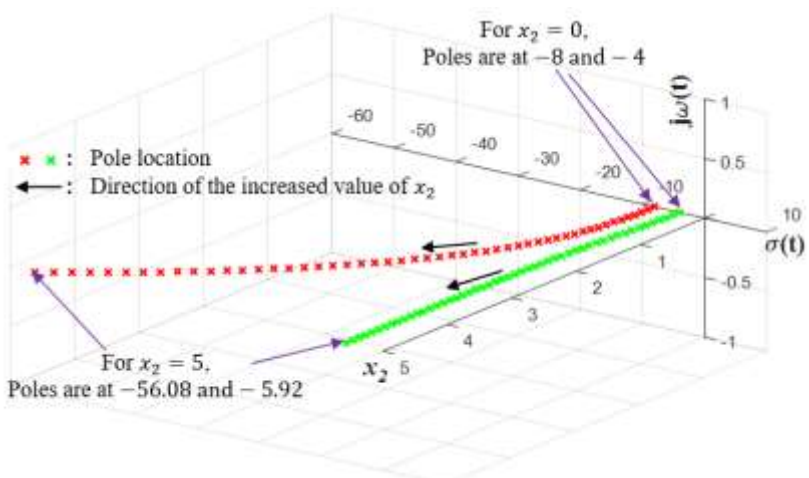

Figure 2.7. Three-dimensional dynamic root locus of the nonlinear dynamic system represented by state-space, $\dot{x_1} = -6x_1 + 2x_2$, $\dot{x_2} = 2x_1 - 6x_2 - 2{x_2}^3$. The third axis represents the system state x_2.

Example 2.4:

The state and output equations of a simplified model of a single link manipulator with a flexible joint system are given by Eq. 2.30. This example is adapted from [7].

$$\begin{aligned} \dot{x_1} &= x_2 \\ \dot{x_2} &= -x_1 - x_2 - x_3 + u(t) \\ \dot{x_3} &= x_4 \end{aligned} \tag{2.30}$$

$$\dot{x_4} = -x_1 - \left\{1 + \frac{sin(x_3)}{x_3}\right\} x_3 - x_4$$

and the output,

$$y = x_3$$

where x_1, x_2, x_3, and x_4 are the states of the system. $u(t)$ is the control input, and y is the output. $x_1 = \theta_m$, $x_2 = \dot{\theta_m}$, $x_3 = \theta_l$, $x_4 = \dot{\theta}_l$. θ_m and θ_l are the relative angular displacement of the joint actuator and relative displacement of the end effector, respectively. The state x_3 dependent sine function $\frac{sin(x_3)}{x_3}$ creates the nonlinearity in the system.

The system matrix $\mathbf{A}(\mathbf{x}, t) = \begin{bmatrix} 0 & 1 & 0 & 0 \\ -1 & -1 & -1 & 0 \\ 0 & 0 & 0 & 1 \\ -1 & 0 & -\left\{1 + \frac{sin(x_3)}{x_3}\right\} & -1 \end{bmatrix}$, the input matrix $\mathbf{B}(\mathbf{x}, t) = \begin{bmatrix} 0 \\ 1 \\ 0 \\ 1 \end{bmatrix}$, and the output matrix $\mathbf{C}(\mathbf{x}, t) = [0 \quad 0 \quad 1 \quad 0]$. The equivalent block diagram is,

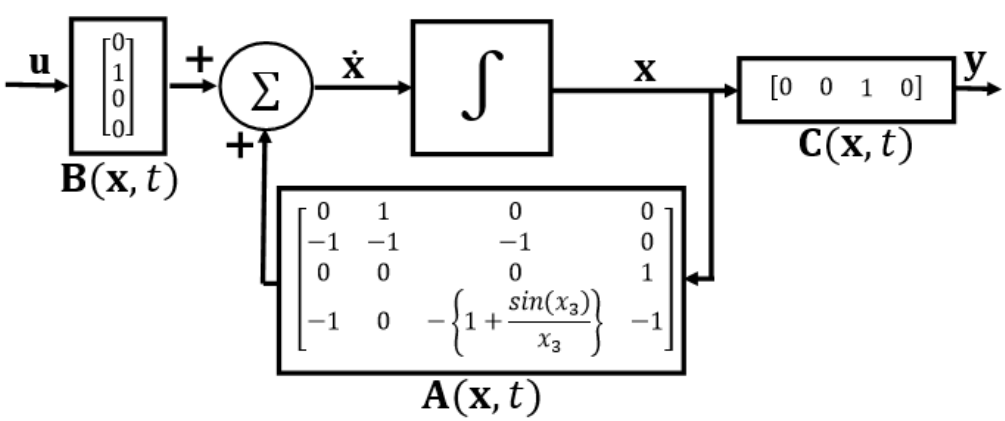

Figure 2.8. An equivalent block diagram of the simplified model of a single link manipulator with a flexible joint system presented by Eq. 2.30.

The dynamic characteristic equation $\mathbf{det}(g\mathbf{I} - \mathbf{A}(\mathbf{x}, t)) = 0$ is,

$$g^4 + 2g^3 + (3 + \varphi)g^2 + (2 + \varphi)g + \varphi = 0 \tag{2.31}$$

where $\varphi = \frac{\sin x_3}{x_3}$. The roots of this dynamic characteristic equation, Eq. (2.31), are a function of the state x_3 dependent sinusoidal term φ, and given by

$$
\begin{aligned}
g_{1,2} &= \frac{1}{2}\left(-1 \pm \sqrt{2\sqrt{\varphi^2+4} - 2\varphi - 3}\right) \\
g_{3,4} &= \frac{1}{2}\left(-1 \pm \sqrt{-2\varphi - 2\sqrt{\varphi^2+4} - 3}\right)
\end{aligned}
\tag{2.32}
$$

Rearranging Eq. (2.32),

$$
1 + \frac{\varphi(g^2+g+1)}{g(g^3+2g^2+3g+2)} = 0 \tag{2.33}
$$

Comparing Eq. (2.33) with (2.16), the nonlinear system has two conjugate dynamic poles and a conjugate dynamic zero in the complex g −plane. $\varphi = \frac{\sin x_3}{x_3}$ is the state x_3 dependent periodic gain and determines the movement of the dynamic poles. Initial dynamic poles are located at $g_1 = 0 + j0$, $g_2 = -1 + j0$, and $g_{3,4} = -0.5 \pm j1.32$.

A three-dimensional sketch of the dynamic root locus of the nonlinear system Eq. (2.30) varying the system state x_3 is shown in Figure 2.9. Arrowhead indicates the direction of the increased value of x_3. A two-dimensional projection is displayed in Figure 2.10.

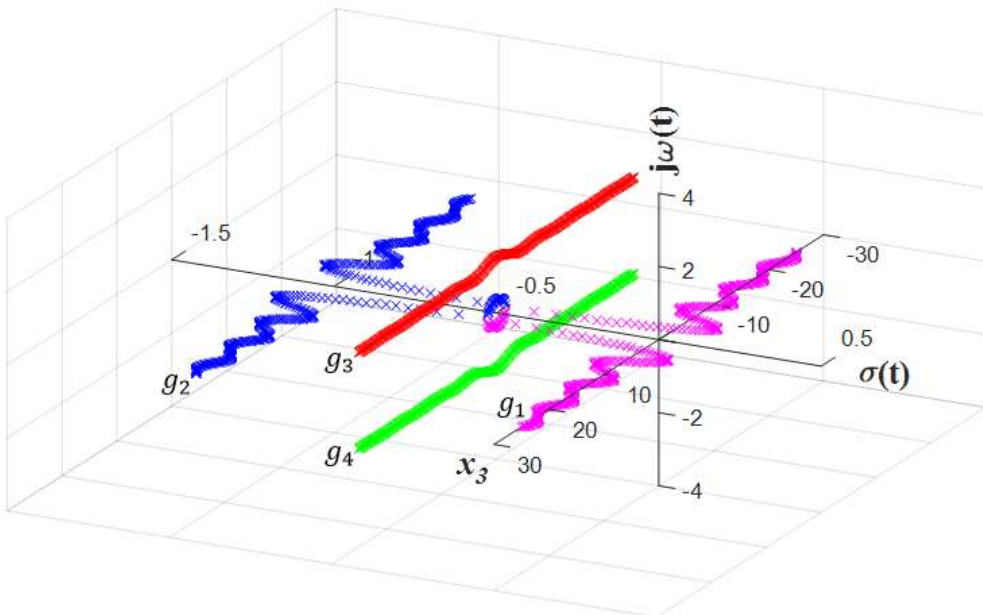

Figure 2.9. Three-dimensional dynamic root locus of the nonlinear system defined by Eq. 2.30. The third axis is presenting the system state x_3.

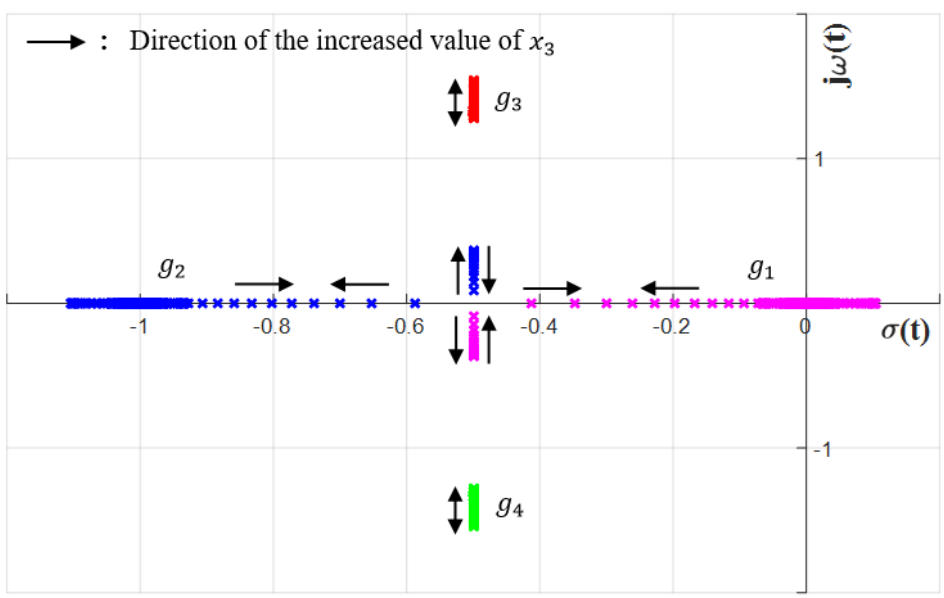

Figure 2.10. A two-dimensional projection of a three-dimensional dynamic root locus of the nonlinear system defined by Eq. 2.30. The horizontal axis is the real axis $\boldsymbol{\sigma(t)}$, the vertical axis is the imaginary axis $\boldsymbol{j\omega(t)}$, and the third axis represents the system state x_3.

The locations of the poles g_1, g_2, g_3, and g_4 in the complex g −plane are a function of the system state x_3 explicitly and time t implicitly. Because of the presence of the state-dependent dynamic gain $\varphi = \frac{\sin x_3}{x_3}$ in Eq. (2.33), an oscillatory behavior of dynamic poles is observed on the dynamic root locus. g_1 and g_2 are complex for the value of the system state x_3 between $-1.65 < x_3 < 1.65$ and other than that they are on the real axis. g_3 and g_4 are complex conjugate dynamic poles.

Example 2.5:

Consider a third-order nonlinear system,

$$\begin{aligned} \dot{x_1} &= x_2 \\ \dot{x_2} &= x_3 \\ \dot{x_3} &= -100x_1 - (50 + 5x_1)x_2 - (14 + x_1)x_3 + u(t) \end{aligned} \tag{2.34}$$

and the output,

$$y = 5x_1 + x_2$$

where $x_1 = x$, $x_2 = \dot{x}$, and $x_3 = \ddot{x}$ are the states of the dynamic system. The System matrix $\mathbf{A}(\mathbf{x}, t) = \begin{bmatrix} 0 & 1 & 0 \\ 0 & 0 & 1 \\ -100 & -(50 + 5x_1) & -(14 + x_1) \end{bmatrix}$, the input matrix $\mathbf{B}(t) = \begin{bmatrix} 0 \\ 0 \\ 1 \end{bmatrix}$, and the output matrix $\mathbf{C}(\mathbf{x}, t) = [5 \quad 1 \quad 0]$. The presence of state x_1 dependent term $-(50 + 5x_1)$ and $-(14 + x_1)$ in the system matrix $\mathbf{A}(\mathbf{x}, t)$ creates the nonlinearity. An equivalent block diagram is,

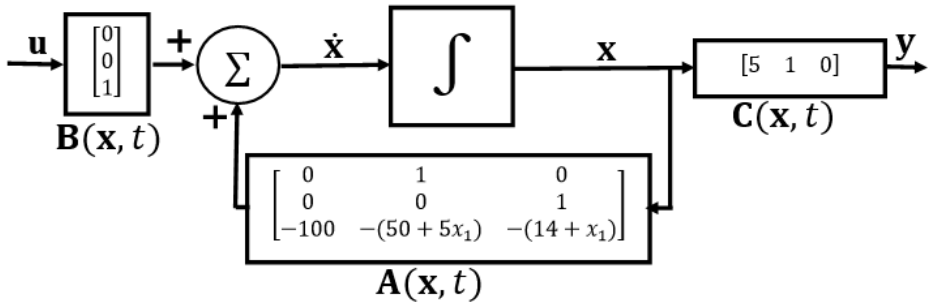

Figure 2.11. An equivalent block diagram of the nonlinear dynamic system defined by Eq. 2.34.

The dynamic characteristic equation $\mathbf{det}(g\mathbf{I} - \mathbf{A}(\mathbf{x}, t)) = 0$ is,

$$g^3 + (14 + x_1)g^2 + (50 + 5x_1)g + 100 \ = 0 \tag{2.35}$$

The roots of this dynamic characteristic equation, Eq. (2.35), are function of state x_1. Rearranging Eq. (2.35),

$$1 + \frac{x_1\, g(g+5)}{(g+10)(g+2+j2.5)(g+2-j2.5)} = 0 \tag{2.36}$$

Comparing Eq. (2.36) with (2.16), the nonlinear system has a conjugate dynamic pole located at $-2 \pm j2.5$, and a real pole located at -10 in the complex g −plane. There are two dynamic zeros located at 0 and -5, respectively. The state x_1 dependent dynamic gain $\mathrm{K}(\mathbf{x}, t) = x_1$ determines the locus of dynamic poles in the complex g −plane. A three-dimensional sketch of the dynamic root locus of the nonlinear system Eq. (2.35) varying the system state x_1 is shown in Figure 2.12. The arrowhead indicates the direction of the increased value of x_1 from zero to infinity.

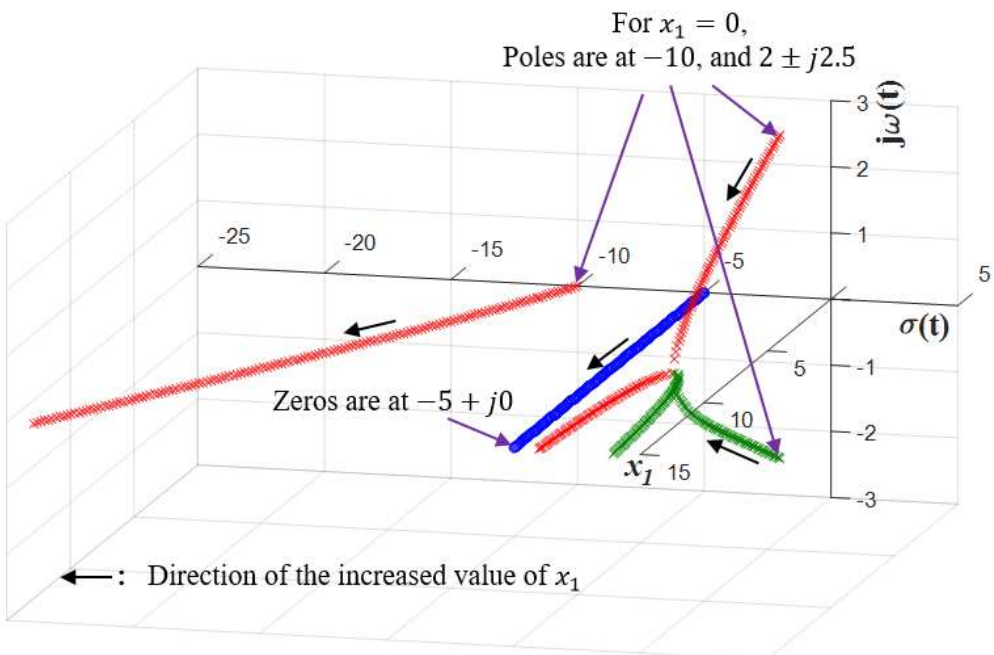

Figure 2.12. Dynamic root locus of the nonlinear system defined by Eq. 2.34 for the increased value of the system state x_1 from zero to infinity. The third axis is representing x_1.

A two-dimensional projection of the three-dimensional dynamic root locus Figure 2.12 is shown in Figure 2.13.

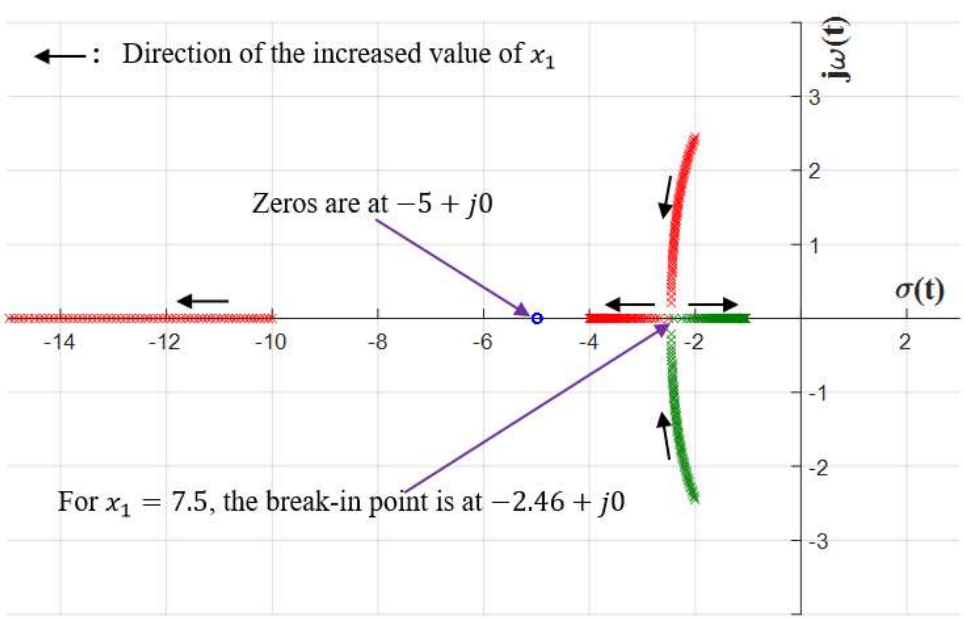

Figure 2.13. A two-dimensional projection of the three-dimensional dynamic root locus of the nonlinear system defined by Eq. 2.34. The horizontal axis is the real axis $\boldsymbol{\sigma}(\boldsymbol{t})$, the vertical axis is the imaginary axis $\boldsymbol{j\omega}(\boldsymbol{t})$, and the third axis is representing the system state x_1.

An increased value of x_1 makes both dynamics conjugate poles move towards each other creating a break-in point on the real axis at $-2.46 + j0$ for $x_1 = 7.5$, and then one pole travels towards to the origin (0,0) and another pole moves to the dynamic zero located at $-10 + j0$. The third dynamic pole moves to infinity as shown in the Figures 2.12 and 2.13.

The verification of the examples presented in this chapter are given in Appendix A.

2.5 Summary

In this chapter, a nonlinear dynamic system representation and some mathematical background in the complex g −plane were given, and it was illustrated that s −plane is a subset of g −plane. The state-space representation of a nonlinear dynamic system was introduced in Section 2.1. The state-space representation of a linear time-invariant system is a subset of general state-space representation of a nonlinear dynamic system, Eq. 2.4. Section 2.1 was used to apprise g operator and the three-dimensional complex g −plane. The definition and mathematical derivation of the g −transfer matrix, which relates the input vector $\boldsymbol{y}(\boldsymbol{t})$ to the output vector $\boldsymbol{u}(\boldsymbol{t})$, were also introduced in this section. The formation of the dynamic characteristic equation $\mathbf{det}(g\mathbf{I} - \mathbf{A}(\mathbf{x}, t)) = 0$ and the definition of dynamic poles and zeros on the complex g −plane were also discussed here. The definition and the procedure of sketching of the dynamic root locus were explained in Section 2.3.

Five numerical examples were presented at the end of the chapter to illustrate the concepts.

Chapter 3

Nonlinear Systems Stability Analysis Using the Dynamic Routh's Criterion and the Development of Dynamic Nyquist Criterion

As discussed in Chapter 2, a nonlinear dynamic system can be represented by the state and output equations [6],

$$\begin{aligned} \dot{\mathbf{x}}(t) &= \mathbf{A}(\mathbf{x},t)\mathbf{x}(t) + \mathbf{B}(t)\mathbf{u}(t), \quad \mathbf{x}(0) \\ \mathbf{y}(t) &= \mathbf{C}(\mathbf{x},t)\mathbf{x}(t) + \mathbf{D}(t)\mathbf{u}(t) \end{aligned} \tag{3.1}$$

where $\mathbf{A}(\mathbf{x},t) = \left[a_{ij}(\mathbf{x},t)\right] \in \Re^{n\times n}$ is the system matrix. $\mathbf{B}(t) \in \Re^{n\times m}$ is the input matrix where $m \leq n$. $\mathbf{C}(\mathbf{x},t) \in \Re^{l\times p}$ is the output matrix where $1 \leq l \leq p$. $\mathbf{D}(t) \in \Re^{l\times m}$ is the feed-forward matrix. The dynamic characteristic equation is [6],

$$\mathbf{det}(g\mathbf{I} - \mathbf{A}(\mathbf{x},t)) = 0 \tag{3.2}$$

where $\mathbf{I}$ is a $n \times n$ identity matrix. The elements of the matrix $\mathbf{A}(\mathbf{x},t)$ are a constant or a function of states $\mathbf{x}$ and/or time t.

The dynamic characteristic equation can also be written as [6],

$$a_n g^n + a_{n-1} g^{n-1} + \cdots + a_1 g + a_0 = 0 \tag{3.3}$$

where $a_i = a_i(\mathbf{x},t)$, $i = 0,1,2,3,\ldots,n$, is the coefficient of g^i and it is constant or a function of system states $\mathbf{x}$ and/or time t. The roots of the dynamic characteristic equation are the dynamic poles of the nonlinear dynamic system defined by Eq. (3.1).

In this chapter, a comprehensive numerical analysis of the stability analysis of a nonlinear system using the dynamic Routh's stability analysis of [6] is presented. The dynamic Routh's

stability criterion is extended for the phase plane analysis. The contributions of this chapter also lie in the relative stability analysis, as well as stability in the frequency domain with the commencement of dynamic gain and phase margin. A dynamic Nyquist stability criterion is developed in Section 3.3. The dynamic Nyquist and Bode plots are also introduced. A study of the interrelationship between the dynamic root locus and the dynamic Nyquist and Bode plots with the help of an example is also presented.

3.1 Dynamic Routh's Stability Criterion

The dynamic pole locations in the complex g −plane determine the stability of a nonlinear and/or time-variant dynamic system. At least one of these dynamic poles in the right-half side of the complex g −plane can make the system unstable by increasing the transient response monotonically or oscillating with rising amplitude with the increase of system states $\mathbf{x}$ and/or time t. On the other hand, an equilibrium condition can be achieved by keeping all the dynamic poles on the left-half side of the complex g −plane at any condition. Thus, the stability of a nonlinear and/or time-varying dynamic system can be guaranteed if and only if all the dynamic poles lie in the left-half side of the complex g −plane. The definition of stability region in the complex g −plane is shown in Figure 3.1.

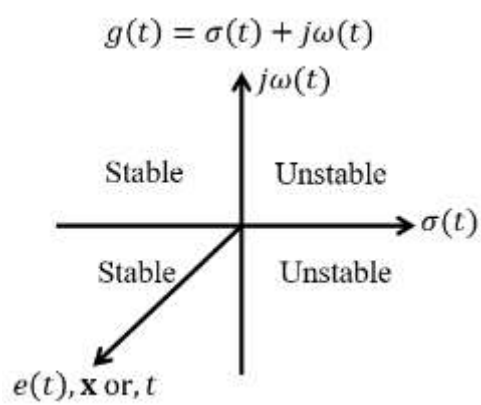

Figure 3.1: The definition of stability region in the complex g −plane, $g(t) = \sigma(t) + j\omega(t)$.

The dynamic Routh's stability criterion and the dynamic Routh's array together give us a quantitative idea about the number of dynamic poles located on the right-half side of the complex g −plane without solving any complex mathematical equations.

The dynamic Routh's array of the dynamic characteristic equation, Eq. (3.3), is shown in Table 3.1 [6]. As illustrated in Chapter 2, the coefficients of the dynamic characteristic equation contain the states $\mathbf{x}$ and/or time t dependent nonlinear terms, so it is imminent that the elements of the dynamic Routh's array also contain the states $\mathbf{x}$ and/or time t dependent nonlinear terms. Elements of the dynamic Routh's array can be a constant, a function of system states $\mathbf{x}$ and/or time t.

Table 3.1: Dynamic Routh's Array

g^n	a_n	a_{n-2}	a_{n-4}	a_{n-6}	$\cdots$
g^{n-1}	a_{n-1}	a_{n-3}	a_{n-5}	a_{n-7}	$\cdots$
g^{n-2}	$\dfrac{-\begin{vmatrix} a_n & a_{n-2} \\ a_{n-1} & a_{n-3} \end{vmatrix}}{a_{n-1}} = b_1$	$\dfrac{-\begin{vmatrix} a_n & a_{n-4} \\ a_{n-1} & a_{n-5} \end{vmatrix}}{a_{n-1}} = b_2$	$\dfrac{-\begin{vmatrix} a_n & a_{n-6} \\ a_{n-1} & a_{n-7} \end{vmatrix}}{a_{n-1}} = b_3$	$\cdots$	$\cdots$
g^{n-3}	$\dfrac{-\begin{vmatrix} a_{n-1} & a_{n-3} \\ b_1 & b_2 \end{vmatrix}}{b_1} = c_1$	$\dfrac{-\begin{vmatrix} a_{n-1} & a_{n-5} \\ b_1 & b_3 \end{vmatrix}}{b_1} = c_2$	$\cdots$	$\cdots$	$\cdots$
$\vdots$		$\vdots$			
$\vdots$		$\vdots$			
g^1		$\vdots$			
g^0		$\vdots$			

Dynamic Routh's stability criterion [6]:

(i) A nonlinear and/or time-varying dynamic system is necessarily stable if all the elements of the first column of the dynamic Routh's array have a positive non-zero value.

(ii) An oscillatory dynamic pole on the imaginary axis is present for a nonlinear and/or time-varying dynamic system if a zero is present at any rows of the first column of the dynamic Routh's array.

(iii) The number of dynamic roots of the dynamic characteristic equation located on the right-half side of the complex g −plane is equal to the number of sign changes in the first column of the dynamic Routh's array.

The stability analysis of a linear time-invariant dynamic system using the Routh's stability criterion is a subset of the stability analysis of a nonlinear and/or time-varying dynamic system having dynamic poles. The dynamic Routh's stability criterion is applicable to a linear, nonlinear, time-invariant, and time-variant dynamic systems. In other words, the dynamic Routh's stability criterion gives a complete scenario of the Routh's stability criterion.

3.2 Illustrative Numerical Examples

In the preceding sections, the stability analysis of a dynamic system based on the dynamic pole motion in the complex g −plane, dynamic Routh's stability criterion, is discussed. In this section, several examples of nonlinear dynamic systems are taken, and the dynamic Routh's stability criterion is applied to do a comprehensive numerical analysis of their stability conditions. The simulation works presented in this section are performed by using software packages: MATLAB r2016a, and SIMULINK v8.7.

Example 3.1:

Consider a nonlinear time-invariant second-order system with a nonlinear damping and a linear spring, presented by

$$\ddot{x} + (1 - x^2)\dot{x} + x = u(t) \tag{3.4}$$

Nonlinearity arises in this system because of the presence of state dependent nonlinear damping term $(1 - x^2)$. This system can be represented to a state-space model by using the following equations,

$$\begin{aligned} \dot{x_1} &= x_2 \\ \dot{x_2} &= -x_1 - (1 - {x_1}^2)x_2 + u(t) \end{aligned} \tag{3.5}$$

where x_1 and x_2 are the states of the system. The output is,

$$y = x_1 \tag{3.6}$$

Equations **(**3.5) and (3.6) can also be represented by

$$\begin{aligned} \dot{\mathbf{x}}(t) &= \mathbf{A}(\mathbf{x}, t)\mathbf{x}(t) + \mathbf{B}(t)\mathbf{u}(t) \\ \mathbf{y}(t) &= \mathbf{C}(\mathbf{x}, t)\mathbf{x}(t) \end{aligned} \tag{3.7}$$

where

$\mathbf{x} \in \Re^n$: the state vector,

$\dot{\mathbf{x}} \in \Re^n$: the derivation of the state vector $\mathbf{x}$ to time t,

$\mathbf{y} \in \Re^p$: the output vector, and

$\mathbf{u} \in \Re^m$: the control input.

System matrix $\mathbf{A}(\mathbf{x}, t) = \begin{vmatrix} 0 & 1 \\ -1 & -(1 - {x_1}^2) \end{vmatrix}$.

Input matrix $\mathbf{B}(t) = \begin{vmatrix} 0 \\ 1 \end{vmatrix}$.

Output matrix $\mathbf{C}(\mathbf{x}, t) = |1 \quad 0|$.

The dynamic characteristic equation is defined as $\mathbf{det}(g\mathbf{I} - \mathbf{A}(\mathbf{x}, t)) = 0$, and given by

$$g^2 + (1 - {x_1}^2)g + 1 = 0 \tag{3.8}$$

where g is a differential operator, $\frac{d}{dt}$. The dynamic Routh's array of this dynamic characteristic equation is,

$$\begin{array}{c|cc} g^2 & 1 & 1 \\ g^1 & (1-{x_1}^2) & 0 \\ g^0 & 1 & 0 \end{array} \tag{3.9}$$

Investigating this dynamic Routh's array Eq. (3.9) we can summarize some important conclusions:

(i) As we know from the dynamic Routh's stability criterion that a nonlinear and/or time-variant system is necessarily stable if all the elements of the first column of the dynamic Routh's array have positive non-zero values. Thus, the nonlinear dynamic system Eq. (3.4) is stable if and only if $(1-{x_1}^2) > 0$, where x_1 is system state. This is shown graphically in Figure 3.2. The horizontal axis represents the time t dependent system state x_1, and the vertical axis represents $(1-{x_1}^2)$. In other words, the nonlinear time-invariant dynamic system Eq. (3.4) is stable for the values of x_1 where $|x_1| < 1$.

(ii) According to dynamic Routh's stability criterion, there exist an oscillatory dynamic pole on the imaginary axis of the complex g −plane of a nonlinear and/or time-variant dynamic system if a zero is present at any rows of the first column of the dynamic Routh's array. Examining the first column of the dynamic Routh's array Eq. (3.9), a zero is present if and only if $(1-{x_1}^2) = 0$ or $|x_1| = 1$. If $|x_1| = 1$, then the dynamic characteristic equation becomes $g^2 + 1 = 0$ and system has a conjugate imaginary pole located at $g = \pm j$.

(iii) The dynamic Routh's stability criterion states that the number of dynamic roots of the dynamic characteristic equation located in the right-half side of the complex g −plane is equal to the number of sign changes in the first column of the dynamic

Routh's array. For example, if $(1 - x_1{}^2) < 0$ or $|x_1| > 1$, then there are two sign changes of the elements of the first column of the dynamic Routh's array. So, for $|x_1| > 1$, there are two dynamic poles located in the right-half side of the complex g −plane. On the other hand, if $(1 - x_1{}^2) > 0$ or, $|x_1| < 1$, there is no sign changes on the first column of the dynamic Routh's array, i.e., no dynamic poles are located in the right-half side of the complex g −plane.

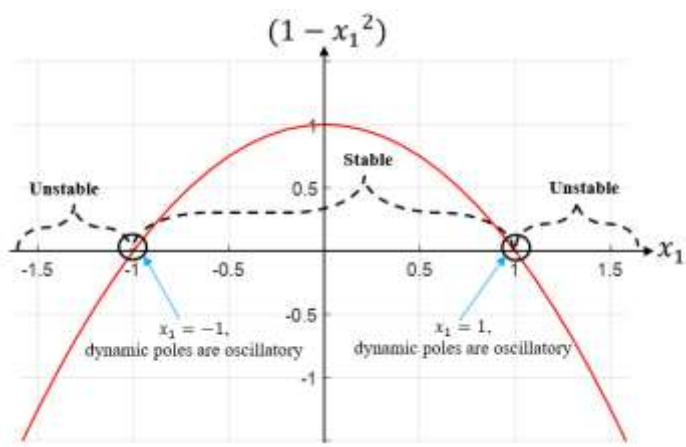

Figure 3.2. Graphical representation of the stability region of the dynamic characteristic equation, $g^2 + (1 - x_1{}^2)g + 1 = 0$.

It is clear that the dynamic roots of the dynamic characteristic equation, Eq. (3.9), are not static because of the state x_1 dependent nonlinear term $(1 - x_1{}^2)$. The dynamic root locus can be drawn by placing through every point in the complex g −plane to locate the dynamic roots of the system as states x_1 is varied from zero to infinity. Figure 3.3 shows the dynamic root locus in the complex g −plane of the nonlinear system Eq. (3.4). The horizontal axis defines the real part of the complex dynamic poles, and the vertical axis indicates the imaginary part. The location of the dynamic poles changes explicitly with the change of system state x_1 while implicitly with time t. Initially when $|x_1| < 1$, the system has a conjugate dynamic pole located in the left-half side of the complex g −plane and with the increase of system state x_1 both dynamic poles shifted towards the imaginary axis as indicated by a dotted arrowhead in Figure 3.3. When $|x_1| = 0$, both dynamic poles are located on the imaginary axis showing a sinusoidal natural

response with a frequency equal to the location of the imaginary axis, $\pm j$. For the values of $|x_1| > 1$, both conjugate dynamic poles move to the right-half side of the complex g −plane causing an amplification of system motion with the increase of time, i.e., instability region.

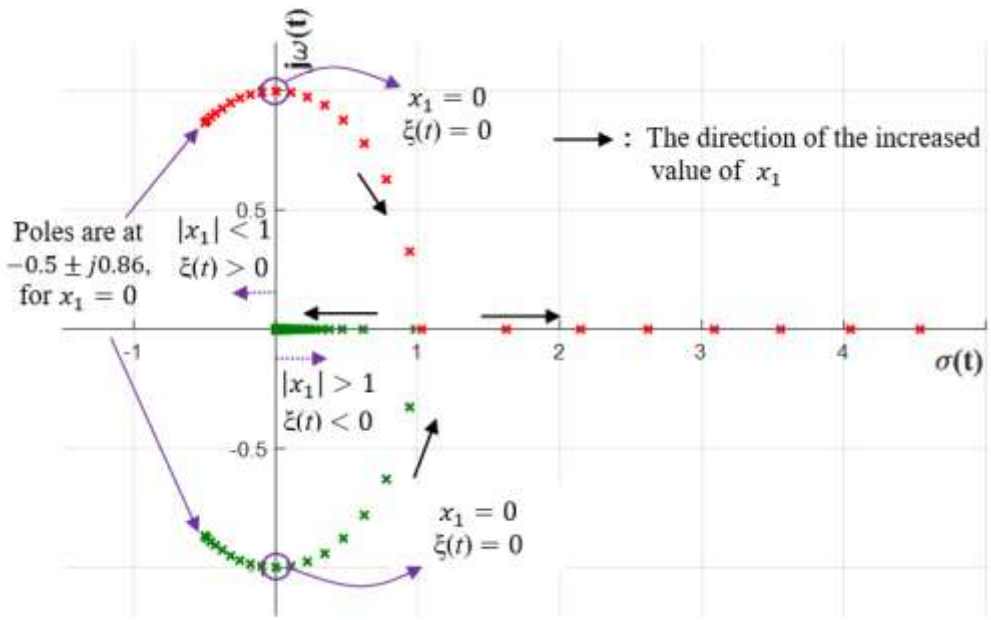

Figure 3.3. Dynamic root locus of the characteristic equation, $g^2 + (1 - {x_1}^2)g + 1 = 0$. The horizontal axis is the real axis, the vertical axis is the imaginary axis, and the third axis is representing system state x_1.

A comparison between the nonlinear time-invariant second-order dynamic system Eq. (3.4) with the general transfer function of a second-order differential equation $y(t) = \frac{\omega_n^2 u(t)}{g^2 + 2\xi\omega_n g + \omega_n^2}$ leads us to an inverse relationship between system states x_1 and the damping ratio $\xi(t)$, and it is given by the Eq. (3.10). The graphical representation is shown in Figure 3.4.

$$\begin{aligned} \xi(t) &= \frac{(1 - {x_1}^2)}{2} \\ \omega_n(t) &= 1 \end{aligned} \tag{3.10}$$

where $\omega_n(t)$ is the time and state-dependent dynamic natural frequency.

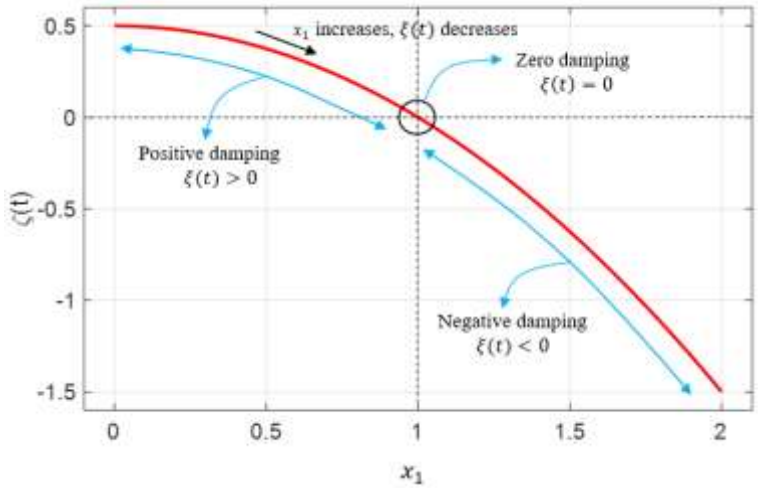

Figure 3.4. An inverse relation between system state x_1 and the dynamic damping ratio $\xi(t)$ of the nonlinear system, $\ddot{x} + (1 - x^2)\dot{x} + x = u(t)$.

As mentioned in Chapter 3, because of the presence of a nonlinear relationship between the damping ratio $\xi(t)$ and time t dependent system state x_1, a time t dependent variation on damping ratio $\xi(t)$ is observed. This changing nature of system damping ratio $\xi(t)$ with time t is called dynamic damping ratio. Starting from a zero initial condition, as system state x_1 increases to a value of 2 with the increase of time t, dynamic damping ratio $\xi(t)$ decreases from an initial value of 0.5 to a value of -1.5. When $x_1 < 1$, the system has positive damping (i.e., $\xi(t) > 0$, dynamic conjugate poles are located in the left-half side of the complex g −plane) and energy is dissipated from the system resulting in a decaying motion. On the other hand, if $x_1 > 1$, negative damping (i.e., $\xi(t) < 0$, the dynamic conjugate poles are located in the right-half side of the complex g −plane) happens, i.e., adding energy to the system resulting in an amplification of the motion. The moment $x_1 = 0$ is called a zero damping situation (i.e., $\xi(t) = 0$, both dynamic conjugate poles are located on the $j\omega$ axis of the complex g −plane) resulting in an oscillatory motion. The dynamic damping ratio $\xi(t)$ for various pole locations in the complex g −plane is shown in Figure 3.3.

Some exciting but powerful features can be explained in here. As discussed before, system dynamics changes with the increase or decrease of the system state x_1 and system state x_1 is implicitly time t dependent; thus the nonlinear system Eq. (3.4) shows a state x_1 and time t dependent frequency response. The dynamic Bode plot is a state x_1 and time t dependent

frequency response plot. It is a three-dimensional frequency response plot. The horizontal axis represents the change of frequency in a logarithmic scale, and the vertical axis represents the magnitude (in dB) and the phase (in degree). Another axis represents the change of time t or system states **x** of the nonlinear system. Figure 3.5 shows the dynamic Bode plot of the nonlinear dynamic system Eq. (3.4).

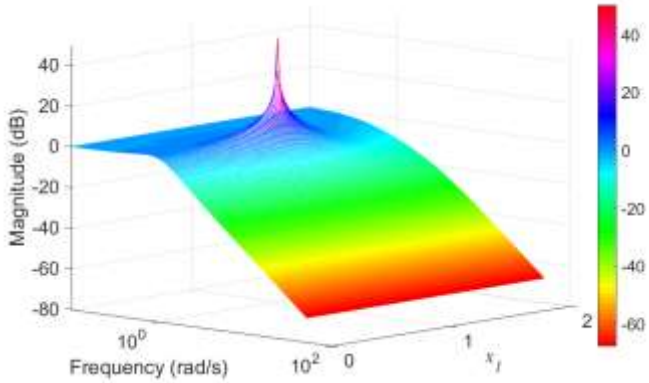

(a) Three-dimensional magnitude frequency response plot.

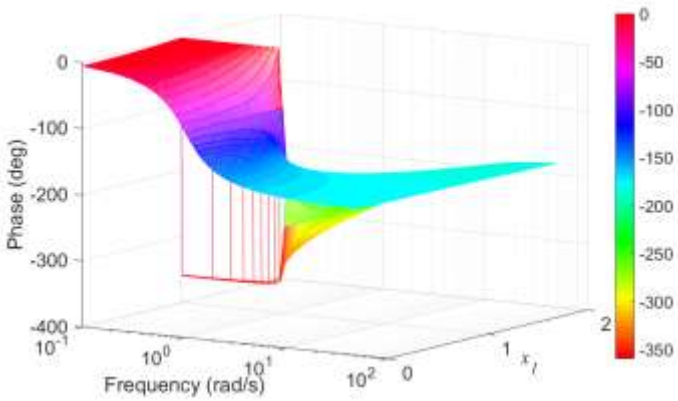

(b) Three-dimensional phase frequency response plot.

Figure 3.5. Dynamic Bode plot, a three-dimensional Bode plot of the second-order nonlinear system $\ddot{x} + (1 - x^2)\dot{x} + x = u(t)$. The third axis represents the system state x_1.

A two-dimensional sketch of the three-dimensional magnitude and phase frequency response plot of the nonlinear system Eq. (3.4) for the various values of the system state x_1 and the associated dynamic damping ratio $\xi(t)$ is shown in Figure 3.6.

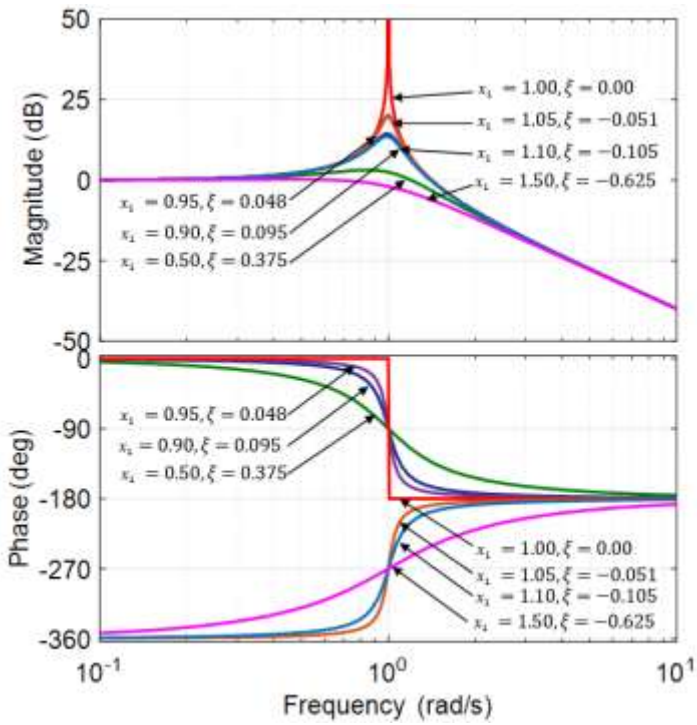

Figure 3.6. Magnitude and phase frequency response of the nonlinear system, $\ddot{x} + (1 - x^2)\dot{x} + x = u(t)$ for the various values of the system state x_1.

For a second order system, the peak resonance and the bandwidth are related to the damping ratio of the system [27]. As said before, the nonlinearity arises in the system because of the presence of the nonlinear damping term $(1 - {x_1}^2)$. As system state x_1 varies with time t, damping ratio also changes according to Eq. (3.10). It is seen from Figures 3.5 and 3.6 that lower the damping ratio higher the peak resonance and vice versa. The resonance happens at the frequency equal to 1 rad/s. From the phase frequency response plot, the damping ratio becomes smaller; and the phase curve becomes steeper. Investigating Figure 3.6, we see that for the values $x_1 < 1$, system Bode plot starts from 0^0 and never reaches to -180^0, and when $x_1 > 1$, the system has a Bode plot always lower than -180^0.

As a large peak resonance correspondence to a large peak overshoot in the response, a system may be stable at low frequency and high frequency, but unstable near the resonant frequency. As mentioned earlier, the input is a function of both amplitude and frequency, and thus, the stability of a nonlinear system depends on the amplitude and frequency of the input signal as well.

The stability of the nonlinear time-invariant dynamic system in the frequency domain is defined by developing a dynamic Nyquist stability criterion. A detailed treatment is given in Section 3.3.

Example 3.2:

Consider another nonlinear time-invariant second-order system with a nonlinear damping $\frac{(x^2-1)}{2}$ and single input $u(t)$,

$$\ddot{x} + (x^2 - 1)\dot{x} + x = u(t) \tag{3.11}$$

The state-space model of this nonlinear dynamic system can be represented by

$$\begin{aligned} \dot{x_1} &= x_2 \\ \dot{x_2} &= -x_1 - ({x_1}^2 - 1)x_2 + u(t) \end{aligned} \tag{3.12}$$

where x_1 and x_2 are representing the states of the system. The output y is,

$$y = x_1 \tag{3.13}$$

The vector-matrix form of the state-space model Eq. (3.12) and (3.13) is,

$$\begin{aligned} \dot{\mathbf{x}}(t) &= \mathbf{A}(\mathbf{x}, t)\mathbf{x}(t) + \mathbf{B}(t)\mathbf{u}(t) \\ \mathbf{y}(t) &= \mathbf{C}(\mathbf{x}, t)\mathbf{x}(t) \end{aligned} \tag{3.14}$$

where

$\mathbf{x} \in \Re^n$: the state vector,

$\dot{\mathbf{x}} \in \Re^n$: the derivation of the state vector $\mathbf{x}$ to time t,

$\mathbf{y} \in \Re^p$: the output vector, and

$\mathbf{u} \in \Re^m$: the control input.

System matrix $\mathbf{A}(\mathbf{x}, t) = \begin{vmatrix} 0 & 1 \\ -1 & -({x_1}^2 - 1) \end{vmatrix}$.

Input matrix $\mathbf{B}(t) = \begin{vmatrix} 0 \\ 1 \end{vmatrix}$.

Output matrix $\mathbf{C}(\mathbf{x}, t) = |1 \quad 0|$.

The dynamic characteristic equation $\mathbf{det}\big(g\mathbf{I} - \mathbf{A}(\mathbf{x}, t)\big) = 0$ of the nonlinear system defined by Eq. (3.14) is given by

$$g^2 + ({x_1}^2 - 1)g + 1 = 0 \tag{3.15}$$

where g is a differential operator, $\frac{d}{dt}$. The dynamic Routh's array of this dynamic characteristic equation, Eq. (3.15), is,

$$\begin{array}{c|cc} g^2 & 1 & 1 \\ g^1 & ({x_1}^2 - 1) & 0 \\ g^0 & 1 & 0 \end{array} \tag{3.16}$$

Applying the dynamic Routh's stability criterion to this dynamic Routh's array Eq. (3.16) we can define the stability of the nonlinear dynamic system Eq. (3.11) as,

(i) The nonlinear time-invariant dynamic system Eq. (3.11) is stable if and only if $({x_1}^2 - 1) > 0$, where x_1 represents system state. Graphical presentation of the stability region is shown in Figure 3.7. The horizontal axis represents the time t dependent system states x_1, and the vertical axis represents $({x_1}^2 - 1)$. The nonlinear dynamic

system represented by Eq. (3.11) is stable for the values of x_1, where $|x_1| > 1$, i.e., $-1 > x_1 > 1$.

(ii) A zero is present in the second row of the first column of the dynamic Routh's array Eq. (3.16) if and only if $({x_1}^2 - 1) = 0$ or, $|x_1| = 1$. If $|x_1| = 1$, then the dynamic characteristic equation, Eq. (3.15), becomes $g^2 + 1 = 0$ and the conjugate imaginary poles are located at $g = \pm j$.

(iv) If $({x_1}^2 - 1) < 0$ or $|x_1| < 1$ then there are two sign changes in the elements of the first column of the dynamic Routh's array Eq. (3.16), i.e., if $|x_1| < 1$ both conjugate dynamic poles located in the right-half side of the complex g −plane. Besides, there are no sign changes on the first column of the dynamic Routh's array if $({x_1}^2 - 1) > 0$. In other words, there are no dynamic poles located in the right-half side of the complex g −plane for $|x_1| > 1$.

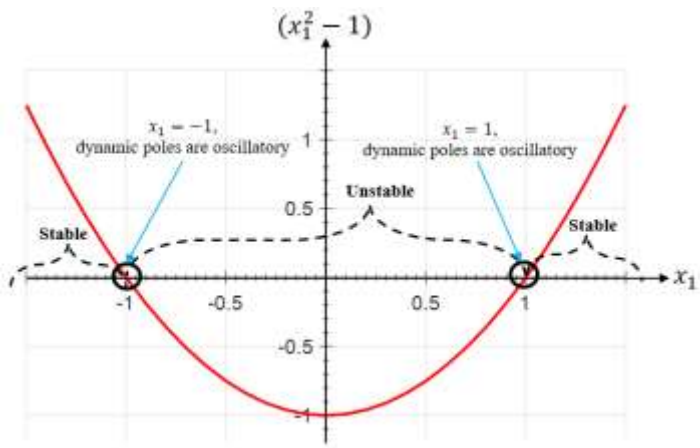

Figure 3.7. Graphical representation of the stability region of the dynamic characteristic equation, $g^2 + ({x_1}^2 - 1)g + 1 = 0$.

Figure 3.8 shows the dynamic root locus of the nonlinear system Eq. (3.12). If $|x_1| < 1$, the system has a conjugate dynamic pole located on the right-half side of the complex g −plane, i.e., in the unstable region. In other words, the system starts with a negative dynamic damping

ratio $\xi(t) < 0$ and the negative damping will pump energy to the system resulting in an amplification of the motion. With the rise of time t and system state x_1 these conjugate dynamic poles will shift towards the imaginary axis. When $|x_1| = 0$, both dynamic poles are located on the imaginary axis and the system dynamic damping ratio $\xi(t) = 0$. For the values of $|x_1| > 1$, the conjugate dynamic poles move to the left-half side of the complex g −plane, i.e., stable region. The dynamic damping ratio becomes positive in sign, i.e., $\xi(t) > 0$ and energy is absorbed from the system resulting in a decreasing motion.

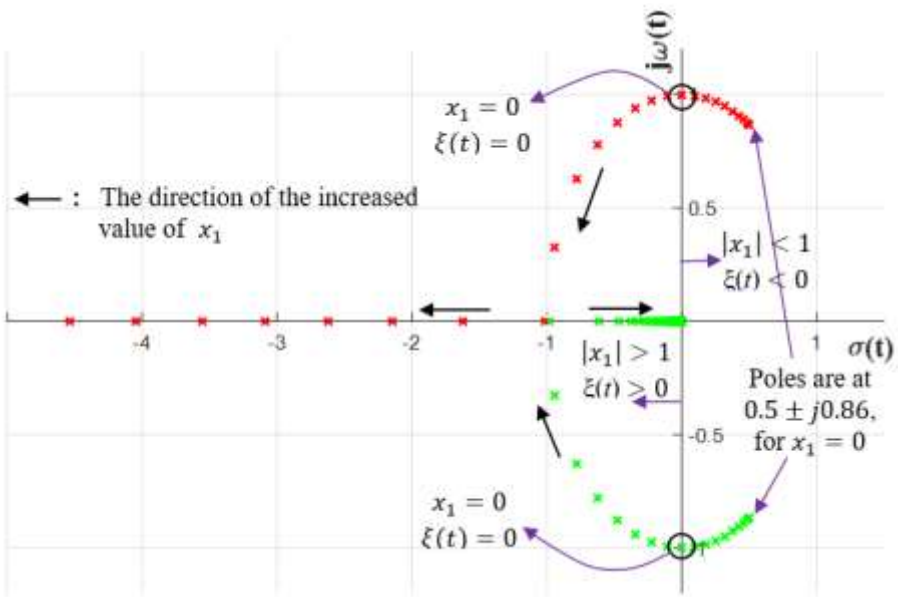

Figure 3.8. Dynamic root locus of the dynamic characteristic equation, $g^2 + ({x_1}^2 - 1)g + 1 = 0$. The third axis is representing the system state x_1.

Figure 3.9 shows a three-dimensional dynamic Bode plot of the nonlinear system, Eq. (3.11), graphically. Figure 3.10 gives a two-dimensional sketch of the magnitude and phase frequency response plot of the same nonlinear system expressed for the various values of the system state x_1. For the values of $x_1 < 1$, the phase frequency response plot starts from -360^0 and never reaches to -180^0, and for $x_1 > 1$, the system has a phase frequency response always higher than -180^0.

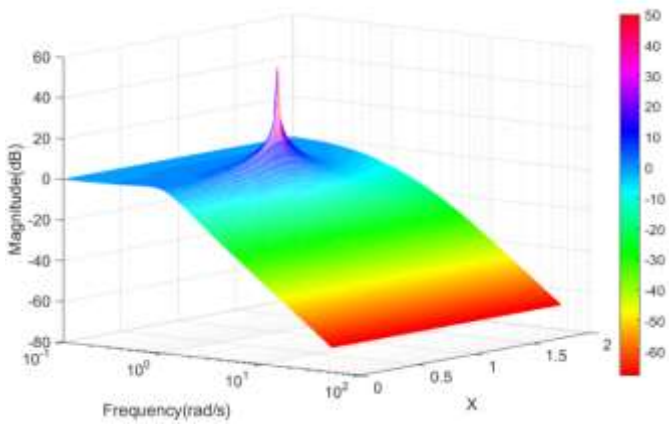

(a) Three-dimensional magnitude frequency response plot.

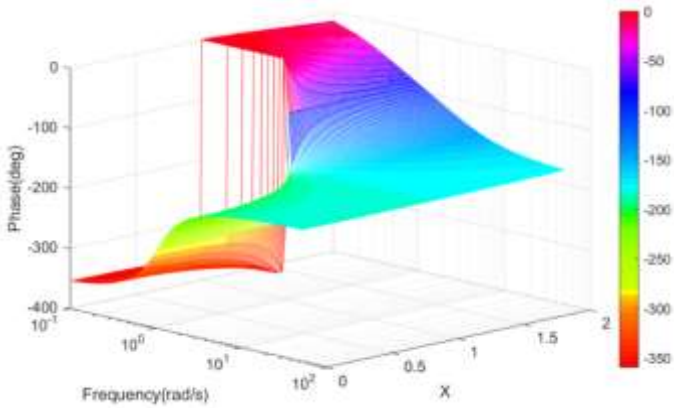

(b) Three-dimensional phase frequency response plot.

Figure 3.9. Dynamic Bode plot, a three-dimensional bode plot of the nonlinear system $\ddot{x} + (x^2 - 1)\dot{x} + x = u(t)$. The third axis represents the system state x_1.

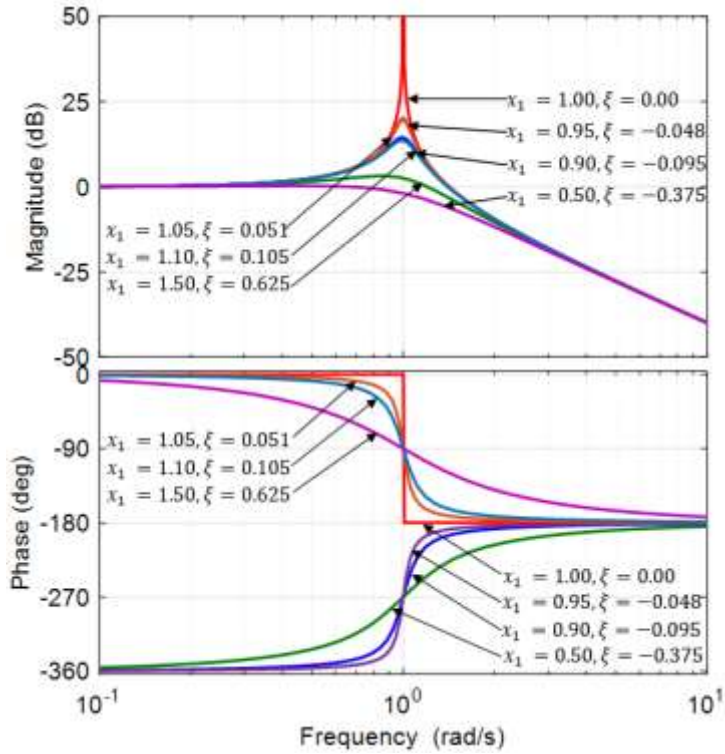

Figure 3.10. Magnitude and phase frequency response of the nonlinear system $\ddot{x} + (x^2 - 1)\dot{x} + x = u(t)$ for the various values of the system state x_1.

From the state-space model of the nonlinear system Eq. (3.12), it can be shown that nonlinear system Eq. (3.11) has only one equilibrium point located at the origin $(0,0)$. From Eq. (3.16), it is clear that the boundary condition for the stability of the same system is $-1 > x_1 > 1$. The phase portrait analysis is a graphical method of studying second-order system dynamics [2]. It is divided into four quadrants, and each axis represents each state of the dynamic system. The horizontal axis represents the position x_1, and the vertical axis represents the velocity x_2 (where $x_2 = \dot{x_1}$). $-1 > x_1 > 1$ is the stability boundary of the nonlinear dynamic system Eq. (3.11), identified by using the dynamic Routh's stability criterion, divides each of these four quadrants into two parts: stable and unstable region, as shown in the Figure 3.11(a). Phase portrait of the system is drawn for initial condition $(0.5,1)$ is shown in Figure 3.11(b).

As we mentioned in our earlier discussion, because of the state and time-dependent nonlinear damping term $({x_1}^2 - 1)$, the nonlinear system Eq. (3.11) exhibits time and state-

dependent damping ratio $\xi(t) = \frac{{x_1}^2-1}{2}$. Natural frequency $\omega_n = 1$. This dynamic nature of damping ratio demonstrates a negative damping for $|x_1| < 1$ ($\xi(t) < 0$, i.e., dissipation of energy from the system resulting in a decaying motion), a zero damping for $|x_1| = 1$ ($\xi(t) = 0$, i.e., neither adding nor dissipation of energy), and a positive damping for $|x_1| > 1$ ($\xi(t) > 0$, i.e., energy is added to the system resulting in an amplification of motion). Thus, a perpetuation of periodic oscillation is expected at the steady-state motion of the system, creating a limit cycle to the phase portrait.

Using the dynamic Routh's stability criterion, it can also be shown that on the 1st quadrant ($x_1: +ve, x_2: +ve$) of the phase portrait Fig 3.11(a), stability is defined by the region where $\dot{x_2}: -ve$ and $\dot{x_2}: +ve$ define the unstable region on the 1st quadrant. Similarly $\dot{x_2}: +ve$ and $\dot{x_2}: -ve$ define the stable and unstable region respectively in the 3rd quadrant ($x_1: -ve, x_2: -ve$) of the phase portrait. In the 4th quadrant ($x_1: +ve, x_2: -ve$), a $+ve$ value of $\dot{x_2}$ shifts the system dynamics to the 1st quadrant and a $-ve$ value of $\dot{x_2}$ shifts the system dynamics to the 3rd quadrant. On the other hand, in the 2nd quadrant ($x_1: -ve, x_2: +ve$) a $+ve$ values of $\dot{x_2}$ shifts the system dynamics to the 1st quadrant and a $-ve$ values of $\dot{x_2}$ shifts the system dynamics to the 3rd quadrant. The value of $\dot{x_2}$ is calculated by using the state-space equations, Eq. (3.12), for various values of system states x_1 and x_2.

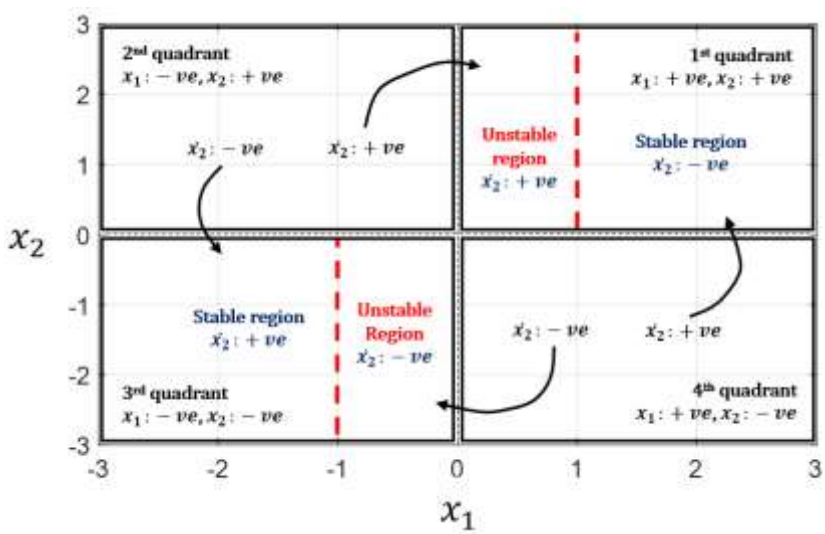

(a) Graphical representation of the stability region on the phase plane.

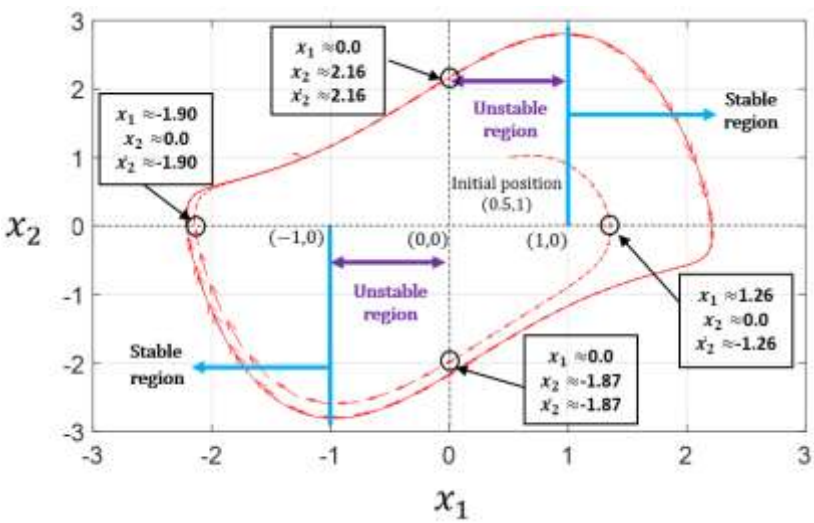

(b) Phase portrait of the system, $\ddot{x} + (x^2 - 1)\dot{x} + x = 0$ for an initial condition $(0.5,1)$.

Figure 3.11. The phase portrait of the nonlinear time-variant dynamic system,

$$\ddot{x} + (x^2 - 1)\dot{x} + x = 0.$$

Figure 3.11(b) exposes the phase portrait plot of the nonlinear dynamic system Eq. (3.11). At the beginning of time and with the initial condition $(x_1, x_2) = (0.5,1)$, the system dynamics is located on the unstable region of the 1st quadrant (Figure 3.11(b)). $\dot{x}_2$ is $+ve$ in this unstable region, and it causes to rise system position x_1 and velocity x_2, simultaneously. This increasing values of x_1 and x_2 take the system dynamics to the stable region of the 1st quadrant where $x_1 > 1$. Acceleration, $\dot{x}_2$ is $-ve$ in this stable region, and eventually, it induces x_2 to decay but x_1 to increase. System dynamics cross the horizontal axis at the point $(x_1, x_2) \approx (1.26,0.0)$ with a $-ve$ acceleration, $\dot{x}_2 \approx$-1.26. A $-ve$ acceleration in the 4th quadrant constrain to shift the system dynamics to the unstable region of the 3rd quadrant. However, a $-ve$ acceleration in the 3rd quadrant make the dynamic system unstable with a declining x_1 and x_2, synchronously. When position x_1 becomes less than -1, i.e., $x_1 < -1$, at that moment $\dot{x}_2$ becomes $+ve$ and system dynamics enter to the stable region of the 3rd quadrant, i.e., induce x_2 to rise but x_1 to decrease. Eventually, system dynamics cross the horizontal axis from the 3rd quadrant to enter 2nd quadrant at $(x_1, x_2) \approx (-1.90,0.0)$ with $\dot{x}_2 \approx$-1.90. This $-ve$ value of $\dot{x}_2$ in the 2nd quadrant retake the dynamics in the unstable region of the 1st quadrant. This process continues creating a steady state sustained periodic oscillations called a limit cycle. The

amplitude and frequency of a limit cycle depend on the position feedback $K_p(e,t)$ and velocity feedback $K_v(e,t)$ of the dynamic system. For various initial conditions with each position feedback $K_p(e,t)$ and velocity feedback $K_v(e,t)$, there exists only one unique limit on the phase portrait.

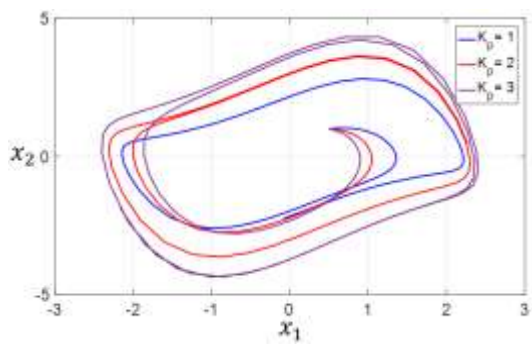

(a) Phase portrait for various values of K_p. $K_p = 1, K_p = 2, K_p = 3$.

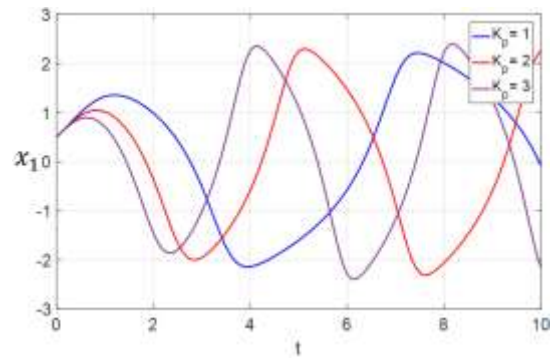

(b) Time response for various values of K_p. $K_p = 1, K_p = 2, K_p = 3$.

Figure 3.12. Effect of changing the values of K_p of the oscillatory dynamic system $\ddot{x} + (x^2 - \alpha)\dot{x} + K_p x = 0$ with an initial condition $(x_1, x_2) = (0.5,1)$. α is kept constant $\alpha = 1$.

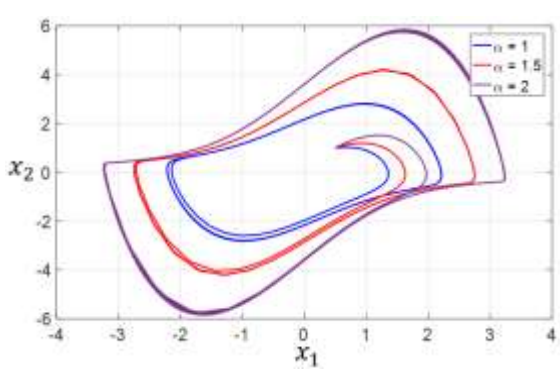

(a) Phase portrait for various values of . $\alpha = 1, \alpha = 1.5, \alpha = 2$.

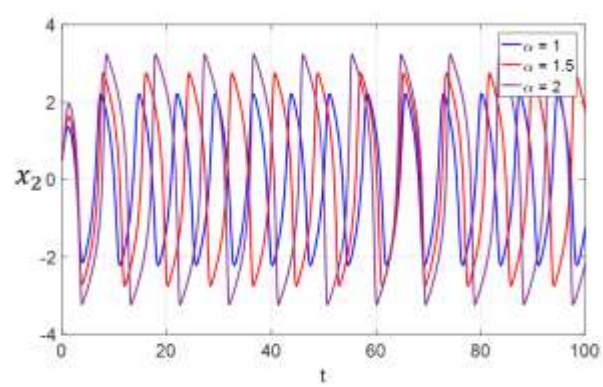

(b) Time response for various values of α. $\alpha = 1, \alpha = 1.5, \alpha = 2$.

Figure 3.13. Effect of changing the values of α of the oscillatory dynamic system $\ddot{x} + (x^2 - \alpha)\dot{x} + K_p x = 0$ with an initial condition $(x_1, x_2) = (0.5,1)$.

K_p is kept constant, $K_p = 1$.

From the above interpretation of the phase portrait of the nonlinear system Eq. (3.11) applying the dynamic Routh's stability criterion, it is interesting to note that this nonlinear differential system can be designed as an oscillator of various amplitude and frequency by comprehending a variable position and variable velocity feedback parameters K_p and α, respectively. For example, the overall system dynamics of an oscillator is given by

$$\ddot{x} + (x^2 - \alpha)\dot{x} + K_p x = 0 \tag{3.17}$$

where K_p and α both are positive numbers, and they control the frequency and the amplitude of oscillation, respectively. Figure 3.12 and 3.13 illustrate the effect of changing K_p and α with an initial condition $(x_1, x_2) = (0.5,1)$. According to dynamic Routh's stability criterion, K_p does not affect the stability of this particular example. The stability only depends on the value of α. For example, the stability of the nonlinear dynamic system Eq. (3.17) is guaranteed for various values of variable velocity feedback parameters $\alpha = 1$, $\alpha = 1.5$, and $\alpha = 2$ if and only if $|x_1| > 1$, $|x_1| > \sqrt{1.5}$, and $|x_1| > \sqrt{2}$, respectively.

Example 3.3:

Consider a second-order nonlinear system with a nonlinear spring,

$$\ddot{x} + 0.6\dot{x} + (3 + x)x = 0 \tag{3.18}$$

The state-space model of this nonlinear dynamic system is,

$$\begin{aligned} \dot{x_1} &= x_2 \\ \dot{x_2} &= -(3 + x_1) - 0.6x_2 \end{aligned} \tag{3.19}$$

where x_1 and x_2 are states of the dynamic system. The system matrix $\mathbf{A}(\mathbf{x}, t)$ of this state-space model is given by

$$A = \begin{bmatrix} 0 & 1 \\ -(3 + x_1) & -0.6 \end{bmatrix} \tag{3.20}$$

The dynamic characteristic equation $\mathbf{del}(g\mathbf{I} - \mathbf{A}(\mathbf{x}, t)) = 0$ of the Eq. (3.18) is,

$$g^2 + 0.6g + (3 + x_1) = 0 \tag{3.21}$$

where g is a differential operator, $\frac{d}{dt}$. The dynamic Routh's array of the dynamic characteristic equation, Eq. (3.21), is,

$$\begin{array}{c|cc} g^2 & 1 & (3 + x_1) \\ g^1 & 0.6 & 0 \\ g^0 & (3 + x_1) & 0 \end{array} \tag{3.22}$$

Applying the dynamic Routh's stability criterion to this dynamic Routh's array, we can finalize some conclusive deduction. For $x_1 < -3$, the second-order nonlinear system Eq. (3.18) has one of its conjugate dynamic poles located on the right-hand side of the complex g −plane and another is located on the left-hand side. With the increased value of the system state x_1, both dynamic poles move towards each other. When $x_1 = -3$, one of the dynamic pole is located on the origin $(0,0)$. Both conjugate poles are located on the left-hand side of the complex g −plane if $x_1 > -3$. If the system state x_1 is increased still further, then both dynamic poles keep traveling to infinity after creating a breakaway point at $(-0.3,0)$. Figure 3.14 shows a three-dimensional plot of the dynamic root locus in the complex g −plane varying the system states x_1. A two-dimensional graphical representation of the same plot is shown in Figure 3.15. The third axis represents the system state x_1.

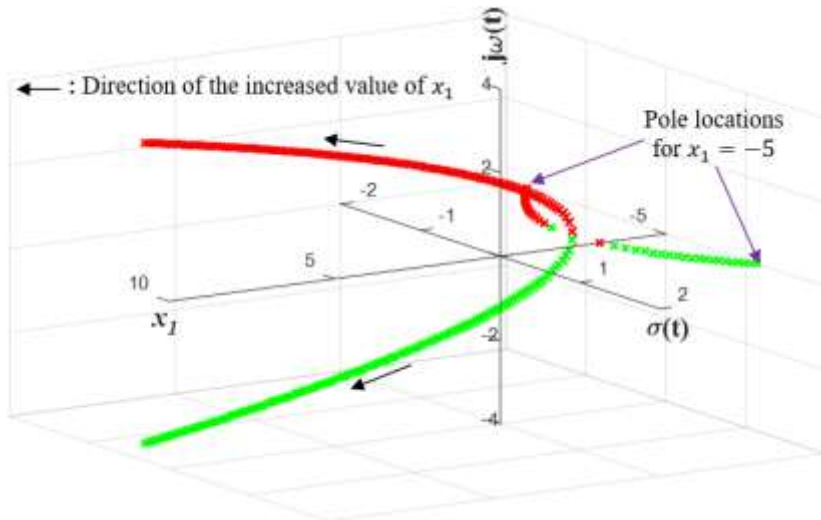

Figure 3.14. A three-dimensional sketch of the dynamic root locus of the characteristic equation $g^2 + 0.6g + (3 + x_1) = 0$. The third axis represents the system state x_1. The left-half side (LHS) is a stable region, and the right-half side (RHS) is an unstable region.

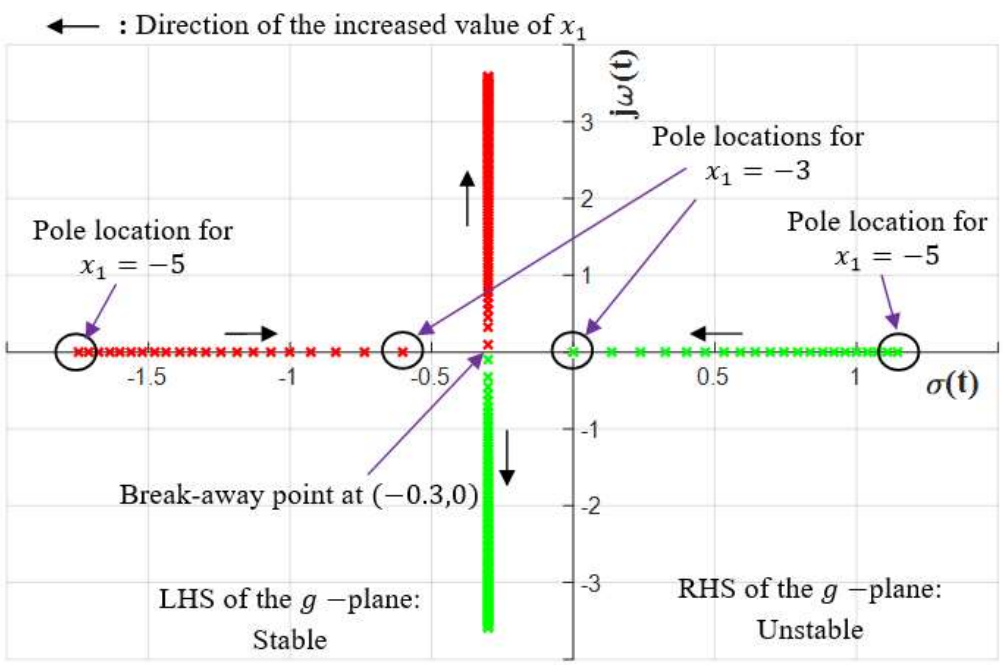

Figure 3.15. A two-dimensional projection of the three-dimensional dynamic root locus of the characteristic equation, $g^2 + 0.6g + (3 + x_1) = 0$. The horizontal axis is the real axis, the

vertical axis is the imaginary axis, and the third axis represents system state x_1. The left-half side (LHS) is the stable region, and the right-half side (RHS) is an unstable region.

Example 3.4:

Sometimes more than one parameter may affect the behavior of the dynamic poles in the design problems [5]. The dynamic root locus technique can also investigate such realism. If more than one parameter (one at a time keeping other parameters constant) is varied from a zero to infinity, respectively, the corresponding dynamic root locus is called dynamic root contour.

Consider the state-space representation of a second-order nonlinear system,

$$\dot{x_1} = \mu x_1^2 x_2 - x_2 \sin x_1$$
$$\dot{x_2} = -x_1 - \mu x_1^2 x_2 + x_2 \tag{3.23}$$

and the output is,

$$y = x_1$$

where x_1 and x_2 are system states and μ is a positively valued gain parameter.

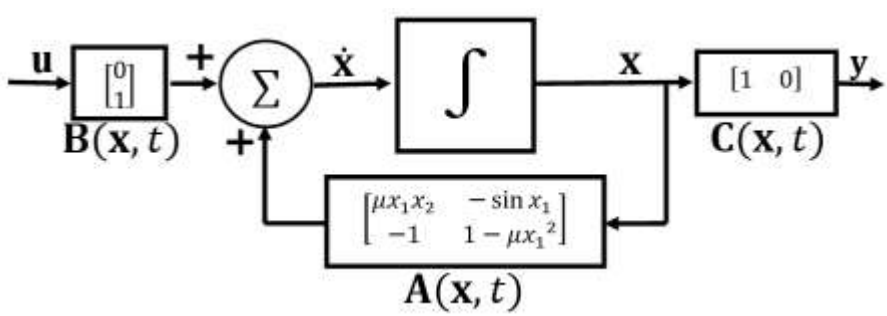

Figure 3.16. The block diagram representation of the second-order nonlinear system, $\dot{x_1} = \mu x_1^2 x_2 - x_2 sin x_1$, $\dot{x_2} = -x_1 - \mu x_1^2 x_2 + x_2$.

The block diagram illustration of the nonlinear dynamic system Eq. (3.23) is shown in Figure 3.16. The system characteristics are involved to two variable parameters, the system state x_1, and the gain parameter μ. For some known values of μ, the effects on the dynamic poles can

be studied from the dynamic characteristic equation of the system. The dynamic characteristic equation, $\mathbf{det}(g\mathbf{I} - \mathbf{A}(\mathbf{x}, t)) = 0$, is given by

$$g^2 + (\mu x_1^2 - 1)g + (\mu x_1^2 - sinx_1) = 0 \tag{3.24}$$

where g is a differential operator, $\frac{d}{dt}$. The dynamic Routh's array is,

$$\begin{array}{c|cc} g^2 & 1 & \mu x_1^2 - sinx_1 \\ g^1 & \mu x_1^2 - 1 & 0 \\ g^0 & \mu x_1^2 - sinx_1 & 0 \end{array} \tag{3.25}$$

Applying the dynamic Routh's stability criterion and from the first column of the dynamic Routh's array, we can conclude that the nonlinear second-order system Eq. (3.23) is stable, if $\mu x_1^2 - sinx_1$ and $\mu x_1^2 - 1$, both are positive definite at any condition. However, since $sinx_1 \leq 1$, so the stability is guaranteed if and only if $\mu x_1^2 > 1$. A similar result of stability requirement can be achieved from a dynamic root contour plot of the same nonlinear system.

The roots of the dynamic characteristic equation, Eq. (3.24), is,

$$g_{1,2} = -\frac{\mu x_1^2 - 1}{2} \pm \frac{1}{2}\sqrt{(\mu^2 x_1^4 + 4\sin x_1 + 1) - 6\mu x_1^2} \tag{3.26}$$

The location of the dynamic conjugate poles $g_{1,2}$ is on either the right-hand side or left-hand side of the complex g −plane depending on the real part of Eq. (3.26), $-\frac{\mu x_1^2 - 1}{2}$. If $\mu x_1^2 - 1$ is $-ve$, then both dynamic conjugate poles are located on the right-hand side of the complex g −plane, i.e., unstable region. On the other hand, if $\mu x_1^2 - 1$ is $+ve$ then both dynamic conjugate poles are on the left-hand side of the complex g −plane and system is stable. Both dynamic conjugate poles are located on the imaginary axis if $\mu x_1^2 - 1 = 0$.

The dynamic root contour of the nonlinear dynamic system Eq. (3.23) can be constructed from the dynamic characteristic equation, Eq. (3.24), by following the general procedure for creating dynamic root locus; varying x_1 and μ, respectively, from a zero to infinity. One of the parameters, e.g., μ is kept in constant value at a time and another parameter, e.g., x_1 is varied from a zero to infinity, and dynamic root locus is sketched. Next, the value of the first parameter, i.e., μ is varied while another parameter, i.e., x_1 is kept constant and sketching the dynamic root locus is repeated. Figure 3.17 and 3.18 presents the dynamic root contours of the dynamic characteristic equation, Eq. (3.24), for three different values of μ ($\mu = 1, \mu = 2, \mu = 3$). Figure 3.17 shows a two-dimensional plot and Figure 3.18 shows a three-dimensional plot. The dynamic root contours start from the initial poles ($g_1 = 0, g_2 = 1$) and terminate at the zeros. The dotted arrowheads on the dynamic root contours plot show the direction of increase of the value of system state x_1.

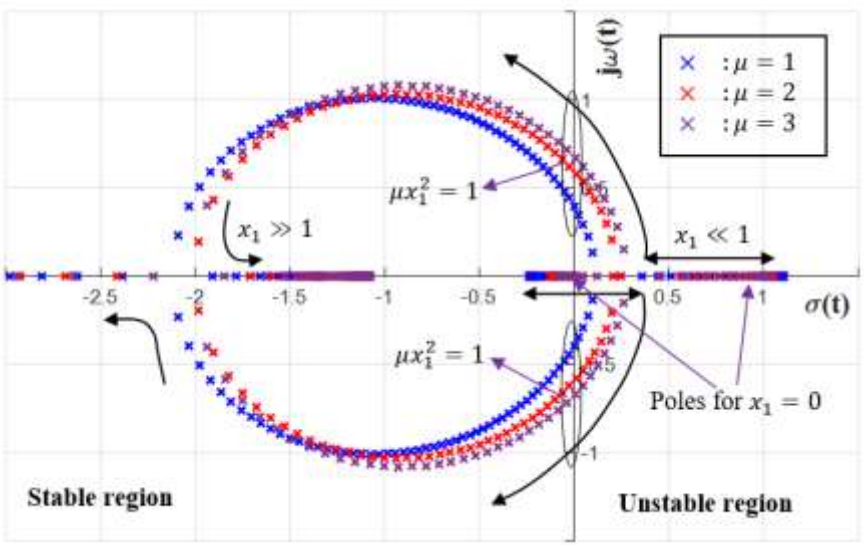

Figure 3.17. A two-dimensional plot of the dynamic root contour of the dynamic characteristic equation $g^2 + (\mu x_1^2 - 1)g + (\mu x_1^2 - sinx_1) = 0$ for three different values of μ: $\mu = 1, \mu = 2, \mu = 3$. The horizontal axis represents the real axis, the vertical axis represents the imaginary axis, and the third axis represents the system state x_1.

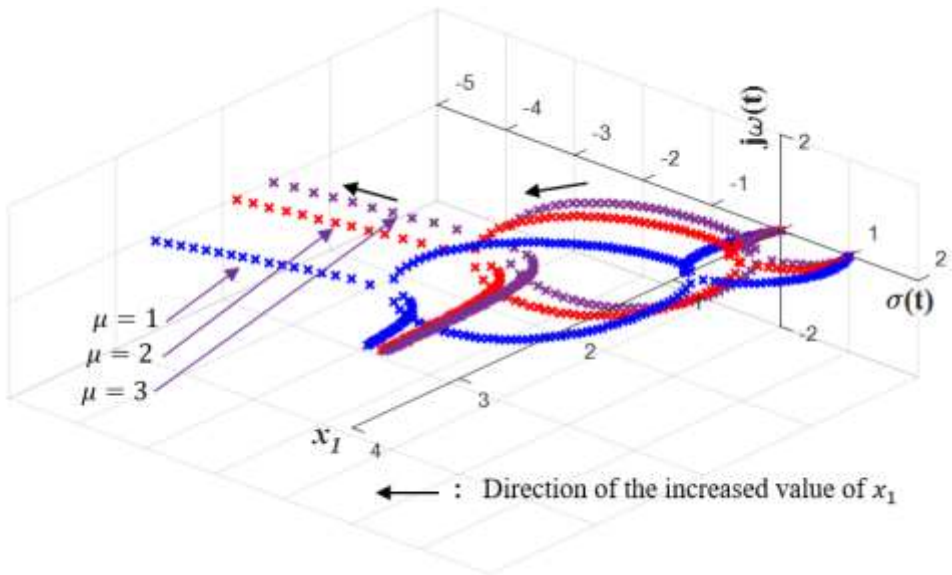

Figure 3.18. A three-dimensional sketch of dynamic root contour plot of the characteristic equation $g^2 + (\mu x_1^2 - 1)g + (\mu x_1^2 - sinx_1) = 0$ for three different values of μ: $\mu = 1, \mu = 2, \mu = 3$. The third axis represents the system state x_1.

The dynamic natural frequency $\omega_n(t)$ and dynamic damping ratio $\xi(t)$ of the second-order nonlinear system Eq. (3.23) is,

$$\omega_n^2(t) = k_p(e,t) = \mu x_1^2 - \sin x_1$$
$$\xi(t) = k_v(e,t) = \frac{\mu x_1^2 - 1}{2\sqrt{\mu x_1^2 - \sin x_1}} \tag{3.27}$$

where $k_p(e,t)$ and $k_v(e,t)$ are the time t dependent position and velocity feedback, respectively. Both natural frequency $\omega_n(t)$ and the damping ratio $\xi(t)$ are a function of μ and system state x_1 explicitly, while time t implicitly. Because of the dynamic nature of the natural frequency $\omega_n(t)$ and the damping ratio $\xi(t)$ of the second-order nonlinear system and their dependency on the sinusoidal function $\sin x_1$, both dynamic poles g_1 and g_2 oscillates on the real axis for small values of x_1, i.e., $x_1 \ll 1$. An increased value of x_1 will eventually cause both dynamic conjugate poles g_1, and g_2 to shift on the left-hand side of the complex g −plane and confirms the stability of the system.

Example 3.5:

Consider a second-order nonlinear system is represented by the state-space equations,

$$\begin{aligned} \dot{x_1} &= x_2 - ax_1(x_1^2 + x_2^2) \\ \dot{x_2} &= -x_1 - ax_2(x_1^2 + x_2^2) \end{aligned} \tag{3.28}$$

where a is a positive real number. The system matrix $\mathbf{A}(\mathbf{x}, t)$ of this nonlinear system Eq. (3.28) is,

$$\mathbf{A}(\mathbf{x}, t) = \begin{vmatrix} -ax_1^2 & 1 - ax_1x_2 \\ -1 - ax_1x_2 & -ax_2^2 \end{vmatrix} \tag{3.29}$$

The dynamic characteristic equation $\mathbf{det}(g\mathbf{I} - \mathbf{A}(\mathbf{x}, t)\ ) = 0$ is,

$$g^2 + a(x_1^2 + x_2^2)g + 1 = 0 \tag{3.30}$$

where g is a differential operator, $\frac{d}{dt}$. The dynamic Routh's array of this dynamic characteristic equation, Eq. (3.30), is,

$$\begin{array}{c|cc} g^2 & 1 & 1 \\ g^1 & a(x_1^2 + x_2^2) & 0 \\ g^0 & 1 & 0 \end{array} \tag{3.31}$$

According to the dynamic Routh's stability criterion, nonlinear system Eq. (3.28) is stable if and only if, the first column of the dynamic Routh's array, Eq. (3.31), has no sign change, i.e., $a(x_1^2 + x_2^2)$ should be positive definite for any values of x_1 and x_2. As a is a positive real number, $a(x_1^2 + x_2^2)$ is also always positive definite, because it is a summation of two real numbers. So, we can conclude that according to the dynamic Routh's stability criterion

nonlinear system Eq. (3.28) is always stable, i.e., system dynamic will always converge to equilibrium for any initial condition of x_1 and x_2. A similar result can be obtained by using Lyapunov's stability method.

Example 3.6:

The dynamic Routh's stability criterion is also applicable to the time-varying dynamic system. Consider a first-order linear time-varying dynamic system,

$$\dot{x_1} = (4t \sin t - 2t)x_1 \tag{3.32}$$

It can be shown very quickly using the dynamic Routh's stability criterion that time-varying linear system Eq. (3.32) is stable if and only if $(4t \sin t - 2t)$ is negative definite at any condition. Figure 3.19 illustrates the dynamic root locus of the same time-varying system. The existence of time t dependent sinusoidal term, $\sin t$, in Eq. (3.32) makes the system dynamic pole to oscillate over the real axis from a stable region to an unstable region and vice versa, with an increase of time t. When $t = 0$s, the dynamic pole is located at the origin $(0,0)$. With the increase of time t, the dynamic pole moves to the left-hand side of the complex g −plane and stays on the left-half side of the g −plane till $t \approx 0.53$s. When $t > 0.53$s, dynamic pole moves to the right-hand side of the complex g −plane again and stays in the right-half side of the g −plane till $t \approx 2.62$s. For $t > 2.62$s, the dynamic pole again moves to the left-half side of the complex g −plane and so on.

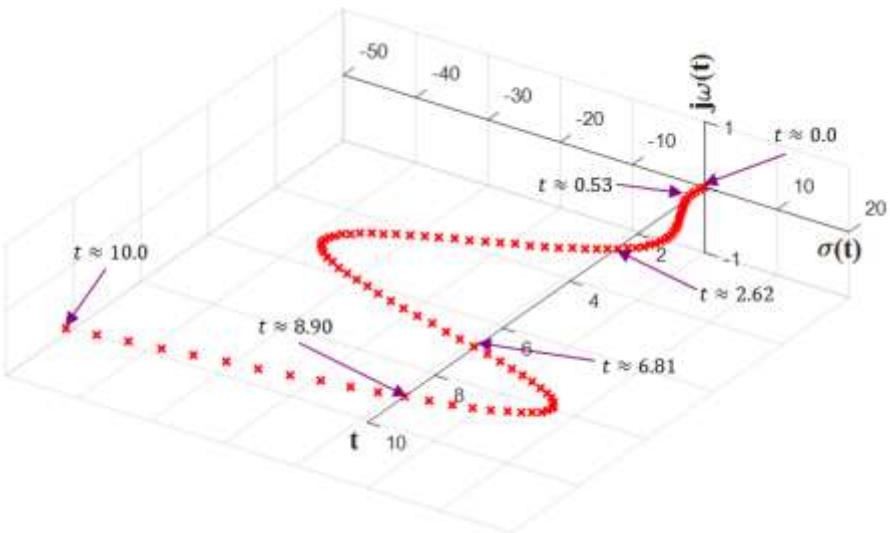

Figure 3.19. The dynamic Root locus of the first-order time-varying dynamic system $\dot{x_1} = (4t \sin t - 2t)x_1$. The third axis is representing time t.

From our knowledge of the study of the linear dynamic system that the transient response of a dynamic system can be described by examining the location of poles, and farther the pole is located from the imaginary axis, the faster the transient system response [4, 5]. As in this particular time-varying dynamic system example, the pole itself is dynamic and each time interval pole moves far from the imaginary axis than before. So the dynamic transient response of each time interval is faster than the previous time interval.

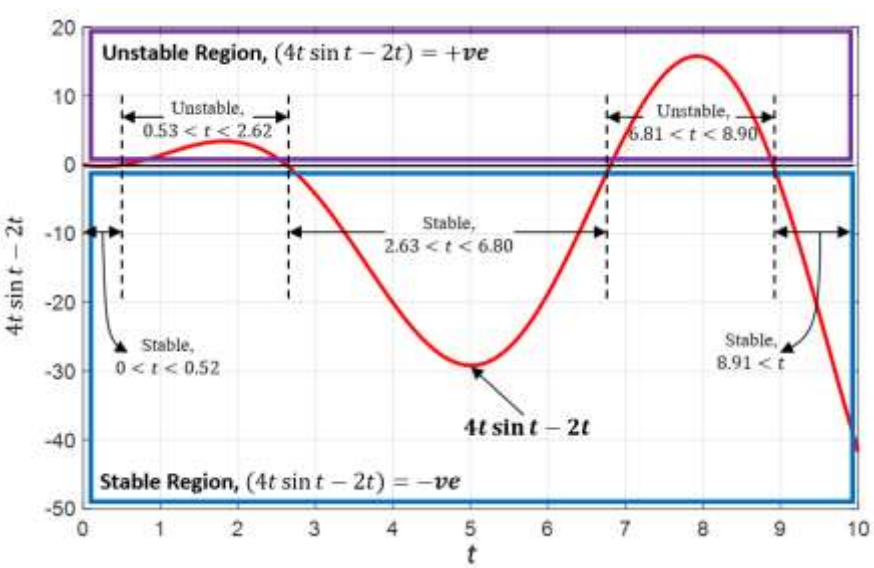

Figure 3.20. The stable and unstable region of the time-varying linear system $\dot{x_1} = (4t \sin t - 2t)x_1$. A positive value of $(4t \sin t - 2t)$ defines the stability, and a negative value of $(4t \sin t - 2t)$ defines the instability situation.

Figure 3.20 shows the stability region of the first-order linear time-varying dynamic system Eq. (3.32). According to the dynamic Routh's stability criterion, the stable region is defined for the values of t so that $(4t \sin t - 2t)$ is negative definite, and the unstable region is defined for the values of t so that $(4t \sin t - 2t)$ is positive definite. For instance, first-order linear time-varying dynamic system Eq. (3.32) is stable between the time span $0s < t < 0.52s$, and unstable between the time span $0.53s < t < 2.62s$. It becomes stable again between $2.63s < t < 6.80s$, and unstable between $6.81s < t < 8.90s$ and so on.

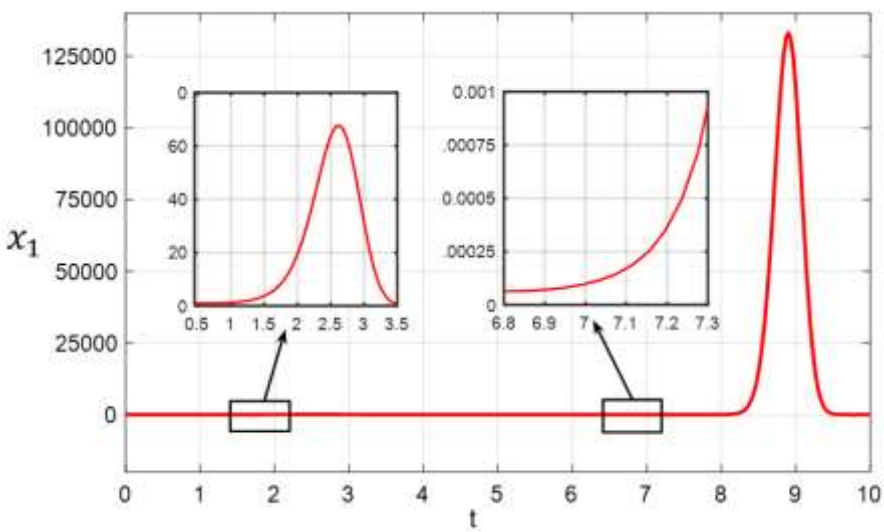

Figure 3.21. System response for the initial condition $x_1 = 1$ of the first-order time-varying linear system $\dot{x_1} = (4t \sin t - 2t)x_1$. The response has two unstable peaks between $0.53s < t < 2.62s$ and $6.81s < t < 8.90s$.

Figure 3.21 shows the first-order time-varying linear system response for the initial condition $x_1 = 1$. According to the stability region illustrated in Figure 3.20, the system dynamic pole oscillates between the unstable right-hand side and stable left-hand side on the real horizontal axis of the complex g −plane. For a 10s simulation time span, dynamic pole stays on

the right-hand side of the complex g −plane between $0.53s < t < 2.62s$ and $6.81s < t < 8.90s$. Similarly, we can see two unstable peaks between the time range $0.53s < t < 2.62s$ and $6.81s < t < 8.90s$ in Figure 3.21. Each of this unstable peak is higher in magnitude than the preceding peak, as dynamic pole moves far from the imaginary axis of the complex g −plane as time t increases.

3.3 Development of the dynamic Nyquist Stability Criterion

In this section, the dynamic Nyquist stability criterion is developed for relative stability analysis of a nonlinear dynamic system in the frequency domain. The interrelationships between the dynamic Root Locus, dynamic Nyquist and Bode plots for a nonlinear dynamic system is also discussed.

Recalling the dynamic characteristic equation, Eq. (2.16),

$$1 + K(\mathbf{x}, t)\frac{\big(g + z_1(\mathbf{x}, t)\big)\big(g + z_2(\mathbf{x}, t)\big)\cdots(g + z_m(\mathbf{x}, t))}{(g + p_1(\mathbf{x}, t))(g + p_1(\mathbf{x}, t))\cdots(g + p_n(\mathbf{x}, t))} = 0 \tag{3.33}$$

$(g + p_i(\mathbf{x}, t))$, $i = 1,2, \ldots, n$, gives the locations of dynamic poles in the complex g −plane and $(g + z_k(\mathbf{x}, t))$, $k = 0,1,2, \ldots, m$, gives the locations of dynamic zeros. $K(\mathbf{x}, t)$ is the system state $\mathbf{x}$ and time t dependent dynamic gain and determines the path of dynamic roots in the complex g −plane.

Equation (3.33) can also be written as

$$1 + \mathbf{L}(g) = 0 \tag{3.34}$$

with

$$\mathbf{L}(g) = K(\mathbf{x}, t)\frac{\big(g + z_1(\mathbf{x}, t)\big)\big(g + z_2(\mathbf{x}, t)\big)\cdots(g + z_m(\mathbf{x}, t))}{(g + p_1(\mathbf{x}, t))(g + p_1(\mathbf{x}, t))\cdots(g + p_n(\mathbf{x}, t))} \tag{3.35}$$

$g \triangleq j\omega$ and ω is in rad/s. The function $\mathbf{L}(g)$ can be written

$$\begin{aligned}\mathbf{L}(g) &= |\mathbf{L}(g)|\angle\mathbf{L}(g) \\ &= K(\mathbf{x},t)\frac{\left|\left(g+z_1(\mathbf{x},t)\right)\right|\cdots\left|\left(g+z_m(\mathbf{x},t)\right)\right|}{\left|\left(g+p_1(\mathbf{x},t)\right)\right|\cdots\left|\left(g+p_n(\mathbf{x},t)\right)\right|}\Big(\angle\left(g+z_1(\mathbf{x},t)\right)+\cdots \\ &\qquad +\angle\left(g+z_m(\mathbf{x},t)\right)-\angle\left(g+p_1(\mathbf{x},t)\right)\cdots \\ &\qquad -\angle\left(g+p_n(\mathbf{x},t)\right)\Big)\end{aligned} \tag{3.36}$$

The dynamic poles and dynamic zeros of $\mathbf{L}(g)$ are (assumed that $\mathbf{L}(g)$ has four dynamic poles and a dynamic zero) shown in Figure 3.22(a).

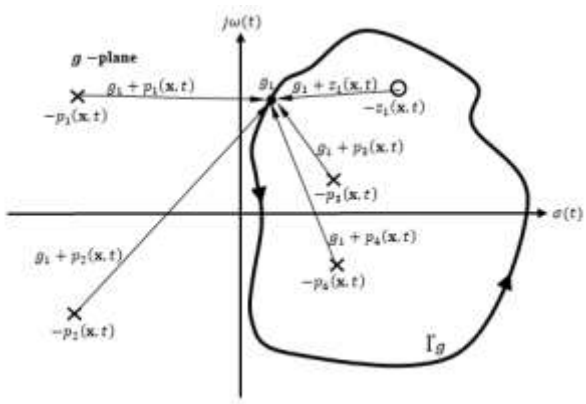

(a)

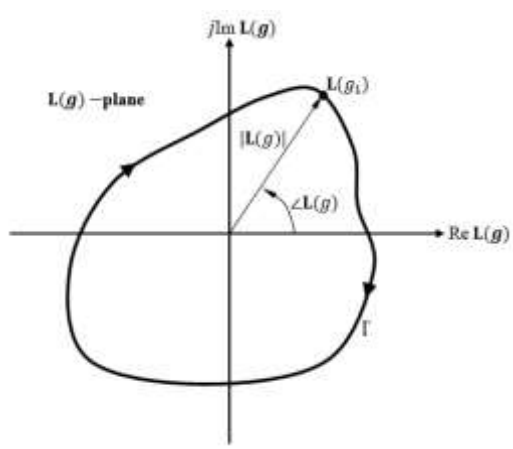

(b)

Figure 3.22: (a) Dynamic pole-zero configuration of $\mathbf{L}(g)$ and an arbitrary g −plane trajectory Γ_g. (b) $\mathbf{L}(g)$ −plane locus, Γ, which corresponds to the Γ_g locus of (a) through one to one mapping.

Figure 3.22(a) shows an arbitrarily chosen trajectory Γ_g in g −plane with an arbitrary point g_1 on the path. The dynamic poles of $\mathbf{L}(g)$ correspond to a negative phase angle, and the dynamic zeros correspond to a positive phase angles in the Eq. 3.36.

If N is the number of encirclement of the origin made by the $\mathbf{L}(g)$ −plane locus Γ, Z is the number of dynamic zeros of $\mathbf{L}(g)$ encircled by the g −plane locus Γ_g in the g −plane, and P is the number of dynamic pols of the $\mathbf{L}(g)$ encirclement by the g −plane locus Γ_g in the g −plane, then according to the principle of the argument,

$$N = Z - P \tag{3.37}$$

If $Z > P$ then N is positive ($\mathbf{L}(g)$ −plane locus will encircle the origin of the $\mathbf{L}(g)$ −plane N times in the same direction as that of Γ_g). If $Z = P$ then N is zero (there is no encirclement to the origin of the $\mathbf{L}(g)$ −plane). If $Z < P$ then N is negative (($\mathbf{L}(g)$ −plane locus will encircle the origin of the $\mathbf{L}(g)$ −plane N times in the opposite direction as that of Γ_g).

If there are N more dynamic zeros than dynamic poles of $\mathbf{L}(g)$, encircled by the g-plane locus Γ_g in a prescribed direction, the net angle traveled by the $\mathbf{L}(g)$ −plane locus as the g-plane locus is equal to

$$2\pi(Z - P) = 2\pi N \tag{3.38}$$

If g −plane locus Γ_g is a Nyquist path in counterclockwise direction, then the stability of a nonlinear dynamic system can be determined by plotting the $\mathbf{L}(g)$ locus for each value of the dynamic gain $\mathrm{K}(\mathbf{x}, t)$, when g takes the values along the Nyquist path, and investing the behavior

of the $\mathbf{L}(g)$ plot with respect to the $(-1, j0)$ point of the $\mathbf{L}(g)$ −plane. It is called the dynamic Nyquist plot of $\mathbf{L}(g)$.

Dynamic Nyquist stability criterion is stated by

For a nonlinear dynamic system to be stable, the dynamic Nyquist plot of $\mathbf{L}(g)$ *must be encircled the* $(-1, j0)$ *point in* $\mathbf{L}(g)$ *−plane as many times as the number of dynamic poles of* $\mathbf{L}(g)$ *that are in the right half of the* g *−plane, and the encirclement, if any, must be made in the clockwise direction.*

Dynamic gain margin: The dynamic gain margin is a measure of the closeness of the dynamic phase-crossover point $\omega_c(t)$ to the $(-1, j0)$ point in the $\mathbf{L}(j\omega)$ −plane, and is given by

$$\text{Dynamic gain margin} = 20\log_{10}\frac{1}{|\mathbf{L}(j\omega_c(t))|}\ \text{dB} \tag{3.39}$$

Dynamic phase margin: The dynamic phase margin is the angle in the degree through which the $\mathbf{L}(j\omega)$ plot must be rotated about the origin so that the dynamic gain-crossover point $\omega_g(t)$ on the $\mathbf{L}(j\omega)$ locus passes through $(-1, j0)$ point in the $\mathbf{L}(j\omega)$ −plane, and is given by

$$\text{Dynamic phase margin} = \angle\mathbf{L}\big(j\omega_g(t)\big) - 180^0 \tag{3.40}$$

The concept is further illustrated by using the following example.

Example 3.7

Consider a third-order dynamic system with a nonlinear spring $(6 + x)$ is,

$$\dddot{x} + 6\ddot{x} + 11\dot{x} + (6 + x)x = u(t) \tag{3.41}$$

The state-space model of this system is,

$$\dot{x_1} = x_2$$
$$\dot{x_2} = x_3$$
$$\dot{x_3} = -(6 + x_1)x_1 - 11x_2 - 6x_3 \tag{3.42}$$

and the output is,

$$y = x_1$$

The System matrix $\mathbf{A}(\mathbf{x}, t) = \begin{vmatrix} 0 & 1 & 0 \\ 0 & 0 & 1 \\ -(6 + x_1) & -11 & -6 \end{vmatrix}$, the input matrix $\mathbf{B}(t) = \begin{vmatrix} 0 \\ 0 \\ 1 \end{vmatrix}$, and the output matrix $\mathbf{C}(\mathbf{x}, t) = |1 \quad 0 \quad 0|$.

The input-output relation regarding g −transfer function is,

$$y(t) = \frac{u(t)}{g^3 + 6g^2 + 11g + (6 + x_1)} \tag{3.43}$$

The dynamic characteristic equation is defined as $\mathbf{det}(g\mathbf{I} - \mathbf{A}(\mathbf{x}, t)) = 0$, and given by

$$g^3 + 6g^2 + 11g + (6 + x_1) = 0 \tag{3.44}$$

The roots of this dynamic characteristic equation, Eq. (3.44), are a function of the system state x_1. Rearranging Eq. (3.44),

$$1 + \frac{x_1}{(g + 1)(g + 2)(g + 3)} = 0 \tag{3.45}$$

The locations of the dynamic poles in the complex g −plane are a function of the system state x_1. A three-dimensional dynamic root locus in the complex g −plane is given in Figure 3.23, and a two-dimensional projection of Figure 3.23 is shown in Figure 3.24. For $x_1 = 0$, the dynamic poles are located at -3, -2, and -1. With an increased value of x_1, a dynamic pole moves to the

left of the $j\omega$ −axis, and the conjugate dynamic poles move towards each other creating a break-away point at -1.4 on the $\sigma(t)$ −axis and then move towards the $j\omega(t)$ −axis, as indicated by the arrowheads in Figures 3.23 and 3.24. For $x_1 < 60$, all the dynamic poles are located on the left-hand side of the g −plane. When $x_1 = 60$, the conjugate dynamic poles are on the $j\omega(t)$ −axis. If x_1 is increased still further, the conjugate dynamic poles are kept on the right-hand side of the complex g −plane.

Applying the dynamic Routh's stability criterion discussed in Section 3.1, the stability of the nonlinear system, Eq. (3.42), can be examined for the various values of state x_1 in a time domain. For instance, the nonlinear system is stable for $x_1 < 60$, have oscillatory dynamic conjugate poles on the $j\omega(t)$ −axis for $x_1 = 60$ and have unstable dynamic conjugate poles on the right-hand side of the $j\omega(t)$ −axis for $x_1 > 60$.

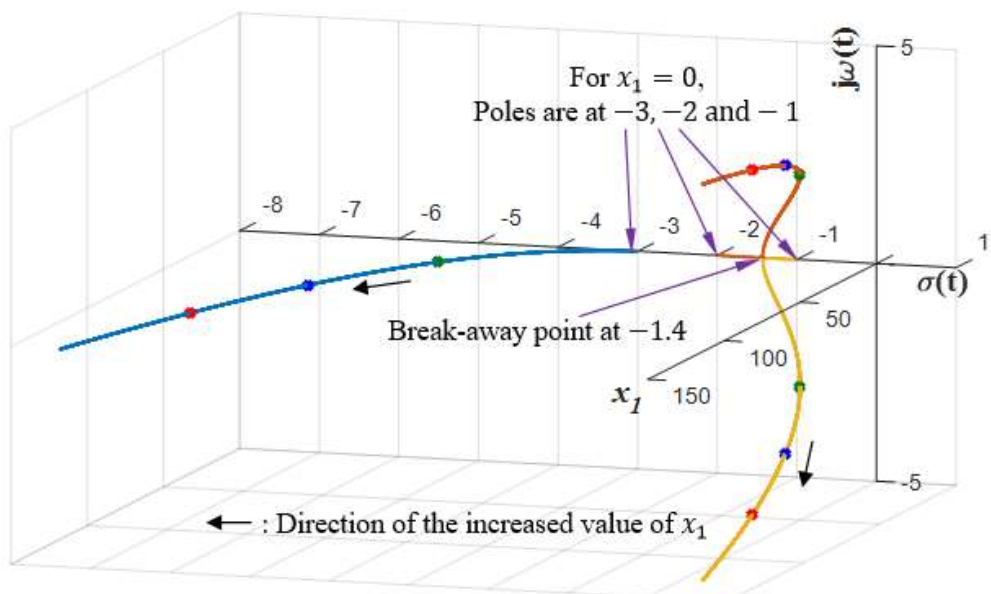

Figure 3.23: A three-dimensional dynamic root locus of the nonlinear system $\dddot{x} + 6\ddot{x} + 11\dot{x} + (6 + x)x = u(t)$. The dynamic poles are on the left-hand side of the complex g −plane for $x_1 < 60$. For $x_1 = 60$, the dynamic conjugate poles are on the $j\omega(t)$ −axis. The dynamic conjugate poles are on the right-hand side of the complex g −plane for $x_1 > 60$.

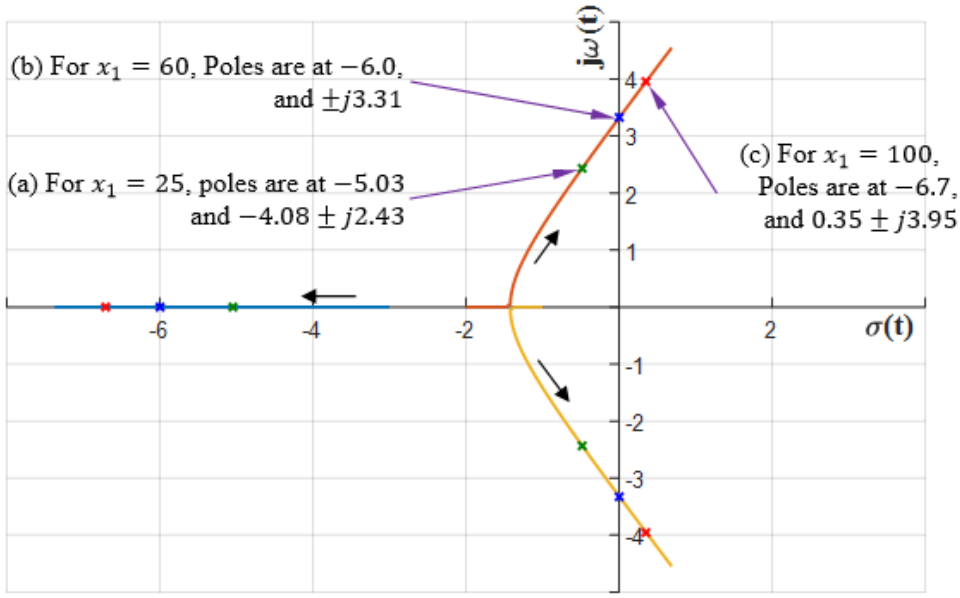

Figure 3.24: A two-dimensional projection of the three-dimensional dynamic root locus Figure 3.23. The location of the dynamic poles changes with the increased value of x_1. For instance, (a) for $x_1 = 25$, poles are at -5.03 and $-4.08 \pm j2.43$, (b) for $x_1 = 60$, poles are at -6.0, and $\pm j3.31$, (c) for $x_1 = 100$, poles are at -6.7, and $0.35 \pm j3.95$.

The relative stability of the nonlinear system in the frequency domain can be measured by means of the dynamic Nyquist plot. The closeness of the dynamic Nyquist plot in the dynamic polar coordinates to the $(-1, j0)$ point, indicates how stable or unstable the nonlinear system is.

From Eq. (3.45), the function $\mathbf{L}(g)$ of the nonlinear system Eq. 3.42 can be written as

$$\begin{aligned} \mathbf{L}(g) &= \frac{x_1}{(g+1)(g+2)(g+3)} \\ &= \frac{x_1}{g^3 + 6g^2 + 11g + 6} \end{aligned} \tag{3.46}$$

Putting $g = j\omega$, we have

$$\mathbf{L}(g) = \frac{x_1}{(j\omega)^3 + 6(j\omega)^2 + 11j\omega + 6}$$
$$= \frac{x_1}{(6 - 6\omega^2) + j(11\omega - \omega^3)} \tag{3.47}$$

Multiplying the numerator and the denominator with $(6 - 6\omega^2) - j(11\omega - \omega^3)$,

$$\mathbf{L}(g) = \frac{x_1\{(6 - 6\omega^2) - j(11\omega - \omega^3)\}}{(6 - 6\omega^2)^2 + (11\omega - \omega^3)^2} \tag{3.48}$$

From Eq. (3.48), the dynamic Nyquist plot crosses the real axis of $\mathbf{L}(g)$ −plane when

$$\frac{-x_1(11\omega - \omega^3)\}}{(6 - 6\omega^2)^2 + (11\omega - \omega^3)^2} = 0 \tag{3.49}$$

Solving Eq. (3.49), the dynamic Nyquist plot crosses the real axis of the $\mathbf{L}(g)$ −plane when $\omega = 0$ rad/s and $\omega = \pm 3.31$ rad/s.

From Eq. (3.48), the dynamic Nyquist plot crosses the imaginary axis of $\mathbf{L}(g)$ −plane when

$$\frac{x_1(6 - 6\omega^2)}{(6 - 6\omega^2)^2 + (11\omega - \omega^3)^2} = 0 \tag{3.50}$$

Solving Eq. (3.50), the dynamic Nyquist plot crosses the imaginary axis of the $\mathbf{L}(g)$ −plane when $\omega = \pm 1.0$ rad/s.

The correspondent dynamic Nyquist plot, step responses, and dynamic magnitude frequency and phase frequency responses to the dynamic root locus, Figures 3.23 and 3.24, for three different values of system state $x_1 = 25$, $x_1 = 60$, and $x_1 = 100$, are shown in Figures 3.25, 3.26, 3.27, 3.28, and 3.29, respectively.

For $x_1 = 25$, the dynamic Nyquist plot intersects the real axis (i.e., dynamic phase crossover point, $\omega_c(t)$) at a point quite far away from $(-1, j0)$ point, and all the dynamic poles are on the left-hand side of the complex g −plane (as shown in Figures 3.23 and 3.24, for $x_1 = 25$), and an equilibrium condition on the response is achieved (as shown in the step response in Figure 3.27, for $x_1 = 25$). As x_1 is increased, the dynamic phase crossover point $\omega_c(t)$ moves closer to $(-1, j0)$ point. For $x_1 = 60$, the nonlinear system has conjugate dynamic poles on the $j\omega$ −axis, and the dynamic Nyquist plot intersects the $(-1, j0)$ point, and the system response has a constant amplitude oscillation in the step response (as shown in the step response in Figure 3.27, for $x_1 = 60$). If x_1 is increased still further, for instance, $x_1 = 100$, the dynamic conjugate poles move to the right-hand side of the g −plane, and the dynamic Nyquist plot encloses the $(-1, j0)$ point. The nonlinear dynamic system becomes unstable in this case with an unbounded response (as shown in the step response in Figure 3.27, for $x_1 = 100$), and the nonlinear system has a negative gain margin and a negative phase margin (as shown in The dynamic magnitude and phase frequency response in Figure 3.28 and 3.29, for $x_1 = 100$).

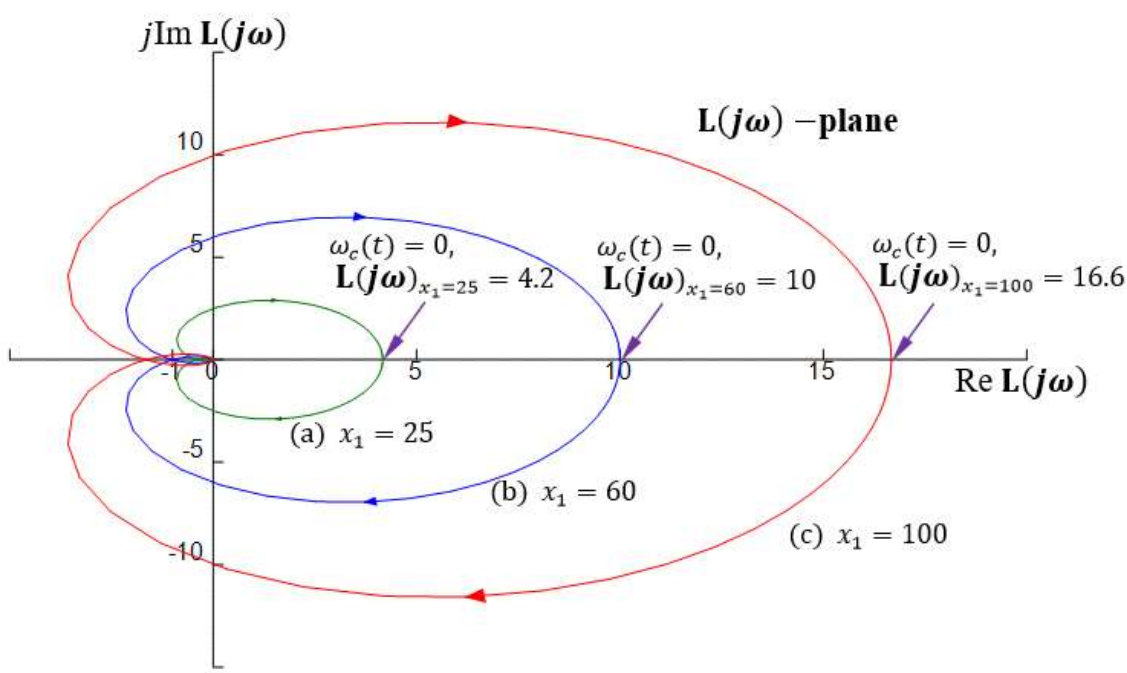

Figure 3.25: The dynamic Nyquist plot of the system defined by Eq. (3.42) for three different values of the system state, (a) $x_1 = 25$, (b) $x_1 = 60$ and (c) $x_1 = 100$. The dotted arrowhead indicates the direction of the increased value of system state x_1.

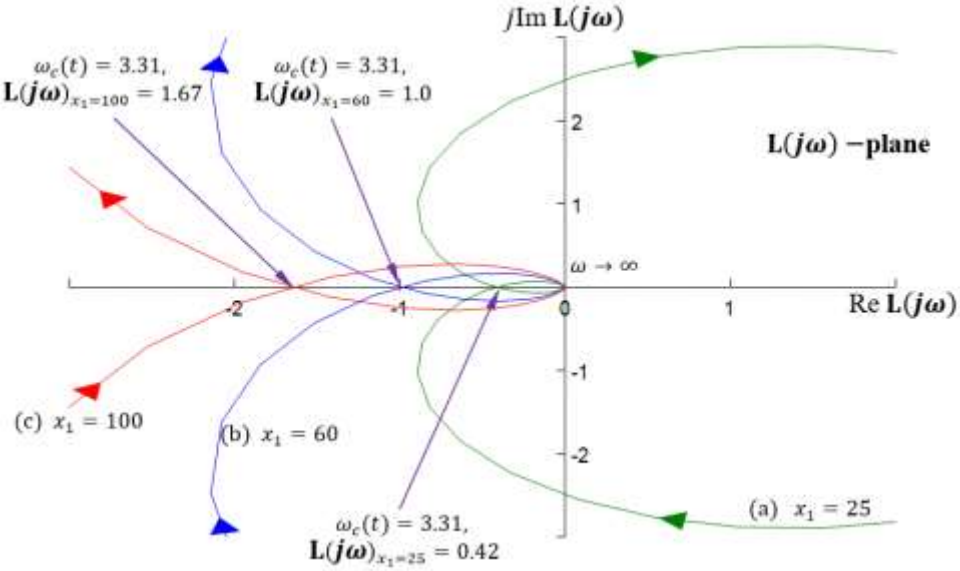

Figure 3.26: A magnified sketch of the dynamic Nyquist plot, Figure 3.25, for three different values of system state (a) $x_1 = 25$, (b) $x_1 = 60$ and (c) $x_1 = 100$.

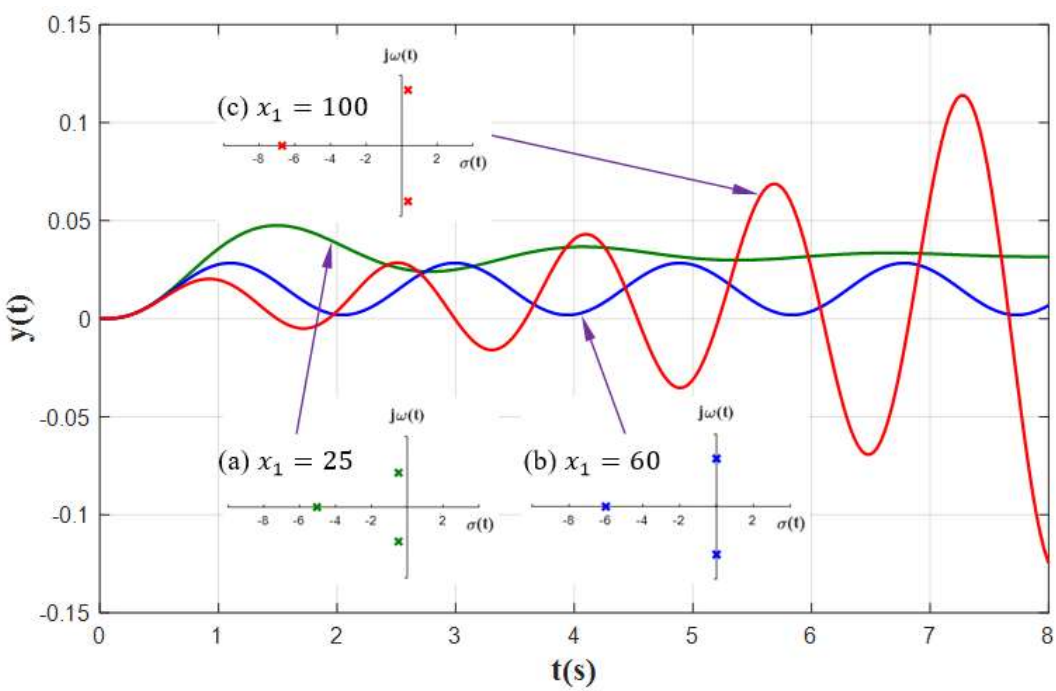

Figure 3.27: The step response of the nonlinear system defined by Eq. (3.42) at three different values of the system state, (a) $x_1 = 25$, (b) $x_1 = 60$ and (c) $x_1 = 100$.

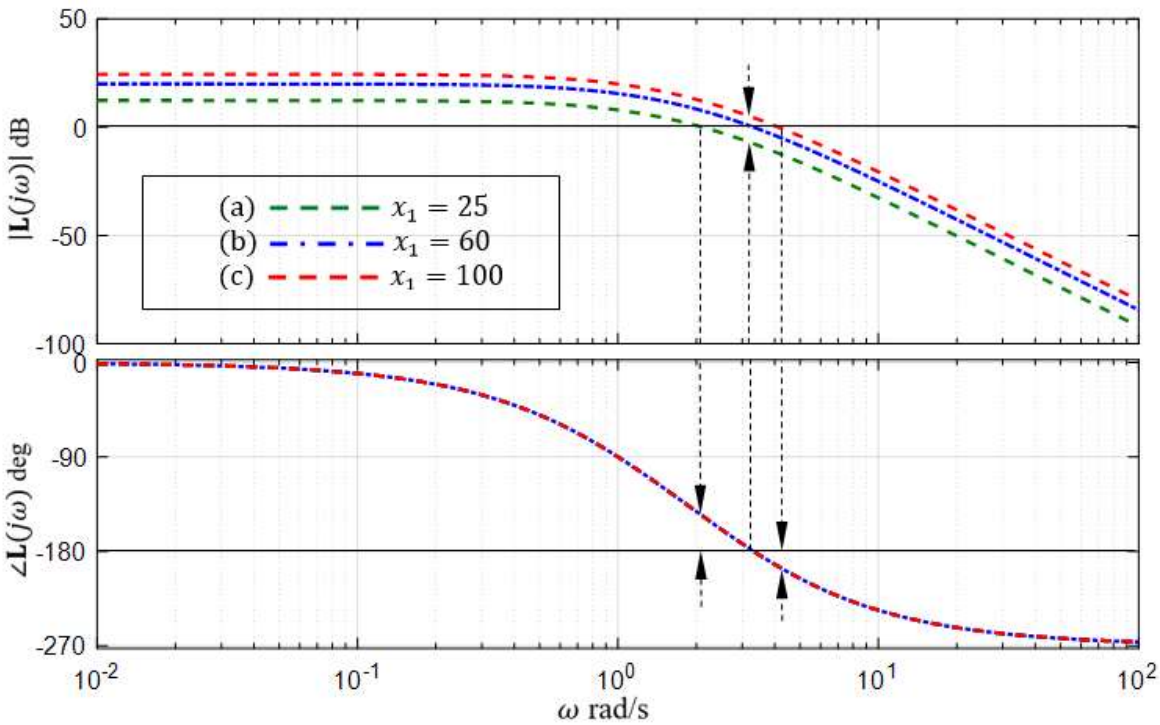

Figure 3.28: The dynamic magnitude and phase frequency response of the nonlinear system defined by Eq. (3.42) for three different values of the system state, (a) $x_1 = 25$, (b) $x_1 = 60$ and (c) $x_1 = 100$.

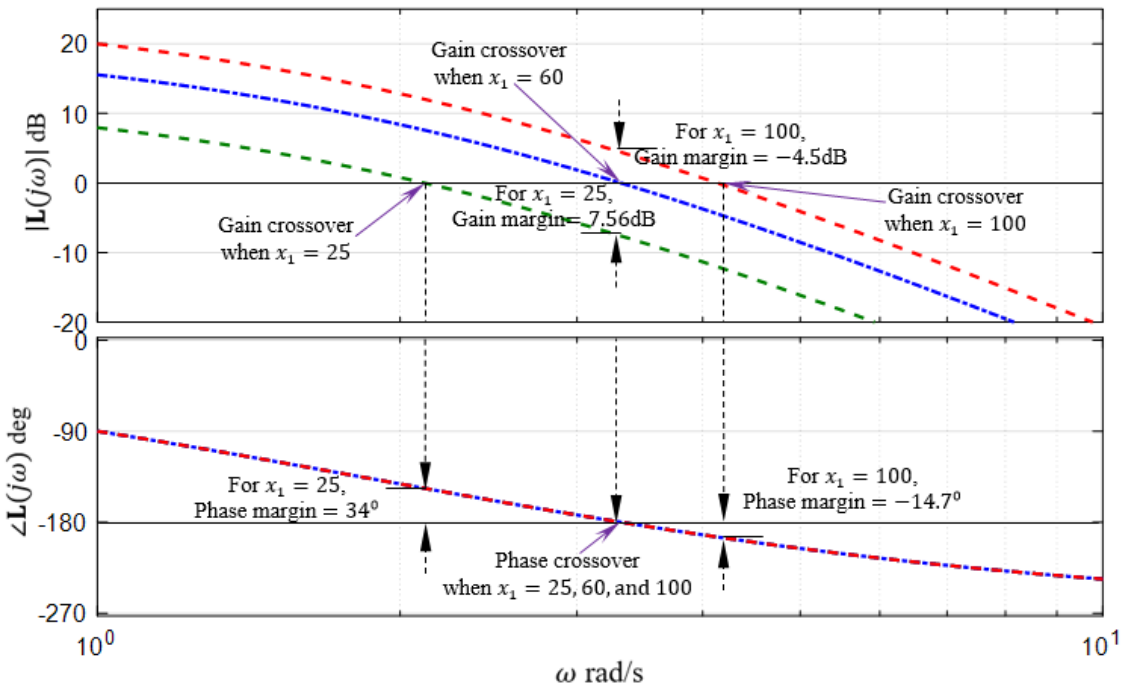

Figure 3.29: A magnified sketch of The dynamic magnitude and phase frequency response, Figure 3.28, for three different values of the system state, (a) $x_1 = 25$, (b) $x_1 = 60$ and (c) $x_1 = 100$, to show the dynamic gain margin and dynamic phase margin.

Figure 3.28 plots the dynamic magnitude and phase frequency response of the nonlinear system defined by Eq. (3.42) for three different values of the system state, (a) $x_1 = 25$, (b) $x_1 = 60$ and (c) $x_1 = 100$. A magnified sketch of the same plot is given in Figure 3.29. The phase crossover frequency is the same for the phase frequency response plot of all three values of the state x_1 and is $\omega_c(t) = 3.3$ rad/s. The magnitude of $\mathbf{L}(j\omega)$ at this frequency is about -7.56dB for $x_1 = 25$, 0dB for $x_1 = 60$, and 4.5dB for $x_1 = 100$. It means that for $x_1 = 25$, if the dynamic gain of the system is increased by 7.5dB, then the magnitude curve will cross the 0dB axis at the phase crossover frequency $\omega_c(t) = 3.3$ rad/s. Therefore the gain margin for $x_1 = 25$ is 7.5dB. Similarly, for $x_1 = 60$ and $x_1 = 100$, the nonlinear system has a gain margin of 0dB and -4.5dB, respectively. A 0dB gain margin means that system is already is the margin of instability, and the dynamic gain can no longer be increased (situation (b) in Figures 3.24 and 3.27). A negative gain margin implies an unstable situation and the dynamic poles are in the right-hand side of the complex g −plane (situation (c) in Figures 3.24 and 3.27).

The dynamic gain crossover and phase crossover frequency are same ($\omega_g(t)$= $\omega_g(t)$=3.31 rad/s) for $x_1 = 60$, as dynamic poles are located on the margin of instability. The dynamic gain crossover frequency $\omega_g(t)$ is at 2.1 rad/s and 4.2 rad/s, for $x_1 = 25$ and $x_1 = 100$, respectively. The dynamic phase margin is 34^0, 0^0 and -14.7^0 for $x_1 = 25$, $x_1 = 60$, and $x_1 = 100$, respectively.

The above discussion can be summarized as, for $x_1 < 60$, the nonlinear system dynamic poles are on the left-hand side of the complex g −plane and stability is guaranteed. For $x_1 = 60$ dynamic poles are on the margin of instability, and for $x_1 > 60$, dynamic poles are on the right-hand side of the complex g −plane creating an unstable situation on the response.

3.4 Summary

In this Chapter 3, an extensive numerical analysis of the stability analysis of a nonlinear dynamic system was studied. A nonlinear system has dynamic poles, and their movement in the complex g −plane is a function of states $\mathbf{x}$ explicitly, while time t implicitly. The stability of a nonlinear system was established applying the dynamic Routh's stability criterion of [6] on the location of the dynamic poles. The location of the dynamic poles in the complex g −plane was determined from the dynamic Routh's array which was constructed from the dynamic characteristic equation of the nonlinear system. A phase plane analysis was also presented by applying the dynamic Routh's stability criterion on it to define the stability region. It is proved that a negative value of acceleration creates stability in the 1st quadrant of a phase plane, and a positive value of acceleration creates stability in the 3rd quadrant.

The dynamic Nyquist plot was developed to study the stability of a nonlinear system in the frequency domain. A dynamic characteristic equation can also be written as

$$1 + \mathbf{L}(g) = 0 \tag{3.51}$$

where

$$\mathbf{L}(g) = K(\mathbf{x}, t)\frac{\big(g + z_1(\mathbf{x}, t)\big)\big(g + z_2(\mathbf{x}, t)\big)\cdots(g + z_m(\mathbf{x}, t))}{(g + p_1(\mathbf{x}, t))(g + p_1(\mathbf{x}, t))\cdots(g + p_n(\mathbf{x}, t))} \tag{3.52}$$

According to the dynamic Nyquist stability criterion, a nonlinear dynamic system is stable, if the dynamic Nyquist plot of $\mathbf{L}(\mathrm{g})$ encircles the $(-1, \mathrm{j}0)$ point in $\mathbf{L}(\mathrm{g})$ $-$plane, in the clockwise direction, as many times as the number of dynamic poles of $\mathbf{L}(\mathrm{g})$ that are in the right half of the complex g $-$plane, and inside the encirclement, if any.

An interrelationship between the dynamic root locus and the dynamic Nyquist and Bode plots was also presented. Several examples were taken from literature, and numerical simulation studies were done to show the efficiency and effectiveness of the proposed dynamic pole movement based nonlinear system stability analysis.

Chapter 4

The Design of a Neuro-controller using g −Plane Approach

Dynamic system behavior can be described regarding its dominant parameters [4, 5]. For a second-order system, the dominant parameters are natural frequency $\omega_n(t)$ and damping ratio $\xi(t)$. It is possible to change the location of the system poles in the complex g −plane by changing the values of the dominant parameters. The dynamic poles change the characteristics of the system response. For example, depending on the location of dynamic poles on g −plane a second-order system exhibits the characteristics much like a first-order system or a damped or an oscillation in its transient response. Indeed, by changing the parameters $\omega_n(t)$ and $\xi(t)$, all possible step responses to a second-order system can be obtained, i.e., undamped ($\xi(t) = 0$), under-damped ($0 < \xi(t) < 1$), critically-damped ($\xi(t) = 1$) and over-damped ($\xi(t) > 1$). An under-damped system yields a faster response, i.e., smaller rise time T_r, with a larger overshoot M_p and a larger settling time T_s [4, 5]. On the other hand, an over-damped system yields a slower response, i.e., smaller rise time T_r, with a zero overshoot $M_p = 0$ [4, 5].

This chapter is devoted to the design of the dynamic pole motion based neuro-controllers. The original works to determine of the neuro-controller parameters were done in [7, 8, 11]. This chapter gives an extensive exploration of various characteristics in the neuro-controller design process. The neuro-controller concept is explained at the beginning of the chapter, and several examples were taken to do a simulation-based study to illustrate the concept. Details of the Simulink models are given in Appendix C.

4.1 Neuro-controller Concept

A controller determines the response of a dynamic system by adjusting the overall dynamics to reach the ideal performance, i.e., fast transient response and nearly zero overshoot. The overall dynamics means the dynamics of a plant along with its controller. The neuro-

controller is a highly nonlinear error-based adaptive controller. A neuro-controller learns from the overall response and adapts its parameters to get the best overall response. Figure 4.1 explains the overall motivation of a neuro-controller. For a large initial error, the overall system exhibits an under-damped and a fast transient response, while for a small error, the overall system exhibits an over-damped and a zero overshoot transient response [7].

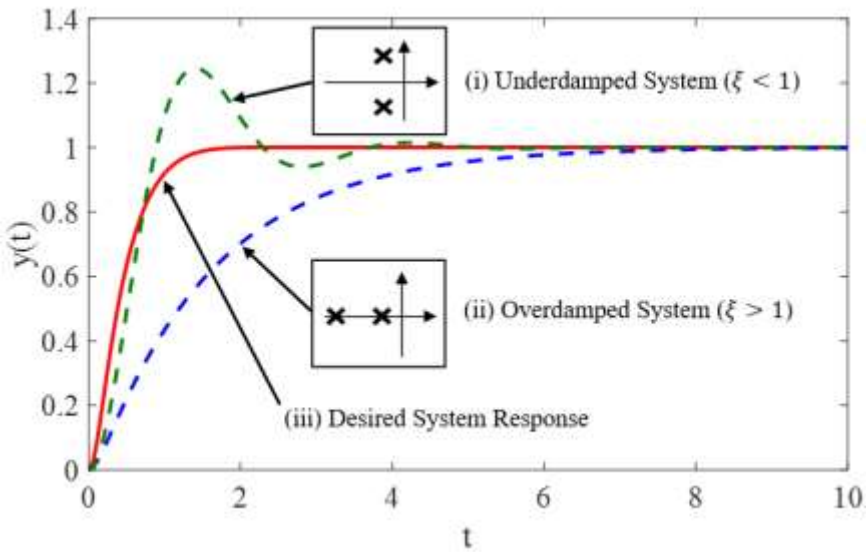

(a) A comparison among (i) an under-damped, (ii) an over-damped and (iii) the desired response curve.

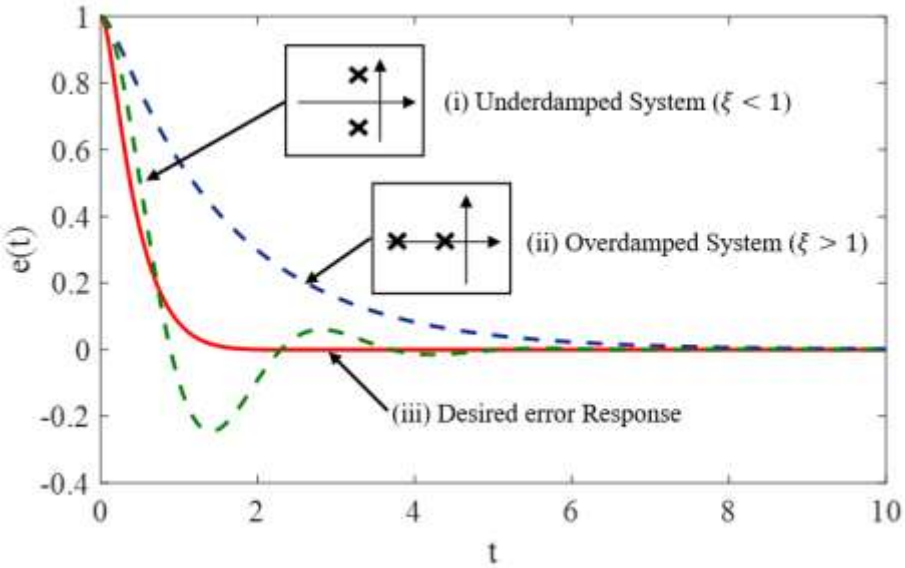

(b) A comparison among (i) an under-damped, (ii) an over-damped and (iii) a desired error response curve of the system.

Figure 4.1. System responses to a unit step input with two different pole locations: (i) under-damped situation ($\xi < 1$), and (ii) over-damped situation ($\xi > 1$). Initially, for a large error, the desired response curve follows an under-damped curve and then settles down to a steady-state value for decreasing errors, i.e., following an over-damped curve. The desired response curve is a marriage between an under-damped and an over-damped response curve [7].

To control the overall system dynamics towards the desired response, parameters of the neuro-controller need to be represented as a function of the overall system error $e(t)$. The design methodology developed in this paper is based on: for an initial large error $e(t)$ the overall system will follow an under-damped system dynamics with a larger bandwidth, i.e., a smaller $\xi(t)$ and a larger $\omega_n(t)$, while for a small error $e(t)$ the overall system will follow an over-damped system dynamics with a smaller bandwidth, i.e., a larger $\xi(t)$ and a smaller $\omega_n(t)$ [7]. Since $\xi(t)$ and $\omega_n(t)$ depend on the velocity feedback K_v and position feedback K_p, respectively, a fast transient response with no overshoot can be achieved if K_p and K_v are defined as a proper function of the overall system error $e(t)$.

4.2 Neuro-controller Design Criteria

The above discussion is summarized to some certain observations by deriving the following design criteria of a neuro-controller [7, 8].

Design criteria I (determination of the overall system response behavior):

(1) If the system error $e(t)$ is large, then make the damping ratio $\xi(t)$ very small and the natural frequency $\omega_n(t)$ very large.

(2) *If the system error $e(t)$ is small, then make the damping ratio $\xi(t)$ very large and the natural frequency $\omega_n(t)$ very small.*

Design criteria II (determination of the parameters of a neuro-controller):

(1) Position feedback $K_p(e,t)$ controls the speed of response, i.e., the natural frequency $\omega_n(t)$ of a system (notice: the bandwidth of the system is determined by the natural frequency $\omega_n(t)$ of a system specifically).

$$K_p(e,t) = \omega_n^2(t) \tag{4.1}$$

(2) Velocity feedback $K_v(e,t)$ controls the brake of response, i.e., the damping ratio $\xi(t)$ of a system specifically.

$$K_v(e,t) = 2\xi(t)\omega_n(t) \tag{4.2}$$

The position feedback $K_p(e,t)$ and velocity feedback $K_v(e,t)$ are the neuro-controller parameters, and they are a function of the error $e(t)$. As error $e(t)$ changes from a large value to a small value, $K_p(e,t)$ is varied from a large value to a small value, and simultaneously $K_v(e,t)$ is varied from a small value to a large value.

To keep the response in an admissible range, the above design procedure introduces a controlled dynamic pole motion of the overall system. The controller parameters are chosen to such an extent that the overall system dynamic poles move as a function of the error $e(t)$ in the complex g −plane to reach a designated response. This controlled way of pole motion is called dynamic pole motion (**DPM**) in the complex g −plane [7, 8]. The proposed neuro-controller is shown in Figure 4.2.

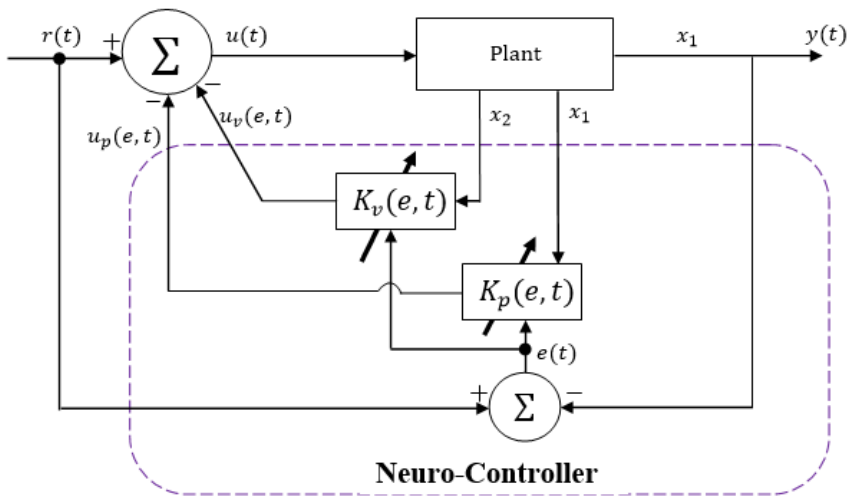

Figure 4.2. A graphical representation of the proposed neuro-controller where $x_2 = \dot{x_1}$. $K_p(e,t)$ and $K_v(e,t)$ are defined according to the design criteria I and II [7, 8].

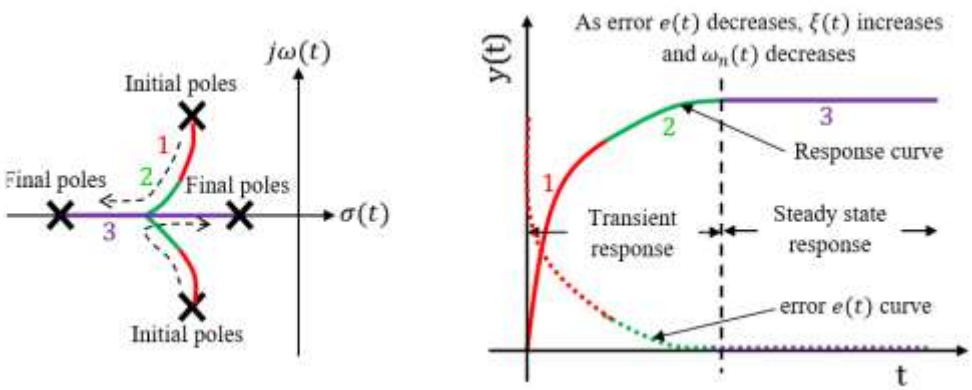

(a) Pole locations on a complex g −plane with a real axis, $\sigma(t)$ and an imaginary axis $j\omega(t)$

(b) Time response

Figure 4.3. The explanation of the dynamic pole motion (**DPM**) concept. Section 1, 2, 3 shows the dynamic pole locations in the complex g −plane in (a), and the correspondent time response of the overall system is shown in (b).

The DPM concept is illustrated graphically in Figure 4.3. The locations of dynamic poles in the complex g −plane are shown in Figure 4.3(a) and the correspondent overall time response is given in Figure 4.3(b). Initially, for a large error $e(t)$ a faster response is achieved by making the damping ratio $\xi(t)$ very small, and the natural frequency $\omega_n(t)$ very large and system performs as an under-damped system. It is shown in Section 1 of Figure 4.3. As the error $e(t)$ decreases, the damping ratio $\xi(t)$ increases and the natural frequency $\omega_n(t)$ decreases, and the system dynamics behave more like to an over-damped system than an under-damped system. It is accomplished by changing the locations of dynamic poles as a function of the system error $e(t)$ in the complex g −plane and shown in Section 2 of Figure 4.3. When the response reaches the desired value, the dynamic poles settle down to a steady-state location exhibited in Section 3 of Figure 4.3.

Several typical step responses of a second-order dynamic system with a neuro-controller for the variation of K_p and K_v are shown in Figure 4.4.

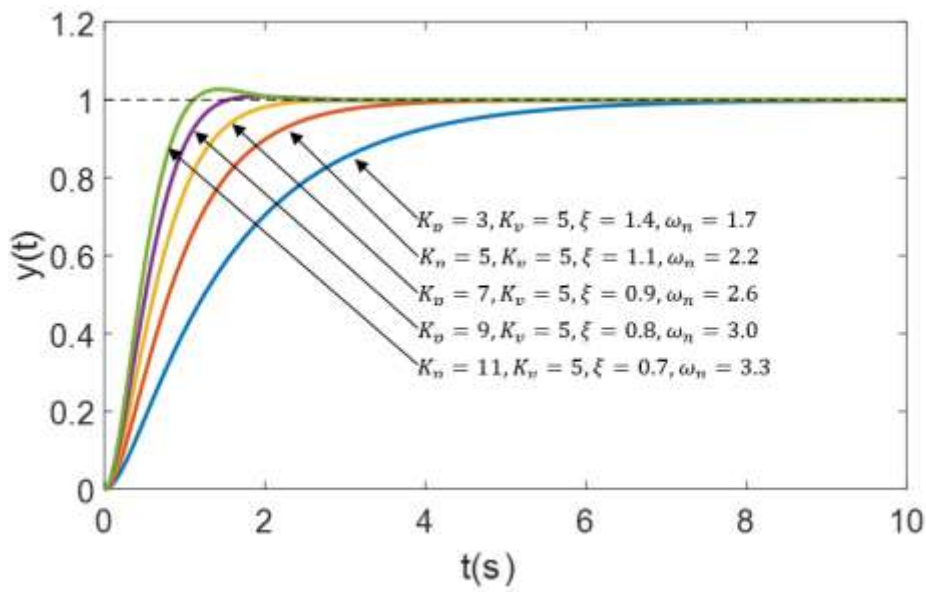

(a) System responses of a typical second-order system with a variable value of K_p and a constant K_v=5 [10, 7].

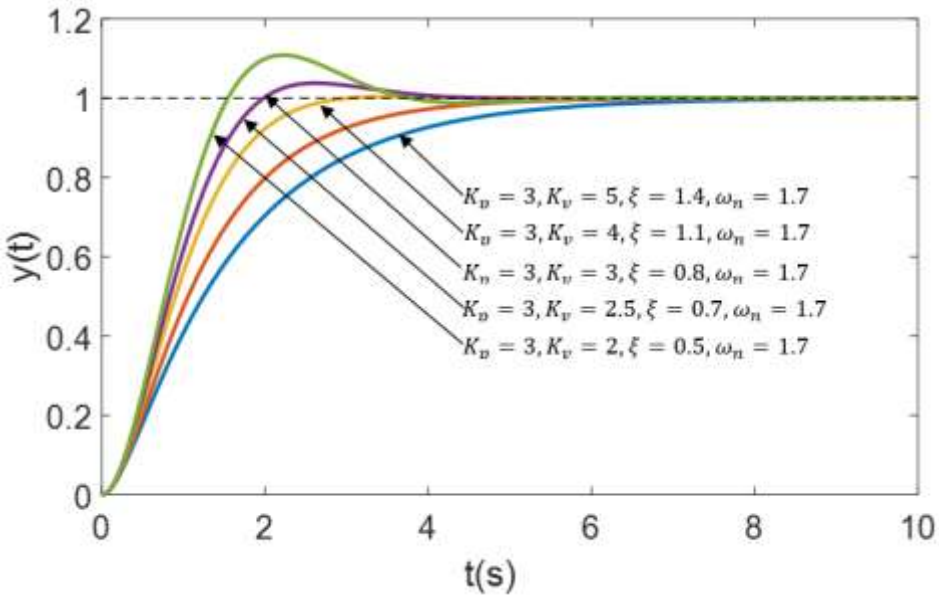

(b) System responses of a typical second-order system with a variable value of K_v and a constant K_p=3 [7, 10].

Figure 4.4. Step responses of a typical second-order system with a neuro-controller for the variation of K_p and K_v, one at a time.

4.3 Controller Design

4.3.1 Determination of Position Feedback $K_p(e,t)$ and Velocity Feedback $K_v(e,t)$

Various types of functions can be designed for the position feedback $K_p(e,t)$ and velocity feedback $K_v(e,t)$ of a neuro-controller by following the design criteria presented in Section 4.2. For example,

$$\begin{aligned} K_p(e,t) &= K_{pf} + \alpha e^2 \\ K_v(e,t) &= K_{vf}\exp(-\beta e^2) \end{aligned} \tag{4.3}$$

where $e = r(t) - y(t)$ is the error signal. α and β are the gain constants and determine the slope of the functions $K_p(e,t)$ and $K_v(e,t)$ as illustrated in Figure 4.5. K_{pf} and K_{vf} are the final steady-state values of $K_p(e,t)$ and $K_v(e,t)$, respectively.

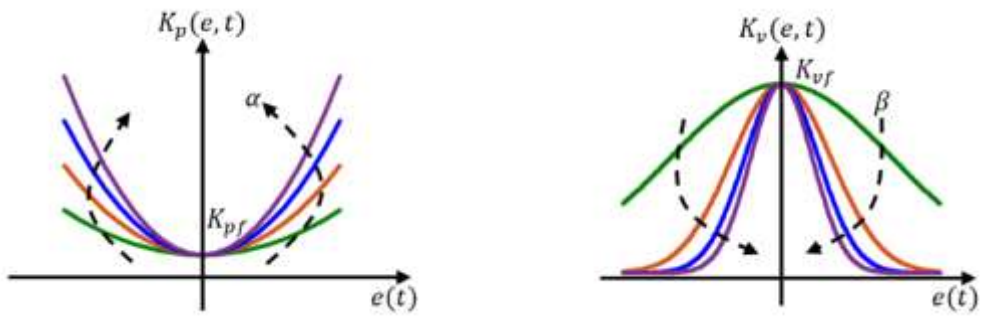

Figure 4.5. Effect of the variation of α and β on the function $K_p(e,t)$ and $K_v(e,t)$, respectively [8].

Several other possible examples are given in Table 4.1.

Table 4.1: Various types of possible functions and their graphical representations for the position feedback $K_p(e,t)$ and velocity feedback $K_v(e,t)$ of a neuro-controller [7, 8, 11].

	$\boldsymbol{K_p(e,t)}$		$\boldsymbol{K_v(e,t)}$	
1	$K_{pf}(1+\alpha\lvert e\rvert)$	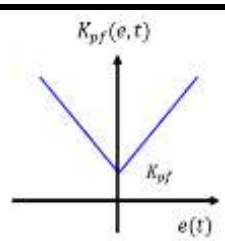	$K_{vf}\dfrac{1}{1+\beta\lvert e\rvert}$	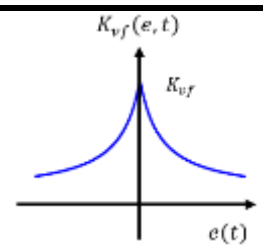
2	$K_{pf}(1+\alpha e^2)$	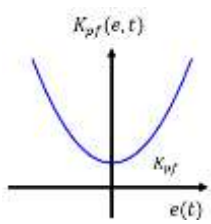	$K_{vf}\dfrac{1}{1+\beta e^2}$	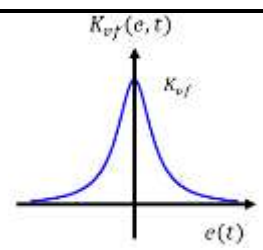

3	$K_{pf} + \alpha e^2$	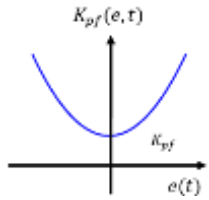	$K_{vf}\exp(-\beta e^2)$	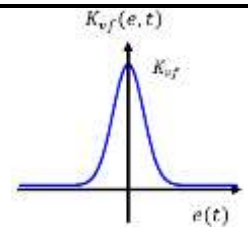

4.3.2 Determination of K_{pf}, K_{vf}, α, and β

As discussed earlier, to achieve a fast response, the overall system must have a larger bandwidth $\omega_{BW}(t)$ for the large error $e(t)$. Position feedback $K_p(e,t)$ determines the bandwidth of a system and is a function of system error $e(t)$. A zero overshoot response is achieved by continuously adjusting the overall system damping ratio $\xi(t)$ as a function of the system error $e(t)$. The position feedback $K_p(e,t)$ and velocity feedback $K_v(e,t)$ are determined in such a way that the overall system has a small damping ratio $\xi(t)$ with a large bandwidth $\omega_{BW}(t)$ for a large error $e(t)$ and a large damping ratio $\xi(t)$ with a small bandwidth $\omega_{BW}(t)$ for a small error $e(t)$. From Figure 4.2, the control input $u(t)$ of the overall system is,

$$u(t) = r(t) - \left[K_p(e,t)x_1 + K_v(e,t)x_2\right] \tag{4.4}$$

with
the position feedback gain $K_p(e,t) = K_{pf} + \alpha e^2$,
the velocity feedback gain $K_v(e,t) = K_{vf}exp[-\beta e^2]$, and
the error $e(t) = r(t) - y(t)$.

From Eq. 4.4, four parameters K_{pf}, K_{vf}, α and β need to be adjusted to get the desired response of a system by continually adjusting the overall system dynamics. These four parameters are chosen using the following criteria [7, 8],

(1) α and β: the initial position of the poles should have a very small damping $\xi(t)$ and a larger bandwidth $\omega_{BW}(t)$.

(2) K_{pf} and K_{vf}: the final position of the poles should have a large damping $\xi(t)$ and a smaller bandwidth $\omega_{BW}(t)$.

(3) To ensure the stability of the system, all the dynamic poles of the overall system must have to keep on the left-half side of the complex g −plane at any condition.

The following equations calculate the natural frequency $\omega_n(t)$ and damping ratio $\xi(t)$ of the neuro-controller,

$$\omega_n(t) = \sqrt{K_{pf} + \alpha\{r(t) - x_1\}^2}$$
$$\xi(t) = \frac{K_{vf} exp[-\beta\{r(t) - x_1\}^2]}{2\sqrt{K_{pf} + \alpha\{r(t) - x_1\}^2}} \tag{4.5}$$

It can be noted from Eq. 4.5 that the bandwidth $\omega_{BW}(t)$ and the damping ratio $\xi(t)$ of the overall system change with the change of the system error $e(t)$ and this dynamic behavior are called dynamic bandwidth and dynamic damping ratio, respectively.

4.4 Illustrative Numerical Examples

In the preceding sections, the design of a neuro-controller for a dynamic system based on the concept of the dynamic pole motion in the complex g −plane to achieve a faster transient response with zero overshoot was discussed. In this section, several examples will be discussed, and the neuro-controller parameters will be determined according to the design criteria described in Section 4.2. Simulation works are performed by using the software packages MATLAB r2016a, and SIMULINK v8.7. The dynamic Routh's stability criterion is used to ensure the stability of the overall neuro-controlled system.

Example 4.1:

Consider a linear time-invariant second-order system with a single input $u(t)$ presented by

$$\ddot{x} + 2\dot{x} + 6x = 6u(t) \tag{4.6}$$

The state-space model of the system is,

$$\begin{aligned} \dot{\mathbf{x}}(t) &= \mathbf{A}(\mathbf{x}, t)\mathbf{x}(t) + \mathbf{B}(t)\mathbf{u}(t) \\ \mathbf{y}(t) &= \mathbf{C}(\mathbf{x}, t)\mathbf{x}(t) \end{aligned} \tag{4.7}$$

where

$\mathbf{x} \in \Re^n$: the state vector,

$\dot{\mathbf{x}} \in \Re^n$: the derivation of the state vector $\mathbf{x}$ to time t,

$\mathbf{y} \in \Re^p$: the output vector, and

$\mathbf{u} \in \Re^m$: the control input.

System matrix $\mathbf{A}(\mathbf{x}, t) = \begin{vmatrix} 0 & 1 \\ -6 & -2 \end{vmatrix}$.

Input matrix $\mathbf{B}(t) = \begin{vmatrix} 0 \\ 6 \end{vmatrix}$.

Output matrix $\mathbf{C}(\mathbf{x}, t) = \begin{vmatrix} 1 & 0 \end{vmatrix}$.

As discussed in Chapter 2, the elements of the system matrix $\mathbf{A}(\mathbf{x}, t)$ can be constant (e.g., linear system), or a function of system states $\mathbf{x}$ and/or time t (e.g., nonlinear time-variant system). In this particular linear time-invariant system, Eq. 4.6, the elements of the system matrix $\mathbf{A}(\mathbf{x}, t)$ are constant. The elements of the input matrix $\mathbf{B}(t)$ are constant (e.g., a step input), or a function of amplitude and frequency (e.g., a periodic input).

The neuro-controller parameters $K_{pf} = 40$, $K_{vf} = 6.5$, $\alpha = 18$, and $\beta = 12$ are determined according to the design procedure explained in Section 4.2 and Section 4.3. The neuro-controlled system respond initially as an under-damped system $\xi(t) < 1$ for a larger error $e(t)$ with a higher bandwidth $\omega_{BW}(t)$, and continuously moves towards the characteristics of an over-damped system $\xi(t) > 1$ with a smaller bandwidth $\omega_{BW}(t)$ as system error $e(t)$ decreases. The position feedback $K_p(e, t)$ and velocity feedback $K_v(e, t)$ of the neuro-controller are,

$$K_p(e,t) = 40 + 18e^2$$
$$K_v(e,t) = 6.5\exp[-12e^2] \tag{4.8}$$

The overall response to a step input is shown in Figure 4.6. Initially, at $t = 0$s and the error $e(t) = 100\%$, the system starts with a smaller damping ratio $\xi(t) = 0.036$, i.e., an under-damped system and the bandwidth is $\omega_{BW}(t)$ =42.95. As time t increases and error $e(t)$ decreases, system response follows more to an over-damped system than an under-damped system. For instance, at $t = 0.63s$, the error is $e(t) \approx 2\%$, and the overall system has a damping ratio $\xi(t) = 0.62$ and a bandwidth $\omega_{BW}(t) = 7.5$. The controlled system response is fast with zero overshoot $M_p = 0\%$. The rise time $T_r = 0.11$s and the settling time $T_s = 0.63$s. In comparison with the neuro-controlled system, the uncontrolled system has an overshoot $M_p = 24.56\%$ with a larger rise time $T_r = 0.6$s and a larger settling time $T_s > 5$s. A detail of the Simulink model is given in Appendix C (Figure C.1).

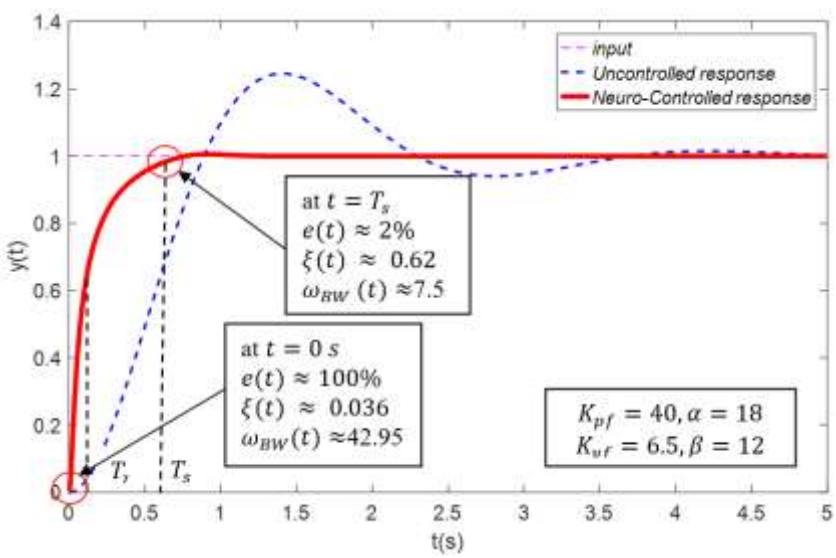

Figure 4.6. The neuro-controlled response of the system $\ddot{x} + 2\dot{x} + 6x = 6u(t)$ to a unit step input. Rise time $T_r = 0.11$s and settling time $T_s = 0.63$s. the neuro-controller parameters are $K_{pf} = 40$, $K_{vf} = 6.5$, $\alpha = 18$ and $\beta = 12$. Blue dotted line is the uncontrolled response of the system.

Figure 4.7 illustrates the overall system dynamic pole motion in the complex g −plane for the decreasing of error $e(t)$. The dynamic poles are located at $-1.0 \pm j27.6$ and $-4.2 \pm j5.28$ for $t = 0$s and $t = 5$s, respectively. Figure 4.7(a) shows a three-dimensional motion of dynamic poles in the complex g −plane and Figure 4.7(b) sketches a two-dimensional projection of pole motion in the complex g −plane. The third axis is representing the system error $e(t)$, and the location of the dynamic poles are changed in the complex g −plane as a function of error $e(t)$ to achieve fast response and zero overshoot.

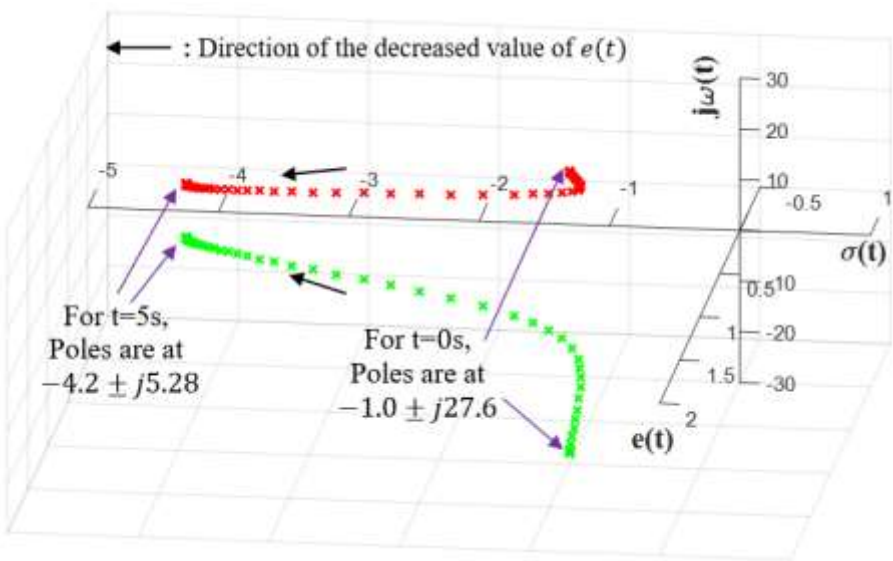

(a) Three-Dimensional motion of dynamic poles.

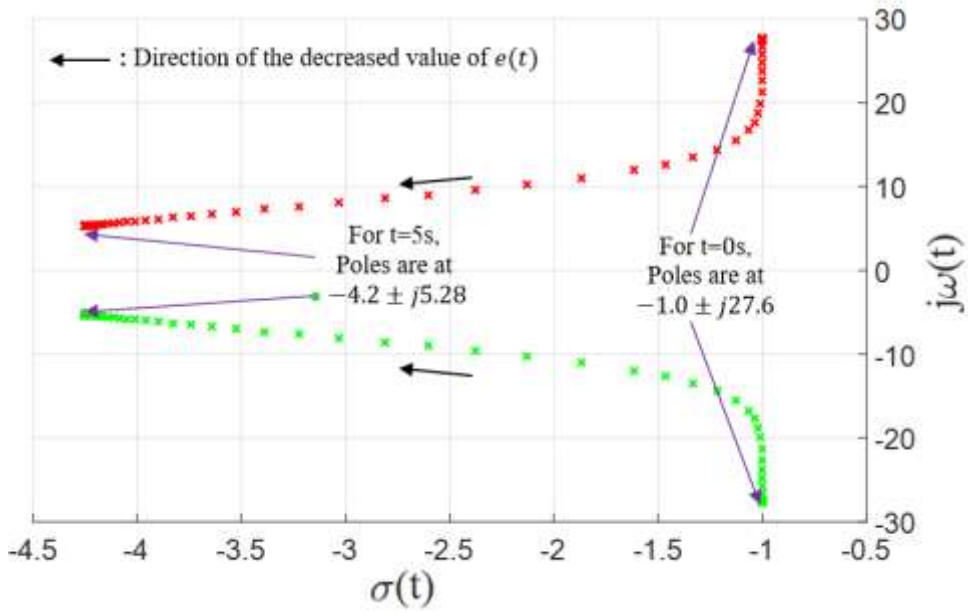

(b) A two-dimensional projection of the three-dimensional dynamic pole motion.

Figure 4.7. Dynamic pole motion of the system $\ddot{x} + 2\dot{x} + 6x = 6u(t)$ with a neuro-controller in the complex g −plane for a decreasing error $e(t)$. The dynamic poles are located at $-1.0 \pm j27.6$ and $-4.2 \pm j5.28$ for $t = 0$s and $t = 5$s, respectively.

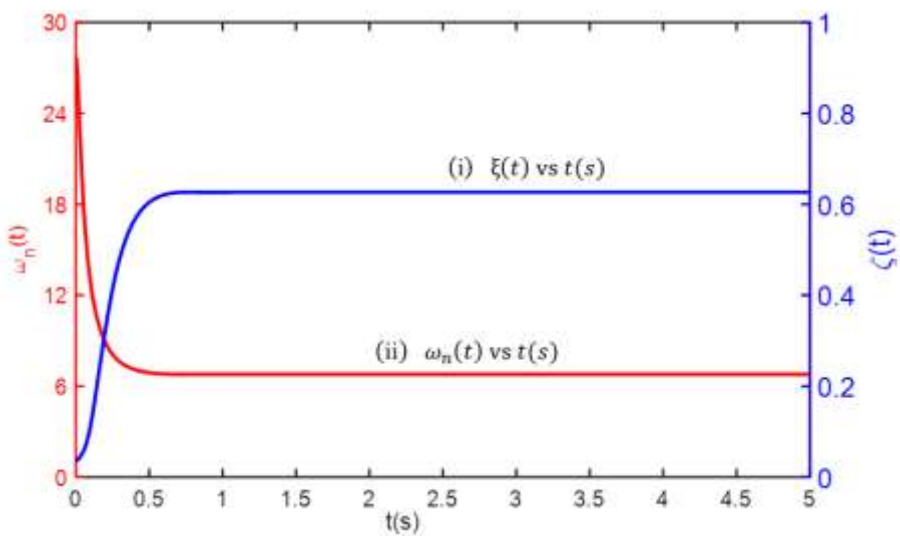

(a) (i) The damping ratio $\xi(t)$ vs. time t and (ii) the natural frequency $\omega_n(t)$ vs. time t.

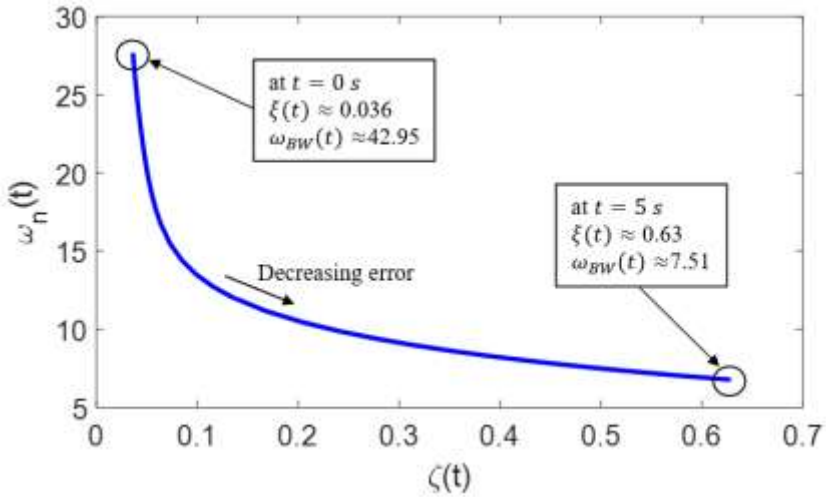

(b) The natural frequency $\omega_n(t)$ vs. the damping ratio $\xi(t)$.

Figure 4.8. A graphical representation of the natural frequency $\omega_n(t)$ vs. the damping ratio $\xi(t)$ with the increase of time t and the decrease of error $e(t)$ of the system $\ddot{x} + 2\dot{x} + 6x = 6u(t)$ with a neuro-controller.

Figure 4.8 illustrates the relationship of the overall system natural frequency $\omega_n(t)$ and damping ratio $\xi(t)$ graphically with the increase of time t and a decrease of error $e(t)$ of the system $\ddot{x} + 2\dot{x} + 6x = 6u(t)$ with a neuro-controller. It is observed that the relation between overall system natural frequency $\omega_n(t)$ and damping ratio $\xi(t)$ is inversely proportional and it is a function of time t and error $e(t)$. The natural frequency $\omega_n(t)$ regulates the speed of the response, and the damping ratio $\xi(t)$ regulates the brake on the response. It is somewhat like 'driving a car.' When the destination is far, and the error $e(t)$ is large then put more gas on the accelerator with no brake, i.e., higher the natural frequency $\omega_n(t)$ and smaller the damping ratio $\xi(t)$. On the other hand, if the destination is closer and error $e(t)$ is small then put more brake with no gas, i.e., lower the natural frequency $\omega_n(t)$ and higher the damping ratio $\xi(t)$.

Figure 4.9 demonstrates the natural frequency $\omega_n(t)$ and the damping ratio $\xi(t)$ at various time t and locations of the neuro-controlled response of the system $\ddot{x} + 2\dot{x} + 6x = 6u(t)$.

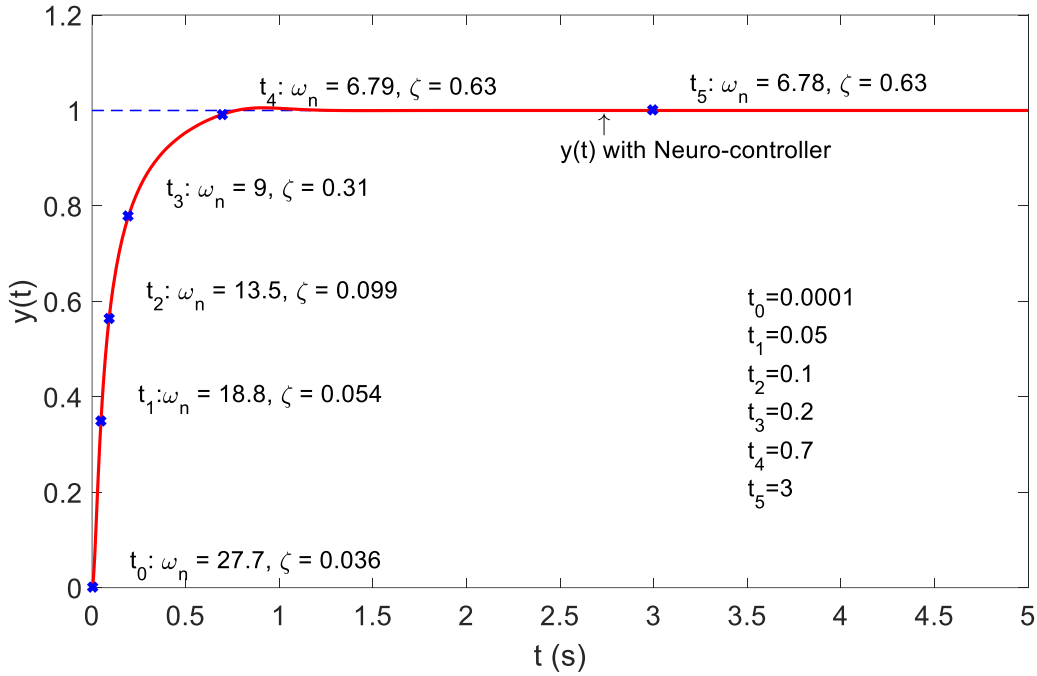

Figure 4.9. The natural frequency $\omega_n(t)$ and the damping ratio $\xi(t)$ at various time t and locations of a unit step response of the system $\ddot{x} + 2\dot{x} + 6x = 6u(t)$.

Example 4.2:

Consider a second-order system with a nonlinear damping $(1 - x^2)$ and an input $u(t)$ presented by a differential equation,

$$\ddot{x} + (1 - x^2)\dot{x} + x = u(t) \tag{4.9}$$

where x is system state. The state-space representation of this nonlinear time-invariant system is,

$$\begin{aligned} \dot{\mathbf{x}}(t) &= \mathbf{A}(\mathbf{x}, t)\mathbf{x}(t) + \mathbf{B}(t)\mathbf{u}(t) \\ \mathbf{y}(t) &= \mathbf{C}(\mathbf{x}, t)\mathbf{x}(t) \end{aligned} \tag{4.10}$$

where

$\mathbf{x} \in \Re^n$: the state vector,

$\dot{\mathbf{x}} \in \Re^n$: the derivation of the state vector $\mathbf{x}$ to time t,

$\mathbf{y} \in \Re^p$: the output vector, and

$\mathbf{u} \in \Re^m$: the control input.

System matrix, $\mathbf{A}(\mathbf{x}, t) = \begin{vmatrix} 0 & 1 \\ -1 & -(1 - {x_1}^2) \end{vmatrix}$.

Input matrix, $\mathbf{B}(t) = \begin{vmatrix} 0 \\ 1 \end{vmatrix}$.

Output matrix, $\mathbf{C}(\mathbf{x}, t) = |1 \quad 0|$.

The block diagram representation of the state-space model of the nonlinear system Eq. 4.10 is given in Figure 4.10.

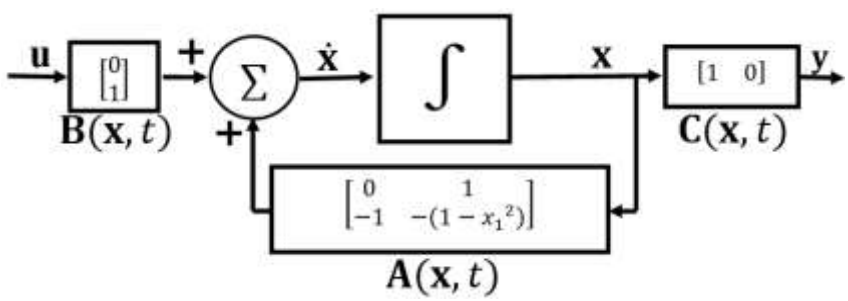

Figure 4.10. Block diagram representation of the state-space model of the nonlinear dynamic system $\ddot{x} + (1 - x^2)\dot{x} + x = u(t)$.

As discussed in Chapter 2 and 3, the dynamic characteristic equation a nonlinear time-invariant system is calculated from $\mathbf{det}(g\mathbf{I} - \mathbf{A}(\mathbf{x}, t)) = 0$ where g is a differential operator ($g \triangleq \frac{d}{dt}$). $\mathbf{I}$ is a $n \times n$ identity matrix. The elements of the system matrix $\mathbf{A}(\mathbf{x}, t)$ are function of states $\mathbf{x}$ and time t, and the coefficients of the dynamic characteristic equation $\mathbf{det}(g\mathbf{I} - \mathbf{A}(\mathbf{x}, t)) = 0$ contain all the state $\mathbf{x}$ and time t dependent terms. $dim[\mathbf{A}(\cdot)] = n \times n$, n is the order of the differential equation.

The dynamic characteristic equation of the nonlinear time-invariant second-order system Eq. 4.9 is,

$$g^2 + (1 - {x_1}^2)g + 1 = 0 \tag{4.11}$$

The dynamic root locus can be obtained by sweeping through every point in the complex g −plane to locate the dynamic roots of the dynamic characteristic equation as system states are varied from a zero to infinity, one at a time. Figure 4.11 gives the dynamic root locus of the dynamic characteristic equation, Eq. 4.11 as system state x_1 is varied. The arrowheads indicate the increased value of x_1.

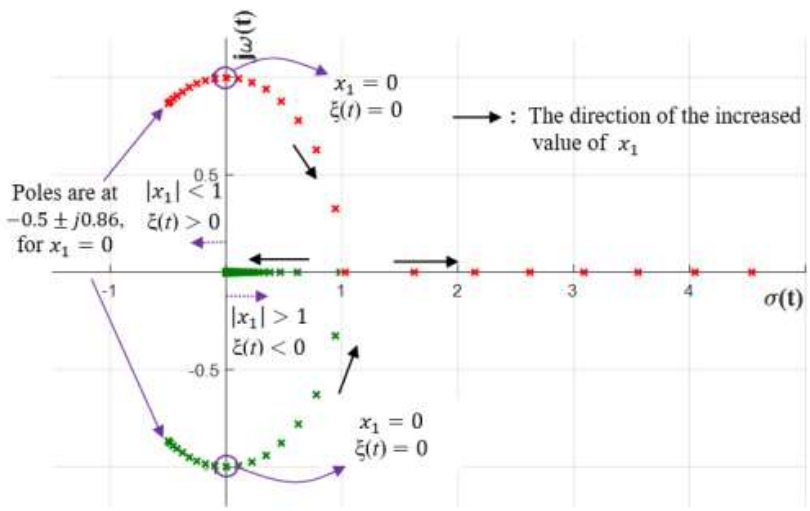

Figure 4.11. Dynamic root locus of the dynamic characteristic equation $g^2 + (1 - {x_1}^2)g + 1 = 0$ as system state x_1 is varied from a zero to infinity.

For $-1 < x_1 < 1$, the conjugate dynamic poles are located on the left-half side of the complex g −plane. With the increases of system state x_1, both dynamic poles start moving toward the right-half side of the g −plane, i.e., unstable region. To ensure the stability of the neuro-controlled system and according to the dynamic Routh's stability criterion presented in Chapter 3, neuro-controller parameters K_{pf}, K_{vf}, α, and β must be determined in such a way that the dynamic poles are always kept on the left-half side of the complex g −plane at any conditions.

According to the design procedure described in Section 4.2 and 4.3, the designed neuro-controller parameters of the nonlinear system, Eq. 4.9, are $K_{pf} = 24$, $K_{vf} = 12$, $\alpha = 150$ and $\beta = 40$. The neuro-controlled response to a step input is shown in Figure 4.12. The rise time $T_r = 0.19$s and the settling time $T_s = 0.49$s. For $t = 0$s, the dynamic poles are located at $-0.5 \pm j13.2$. When $t = 3$s, the dynamic poles move to $-10.65 + j0.0$ and $-2.34 + j0.0$, respectively, in the complex g −plane. The dynamic pole motion of the overall neuro-controlled system with the increase of time t and the decrease of error $e(t)$ in the complex g −plane is plotted in Figure 4.13. A detail of the Simulink model is given in Appendix C (Figure C.2).

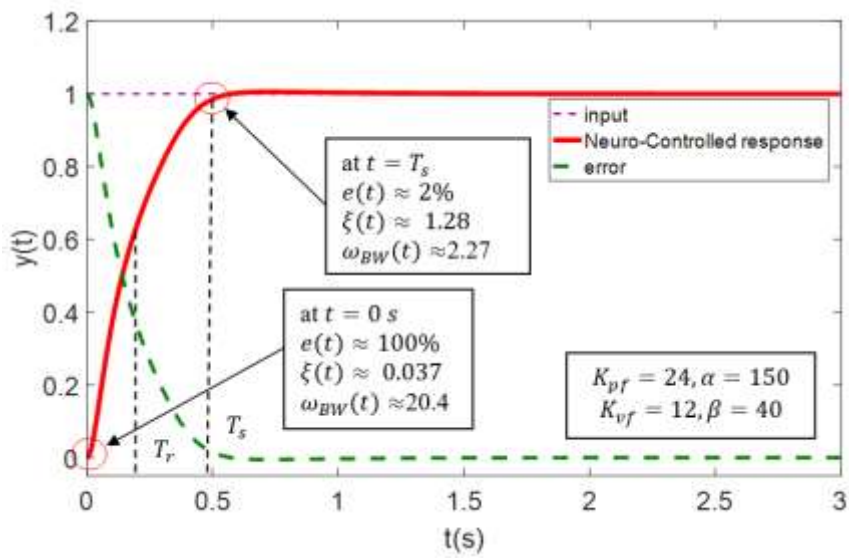

Figure 4.12. Neuro-controlled response of the system $\ddot{x} + (1 - x^2)\dot{x} + x = u(t)$ to a step input. The rise time $T_r = 0.19$s and the settling time $T_s = 0.49$s. The neuro-controller parameters are $K_{pf} = 24$, $K_{vf} = 12$, $\alpha = 150$ and $\beta = 40$. The green dotted line is the system error $e(t)$.

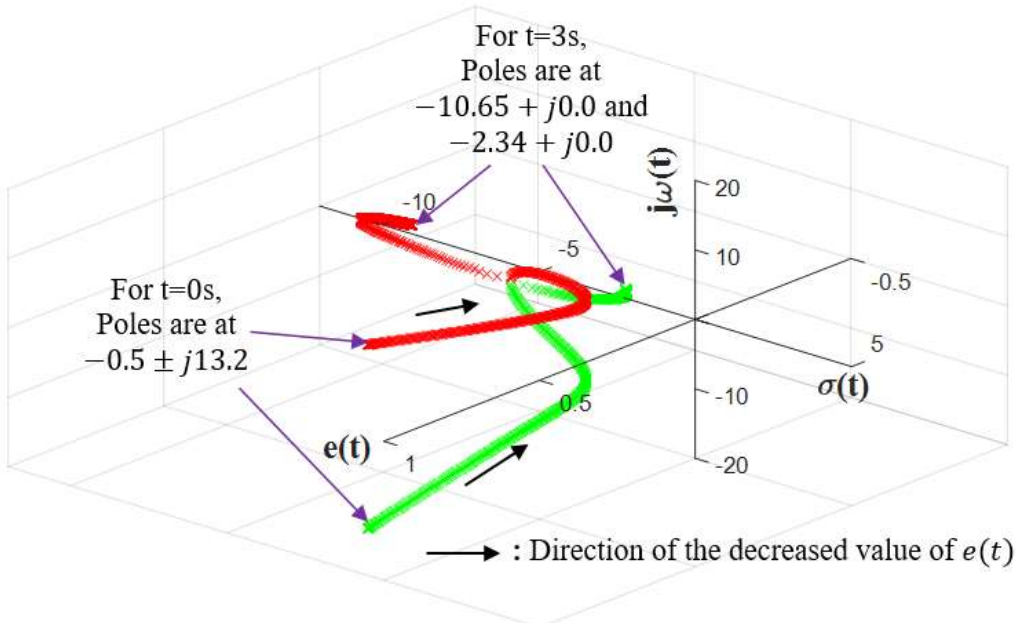

Figure 4.13. Dynamic pole motion of the system $\ddot{x} + (1 - x^2)\dot{x} + x = u(t)$ with a neuro-controller in the complex g −plane for a decreasing error $e(t)$. For $t = 0$s, the dynamic poles are located at $-0.5 \pm j13.2$. When $t = 3$s, the dynamic poles move to $-10.65 + j0.0$ and $-2.34 + j0.0$, respectively.

The position feedback $K_p(e,t)$ and velocity feedback $K_v(e,t)$ of the neuro-controller is,

$$\begin{aligned} K_p(e,t) &= 24 + 150 \times e^2 \\ K_v(e,t) &= 12\exp[-40e^2] + {x_1}^2 \end{aligned} \tag{4.12}$$

where $e(t)$ is the error signal and $\exp[\cdot]$ is an exponential function. Figure 4.14 plots the position feedback $K_p(e,t)$ and the velocity feedback $K_v(e,t)$ of the neuro-controller along with system error $e(t)$. For a large error $e(t)$, the neuro-controller has a higher $K_p(e,t)$ and lower $K_v(e,t)$, or vice versa. At steady-state situation, $K_p(e,t)$, and $K_v(e,t)$ settle themselves to a final value of $K_{pf} = 24$ and $K_{vf} = 12$, respectively. Gain constant $\alpha = 150$ and $\beta = 40$ determine the rate of increasing or decreasing of $K_p(e,t)$, and $K_v(e,t)$ to the system error $e(t)$, respectively.

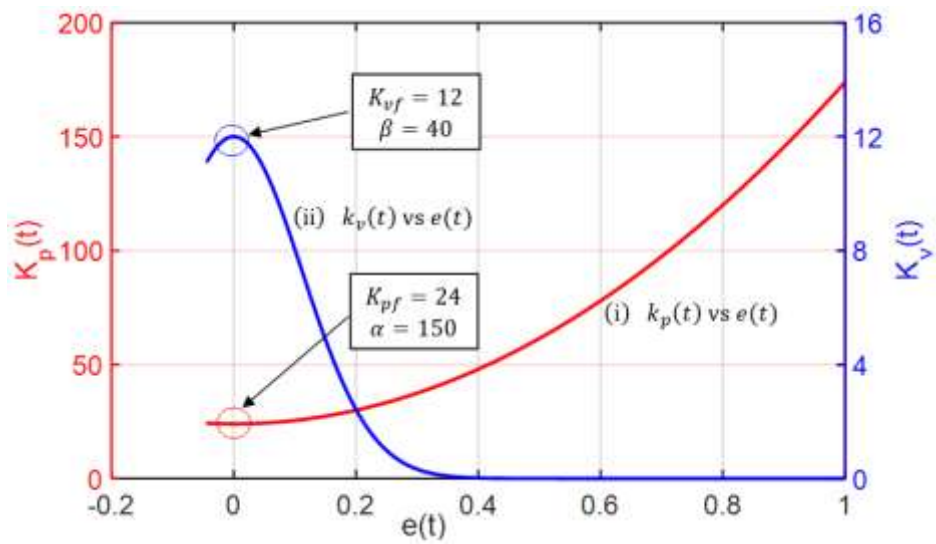

Figure 4.14. The neuro-controller parameters vs. error $e(t)$. (i) The position feedback $K_p(e,t)$ vs. error $e(t)$ and (ii) the velocity feedback $K_v(e,t)$ vs. error $e(t)$.

Figure 4.15 plots the damping ratio $\xi(t)$ of the overall system along with the system error $e(t)$ and time t. As the system dynamics change with time t and error $e(t)$, the damping ratio $\xi(t)$ also changes to get a fast transient response, i.e., very low T_r and T_s with no overshoot $M_p = 0$. When $t = 0$s, damping ratio is $\xi(t)$ =0.037, and the system follows an under-damped and fast response. As the error $e(t)$ is decreased with the increase of time t, the damping ratio $\xi(t)$ is also increased, and the bandwidth $\omega_{BW}(t)$ is decreased, and the system started following to an over-damped system to achieve a zero overshoot $M_p = 0$ in the response. At $t = 3$s, the damping ratio is $\xi(t)$ =1.30. The plot of the dynamic damping ratio $\xi(t)$ along with time t and the error $e(t)$ is shown graphically in Figure 4.15.

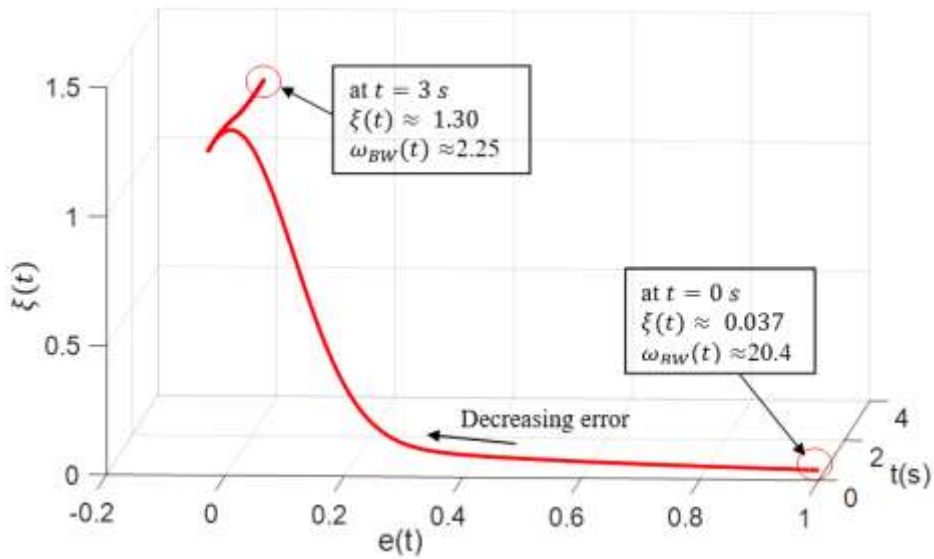

Figure 4.15. The dynamic damping ratio $\xi(t)$ along with time t and the error $e(t)$ of the neuro-controlled system $\ddot{x} + (1 - x^2)\dot{x} + x = u(t)$.

The overall dynamics of the system, Eq. 4.9, with the neuro-controller is,

$$\ddot{\boldsymbol{x}} + \{(1 - {x_1}^2) + 12\exp[-40e^2] + {x_1}^2\}\dot{\boldsymbol{x}} + \{1 + [24 + 150e^2]\}\boldsymbol{x} = \boldsymbol{u}(t) \tag{4.13}$$

The magnitude of the closed-loop frequency response $M(t)$ of the overall neuro-controlled system Eq. 4.13 is,

$$M(t) = \frac{K_{po}(e,t)}{\sqrt{(K_{po}(e,t) - \omega^2)^2 + (\omega K_{vo}(e,t))^2}} \tag{4.14}$$

where ω is the frequency in rad/s.

The overall system position feedback $K_{po}(e,t) = 1 + \{24 + 150e^2\}$,

The overall system velocity feedback $K_{vo}(e,t) = (1 - {x_1}^2) + \{12\exp[-40e^2] + {x_1}^2\}$.

Squaring both sides of Eq. 4.14 and then differentiating with ω^2 and setting the derivative equals to zero gives the maximum resonance value $M_p(t)$ [4].

$$\text{for } 0 \le \xi(t) \le 0.707, \qquad M_p(t) = \frac{1}{2\xi(t)\sqrt{1-\xi(t)^2}}$$
$$\text{for } \xi(t) > 0.707, \qquad M_p(t) = 1 \tag{4.15}$$

where the dynamic damping ratio $\xi(t) = k_{vo}(e,t)/2\sqrt{k_{po}(e,t)}$. From Eq. 4.15, the maximum magnitude of the frequency response curve $M_p(t)$ is inversely related to the dynamic damping ratio $\xi(t)$, and as $\xi(t)$ approaches to zero, $M_p(t)$ approaches to infinity. There will not be a peak at frequencies above zero if $\xi(t) > 0.707$. The relationship between $M_p(t)$ and $\xi(t)$ is shown in Figure 4.16.

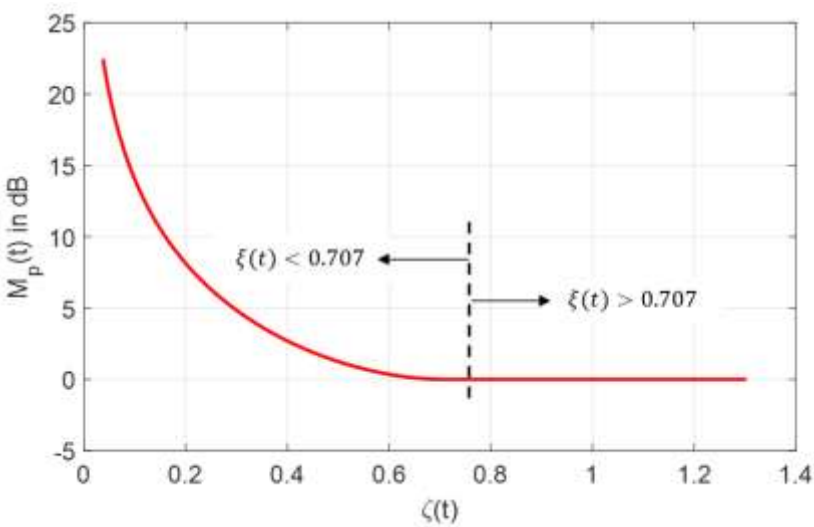

Figure 4.16. The relationship among the maximum magnitude of the frequency response curve $M_p(t)$ and dynamic damping ratio $\xi(t)$.

The variation of the bandwidth of the overall system $\omega_{BW}(t)$ with time t is shown in Figure 4.17. Figure 4.17(a) displays the overall system bandwidth for three different time $t = 0.0$s, $t = 0.25$s and $t = 0.4$s. As the error $e(t)$ decreases, the dynamic damping ratio $\xi(t)$ increases. Because of the inverse relationship among the damping ratio and bandwidth, the dynamic bandwidth $\omega_{BW}(t)$ will also decrease with the increase of the dynamic damping ratio $\xi(t)$. For instance, at time $t = 0.0$s, $t = 0.25$s and $t = 0.4$s, the overall system has a bandwidth

of $\omega_{BW} = 20$ rad/s, $\omega_{BW} = 20$ rad/s and $\omega_{BW} = 20$ rad/s, respectively. Figure 4.17(b) exhibits the relationship of the dynamic bandwidth $\omega_{BW}(t)$ with the error $e(t)$ and time t. Figure 4.17(c) gives a three-dimensional dynamic magnitude frequency plot of the overall neuro-controlled system.

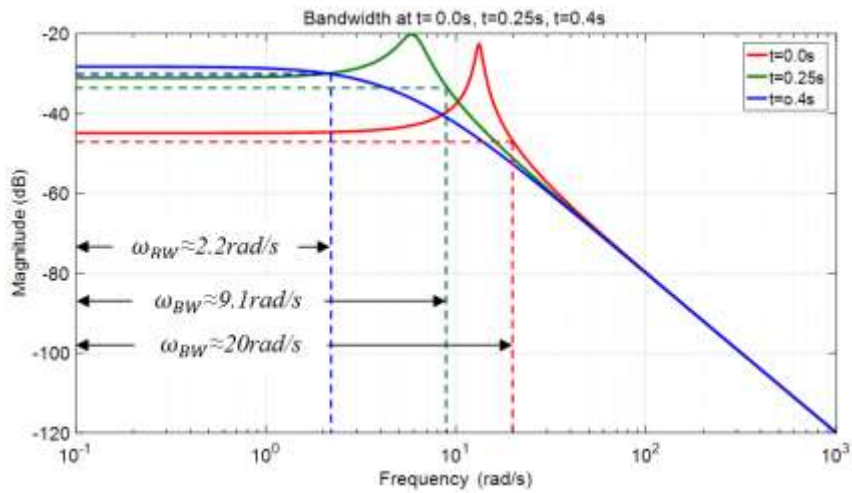

(a) The bandwidth $\omega_{BW}(t)$ of the overall system at $t = 0.0$s, $t = 0.25$s and $t = 0.4$s.

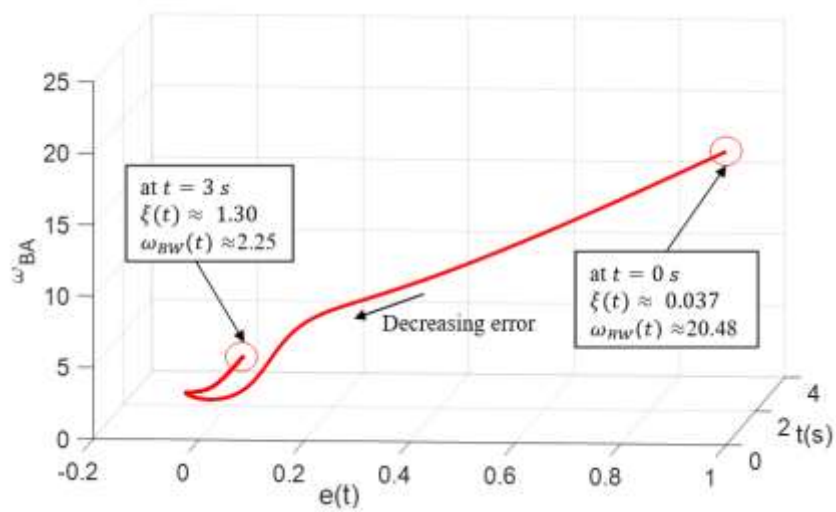

(b) The bandwidth $\omega_{BW}(t)$ of the overall system to the error $e(t)$ and time t.

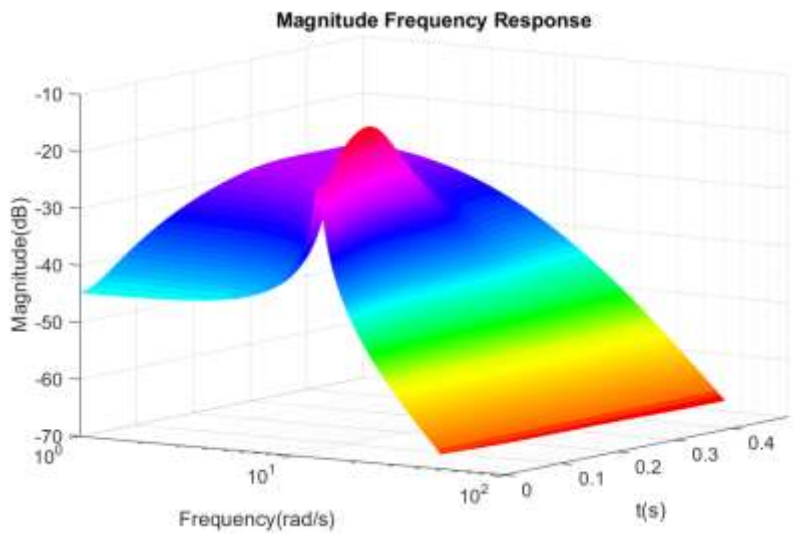

(c) Three-dimensional sketch of the dynamic magnitude frequency plot.

Figure 4.17. The variation of the dynamic bandwidth $\omega_{BW}(t)$ of the overall neuro-controlled system at each time interval.

According to the dynamic Routh's stability criterion (discussed in Chapter 3), the stability is guaranteed for a dynamic system (linear, nonlinear, time-invariant or time-variant) if and only if all the dynamic roots of the dynamic characteristic equation $\mathbf{det}(g\mathbf{I} - \mathbf{A}(\mathbf{x}, t)) = 0$ are kept on the left-half side of the complex g −plane [6]. $\mathbf{I}$ is an $n \times n$ identity matrix, and $\mathbf{A}(\mathbf{x}, t)$ is the system matrix.

The dynamic characteristic equation $\mathbf{det}(g\mathbf{I} - \mathbf{A}(\mathbf{x}, t)) = 0$ of the overall nonlinear system, Eq. 4.13, is given by

$$g^2 + \{(1 - {x_1}^2) + 12\exp[-40e^2] + {x_1}^2\}g + \{1 + [24 + 150e^2]\} = 0 \tag{4.16}$$

where g is a differential operator ($g \triangleq \frac{d}{dt}$). The dynamic Routh's array of the dynamic characteristic equation Eq. 4.16 is,

$$
\begin{array}{c|cc}
g^2 & 1 & \{1+[24+150e^2]\} \\
g^1 & \{(1-{x_1}^2)+12\exp[-40e^2]+{x_1}^2\} & 0 \\
g^0 & \{1+[24+150e^2]\} & 0
\end{array}
\tag{4.17}
$$

Examining the dynamic Routh's array, Eq. 4.17, we can list the overall neuro-controlled system stability.

The overall neuro-controlled system, Eq. 4.13, is stable if and only if $\{(1-{x_1}^2)+12\exp[-40e^2]+{x_1}^2\} > 0$ and $\{1+[24+150e^2]\} > 0$. Both of the elements of the first column of the dynamic Routh's array are positive definite for any values of x_1 and $e(t)$, ensuring that both the dynamic poles are always kept on the left-half side of the complex g −plane. So the stability of the proposed neuro-controlled system, Eq. 4.13, is guaranteed according to the dynamic Routh's stability criterion.

Example 4.3:

A nonlinear time-invariant second-order system is,

$$
\begin{aligned}
\dot{x_1} &= x_2 - ax_1(x_1^2+x_2^2) \\
\dot{x_2} &= -x_1 - ax_2(x_1^2+x_2^2)
\end{aligned}
\tag{4.18}
$$

and the output,

$$y = x_1$$

where a is a positive definite real number. The system matrix $\mathbf{A}(\mathbf{x},t)$ is given by

$$
\mathbf{A}(\mathbf{x},t) = \begin{vmatrix} -a(x_1^2+x_2^2) & 1 \\ -1 & -a(x_1^2+x_2^2) \end{vmatrix}
\tag{4.19}
$$

The elements of matrix $\mathbf{A}(\mathbf{x},t)$ are a function of system states x_1 and x_2, and the states are implicitly time t dependent. The block diagram representation of the state-space model is,

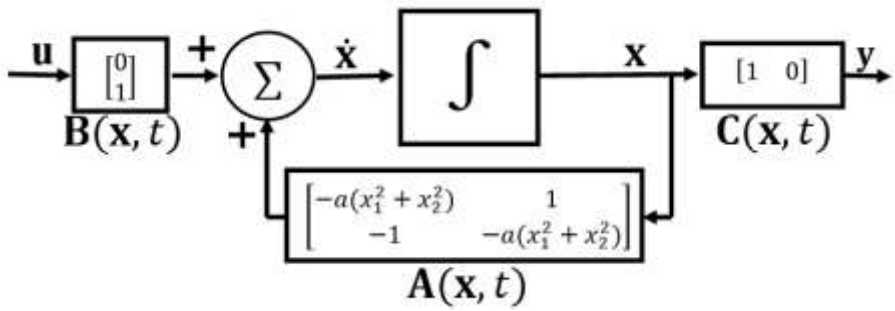

Figure 4.18. Block diagram representation of the state-space model of the nonlinear system, $\dot{x_1} = x_2 - ax_1(x_1^2 + x_2^2)$, $\dot{x_2} = -x_1 - ax_2(x_1^2 + x_2^2)$, and $y = x_1$.

The input-output relationship in terms of g −transfer matrix of the nonlinear time-invariant second-order system Eq. 4.18 is,

$$\mathrm{y}(t) = \left[\frac{1}{g^2 + 2a({x_1}^2 + {x_2}^2)g + a^2({x_1}^2 + {x_2}^2)^2 + 1}\right]u(t) \tag{4.20}$$

Solving the numerator of Eq. 4.20 for g gives the dynamic characteristic equation $\mathbf{det}(g\mathbf{I} - \mathbf{A}(\mathbf{x}, t)) = 0$ of the nonlinear system, Eq. 4.18. From the Eq. 4.20, the system has a conjugate dynamic pole in the complex g −plane.

a is chosen 1. The designed neuro-controller parameters are $K_{pf} = 85$, $K_{vf} = 23$, $\alpha = 50$, and $\beta = 5$. The overall response to a step input is shown in Figure 4.19. At time $t = 0$s, the error is $e(t) = 100\%$, and the neuro-controlled system starts with a damping ratio $\xi(t) = 0.006$, i.e., an under-damped system with a larger bandwidth. At time $t = 0.29s$, the error is $e(t) \approx 2\%$, and the overall system has a damping ratio $\xi(t) = 1.23$. The neuro-controlled response is fast with zero overshoot $M_p = 0\%$. The rise time $T_r = 0.13$s and the settling time $T_s = 0.29$s. A detail of the Simulink model is given in Appendix C (Figure C.3).

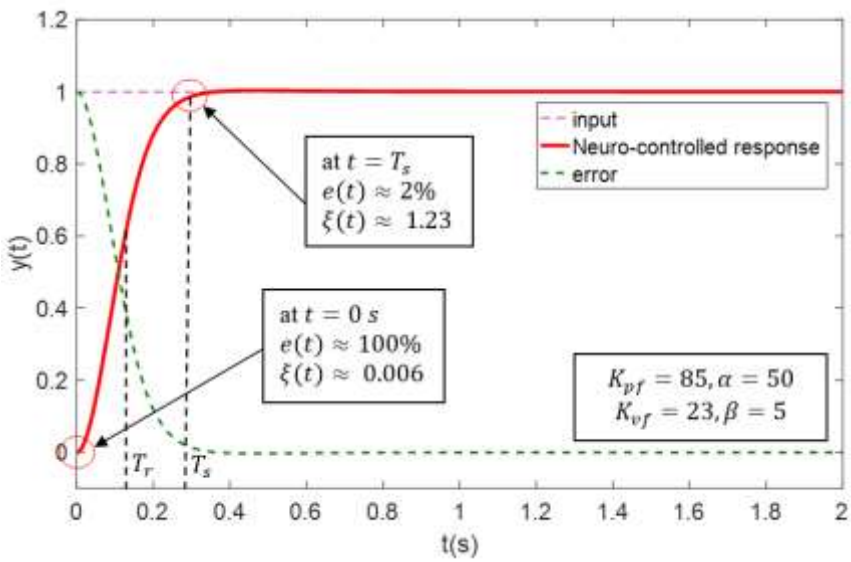

Figure 4.19. The neuro-controlled response of the system defined by Eq. 4.18 to a unit step input. The rise time $T_r = 0.13$s and the settling time $T_s = 0.29$s. the neuro-controller parameters are $K_{pf} = 85$, $K_{vf} = 23$, $\alpha = 50$ and $\beta = 5$. The green dotted line is the system error $e(t)$.

Figure 4.20 demonstrates the natural frequency $\omega_n(t)$ and the damping ratio $\xi(t)$ at various time t and locations of the neuro-controlled response to a step input of the system defined by Eq. 4.18.

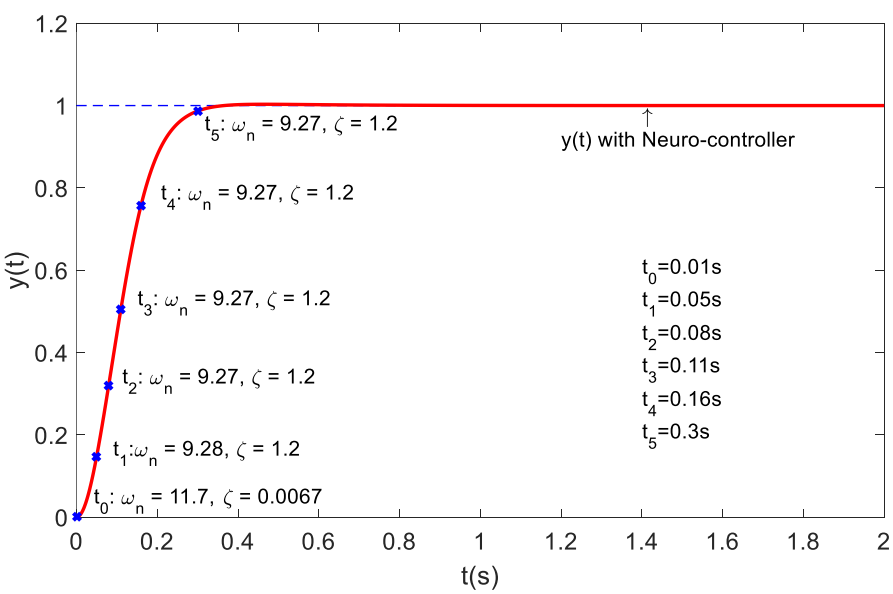

Figure 4.20. The natural frequency $\omega_n(t)$ and the damping ratio $\xi(t)$ at various time t and locations of a unit step neuro-controlled response of the system defined by Eq. 4.18.

Figure 4.21 displays a three-dimensional pole motion plot in the complex g −plane of the overall system for a decreasing error $e(t)$. The third axis of the complex g −plane is representing the system error $e(t)$. When $t = 0$s and $e(t) = 100\%$, the dynamic conjugate poles are located at $-0.07 \pm j11.6$. When $t = 2s$ and $e(t) = 0\%$, dynamic poles are at $-18.3 + j0.0$, and $-4.69 + j0.0$ in the complex g −plane.

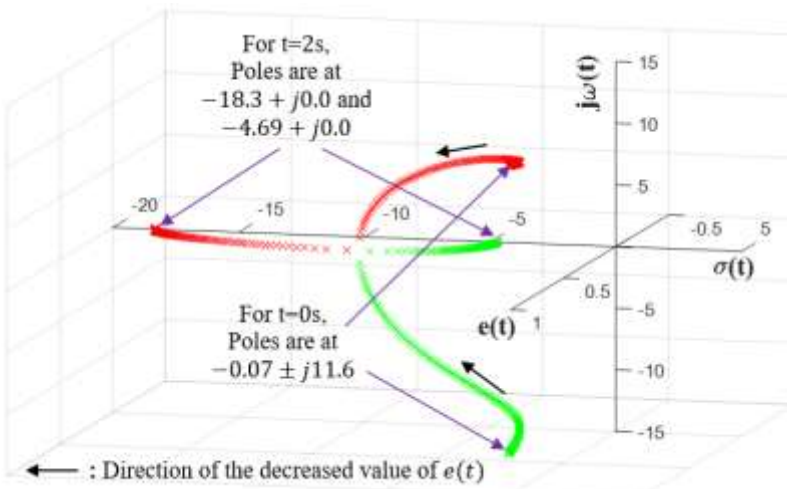

Figure 4.21. The dynamic pole motion of the neuro-controlled system response defined by Eq. 4.18 on the three-dimensional complex g −plane. At $t = 0$s, dynamic poles are at $-0.07 \pm j11.6$ and at t=2s poles are at $-18.3 + j0.0$ and $-4.69 + j0.0$.

The motion of the dynamic poles of the neuro-controlled system in the complex g −plane is determined by the system error $e(t)$. The neuro-controller ensures initial lower damping $\xi(t)$ and higher bandwidth $\omega_{BA}(t)$ of the overall system to achieve a fast response at $t = 0s$. With the increase of time t, neuro-controller keeps updating overall system dominant parameters $\omega_n(t)$ and $\xi(t)$, as a function of the error $e(t)$, to move the system dynamic poles in the complex g −plane such that there is zero overshoot $M_p = 0\%$ on the response. In other words, higher the

damping ratio $\xi(t)$ and lower the bandwidth $\omega_{BA}(t)$ as time t increases and the error $e(t)$ decreases. Figure 4.22 plots the overall system dynamic natural frequency $\omega_n(t)$ and dynamic damping ratio $\xi(t)$ with the increase of time t.

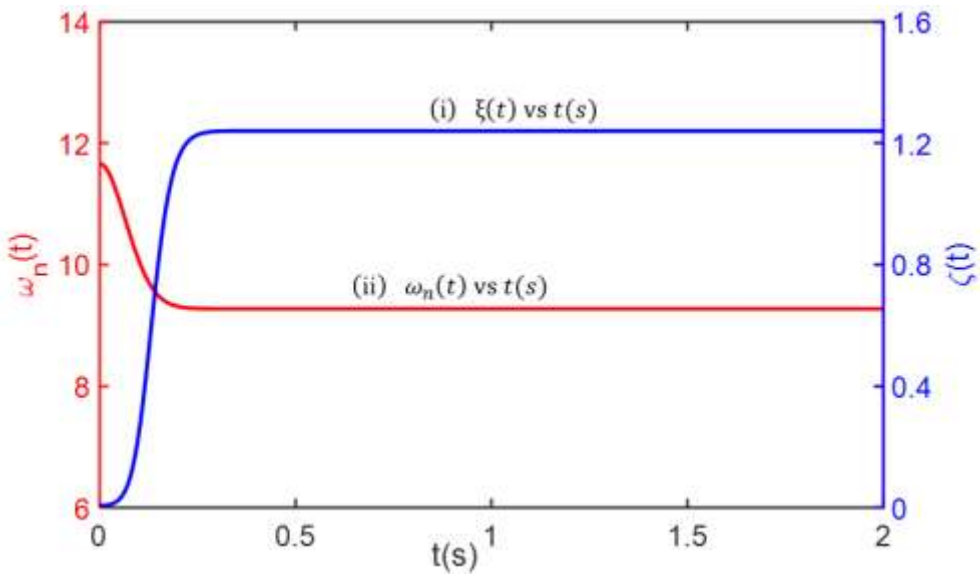

Figure 4.22. A graphical representation of the natural frequency $\omega_n(t)$ vs. damping ratio $\xi(t)$ with the increase of time t of the neuro-controlled system defined by Eq. 4.18.

The position feedback $K_p(e,t)$ and the velocity feedback $K_v(e,t)$ of the neuro-controller is,

$$\begin{aligned} K_p(e,t) &= 85 + 50e^2 \\ K_v(e,t) &= 23\exp[-5e^2] \end{aligned} \tag{4.21}$$

Figure 4.23 plots the position feedback $K_p(e,t)$ and the velocity feedback $K_v(e,t)$ to the system error $e(t)$. For a large error $e(t)$, the overall system has a higher $K_p(e,t)$ and lower $K_v(e,t)$, or vice versa. When $e(t)$ becomes zero, $K_p(e,t)$, and $K_v(e,t)$ settle themselves to a final steady-state value of $K_{pf} = 85$ and $K_{vf} = 23$, respectively. Gain constant $\alpha = 50$, and $\beta = 5$ determines the rate of increasing or decreasing of $K_p(e,t)$, and $K_v(e,t)$, respectively.

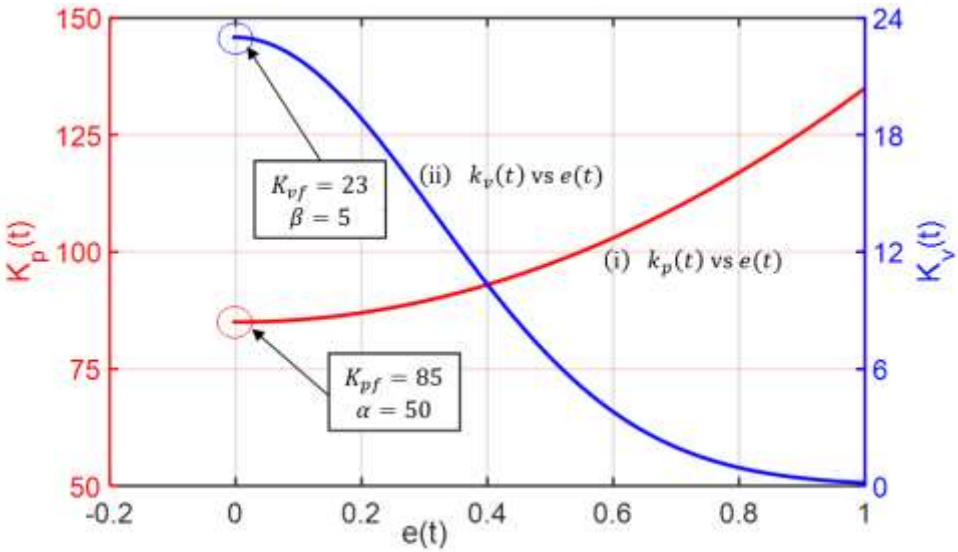

Figure 4.23. The neuro-controller parameters plot to the system error $e(t)$. (i) The position feedback $K_p(e,t)$ vs. error $e(t)$ and (ii) the velocity feedback $K_v(e,t)$ vs. error $e(t)$.

The bandwidth of the overall neuro-controlled system is dynamic. As discussed earlier, the dynamic bandwidth $\omega_{BW}(t)$ of a second-order system depends on the dynamic damping ratio $\xi(t)$. The variation of the bandwidth of the overall neuro-controlled system $\omega_{BW}(t)$ over time t is shown in Figure 4.24. Figure 4.24(a) displays a dynamic bandwidth $\omega_{BW}(t)$ of the overall system for a three different time intervals $t = 0$s, $t = 0.10$s, and $t = 0.15$s. Figure 4.24(b) plots a three-dimensional view of the dynamic magnitude frequency response.

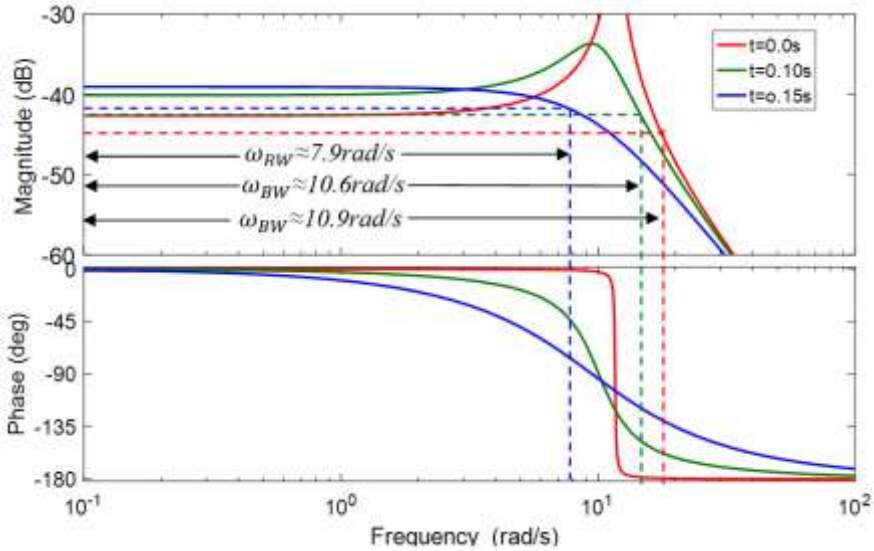

(a) The variation of the bandwidth $\omega_{BW}(t)$ of the overall neuro-controlled system at $t = 0.0$s, $t = 0.10$s, and $t = 0.15$s.

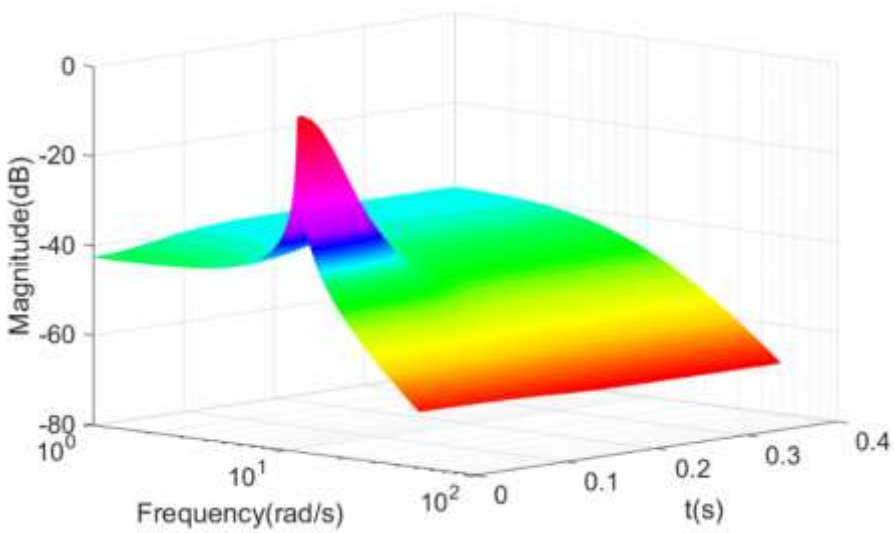

(b) Three-dimensional sketch of the dynamic magnitude frequency plot.

Figure 4.24. The variation of the bandwidth $\omega_{BW}(t)$ of the overall neuro-controlled system defined by Eq. 4.18 at each time interval.

The neuro-controlled response of the system defined by Eq. 4.18 for a periodic input reference $u(t) = \sin\frac{t}{2} + \frac{1}{2}\sin 2t$ is given in Figure 4.25.

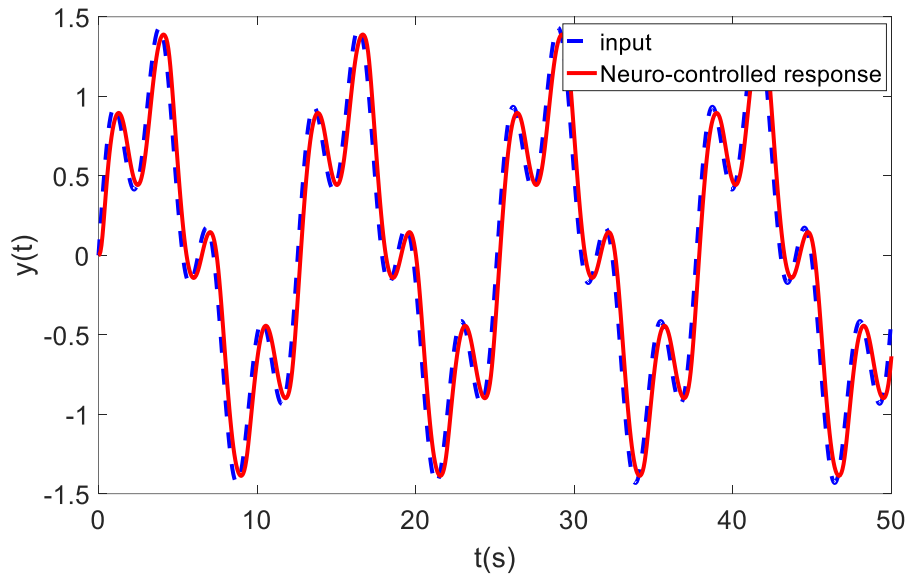

Figure 4.25. The neuro-controlled response for a periodic input reference $u(t) = \sin\frac{t}{2} + \frac{1}{2}\sin 2t$ of the system defined by Eq. 4.18.

According to the dynamic Routh's stability criterion, a second-order differential equation $\ddot{\boldsymbol{x}} + a\dot{\boldsymbol{x}} + b\boldsymbol{x} = \boldsymbol{u}(\boldsymbol{t})$ is stable if and only if coefficient a and b are positive definite, where a and b can be a constant, or a function of system states $\mathbf{x}$ and/or time t [6].

Now, overall dynamics of the neuro-controlled system, Eq. 4.18, is,

$$\ddot{\boldsymbol{x}} + K_{vo}(e,t)\dot{\boldsymbol{x}} + K_{po}(e,t)\boldsymbol{x} = \boldsymbol{u}(\boldsymbol{t}) \tag{4.22}$$

with

The overall system position feedback $K_{po}(e,t) = 1 + a^2({x_1}^2 + {x_2}^2)^2 + [85 + 50e^2]$

The overall system velocity feedback $K_{vo}(e,t) = 2a({x_1}^2 + {x_2}^2) + 23\exp[-5e^2]$

$K_{po}(e,t)$ and $K_{vo}(e,t)$ are positive definite for any values of error $e(t)$ and states x_1, x_2 and the stability of our designed neuro-controlled system Eq. 4.22 is guaranteed according to the dynamic Routh's stability criterion.

Example 4.4:

Consider a nonlinear time-invariant second-order system with an input $u(t)$ is presented by

$$\begin{aligned} \dot{x_1} &= x_2 \\ \dot{x_2} &= -(\sin x_1)x_2 + x_3 \\ \dot{x_3} &= -(30 + {x_2}^2)x_1 - (17 + {x_1}^2)x_2 - 8x_3 + u(t) \end{aligned} \tag{4.23}$$

and the output,

$$y = 5x_1 + x_2$$

where $x_1 = x$, $x_2 = \dot{x}$, and $x_3 = \ddot{x}$ are the states of the dynamic system. y is the output. The system matrix $\mathbf{A}(\mathbf{x},t) = \begin{bmatrix} 0 & 1 & 0 \\ 0 & -\sin x_1 & 1 \\ -(30+{x_2}^2) & -(17+{x_1}^2) & -8 \end{bmatrix}$. The input matrix $\mathbf{B}(t) = \begin{bmatrix} 0 \\ 0 \\ 1 \end{bmatrix}$, and the output matrix $\mathbf{C}(\mathbf{x},t) = [5 \quad 1 \quad 0]$. The state x_1 and x_2 dependent nonlinear elements in the system matrix $\mathbf{A}(\mathbf{x},t)$ create the nonlinearity. The equivalent block diagram is,

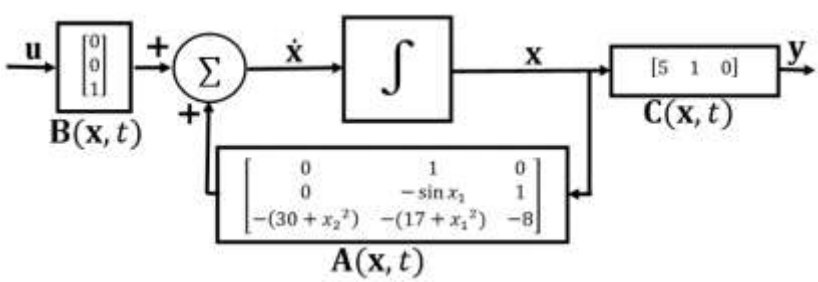

Fig 4.26. The block diagram representation of the state-space model of the nonlinear dynamic system defined by Eq. 4.23.

The input-output relationship regarding the g −transfer matrix of the nonlinear system, Eq. 4.23, is given by

$$\mathrm{y}(t) = \left[\frac{g+5}{g^3 + (8+\sin x_1)g^2 + (17 + {x_1}^2 + 8\sin x_1)g + (30 + {x_2}^2)}\right]\mathrm{u}(t) \tag{4.24}$$

Solving the numerator of Eq. 4.24 for g gives the dynamic characteristic equation $\mathbf{det}(g\mathbf{I} - \mathbf{A}(\mathbf{x}, t)) = 0$ of the nonlinear system, Eq. 4.23. This nonlinear system has three dynamic poles, two of them are conjugate, and a dynamic zero in the complex g −plane.

The neuro-controller parameters are determined according to the design procedure described in Section 4.2 and 4.3. The position feedback $K_p(e,t)$, the velocity feedback $K_v(e,t)$ and the acceleration feedback $K_a(e,t)$ of the neuro-controller are,

$$\begin{aligned} K_p(e,t) &= 650 + 600e^2 \\ K_v(e,t) &= 250\exp[-6e^2] \\ K_a(e,t) &= 25 + e^2 \end{aligned} \tag{4.25}$$

When error $e(t)$ is large, the neuro-controlled ensures that the overall system has a higher $K_p(e,t)$ and lower $K_v(e,t)$, or vice versa. Acceleration feedback $K_a(e,t)$ ensures initial higher acceleration for large error $e(t)$. $K_p(e,t)$, $K_v(e,t)$ and $K_a(e,t)$ settles themselves to a final steady-state value of $K_{pf} = 650$, $K_{vf} = 250$ and $K_{af} = 25$, respectively. Gain constant $\alpha = 600$, $\beta = 6$, and $\gamma = 1$ determine the rate of increasing or decreasing of $K_p(e,t)$, $K_v(e,t)$ and $K_a(e,t)$, respectively. A detail of the Simulink model is given in Appendix C (Figure C.4).

The neuro-controlled system response to a step input is shown in Figure 4.27. The rise time $T_r = 0.14$s and the settling time $T_s = 0.31$s. For $t = 0$s, the conjugate dynamic poles are located at $0.28 \pm j6.07$, and the final locations are at $-5.26 + j1.58$. The third dynamic pole moves from -34.5 to -22.4 on the real axis of the complex g −plane, and the dynamic zero is located at -5. A three-dimensional sketch of the dynamic pole motion of the overall system with

the increase of time t and decrease of the error $e(t)$ in the complex g −plane is plotted in Figure 4.28. The arrowhead indicates the decreased value of the error $e(t)$.

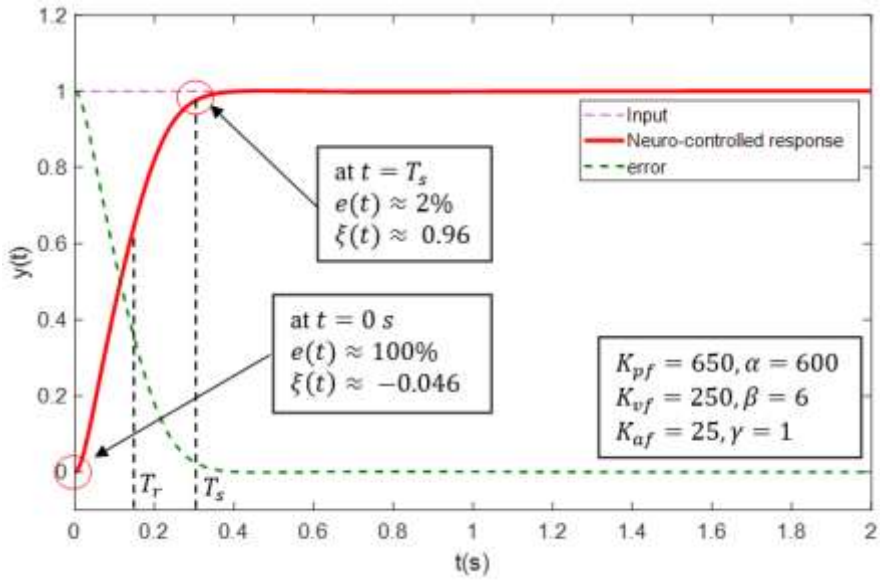

Figure 4.27. The neuro-controlled response of the system defined by Eq. 4.23 to a unit step input. The rise time $T_r = 0.19$s and the settling time $T_s = 0.49$s. The neuro-controller parameters are $K_{pf} = 650$, $K_{vf} = 250$, $K_{af} = 25$, $\alpha = 18$, $\beta = 12$ and $\gamma = 1$. The green dotted line is the system error $e(t)$.

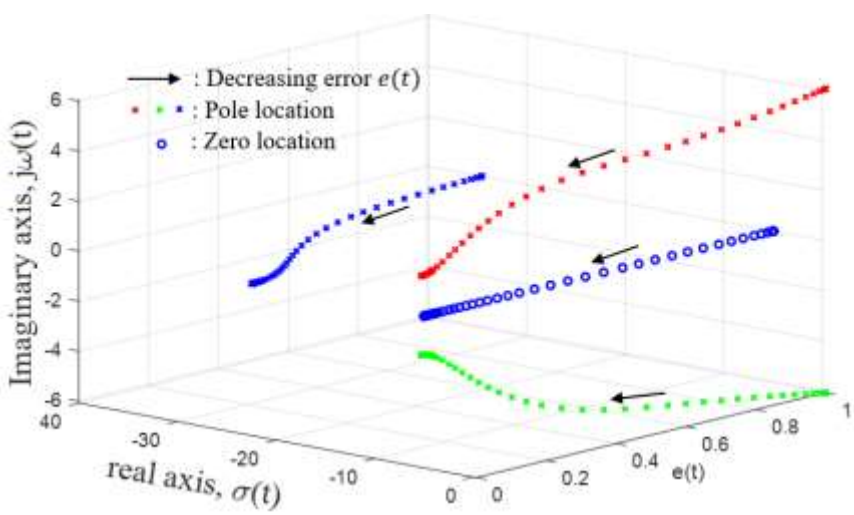

Figure 4.28. The dynamic pole motion of the neuro-controlled system defined by Eq. 4.23 in the complex g −plane.

A two-dimensional projection of the three-dimensional dynamic root locus Figure 4.28 is shown in Figure 4.29.

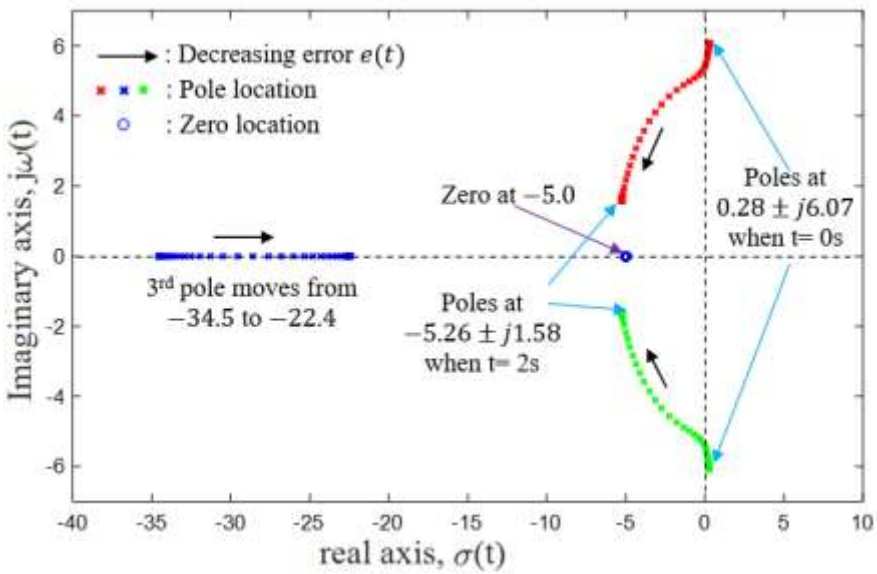

Figure 4.29. A two-dimensional projection of Figure 4.28. When $t = 0$s, the conjugate dynamic poles are located at $0.28 \pm j6.07$, and the final locations are at $-5.26 + j1.58$. The third dynamic pole moves from -34.5 to -22.4 on the real axis of the complex g −plane.

Figure 4.30 plots the position feedback $K_p(e,t)$ and the velocity feedback $K_v(e,t)$ regarding the system error $e(t)$.

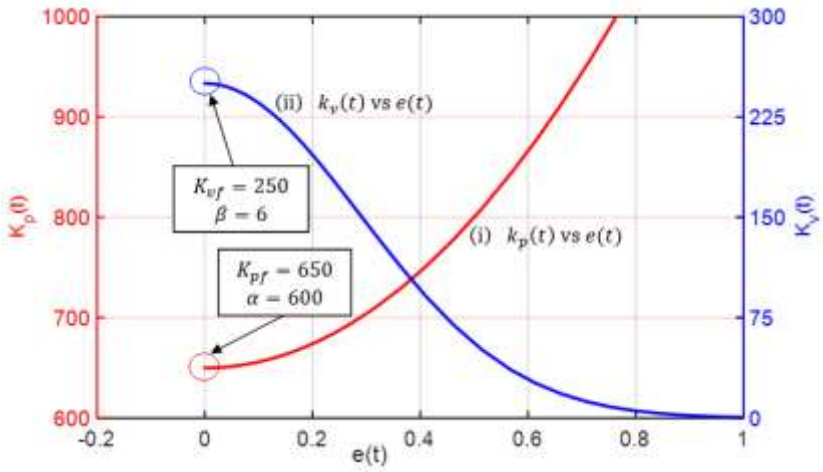

Figure 4.30. The neuro-controller parameters plot to the system error $e(t)$. (i) The position feedback $K_p(e,t)$ vs. error $e(t)$, and (ii) velocity feedback $K_v(e,t)$ vs. error $e(t)$.

Figure 4.31 is showing the relationship of the dynamic natural frequency $\omega_n(t)$ and the dynamic damping ratio $\xi(t)$ of the neuro-controlled system with the increase of time t. Figure 4.32 gives the plot of the dynamic damping ratio $\xi(t)$ of the overall system regarding the system error $e(t)$ and time t. When time $t = 0$s, dynamic damping ratio is $\xi(t) = -0.046$, and the neuro-controlled system follows an under-damped system to get a fast response. As the error $e(t)$ decreases and time t increases, the dynamic damping ratio $\xi(t)$ also increases and the dynamic bandwidth $\omega_{BW}(t)$ decreases to achieve a zero overshoot $M_p = 0\%$ in the response. At $t = 2$s, dynamic damping ratio is $\xi(t)$ =0.957.

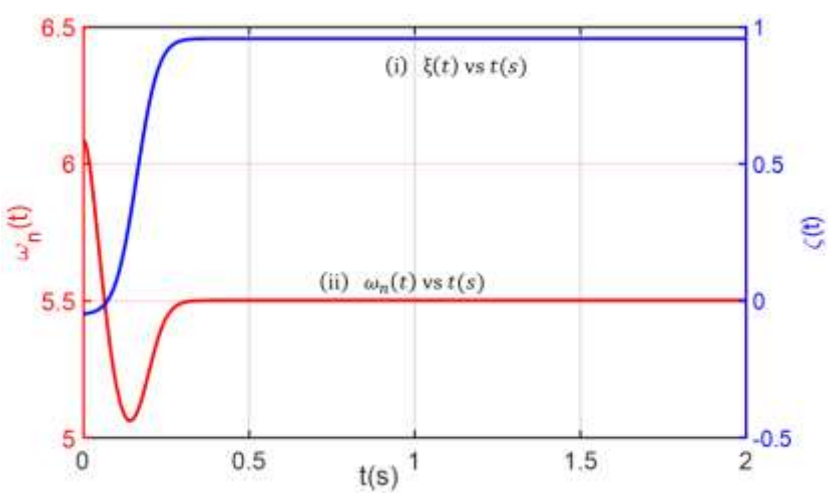

Figure 4.31. A graphical representation of the natural frequency $\omega_n(t)$ vs. damping ratio $\xi(t)$ with the increase of time t of the system defined by Eq. 4.23 with a neuro-controller.

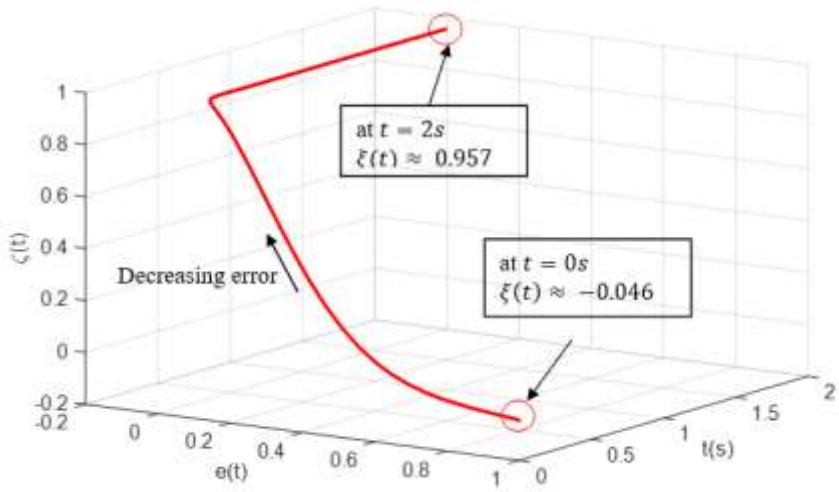

Figure 4.32. The dynamic damping ratio $\xi(t)$ vs. error $e(t)$ and time t of the system defined by Eq. 4.23 with a neuro-controller.

The variation of the bandwidth of the overall system $\omega_{BW}(t)$ at time t is shown in Figure 4.33. Figure 4.33(a) displays the overall system bandwidth for three different time $t = 0.0$s, $t = 0.07$s and $t = 0.2$s. As error $e(t)$ decreases, the dynamic damping ratio $\xi(t)$ increases. Because of the inverse relationship among the damping ratio and the bandwidth, the dynamic bandwidth $\omega_{BW}(t)$ will decrease with the increase of the dynamic damping ratio $\xi(t)$. For example, at time $t = 0.0$s, $t = 0.07$s, and $t = 0.2$s, the overall system has a bandwidth $\omega_{BW} = 9.5$ rad/s, $\omega_{BW} = 8.1$ rad/s, and $\omega_{BW} = 3.7$ rad/s, respectively. Figure 4.16(c) presents a three-dimensional magnitude frequency response plot of the overall neuro-controlled system.

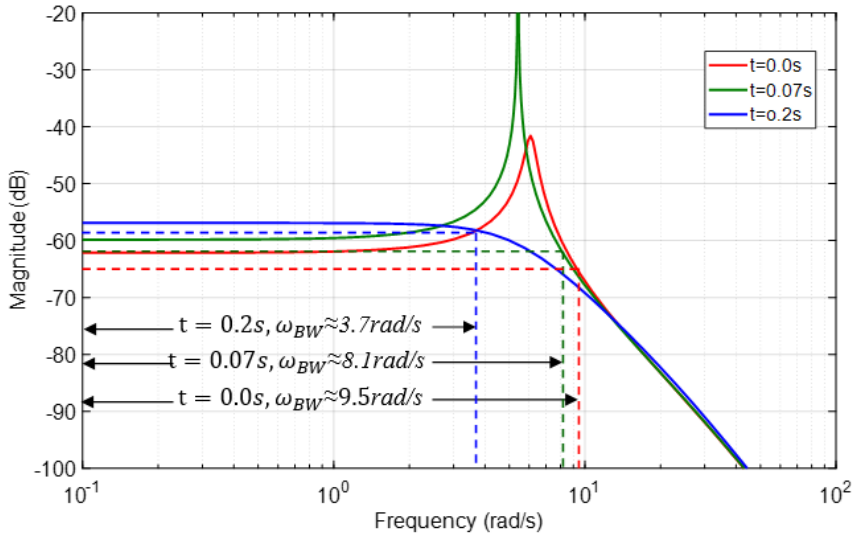

(a) The bandwidth $\omega_{BW}(t)$ of the neuro-controlled system at $t = 0.0$s, $t = 0.07$s and $t = 0.2$s.

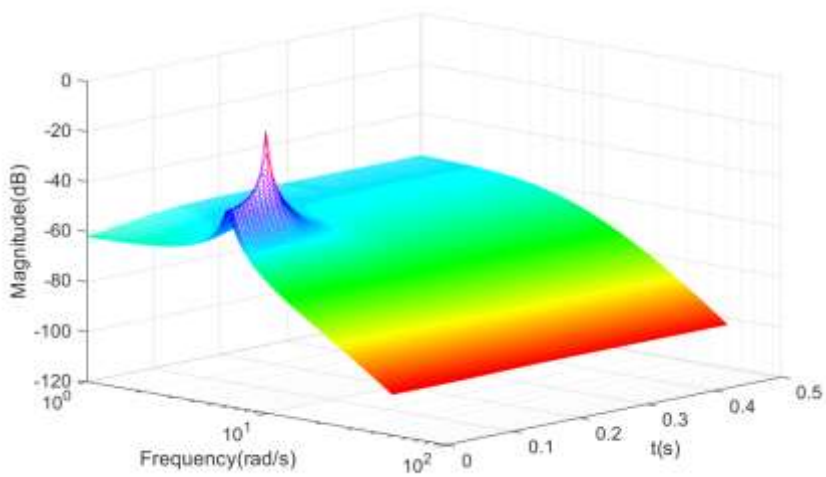

(b) Three-dimensional sketch of the dynamic magnitude frequency response.

Figure 4.33. The variation of the dynamic bandwidth $\omega_{BW}(t)$ of the overall system at each time interval of the overall neuro-controlled system Eq. 4.23.

The neuro-controlled response for a periodic input reference $u(t) = \sin\frac{t}{2} + \frac{1}{2}\sin\frac{3}{4}t + \frac{1}{2}\sin t$ is given in Figure 4.34.

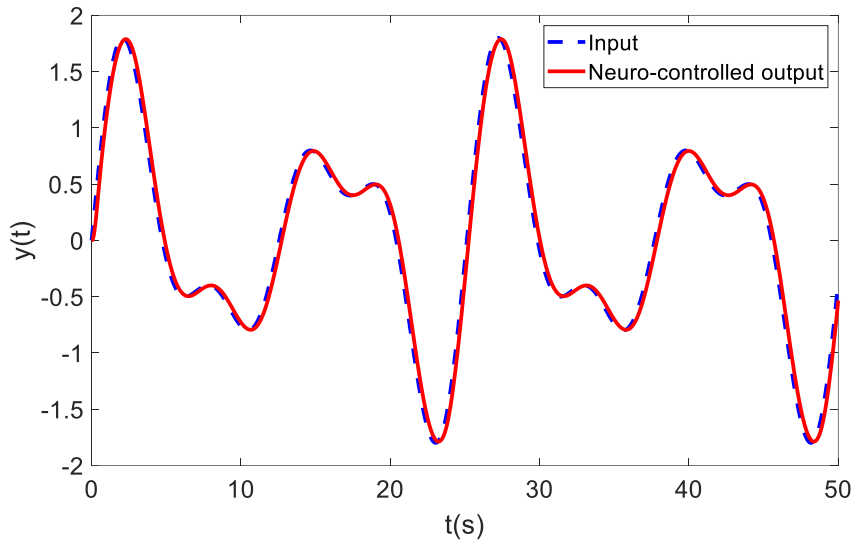

Figure 4.34. The neuro-controlled response for a periodic input reference $u(t) = \sin\frac{t}{2} + \frac{1}{2}\sin\frac{3}{4}t + \frac{1}{2}\sin t$ of the nonlinear system defined by Eq. 4.23.

The dynamic characteristic equation $\mathbf{det}\big(g\mathbf{I} - \mathbf{A}(\mathbf{x}, t)\big) = 0$ of the overall nonlinear system is,

$$g^3 + \{33 + \sin x_1 + e^2\}g^2 + \{(17 + {x_1}^2 + 8\sin x_1) + 250\exp[-6e^2]\}\,g + \{680 + {x_2}^2 + 600e^2\}=0 \tag{4.26}$$

According to the dynamic Routh's stability criterion, a third-order differential equation $\dddot{\boldsymbol{x}} + a\ddot{\boldsymbol{x}} + b\dot{\boldsymbol{x}} + c\boldsymbol{x} = \boldsymbol{u}(\boldsymbol{t})$ is stable if and only if coefficient a, b, and c are positive definite and $ab > c$. a, b and c can be a constant, or a function of system states $\mathbf{x}$ and/or time t.

The overall dynamics of the neuro-controlled system is,

$$\dddot{\boldsymbol{x}} + k_{ao}(e,t)\ddot{\boldsymbol{x}} + K_{vo}(e,t)\dot{\boldsymbol{x}} + K_{po}(e,t)\boldsymbol{x} = \boldsymbol{u}(\boldsymbol{t}) \tag{4.27}$$

with

The overall system position feedback $K_{po}(e,t) = 680 + {x_2}^2 + 600e^2$

The overall system velocity feedback $K_{vo}(e,t) = (17 + {x_1}^2 + 8\sin x_1) + 250\exp[-6e^2]\}$

The overall system acceleration feedback $K_{ao}(e,t) = 33 + \sin x_1 + e^2$

It is visible that $K_{po}(e,t)$, $K_{vo}(e,t)$ and $K_{ao}(e,t)$, are positive definite for any values of error $e(t)$ and system states x_1 and x_2. When $e \to 0$, $k_{ao} \times k_{vo} > k_{po}$ and stability of our designed neuro-controlled system of the nonlinear equation, Eq. 4.23, is guaranteed according to the dynamic Routh's stability criterion.

4.5 Summary

In this Chapter, a dynamic pole motion in the complex g −plane based neuro-controller was designed for a dynamic system to achieve a faster transient response and a zero overshoot on the system response. The neuro-controller is a highly nonlinear controller, and the controller parameters are the position feedback $K_p(e,t)$, and the velocity feedback $K_{vo}(e,t)$. $K_p(e,t)$ and $K_v(e,t)$ are a function of the system error $e(t)$, and various types of possible functions are given at Table 4.1. $K_p(e,t)$ controls the speed of the response, whereas $K_v(e,t)$ controls the brake. The concepts of a neuro-controller were illustrated with the help of four numerical examples.

The neuro-controlled response is very faster without overshoot compared to the uncontrolled response in those four examples. A neuro-controller ensures a smaller damping ratio $\xi(t)$ with a larger bandwidth $\omega_{BW}(t)$ for a large error $e(t)$, and a larger damping ratio $\xi(t)$ with a smaller bandwidth $\omega_{BW}(t)$ for a small error $e(t)$.

Finally, the stability of the designed neuro-controlled systems was established by applying the dynamic Routh's stability criterion.

Chapter 5
Concluding Remarks and Future Work

5.1 Overview and Conclusions

In this thesis, the concepts of dynamic poles, dynamic characteristic equation, dynamic Routh's stability criterion, dynamic Bode and Nyquist plots, for the stability analysis and the neuro-controller design of nonlinear systems, are presented. A dynamic Nyquist criterion is developed to analyze the relative stability as well as the frequency domain characteristics. This research leads us to originate a unifying novel methodology based upon pole motion for the stability analysis and the design of feedback controllers for both linear and nonlinear systems.

A comprehensive numerical analysis is presented. System characteristics, e.g., the stability of the system and the quality of the response, depends on the location of dynamic dominant poles in the complex g −plane. Besides, the location of the dynamic poles in the complex g −plane is a function of system parameters, e.g., system states $\mathbf{x}$. The system states $\mathbf{x}$ depend on time t implicitly and the input signal $\mathbf{u}(t)$ explicitly. The input signal $\mathbf{u}(t)$ is a function of amplitude and frequency. Thus, time t, the system states $\mathbf{x}$, and the input signal $\mathbf{u}(t)$ are responsible for the stability and the quality of response of a nonlinear dynamic system.

The accomplishments of this thesis are summarized below:

(1) A mathematical background on the representation of a nonlinear system and their characteristics in the complex g −plane are presented in Chapter 2. The primary work done at [6] is extended with the inclusion of a general state-space representation of a nonlinear system and its graphical representation, the derivation of the relation among the output vector $\mathbf{y}(t)$ to the input vector $\mathbf{u}(t)$ through the g −transfer matrix, the formation of the dynamic characteristic equation $\mathbf{det}\big(g\mathbf{I} - \mathbf{A}(\mathbf{x}, t)\big) = 0$, dynamic poles and zeros in the complex g −plane, and the

sketching procedure of dynamic root locus and dynamic root contour from the dynamic characteristic equations.

The state and output equations of any nonlinear system are represented by

$$\begin{aligned} \dot{\mathbf{x}}(t) &= \mathbf{A}(\mathbf{x},t)\mathbf{x}(t) + \mathbf{B}(t)\mathbf{u}(t)\ , \quad \mathbf{x}(0) \\ \mathbf{y}(t) &= \mathbf{C}(\mathbf{x},t)\mathbf{x}(t) + \mathbf{D}(t)\mathbf{u}(t) \end{aligned} \tag{5.1}$$

The elements of the system matrix $\mathbf{A}(\mathbf{x},t)$ are the function of states $\mathbf{x}$ and/or time t. The system states $\mathbf{x}$ are a function of input $\mathbf{u}(t)$ in both amplitude and frequency. The state-space representation of a linear time-invariant system is a subset of the general state-space representation of a nonlinear system, Eq. 5.1. The input $\mathbf{u}(t)$ and output $\mathbf{y}(t)$ relation through the g −transfer matrix of a nonlinear system is,

$$\mathbf{y}(t) = \left[\frac{\mathbf{C}(\mathbf{x},t)\mathbf{adj}\big(g\mathbf{I} - \mathbf{A}(\mathbf{x},t)\big)\mathbf{B}(t) + \mathbf{det}\big(g\mathbf{I} - \mathbf{A}(\mathbf{x},t)\big)\mathbf{D}(t)}{\mathbf{det}\big(g\mathbf{I} - \mathbf{A}(\mathbf{x},t)\big)}\right]\mathbf{u}(t) \tag{5.2}$$

Solving the denominator of the g −transfer matrix for g gives the location of dynamic poles in the complex g −plane whereas solving the numerator gives the location of dynamic zeros. The dynamic roots of the dynamic characteristic equation $\mathbf{det}\big(g\mathbf{I} - \mathbf{A}(\mathbf{x},t)\big)$ are [6],

$$g(t) \ = \sigma(t) + j\omega(t) \tag{5.3}$$

where $\sigma(t)$ and $j\omega(t)$ are the state $\mathbf{x}$ and time t dependent real parts and imaginary parts of the dynamic roots $g(t)$, respectively. It is also discussed that s ($\triangleq \frac{d}{dt}$) operator is used only for a linear time-invariant system and is a subset of g operator. g operator is applicable to linear, nonlinear, time-variant, or time-invariant dynamic systems, simultaneously.

Rearranging the dynamic characteristic equation $\mathbf{det}\big(g\mathbf{I} - \mathbf{A}(\mathbf{x},t)\big)$,

$$1 + \frac{\mathrm{K}(\mathbf{x},t)\big(g + z_1(\mathbf{x},t)\big)\big(g + z_2(\mathbf{x},t)\big)\cdots(g + z_m(\mathbf{x},t))}{(g + p_1(\mathbf{x},t))(g + p_1(\mathbf{x},t))\cdots(g + p_n(\mathbf{x},t))} = 0 \tag{5.4}$$

$(g + p_i(\mathbf{x},t))$, $i = 1,2,\ldots.,n$, gives the locations of dynamic poles in the complex g −plane and $(g + z_k(\mathbf{x},t))$, $k = 0,1,2,\ldots,m$, gives the locations of dynamic zeros. $\mathrm{K}(\mathbf{x},t)$ is the system state $\mathbf{x}$ and time t dependent dynamic gain, and determines the path of dynamic roots in the complex g −plane.

The dynamic root contour of a nonlinear and/or time-variant system is sketched on the g −plane by varying multiple parameters, respectively, from zero to infinity.

(2) The stability of a nonlinear system depends on the location of dynamic poles in the complex g −plane. At least one of the dynamic poles on the right-hand side of the complex g −plane makes the system unstable with an increasing amplitude to the response, with a variation of system parameters. The dynamic poles located on the $j\omega$ −axis create an oscillatory response, and the dynamic poles on the left-hand side create a stable equilibrium to the response.

The initial work on the construction of a dynamic Routh's array from a dynamic characteristic equation, $\mathbf{det}\big(g\mathbf{I} - \mathbf{A}(\mathbf{x},t)\big) = 0$, and the absolute stability analysis of a nonlinear system using the dynamic Routh's stability criterion was carried out in [6]. The concept is elaborated for the relative stability analysis in the frequency domain of a nonlinear system with the development of the dynamic Nyquist criterion. The dynamic Nyquist and Bode plots, dynamic gain and phase margins are also introduced in Chapter 3. The dynamic Routh's stability analysis is also applied to do a phase plane analysis of a second-order system to define the stability region.

Dynamic Routh's stability criterion gives a quantitative measure of the locations and number of dynamic poles in the complex g −plane. The elements of the dynamic Routh's array contains the state $\mathbf{x}$ and time t dependent nonlinear terms. The stability analysis of a linear time-invariant dynamic system using Routh's stability criterion is a subset of the stability analysis of a nonlinear system having dynamic poles.

The stability is guaranteed for a nonlinear system if all the elements of the first column of the dynamic Routh's array have a positive non-zero value [6]. A zero at any rows of the first column of the dynamic Routh's array means an oscillatory dynamic pole on the $j\omega$ −axis. The number of dynamic poles located on the right-half side of the complex g −plane is equal to the number of sign changes in the first column of the dynamic Routh's array [6].

Besides, the stability of a nonlinear dynamic system not only depends on the system parameters but also depends on the input signals. The input signals are a function of amplitude and frequency. For instance, a nonlinear is stable for low frequencies and high frequencies but can be unstable for a range of frequencies.

A dynamic Nyquist criterion is developed in this thesis to study the stability of the nonlinear systems in the frequency domain. In the frequency domain, $g \triangleq j\omega$ where ω is in rad/s. The dynamic characteristic equation, Eq. 5.4, can also be written as

$$1 + \mathbf{L}(g) = 0 \tag{5.5}$$

where

$$\mathbf{L}(g) = \frac{\mathrm{K}(\mathbf{x}, t)\big(g + z_1(\mathbf{x}, t)\big)\big(g + z_2(\mathbf{x}, t)\big) \cdots (g + z_m(\mathbf{x}, t))}{(g + p_1(\mathbf{x}, t))(g + p_1(\mathbf{x}, t)) \cdots (g + p_n(\mathbf{x}, t))} \tag{5.6}$$

The dynamic Nyquist criterion is stated by

A nonlinear dynamic system is stable, if the dynamic Nyquist plot of $\boldsymbol{L}(g)$ encircles the $(-1, j0)$ point in $\boldsymbol{L}(g)$ −plane, in the clockwise direction, as many times as the number of dynamic poles of $\boldsymbol{L}(g)$ that are in the right half of the complex g −plane, and inside the encirclement, if any.

(3) The characteristics of a transient response of a nonlinear system also depend on the location of dynamic poles in the complex g −plane. For instance, a second-order system response can be over-damped, under-damped, critically-damped, or undamped based on the location of dynamic poles in the complex g −plane. Chapter 3 is devoted to making a more comprehensive descriptions and analysis of the neuro-controller design techniques primarily developed in [7], with the help of several nonlinear dynamic system examples.

The neuro-controller determines the transient response of a system by adjusting its parameters to locate the dynamic poles in the complex g −plane by changing the overall dynamics of the controlled system. The neuro-controller parameters are position feedback $K_p(e,t)$ and velocity feedback $K_v(e,t)$, and they are not constant rather function of system error, $e(t) = r(t) - y(t)$.

As error changes from a large value to a small value, $K_p(e,t)$ is varied from a very large value to a small value, and simultaneously $K_v(e,t)$ is varied from a very small value to large value, letting for a larger bandwidth for a large error and a smaller bandwidth for a small error [7]. Various types of functions can be designed for $K_p(e,t)$ and $K_v(e,t)$ by following the design criteria. A typical example is,

$$\begin{aligned} K_p(e,t) &= K_{pf} + \alpha e^2(t) \\ K_v(e,t) &= K_{vf}\exp(-\beta e^2(t)) \end{aligned} \tag{5.7}$$

α and β are gain constants which determines the slope of the functions $K_p(e,t)$ and $K_v(e,t)$. K_{vf} and K_{pf} are the final steady-state values.

A proper selection of the controller parameters $K_p(e,t)$ and $K_v(e,t)$ guarantee that the location of the dynamic poles is always kept on the left-hand side of the complex g −plane ensuring the stability of the overall controlled system according to the dynamic Routh's stability criterion, discussed in Chapter 3.

5.2 Future Works

In this thesis, we have successfully established the proof-of-concept of the dynamic pole motion in the complex g −plane based stability analysis and neuro-controller design through the modeling and simulation of some complex nonlinear dynamic systems. Some contentions can be undertaken to extend this research in the future.

(1) We have determined the neuro-controller parameters for the systems with a known dynamics. Neuro-controller design can be extended for partially known dynamic systems with uncertain situations.

(2) The dynamic pole motion based stability analysis and neuro-control concept presented in this thesis can be extended for the efficient optimization and control of the interconnected nonlinear systems with multiple numbers of feedback loops, which usually appears in the field of robotics, traffic, transportation, power, and ecosystem, etc. As the g −transfer matrix is a summation of several rational functions and the dynamic poles and zeros may be unknown. However, a systematic approach based on the pole motion can be carried out to study the multi-loop nonlinear systems.

(3) Throughout this thesis, the optimization and stability properties were discussed for a continuous system without delays. However, the dynamic Routh's stability criterion for the stability analysis and the neuro-controller design for a continuous system can be extended for the discrete systems and the systems with time delays, as well.

(4) The theoretical studies can be applied to create an efficient and adaptive learning algorithm in the disciplines of neural optimization, and neuro-vision systems for their applications to industrial, socio-economical, group decision making and robotic systems.

(5) The neuro-controller designed in this thesis is only for single-input-single-output (SISO) systems. It can be propagated for multi-input-multi-output (MIMO) system, as well.

Appendix A
Verification of Examples

The verification of the examples presented in this thesis is done by the simulation of a nonlinear system. Two steps are followed.

Step 1:

(a) The nonlinear system is simulated for various inputs, e.g. a small positive step input, a large positive step input, a negative step input, and periodic oscillations with various amplitude and frequency, and output response is then plotted using Simulink software.

(b) As nonlinear system dynamics vary with the change of system states and time, the location of poles will also change in the complex plane with the change of system states and time. The system pole locations are drawn by collecting the data from step 1(a) and writing codes in MATLAB software.

Step 2:

(a) A Dynamic characteristic equation is constructed, and dynamic root locus is plotted in the complex g −plane varying system states and using the approach presented in Chapter 2.

(b) A comparison of system response for various inputs from step 1(a) and system pole location plots from step 1(b) and dynamic root locus plots from step 2(a) is done. A uniformity of two root locus plots from step 1(b) and step 2(a), and system responses from step 1(a) and root locus plots from step 2(a) confirms the validity of the examples solved in Chapter 2 and Chapter 3, respectively.

Consider a second-order nonlinear system with a nonlinear spring $(12 + x)$,

$$\ddot{x} + 8\dot{x} + (12 + x)x = u(t)$$

and, output (A.1)

$$y = x$$

System dynamics of this nonlinear equation change with the variation of system state x. The steady-state response of is a function of system states. The steady state response of this nonlinear system is given by

$$y = \frac{u(t)}{12 + x} \tag{A.2}$$

The state-space representation is given by

$$\begin{aligned} \dot{x_1} &= x_2 \\ \dot{x_2} &= -(12 + x_1)x_1 - 8x_2 - u(t) \end{aligned} \tag{A.3}$$

where x_1 and x_2 are the system states.

A.1. Simulation

A.1.1. Simulation for Various Inputs

The nonlinear system Eq. (A.3) is simulated for various inputs, e.g. a small positive step input $u(t) = +50$, a large positive step input $u(t) = +200$, a negative step input $u(t) = -50$, and periodic oscillations with various amplitude and frequency $u(t) = 75 \sin t$, $u(t) = 10 \sin t$, $u(t) = 75 \sin 0.8t$, and output response is then plotted using Simulink software.

Simulation 1: Input Step $u(t) = +50$

The Simulink model of the nonlinear system Eq. (A.3) with step input $u(t) = +50$ is shown in Figure A.1, and the response is overdamped as shown in Figure A.2. The system has a stable response, and steady-state output is 3.274, as calculated from Eq. (A.2). The system states vary from 0~3.274.

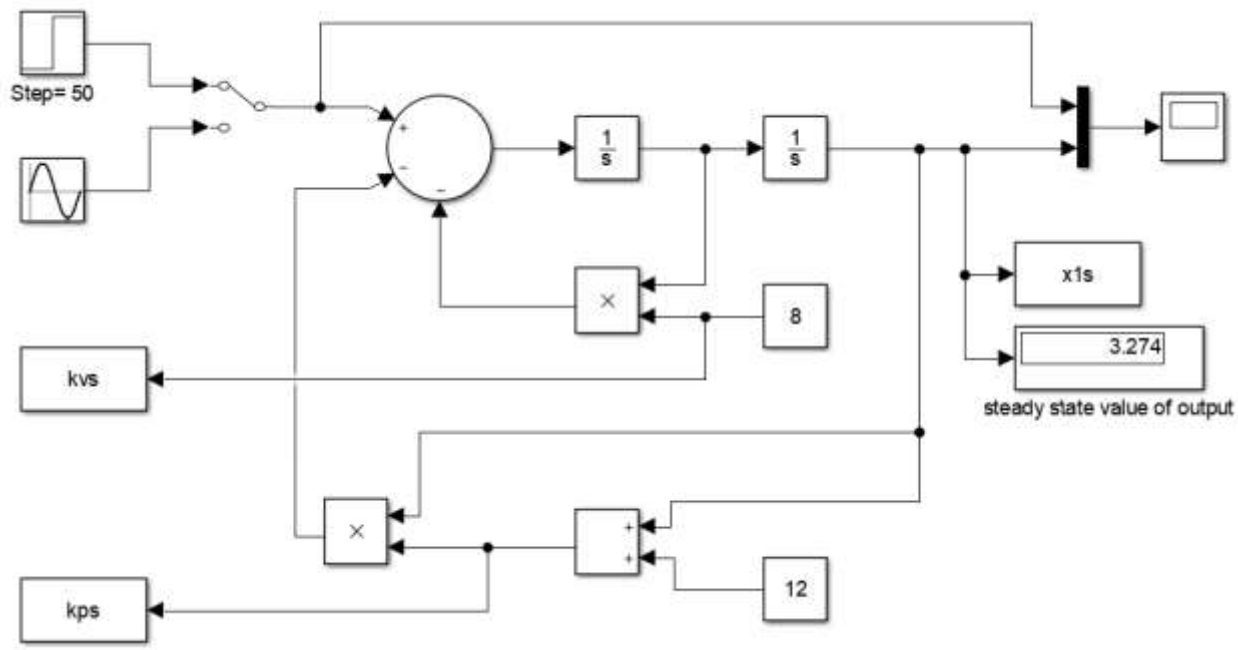

Figure A.1. Simulink model of the nonlinear system Eq. (A.3) with a step input $u(t) = +50$.

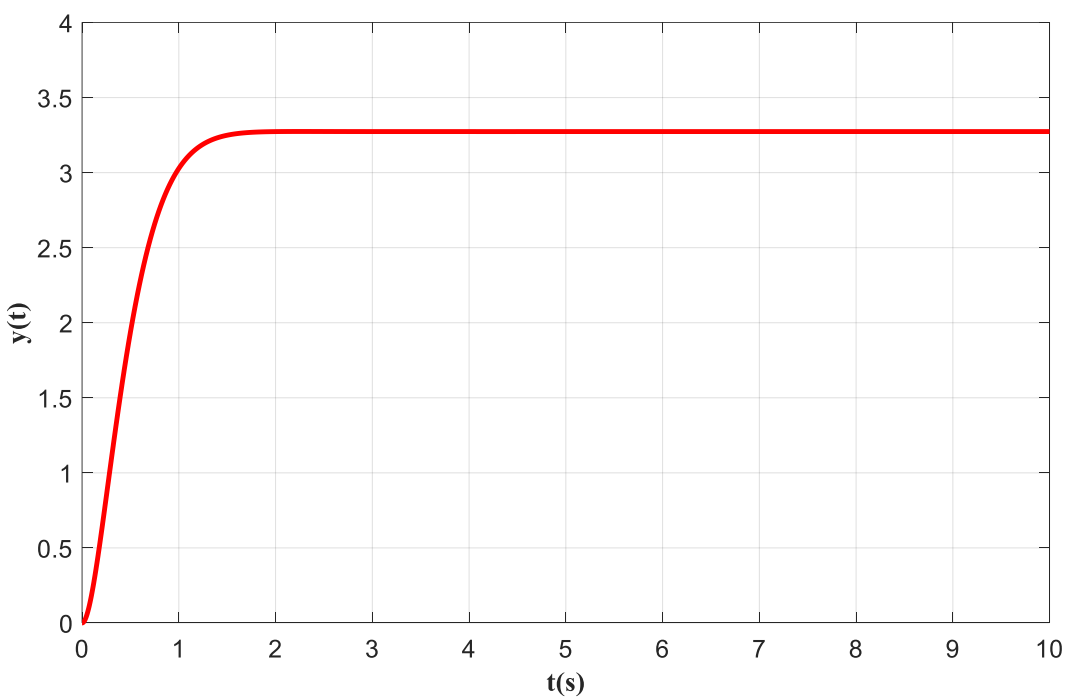

Figure A.2. The overdamped response of the nonlinear system for a step input $u(t) = +50$.

As the system dynamics changes with the variation of system states, the location of poles in the complex plane is plotted by collecting data from Simulink simulation. The locations of the poles of the system in the complex plane are plotted by running the following code in MATLAB and taking the values of position feedback K_{ps} and velocity feedback K_{vs} to form Simulink model (Figure A.1). A three-dimensional plot of the location of roots is shown in Figure A.3, and a two-dimensional plot is given in Figure A.4.

MATLAB code for drawing the root locus from Simulink model (Figure A.1):

```
clc
kp=kps.data; %% Position feedback from simulink
kv=kvs.data; %% velocity feedback from simulink
x1=x1s.data; %% state x1 from simulink
t=kps.time;

%%
for i=1:size(kv)
    num=[1]; % num=1
    Den=[1 kv(i) kp(i)]; %Denominator at each interval
    G(i)=tf(num,Den); %% Transfer function at each interval
    i=i+1;
end
%%
i=1;
for i=1:size(kv)
    rt(i,:)=pole(G(i)); % dynamic Poles of the transfer function at each time
interval
    re1(i)=real(rt(i,1));% real part of the dynamic pole 1
    im1(i)=imag(rt(i,1));% imaginary part of dynamic pole 1
    re2(i)=real(rt(i,2));% real part of the dynamic pole 2
    im2(i)=imag(rt(i,2)); % imaginary part of dynamic pole 2
end
%%
figure(1)
plot(re1,im1,'xr');hold on; % plot pole 1 on the complex g-plane
plot(re2,im2,'xg');hold on; % plot pole 2 on the complex g-plane
xlabel('\fontsize{30}\fontname{Times}\bf\sigma(t)');
ylabel('\fontsize{30}\fontname{Times}\bfj\omega(t)')
grid on
hAxis = gca;
hAxis.XRuler.FirstCrossoverValue  = 0; % X crossover with Y axis
hAxis.YRuler.FirstCrossoverValue  = 0; % Y crossover with X axis
```

```
%%
figure(2)
plot3(x1,re1,im1,'xr');hold on; % plot pole 1 on the 3D complex g-plane
plot3(x1,re2,im2,'xg');hold on; % plot pole 2 on the 3D complex g-plane
xlabel('\fontsize{20}\fontname{Times}\bfx_1(t)');
ylabel('\fontsize{20}\fontname{Times}\bf\sigma(t)');
zlabel('\fontsize{20}\fontname{Times}\bfj\omega(t)')
grid on
set(gca,'XDir','reverse');
set(gca,'YDir','reverse');
hAxis = gca;
hAxis.XRuler.FirstCrossoverValue  = 0; % X crossover with Y axis
hAxis.YRuler.FirstCrossoverValue  = 0; % Y crossover with X axis
hAxis.ZRuler.FirstCrossoverValue  = 0; % Z crossover with X axis
hAxis.ZRuler.SecondCrossoverValue = 0; % Z crossover with Y axis
hAxis.XRuler.SecondCrossoverValue = 0; % X crossover with Z axis
hAxis.YRuler.SecondCrossoverValue = 0; % Y crossover with Z axis
```

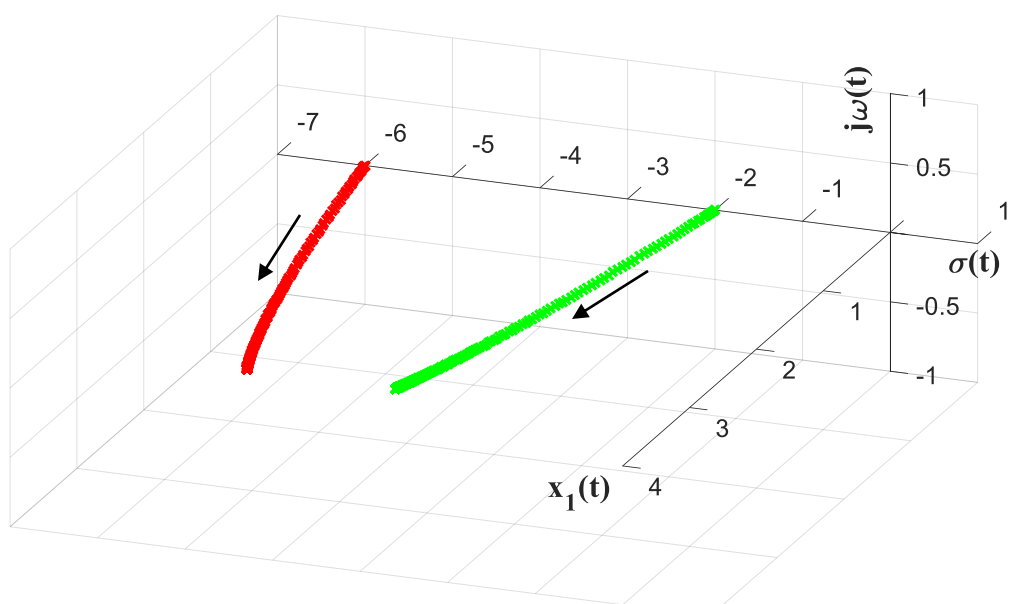

Figure A.3. A three-dimensional plot of the location of poles in the complex plane of the nonlinear system for step input $u(t) = +50$.

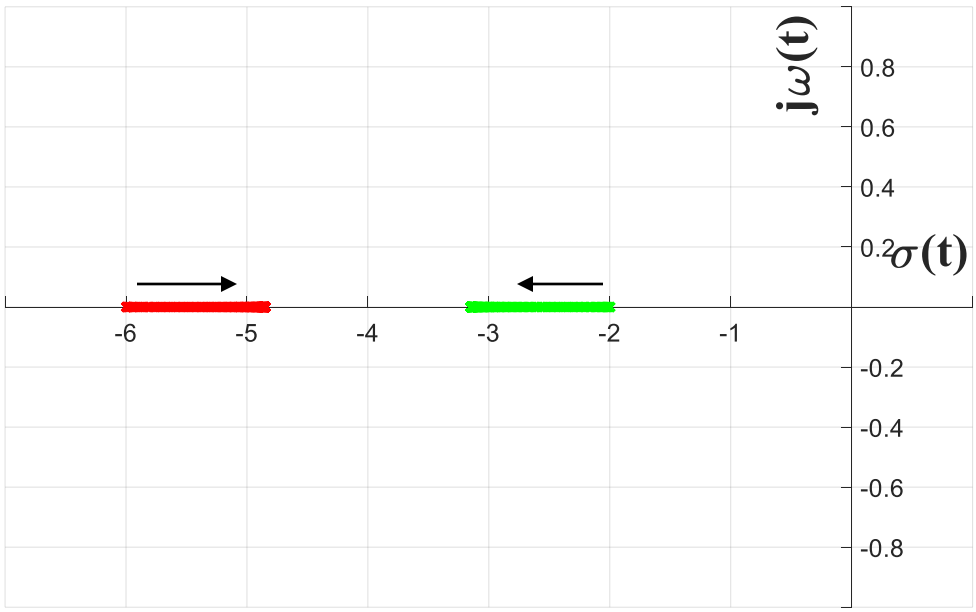

Figure A.4. A two-dimensional projection of the three-dimensional dynamic root locus plot Figure A.3.

It is noted that all poles are located on the left-hand side real axis of the complex plane and system response is overdamped as shown in Figure A.2.

Simulation 2: Input Step $u(t) = +200$

The step input is increased to $u(t) = +200$ as shown in Simulink model Figure A.5 and the response is shown in Figure A.6. The system has an underdamped response, and the steady-state output is 9.362. The system states vary from 0~9.362. The system has complex poles in the left-hand side of the complex plane, and pole locations are plotted in the Figures A.7 and A.8.

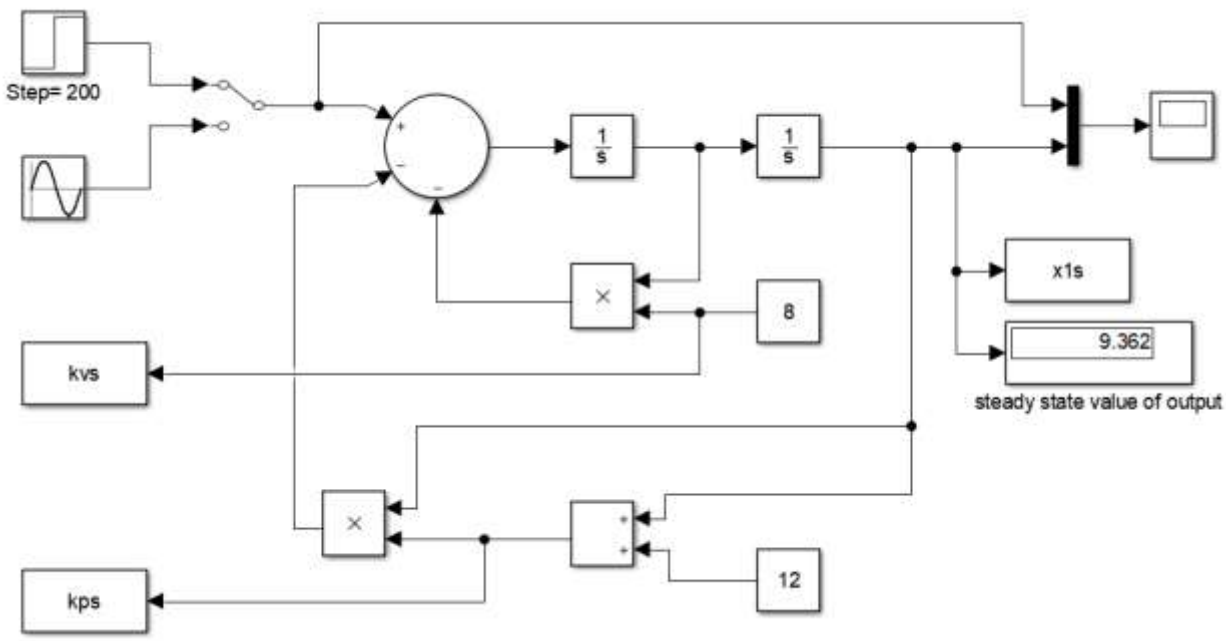

Figure A.5. Simulink model of the nonlinear system Eq. (A.3) with a step input $u(t) = +200$.

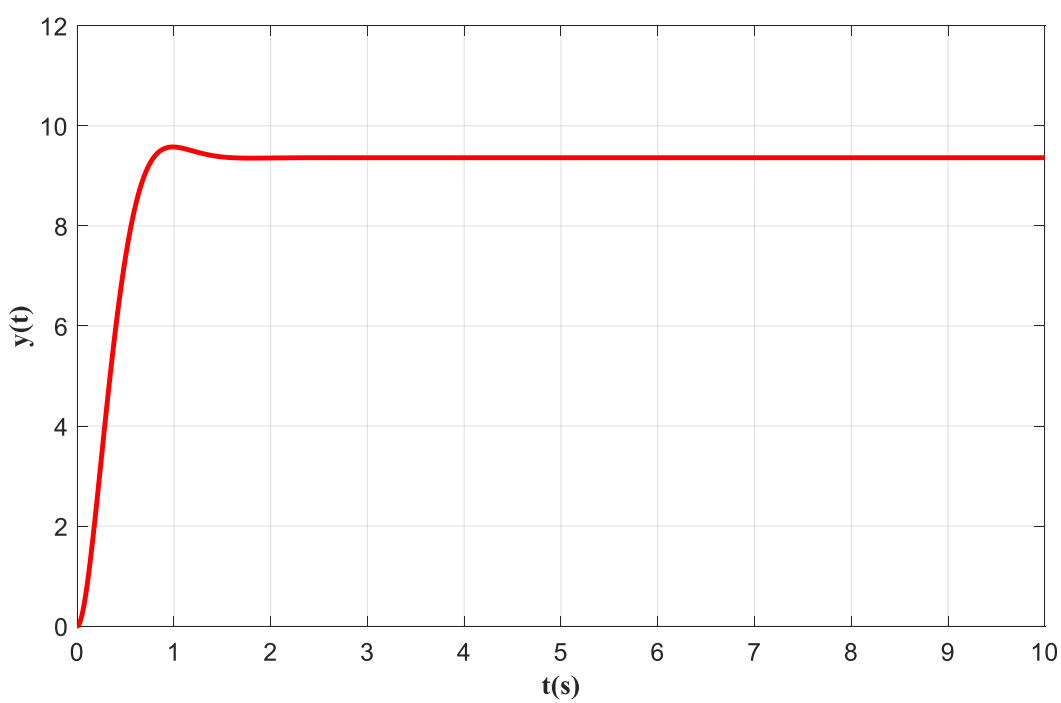

Figure A.6. The underdamped response of the nonlinear system for a step input $u(t) = +200$.

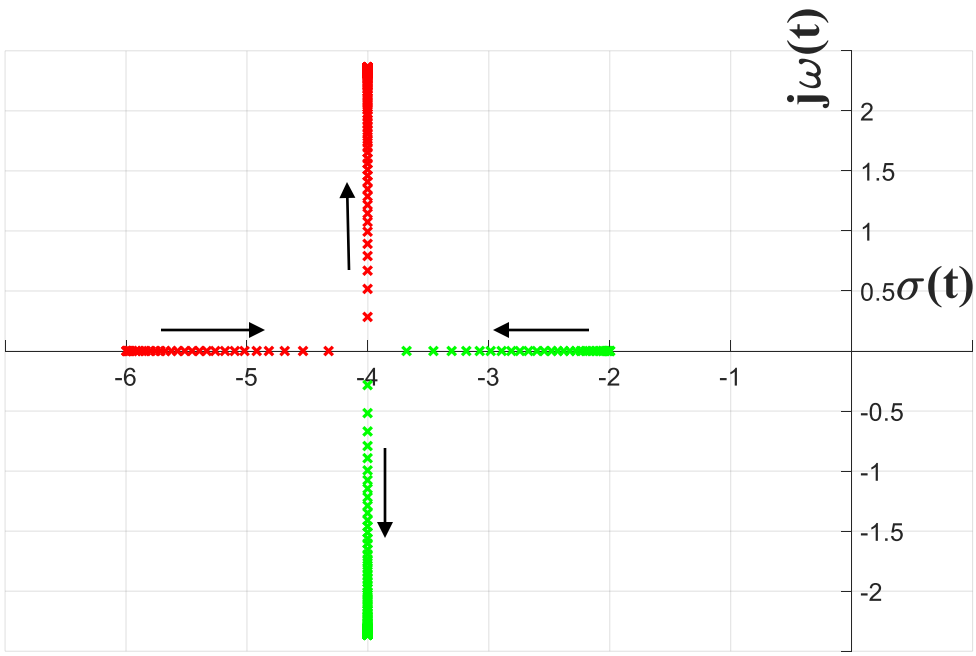

Figure A.7. A three-dimensional plot of the location of poles in the complex plane of the nonlinear system for step input $u(t) = +200$.

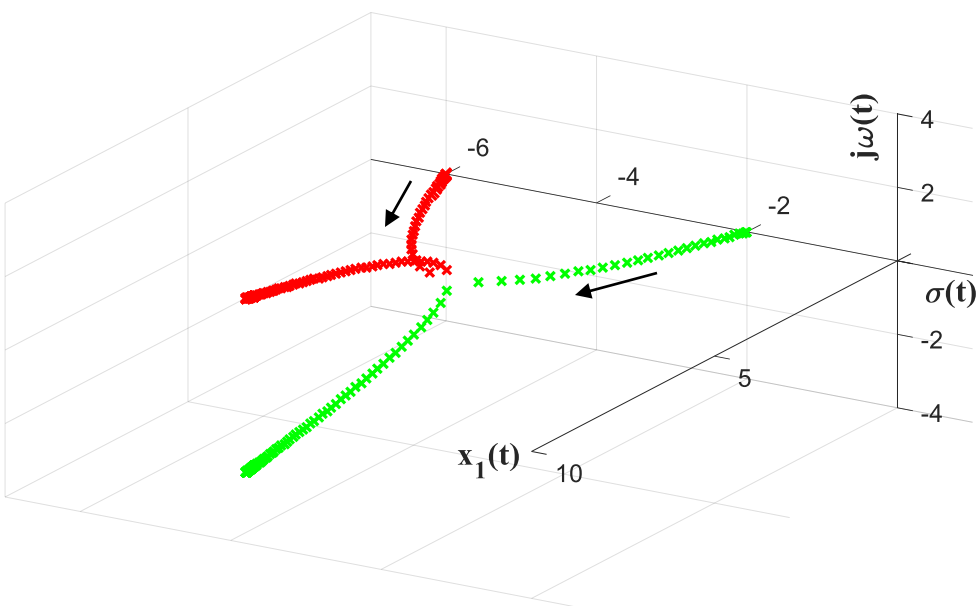

Figure A.8. A two-dimensional projection of the three-dimensional root locus Figure A.7.

Simulation 3: Input Step $u(t) = -50$

The step input is decreased to $u(t) = -50$ as shown in Simulink model Figure A.9, and the system response is shown in Figure A.10. The system has an unstable response, and the pole locations are plotted in the Figures A.11 and A.12. The system states vary from $-\text{inf} \sim 0$. One of the system poles moves to the right-hand side of the complex plane for system state $x_1 < -12$.

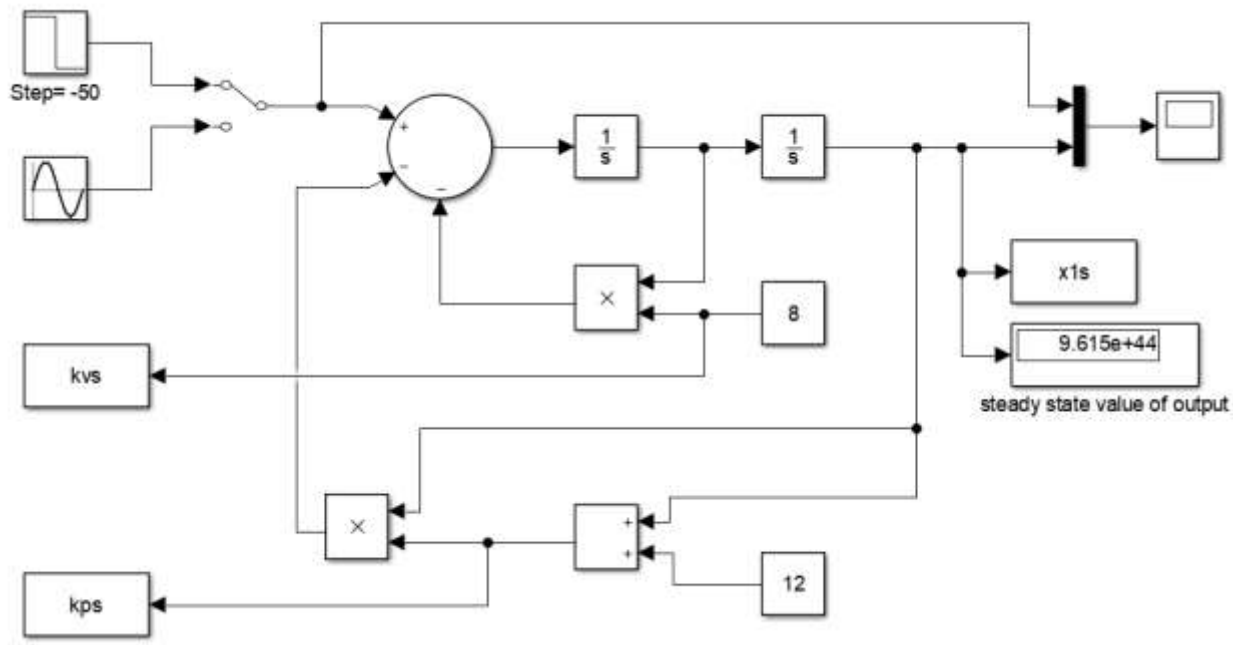

Figure A.9. Simulink model of the nonlinear system Eq. with step input $u(t) = -50$.

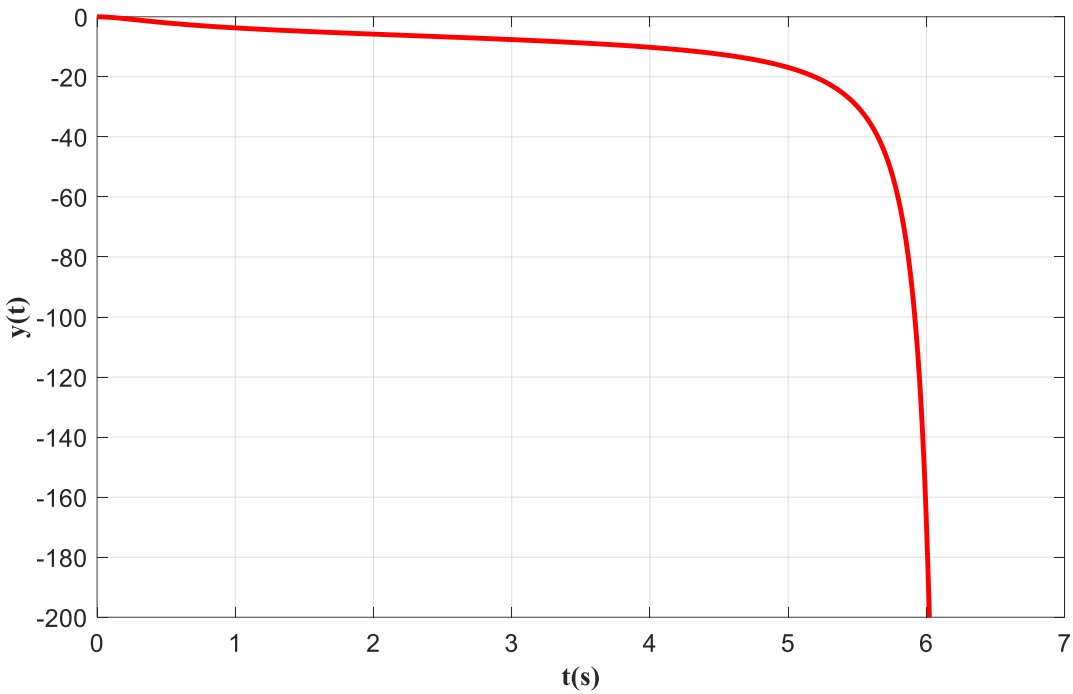

Figure A.10. The unstable response of the nonlinear system for a step input $u(t) = -50$.

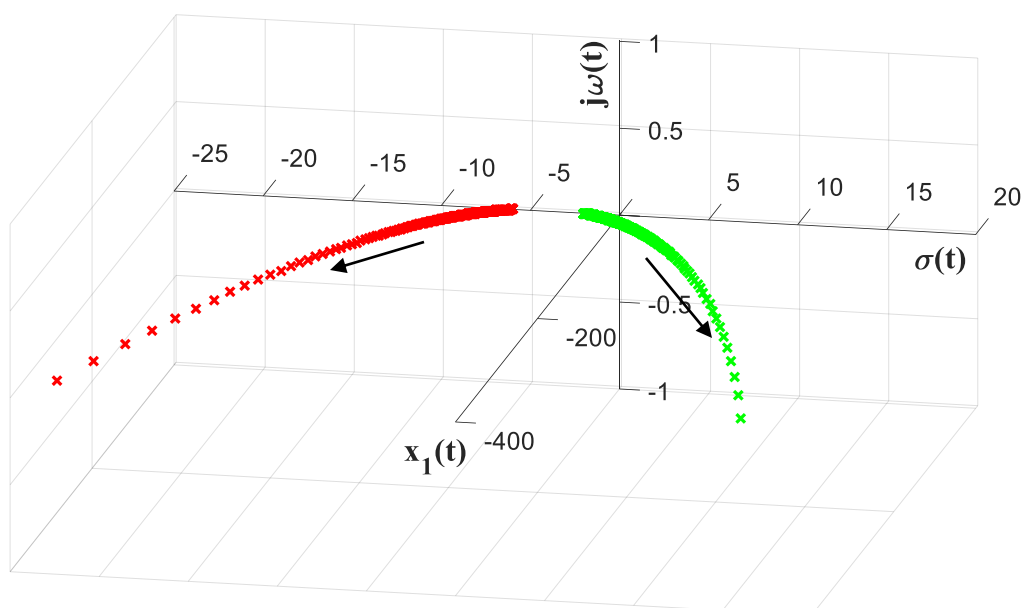

Figure A.11. A three-dimensional plot of the location of poles in the complex plane of the nonlinear system for step input $u(t) = -50$.

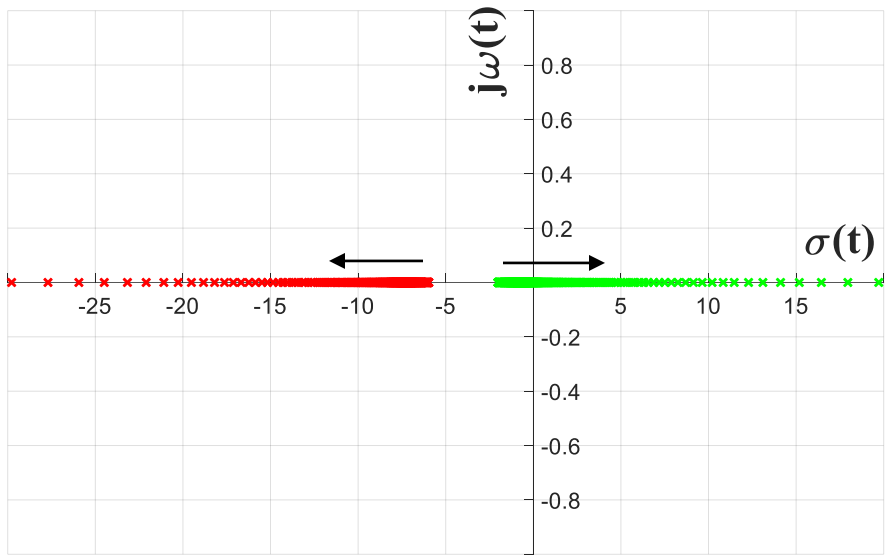

Figure A.12. A two-dimensional projection of the three-dimensional root locus Figure A.11.

Simulation 4: Periodic Input $u(t) = 75 \sin t$

The output response for a sinusoidal input with an amplitude $\mathrm{A} = 75$ and an angular frequency $\omega = 1$ rad/s, i.e., $u(t) = 75 \sin t$ is shown in Figure A.14. The Simulink model is shown in Figure A.13. The system states vary from $-9.9 \sim +4.42$. The output response is stable and periodic but highly distorted because of the state dependency on the output response as given by Eq. (A.2).

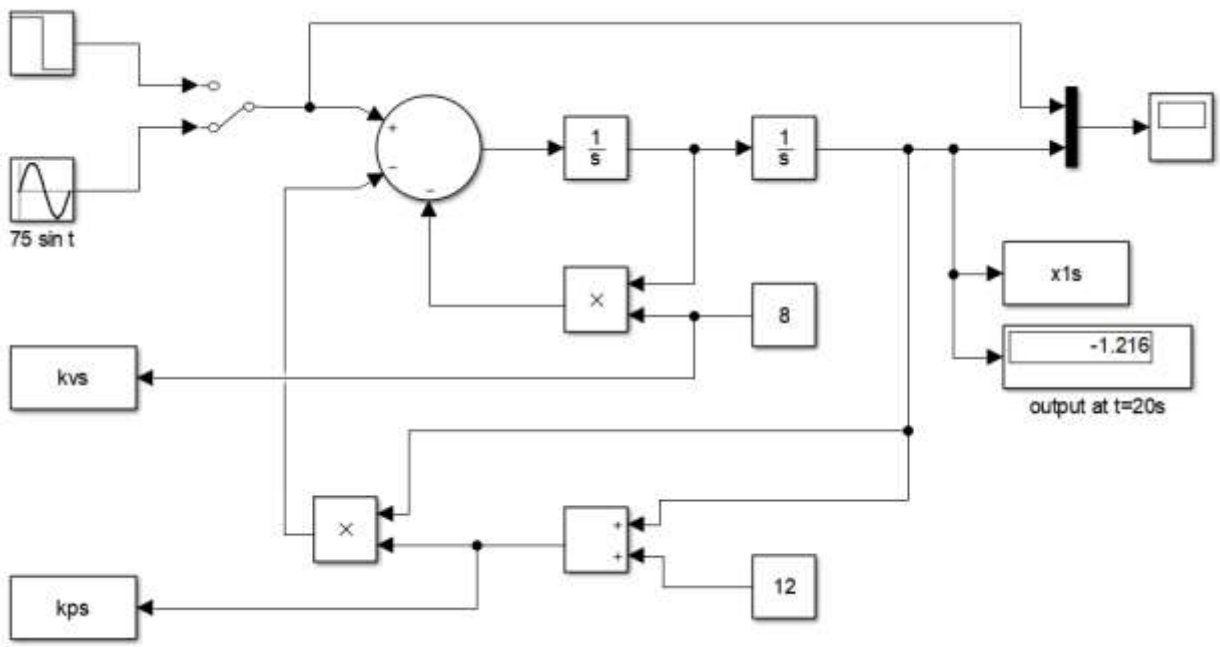

Figure A.13. Simulink model of the nonlinear system Eq. (A.3) with an input $u(t) = 75 \sin t$.

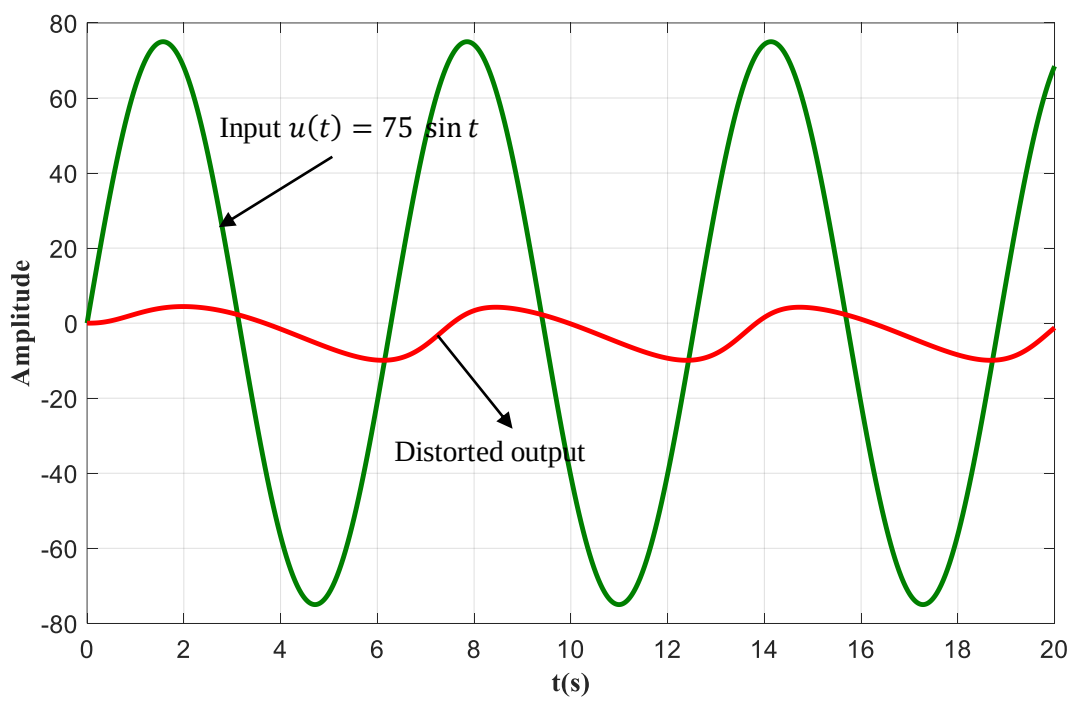

Figure A.14. The stable response of the nonlinear system for an input $u(t) = 75 \sin t$.

Figure A.15 gives a root locus vs. time $t(s)$ plot whereas Figure A.16 gives a root locus vs. system state x_1 plot. The roots are on the left half of the complex plane showing the stability of the system for an input $u(t) = 75 \sin t$.

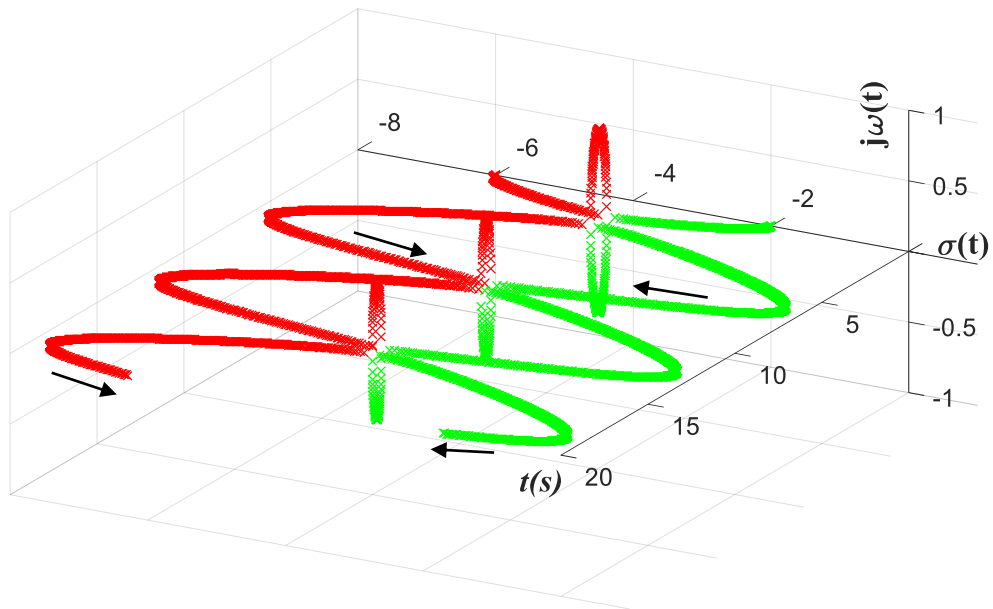

Figure A.15. The location of poles vs. time $t(s)$ in the complex plane of the nonlinear system for an input $u(t) = 75 \sin t$.

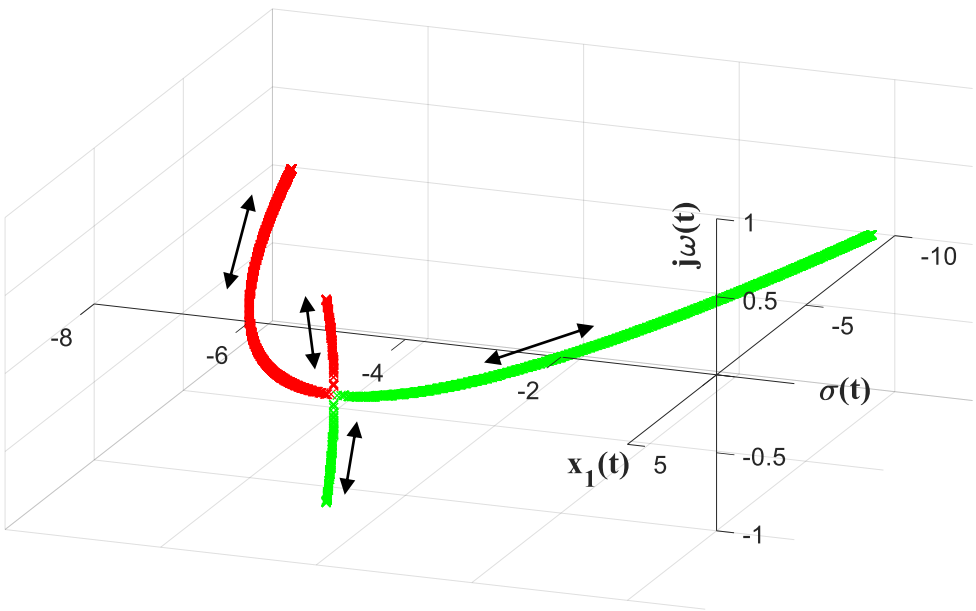

Figure A.16. The location of poles vs. system state x_1 in the complex plane of the nonlinear system for an input $u(t) = 75 \sin t$.

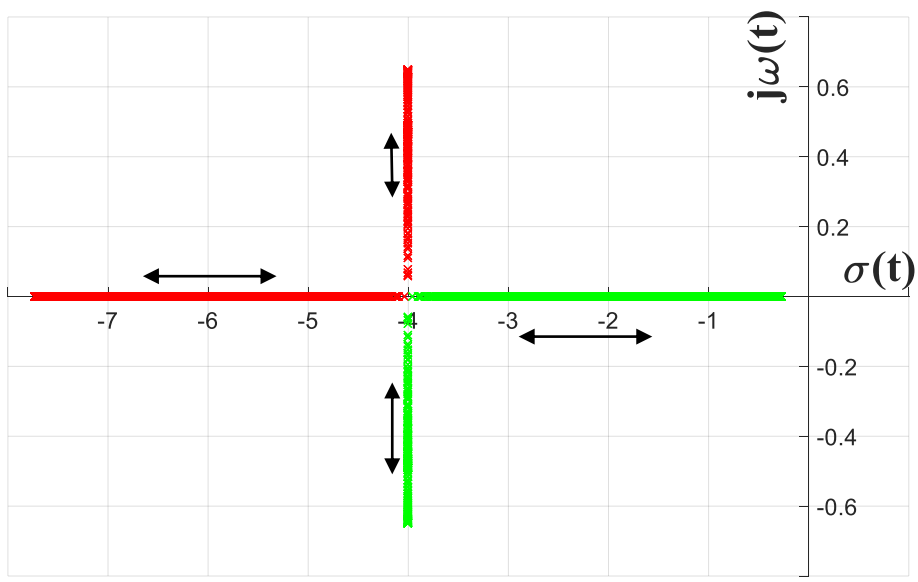

Figure A.17. A two-dimensional projection of the three-dimensional dynamic root locus Figures A.15 and A.16.

Simulation 5: Periodic Input $u(t) = 10 \sin t$

The input amplitude is reduced to $A = 10$, but the angular frequency is kept $\omega = 1$, i.e. input $u(t) = 10 \sin t$. The output response is stable and periodic but less distorted compared to the Figure A.14 ($u(t) = 75 \sin t$). The system states vary from $-0.766 \sim +0.712$.

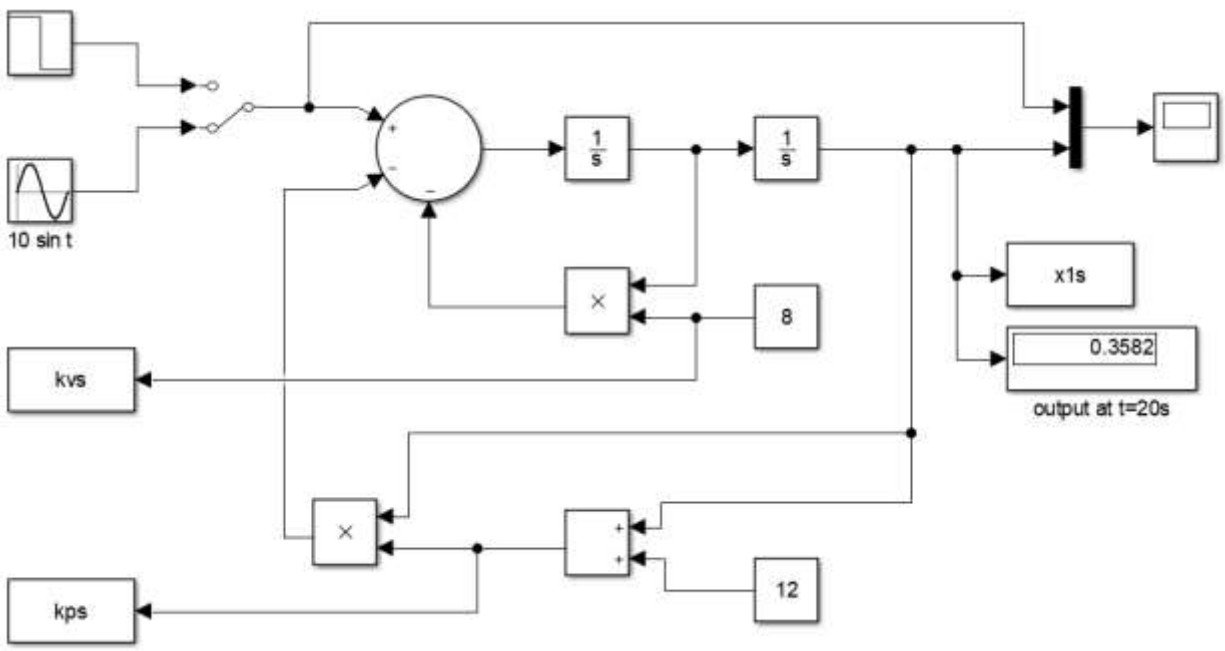

Figure A.18. Simulink model of the nonlinear system Eq. (A.3) with an input $u(t) = 10 \sin t$.

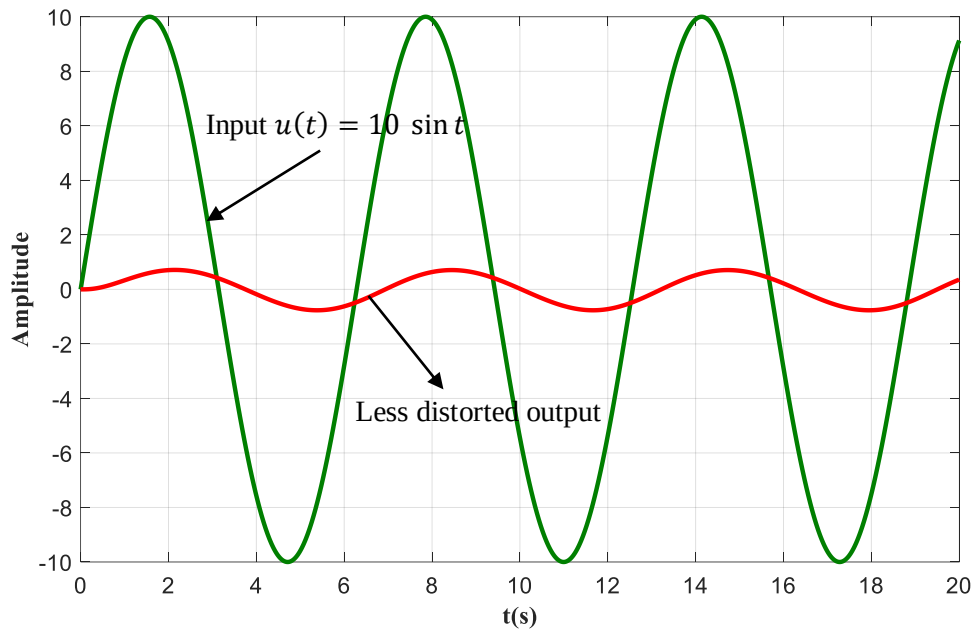

Figure A.19. The stable response of the nonlinear system Eq. (A.3) for an input $u(t) = 10 \sin t$.

Figure A.20 gives a root locus vs. time $t(s)$ plot whereas Figure A.21 gives a root locus vs. system state x_1 plot. The roots are on the left-hand side real axis of the complex plane showing the stability of the system for an input $u(t) = 10 \sin t$.

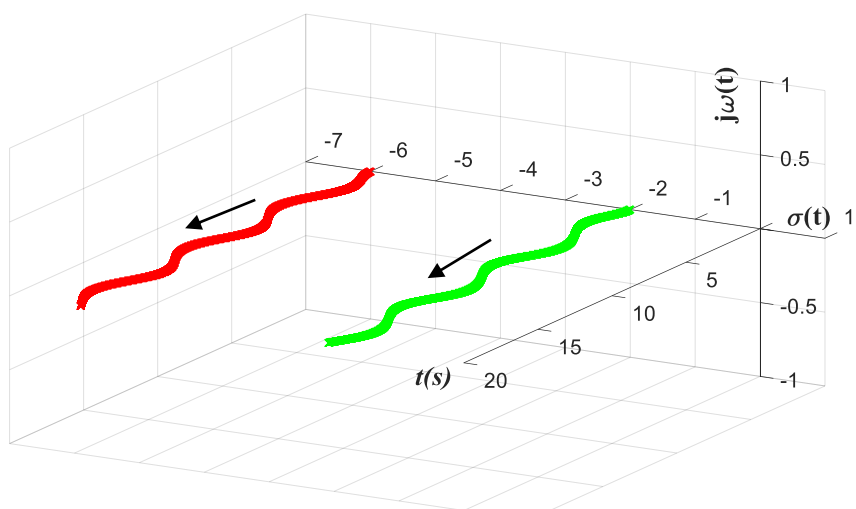

Figure A.20. The location of poles vs. time $t(s)$ in the complex plane of the nonlinear system for an input $u(t) = 10 \sin t$.

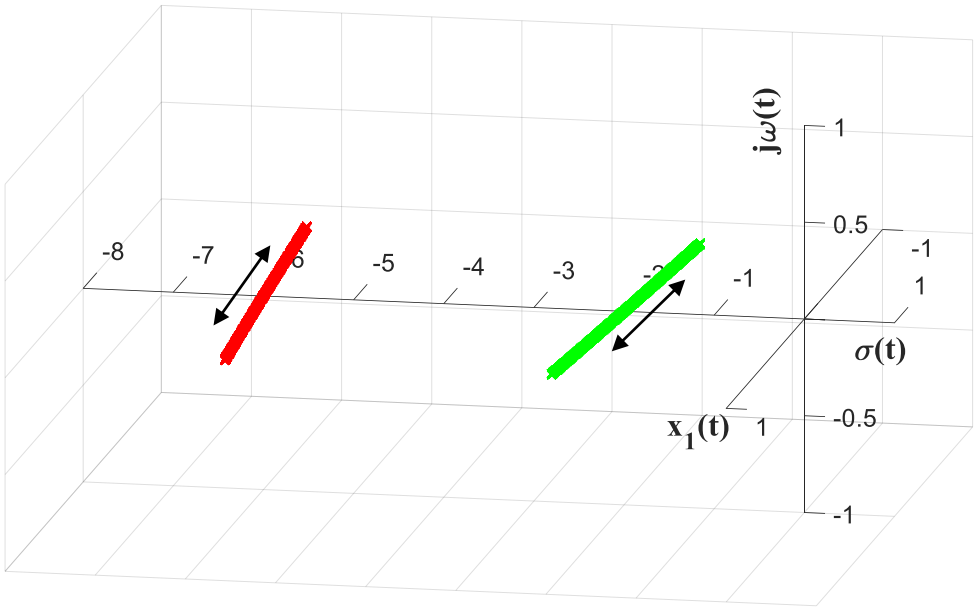

Figure A.21. The location of poles vs. system state x_1 in the complex plane of the nonlinear system for an input $u(t) = 10 \sin t$.

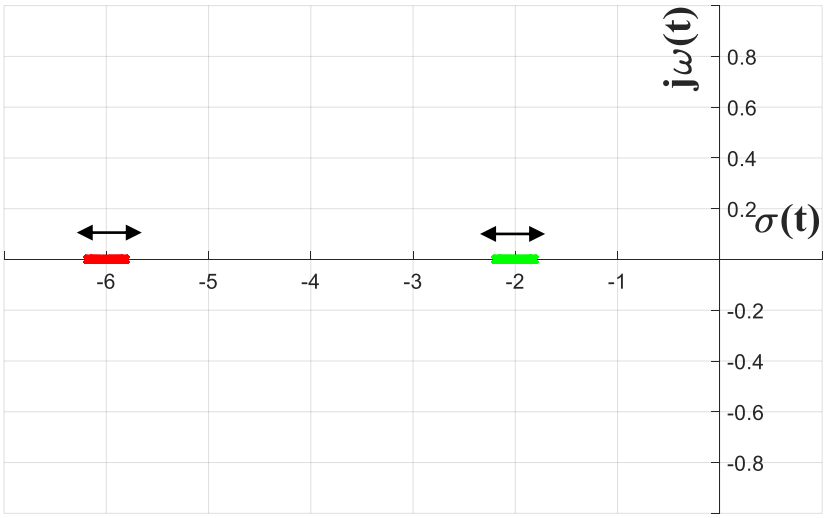

Figure A.22. A two-dimensional projection of the three-dimensional dynamic root locus Figures A.20 and A.21.

Simulation 6: Periodic Input $u(t) = 75 \sin 0.8t$

The input amplitude is kept constant $A = 75$, but the angular frequency is reduced to $\omega = 0.8$, i.e. $u(t) = 75 \sin 0.8t$. The output response is unstable is shown in Figure A.24, because of the low pass filter effect of the nonlinear system. The roots move to the right-hand side of the complex plane showing the unstable condition in Figures A.25, A.26, and A.27. The system states vary from $-\text{inf} \sim +04.47$.

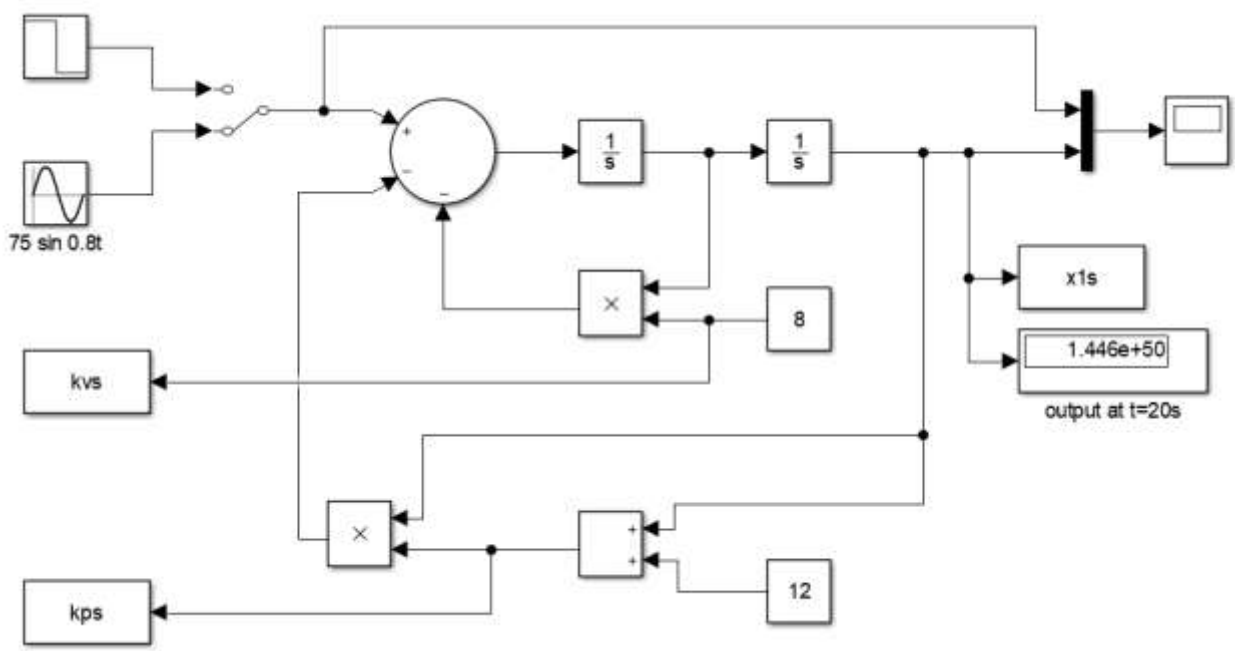

Figure A.23. Simulink model of the nonlinear system Eq. (A.3) with an input $u(t) = 75\sin 0.8t$.

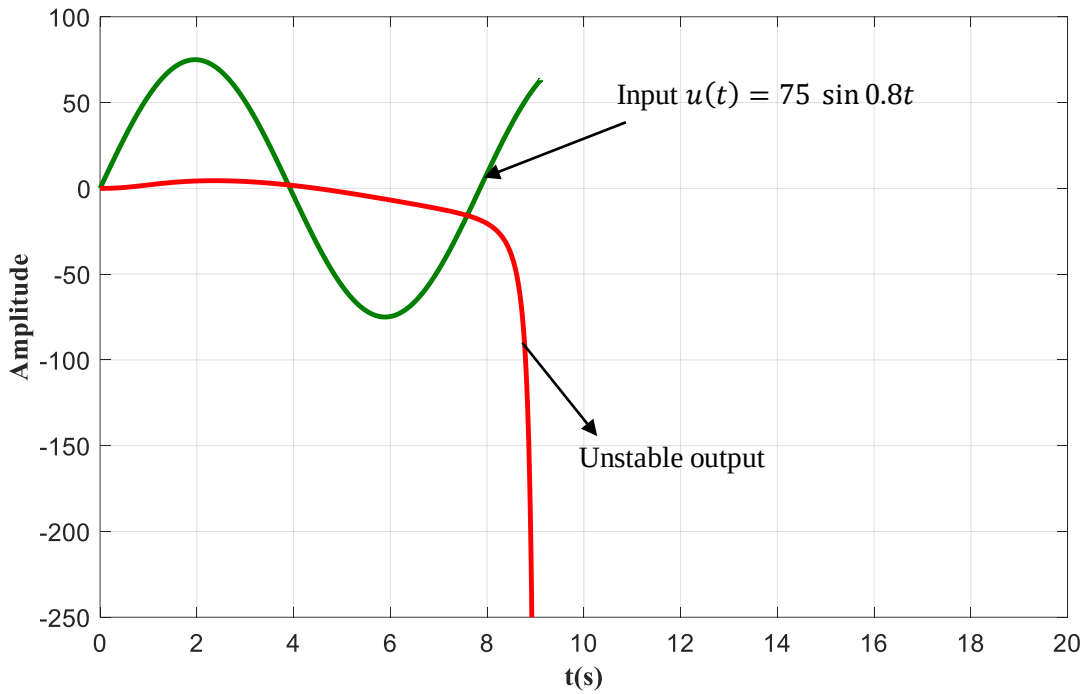

Figure A.24. The unstable response of the nonlinear system Eq. (A.3) for an input $u(t) = 75\sin 0.8t$.

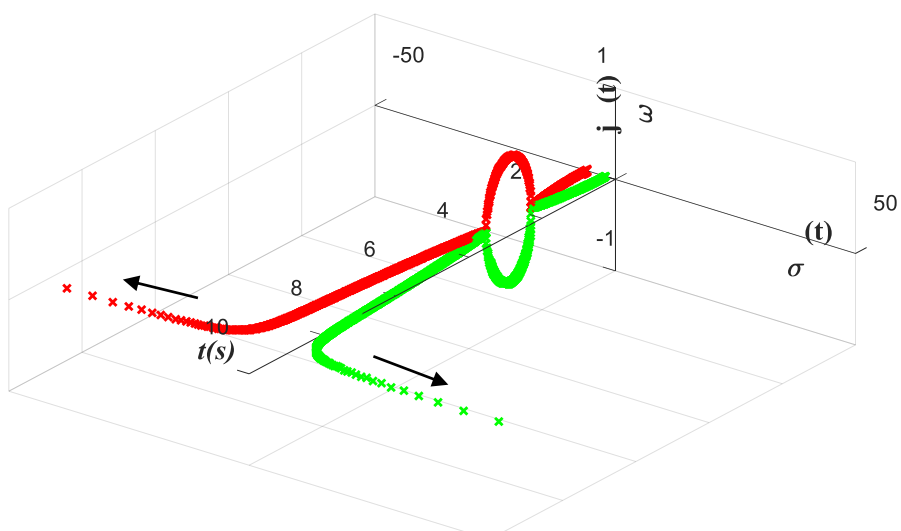

Figure A.25. The location of poles vs. time $t(s)$ in the complex plane of the nonlinear system for an input $u(t) = 75 \sin 0.8t$.

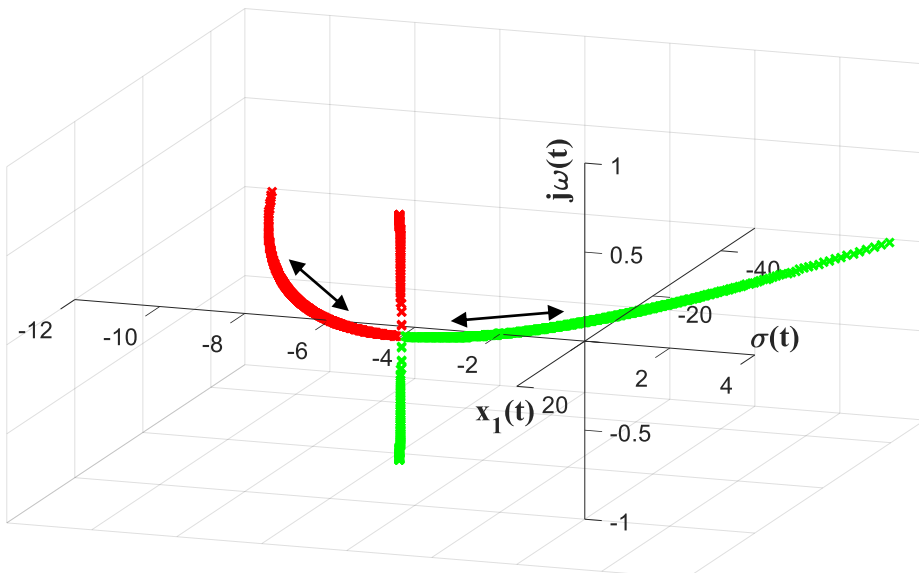

Figure A.26. The location of poles vs. system state x_1 in the complex plane of the nonlinear system for an input $u(t) = 75 \sin 0.8t$.

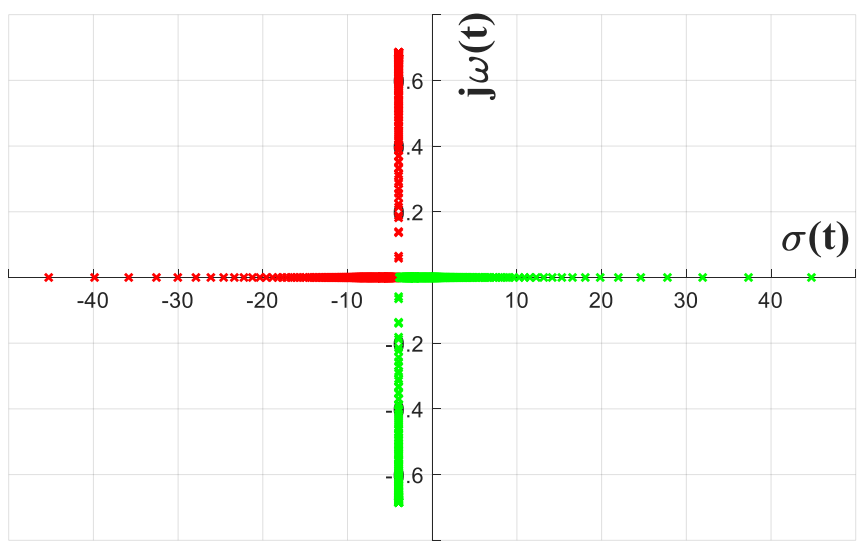

Figure A.27. A two-dimensional projection of a three-dimensional dynamic root locus plots Figures A.25 and A.26.

A.1.2. Dynamic Characteristic Equation and Dynamic Root Locus Plot

In this section, the dynamic characteristic equation of the nonlinear system is constructed, and dynamic root locus is plotted according to the dynamic root locus drawing techniques presented at Chapter 2. A dynamic Routh's table as given in Chapter 3 is then created to show the stability region. The results are then compared with the simulation results presented at Section A.1.1 to show the validity of the proposed stability approach.

According to the techniques presented in Section 2.2, the dynamic characteristic equation of the nonlinear system Eq. (A.3) is

$$g^2 + 8g + (12 + x_1) = 0 \tag{A.4}$$

The dynamic Routh's table is given by

$$\begin{array}{c|cc} g^2 & 1 & 12 + x_1 \\ g^1 & 8 & 0 \\ g^0 & 12 + x_1 & 0 \end{array} \tag{A.5}$$

According to the dynamic Routh's criterion presented in Chapter 3, the nonlinear system Eq. (A.3) is stable, if and only if $12 + x_1 > 0$, or, $x_1 < -12$.

Rearranging Eq. (A.4),

$$1 + \frac{x_1}{g^2 + 8g + 12} = 0 \tag{A.6}$$

or,

$$1 + \frac{x_1}{(g+2)(g+6)} = 0 \tag{A.7}$$

As given in Section 2.3, the dynamic root locus starts from $g_{1,2} = -2\ \&-6$, and the dynamic pole locations are changed in the complex g −plane with the variation of system states x_1.

The MATLAB code for drawing the dynamic root locus from the dynamic characteristic equation Eq. (A.6) varying system state x_1 is given below:

```
clc
clear all
i=1;
for x1=0:.01:3.27 %% value of system state x1
    rt(i,:)=roots([1   8   (x1+12)]);   %%   dynamic   roots   of   the   dynamic
characteristic equation
    re1(i)=real(rt(i,1)); %% real part of the dynamic pole 1
    im1(i)=imag(rt(i,1)); %  imaginary part of the dynamic pole 1
    re2(i)=real(rt(i,2)); %  real part of the dynamic pole 2
    im2(i)=imag(rt(i,2)); %  imaginary part of the dynamic pole 1
    y(i)=x1;
    i=i+1;
end

figure(1)
plot3(y,re1,im1,'rx');hold on; % plot dynamic pole 1 on the 3D complex g-
plane
plot3(y,re2,im2,'gx');hold on; % plot dynamic pole 2 on the 3D complex g-
plane
xlabel('\fontsize{20}\fontname{Times}\bf\itx_1');
ylabel('\fontsize{20}\fontname{Times}\bf\sigma(t)');
zlabel('\fontsize{20}\fontname{Times}\bfj\omega(t)')
grid on
set(gca,'XDir','reverse');
set(gca,'YDir','reverse');
hAxis = gca;
hAxis.XRuler.FirstCrossoverValue  = 0; % X crossover with Y axis
hAxis.YRuler.FirstCrossoverValue  = 0; % Y crossover with X axis
hAxis.ZRuler.FirstCrossoverValue  = 0; % Z crossover with X axis
hAxis.ZRuler.SecondCrossoverValue = 0; % Z crossover with Y axis
hAxis.XRuler.SecondCrossoverValue = 0; % X crossover with Z axis
hAxis.YRuler.SecondCrossoverValue = 0; % Y crossover with Z axis
```

```
%%
figure(2)
plot(re1,im1,'rx');hold on; % plot pole 1 on the complex g-plane
plot(re2,im2,'gx');hold on; % plot pole 2 on the complex g-plane
xlabel('\fontsize{20}\fontname{Times}\bf\sigma(t)');
ylabel('\fontsize{20}\fontname{Times}\bfj\omega(t)')
grid on
hAxis = gca;
hAxis.XRuler.FirstCrossoverValue  = 0; % X crossover with Y axis
hAxis.YRuler.FirstCrossoverValue  = 0; % Y crossover with X axis
```

Simulation 7: Dynamic Root Locus Plot for $x_1 = 0{\sim}3.274$

For a step input $u(t) = +50$, the system states vary from 0~3.274 (Section A.1.1 Simulation 1). A three-dimensional dynamic root locus of the characteristic equation $g^2 + 8g + (12 + x_1) = 0$ is shown in Figure A.28 varying system state x_1 from 0~3.274. The horizontal axis is the real axis $\boldsymbol{\sigma(t)}$, the vertical axis is the imaginary axis $\boldsymbol{j\omega(t)}$, and the third axis represents the system state x_1. The dynamic poles are on the real axis of the left-hand side of the complex g −plane, similar to the root locus drawing at Section A.1.1 Simulation 1.

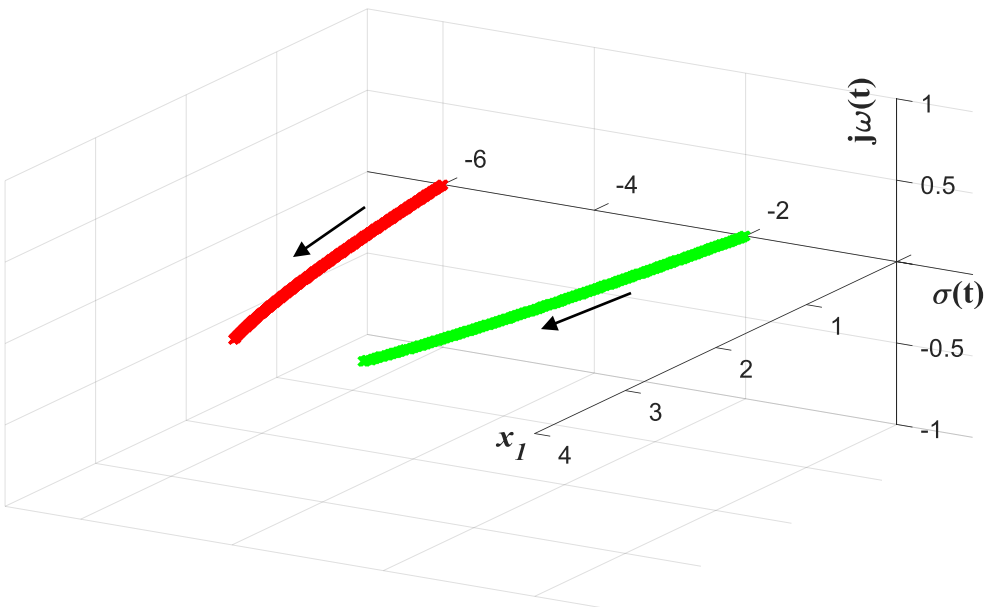

Figure A.28. A three-dimensional dynamic root locus of the characteristic equation $g^2 + 8g + (12 + x_1) = 0$ varying the system state x_1 from 0~3.274.

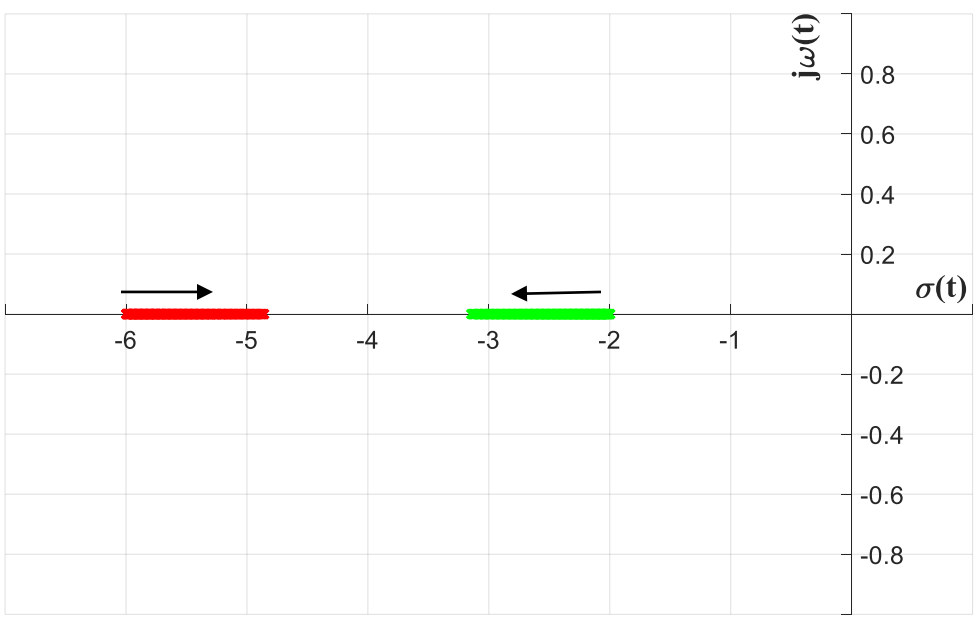

Figure A.29. A two-dimensional projection of a three-dimensional dynamic root locus plot Figure A.28 varying the system state x_1 from 0~3.274.

The Dynamic root locus starts from $\sigma(t) = -2$ and $(t) = -6$, and as system states, x_1 increases dynamic poles move towards each other, and they are located on the real axis similar to Figure A.4 at Section A.1.1. Nonlinear dynamic system response is overdamped.

Simulation 8: Dynamic Root Locus Plot for $x_1 = 0{\sim}9.362$

For a step input $u(t) = +200$, the system states vary from 0~9.362 (Section A.1.1 Simulation 2). A three-dimensional dynamic root locus of the characteristic equation $g^2 + 8g + (12 + x_1) = 0$ varying System state x_1 from 0~9.362 is shown in Figure A.30. The horizontal axis is the real axis $\boldsymbol{\sigma(t)}$, the vertical axis is the imaginary axis $\boldsymbol{j\omega(t)}$, and the third axis represents the system state x_1. The dynamic poles are on the left-hand side of the complex g −plane, similar to the root locus drawing at Section A.1.1 Simulation 2.

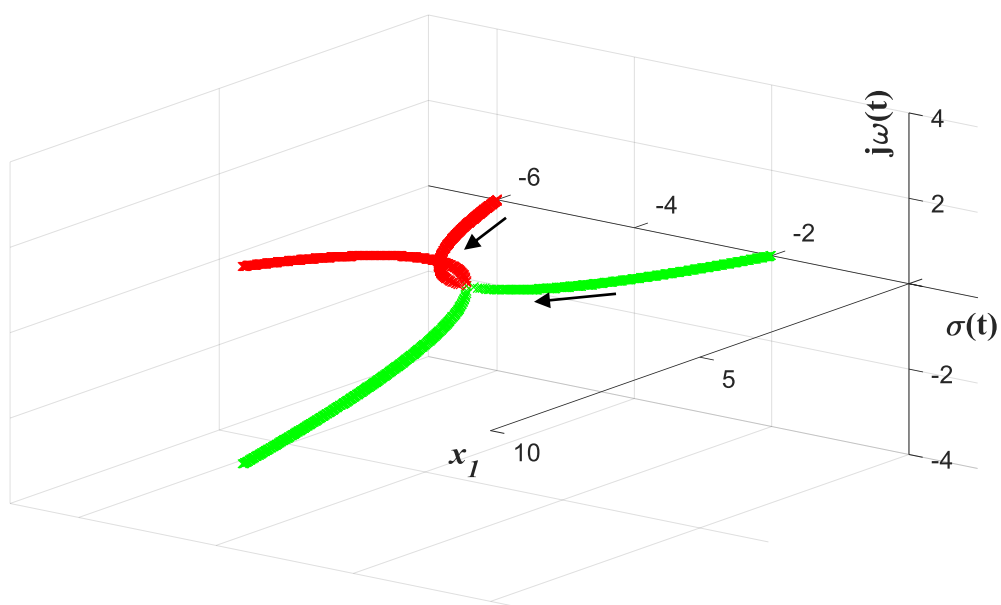

Figure A.30. A three-dimensional dynamic root locus of the characteristic equation $g^2 + 8g + (12 + x_1) = 0$ varying System state x_1 from 0~9.362.

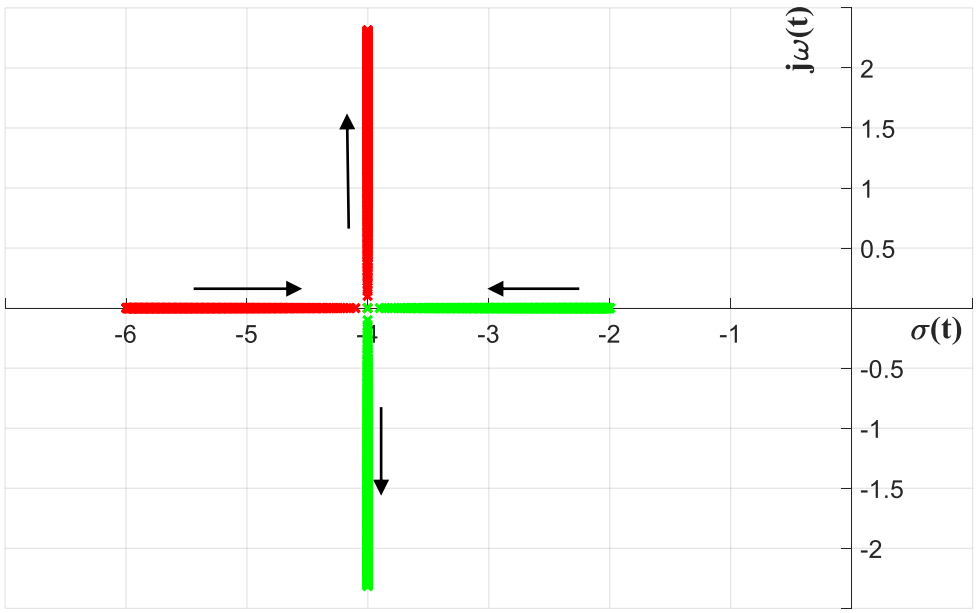

Figure A.31. A two-dimensional projection of a three-dimensional dynamic root locus Figure A.30.

The dynamic root locus starts from $\boldsymbol{\sigma(t)} = -2$ and $\boldsymbol{\sigma(t)} = -6$, and as system states x_1 increases dynamic poles moves towards each other and creates a breakaway point at $\boldsymbol{\sigma(t)} = -4$ on the real axis similar to Figures A.7 and A.8 at Section A.1.1 Simulation 2. Nonlinear dynamic system response is an underdamped system.

Simulation 9: Dynamic Root Locus Plot for $x_1 = -\text{inf}\sim 0$

For a step input $u(t) = -50$, the system states vary from $-\text{inf}\sim 0$ (Section A.1.1 Simulation 3). A three-dimensional dynamic root locus of the characteristic equation $g^2 + 8g + (12 + x_1) = 0$ varying System state x_1 from $-400\sim 0$ is shown in Figure A.32. The horizontal

axis is the real axis $\boldsymbol{\sigma(t)}$, the vertical axis is the imaginary axis $\boldsymbol{j\omega(t)}$, and the third axis represents the system state x_1.

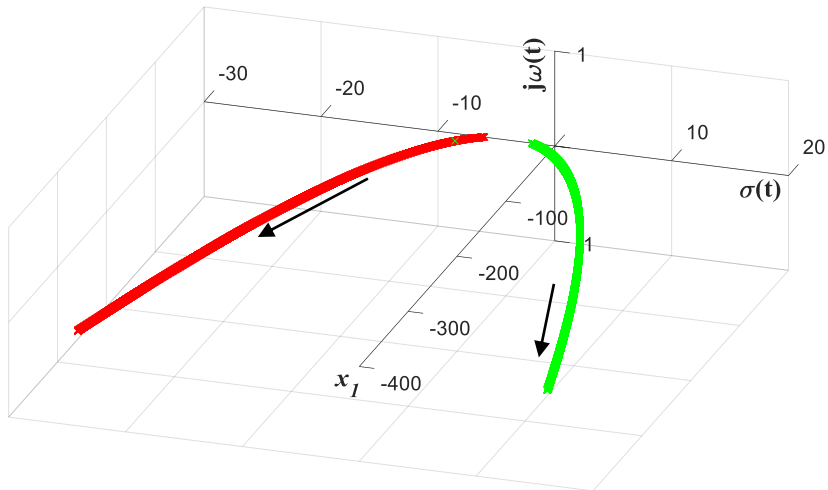

Figure A.32. A three-dimensional dynamic root locus of the dynamic characteristic equation $g^2 + 8g + (12 + x_1) = 0$ varying the system state x_1 from -400~0.

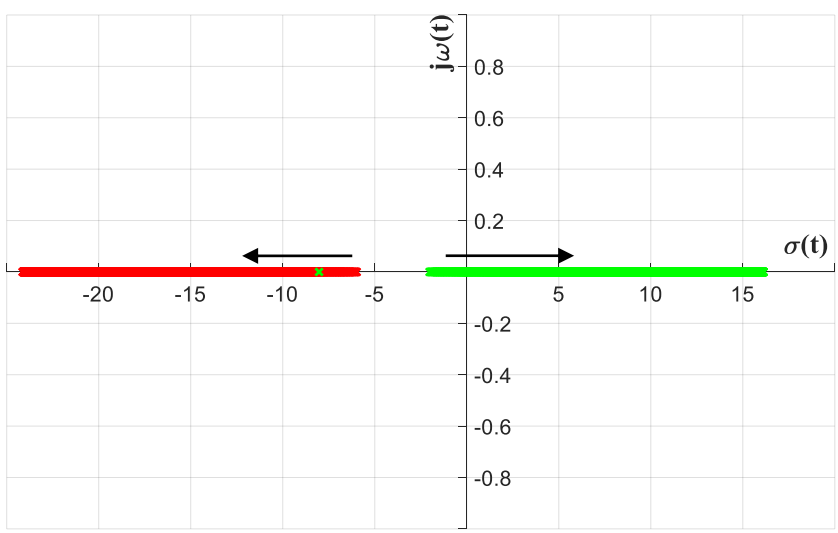

Figure A.33. A two-dimensional projection of the three-dimensional dynamic root locus Figure A.32.

The dynamic root locus starts from $\boldsymbol{\sigma(t)} = -2$ and $\boldsymbol{\sigma(t)} = -6$, and as system states x_1 decreases dynamic poles moves from each other and crosses the imaginary axis for $x_1 = -12$ on the real axis similar to Figures A.11 and A.12. Nonlinear dynamic system response is unstable.

Simulation 10: Dynamic Root Locus Plot for $x_1 = -9.9 \sim +4.42$

For a periodic input $u(t) = 75 \sin t$, the system states vary from $-9.9 \sim +4.42$ (Section A.1.1 Simulation 4). A three-dimensional dynamic root locus of the characteristic equation $g^2 + 8g + (12 + x_1) = 0$ varying system state x_1 from $-9.9 \sim +4.42$ is shown in Figure A.34. The horizontal axis is the real axis $\boldsymbol{\sigma(t)}$, the vertical axis is the imaginary axis $\boldsymbol{j\omega(t)}$, and the third axis represents the system state x_1.

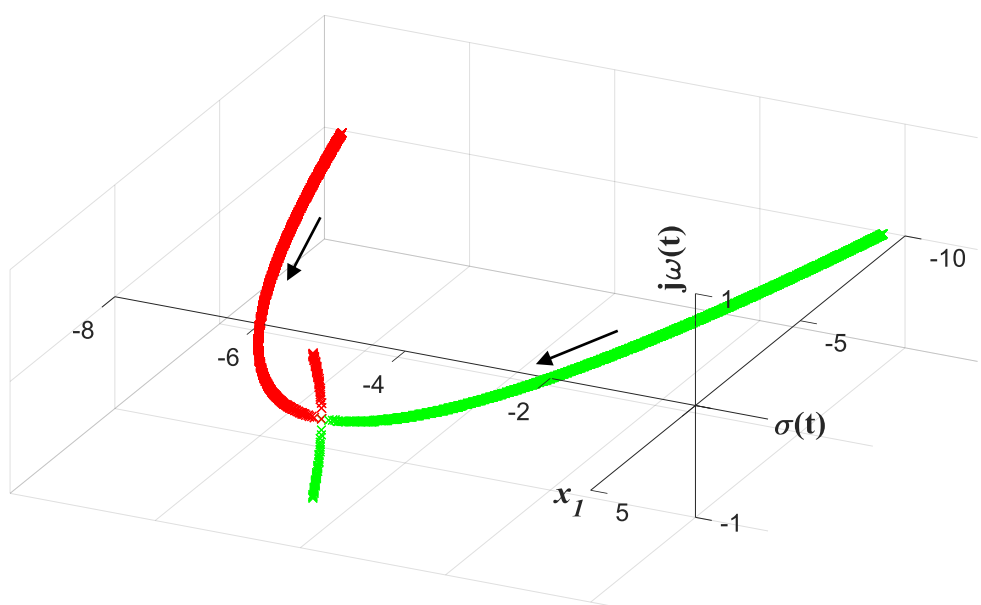

Figure A.34. A three-dimensional dynamic root locus of the dynamic characteristic equation $g^2 + 8g + (12 + x_1) = 0$ varying the system state x_1 from $-9.9 \sim +4.42$.

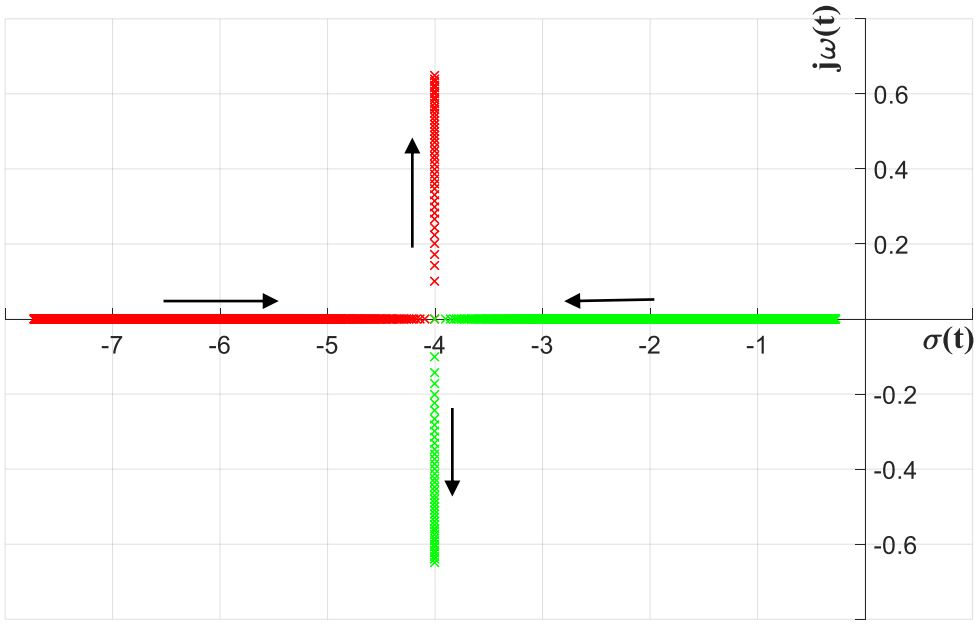

Figure A.35. A two-dimensional projection of the three-dimensional dynamic root locus Figure A.33.

The dynamic poles oscillate on the real axis and are kept on the left-hand side of the complex g −plane similar to Figures A.15, A.16, and A.17. Nonlinear dynamic system response is stable.

Simulation 11: Dynamic Root Locus Plot for $x_1 = -0.766 \sim +0.712$

For a periodic input $u(t) = 10 \sin \mathrm{t}$, the system states vary from $-0.766 \sim +0.712$ (Section A.1.1 Simulation 5). A three-dimensional dynamic root locus of the characteristic equation $g^2 + 8g + (12 + x_1) = 0$ varying system state x_1 from $-0.766 \sim +0.712$ is shown in Figures A.35 and A.36.

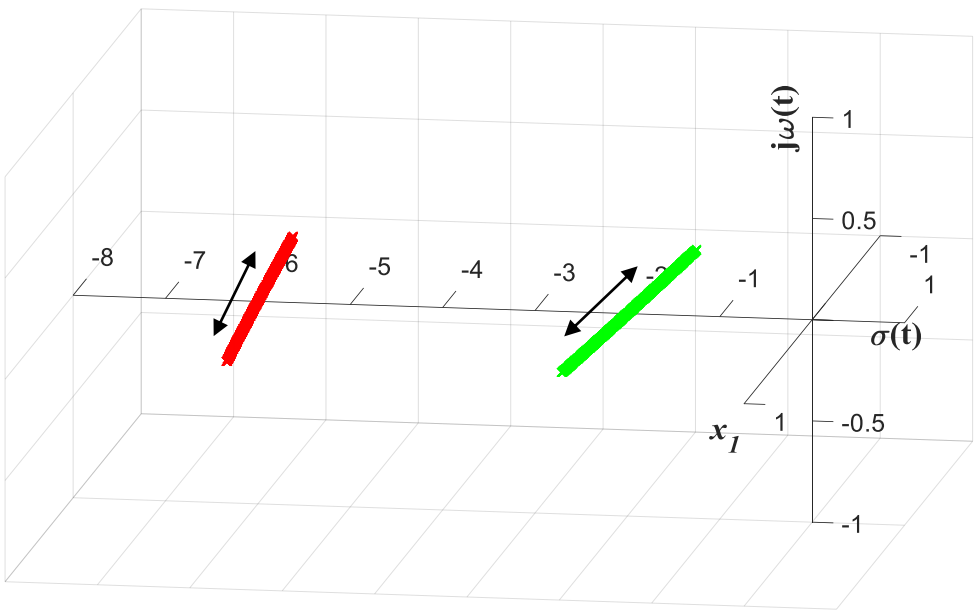

Figure A.36. A three-dimensional dynamic root locus of the dynamic characteristic equation $g^2 + 8g + (12 + x_1) = 0$ varying the system state x_1 from $-0.766 \sim +0.712$.

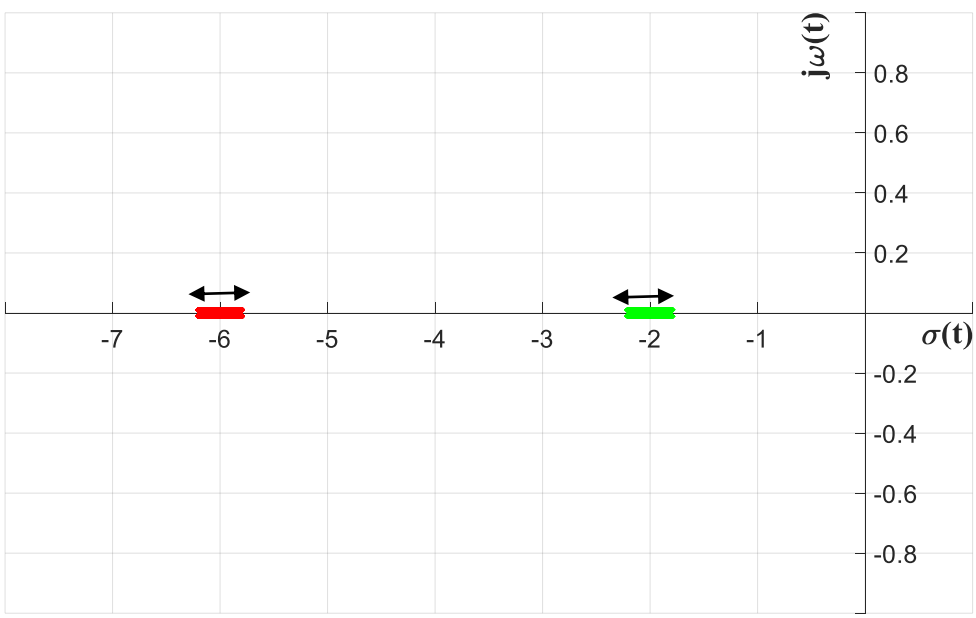

Figure A.37. A two-dimensional projection of the three-dimensional dynamic root locus Figure A.35.

The value for the system states x_1 varies from $-0.766\sim+0.712$ the dynamic poles are kept on the left-hand side of the complex g −plane and the real axis similar to Figures A.20, A.21, and A.22. Nonlinear dynamic system response is stable.

Simulation 12: Dynamic Root Locus Plot for $x_1 = -\text{inf}\sim+04.47$

For a periodic input $u(t) = 75\sin 0.8\text{t}$, the system states vary from $-\text{inf}\sim+04.47$ (Section A.1.1 Simulation 6). A three-dimensional dynamic root locus of the characteristic equation $g^2 + 8g + (12 + x_1) = 0$ varying system state x_1 from $-20\sim+4.47$ is shown in Figure A.37. For $x_1 < -12$, one of the dynamic poles moves to the right-hand side of the complex g −plane and the nonlinear system Eq. (A.3) becomes unstable.

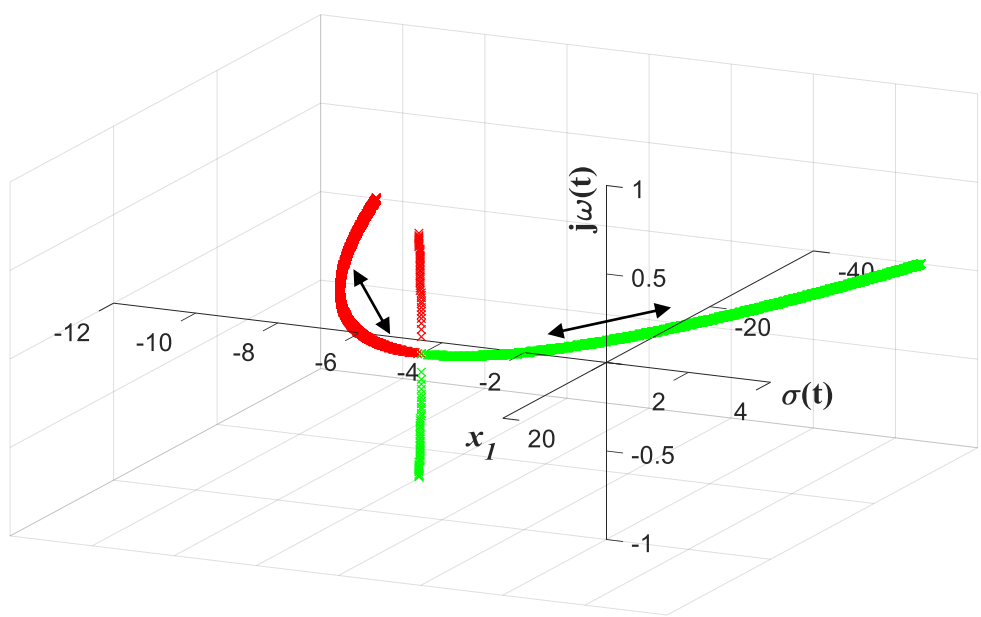

Figure A.38. A three-dimensional dynamic root locus of the dynamic characteristic equation $g^2 + 8g + (12 + x_1) = 0$ varying the system state x_1 from $-20\sim+4.47$.

From the above discussion, it can be concluded that the performance of a nonlinear system, i.e. stability and transient response depends on the system states. System states are a function of the input signal, and the input signal is a function of amplitude and frequency. So, nonlinear system performance depends on the amplitude and frequency of the input signal $u(t)$.

At Section A.1.1, a nonlinear system represented by $\ddot{x} + 8\dot{x} + (12 + x) = u(t)$ is simulated for various inputs, e.g. a small positive step input $u(t) = +50$, a large positive step input $u(t) = +200$, a negative step input $u(t) = -50$, and a periodic oscillations with various amplitude and frequency $u(t) = 75 \sin t$, $u(t) = 10 \sin t$, $u(t) = 75 \sin 0.8t$, and the output response is then plotted using the Simulink software. At Section A.1.2, a dynamic characteristic equation is constructed, and dynamic root locus is plotted in the complex g −plane varying system states using the approach presented in Chapter 2. The nonlinear system responses and the system pole location plot from Section A.1.1, and the dynamic root locus plot from Section A.1.2 is identical, and a uniformity confirms the validity of the examples solved in this thesis.

Appendix B

Linearization vs. Dynamic Pole Motion Approach

Linearization of a nonlinear system to an operating point is an approximate model of a nonlinear system, and it gives a good estimate when the perturbations around the operating point is very small or the system is almost linear [2]. But linearization fails to give the correct result always e.g. a highly nonlinear system where a small perturbation can create a large displacement or if perturbations are not small. But the dynamic pole motion approach, presented in Chapters 2 and 3, give the exact scenario of the system performance.

Consider the example from Appendix A, Eq. (A.1), again,

$$\ddot{x} + 8\dot{x} + (12 + x)x = u(t)$$

and, output (B.1)

$$y = x$$

The state-space representation is given by

$$\begin{aligned} \dot{x_1} &= x_2 \\ \dot{x_2} &= -(12 + x_1)x_1 - 8x_2 - u(t) \end{aligned} \tag{B.2}$$

where x_1 and x_2 are the system states.

For $u(t) = +50$, the equilibrium point is $(x_1, x_2) = (3.2736,0)$. The linearized model of the nonlinear system Eq. (B.2) on the equilibrium point $(3.2736,0)$ is,

$$\begin{bmatrix} \delta x_1 \\ \delta x_2 \end{bmatrix} = \mathbf{A} \begin{bmatrix} \delta x_1 \\ \delta x_2 \end{bmatrix} + \mathbf{B}\, \delta u \tag{B.3}$$

and, output

$$y = \mathbf{C}\begin{bmatrix}\delta x_1\\ \delta x_2\end{bmatrix} + \mathbf{D}\,\delta u$$

where, the linearized system matrix $A = \begin{bmatrix} 0 & 1 \\ -18.5472 & -8 \end{bmatrix}$, the linearized input matrix $B = \begin{bmatrix} 0 \\ 1 \end{bmatrix}$, the linearized output matrix $C = [1 \quad 0]$, and the linearized feed-forward matrix $D = [0]$.

The MATLAB code for performing the linearization is:

```
clc
clear
syms x1 x2 u
f1=x2;                  %% x1dot= x2
f2=-(12+x1)*x1-8*x2+u; %% x2dot= -(12+x1)*x1-8*x2+u
g1=x1;                  %% y=x1
g2=0;
A=jacobian([f1,f2],[x1,x2]) %% Jacobian of system matrix A
B=jacobian([f1,f2],[u]);%% Jacobian of input matrix B
C=jacobian([g1,g2],[x1]);C=C'; %%Jacobian of output matrix C
D=jacobian([g1 g2],[u]);D=D'; %%Jacobian of feed-forward matrix D

x1=3.2736  %% Equilibrium point
A=eval(A)  %% Evaluate matrix A at Equilibrium
```

And the output is:

```
Command Window

A =

[            0,  1]
[ - 2*x1 - 12, -8]


B =

 0
 1


C =

[ 1, 0]


D =

[ 0, 0]


x1 =

    3.2736


A =

         0    1.0000
  -18.5472   -8.0000

>>
```

The linearized model is simulated the operating point $u(t) = +50$, and at the operating point it gives the same steady-state output as the nonlinear system as shown in Figure B.2. The Simulink model is given in the Figure B.1.

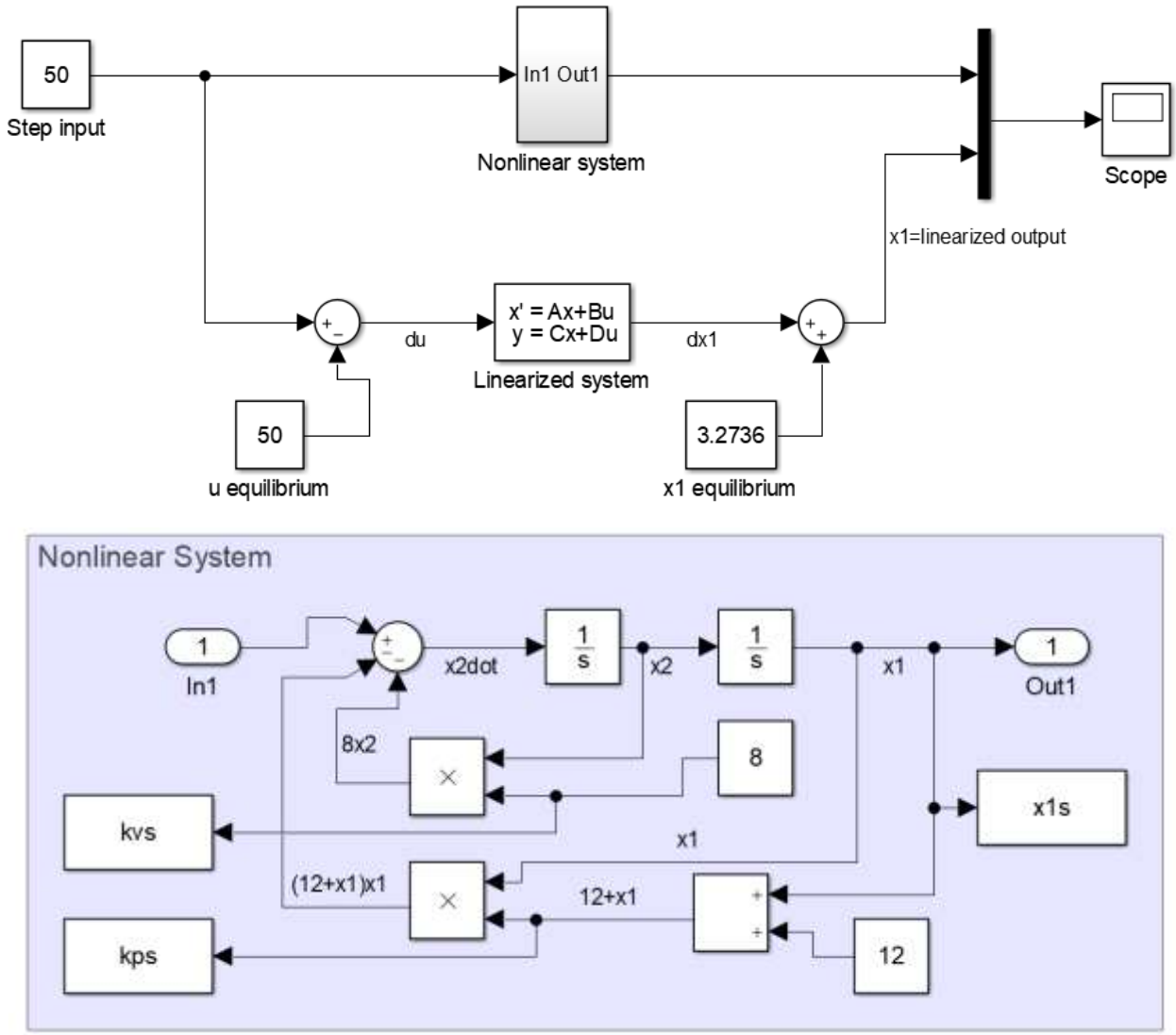

Figure B.1. Simulink model of the nonlinear system Eq. (B.2) and its linearized model Eq. (B.3) at the operating point $u(t) = +50$.

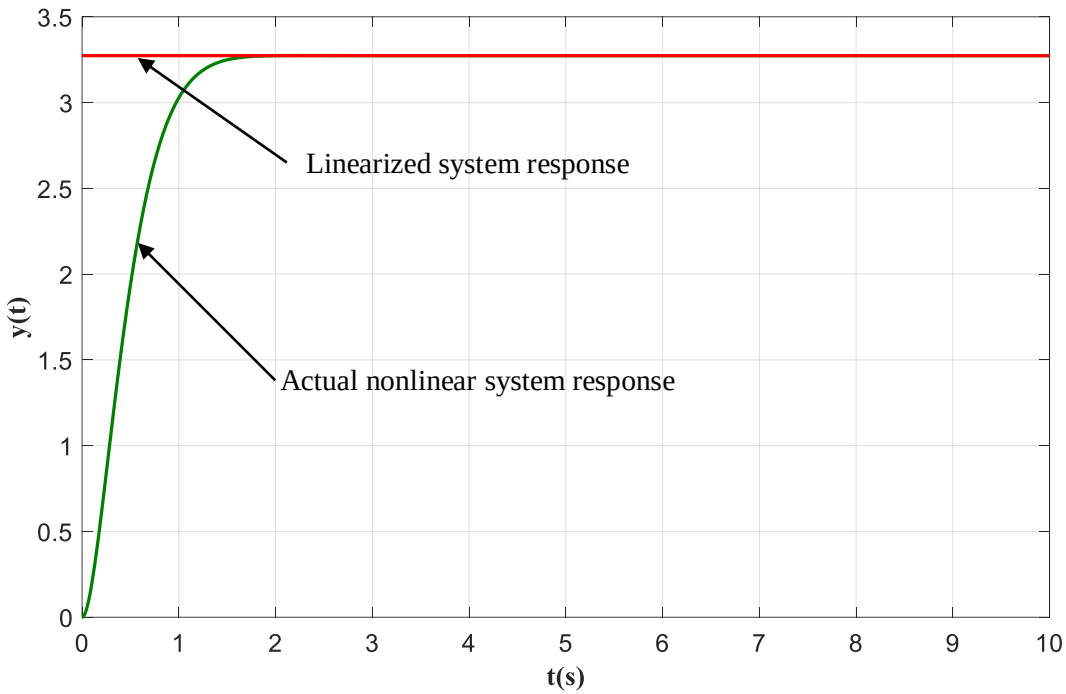

Figure B.2. The output of the nonlinear system Eq. (B.2) and its linearized model Eq. (B.3) at the operating point $u(t) = +50$.

The location of the poles of the linearized model and the locations of the dynamic poles of the actual nonlinear system is given in the Figure B.3. The linearized model has a complex pole whereas the original system has a dynamic real pole on the complex g −plane. The pole location of the linearized model is fixed but for the actual nonlinear system, it moves with the change system states.

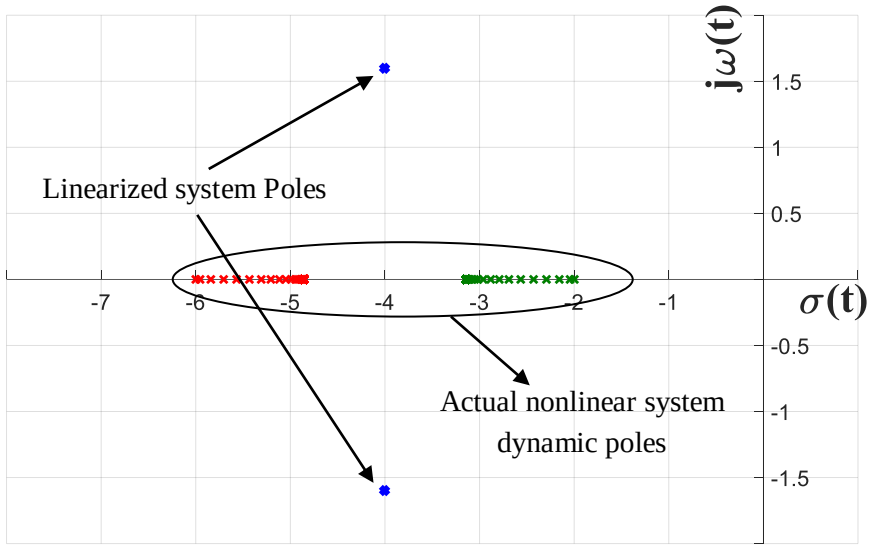

Figure B.3. The pole locations of the nonlinear system Eq. (B.2) and its linearized model Eq. (B.3) at the operating point $u(t) = +50$.

When the perturbation increases, the error of the output of the linearization model than the actual nonlinear system also increases. For example, Figure B.4 shows the output response of the linearized model and the actual nonlinear system for a small perturbation $\delta u = 0.5$ i.e. $u(t) = +50.5$.

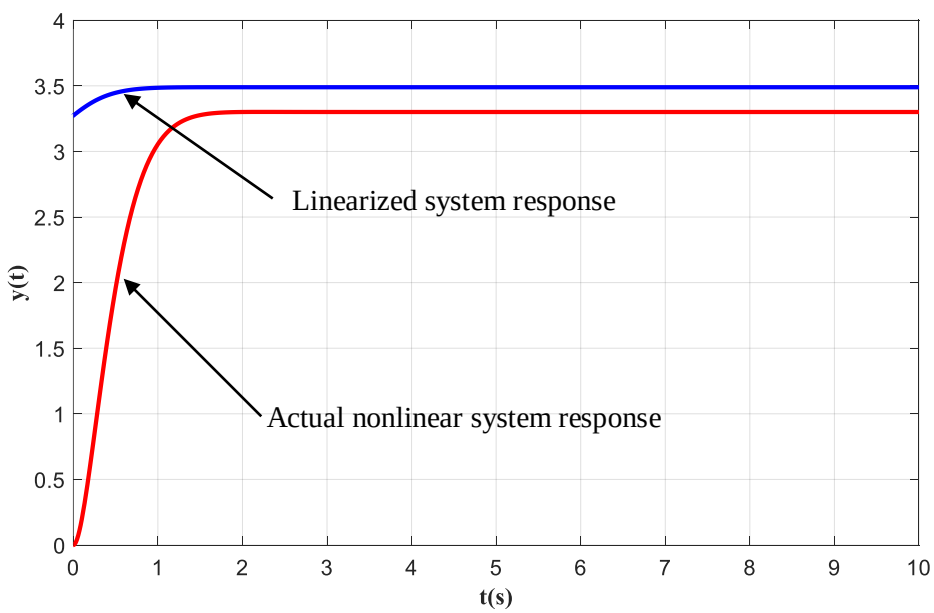

Figure B.4. The output of the nonlinear system Eq. (B.2) and its linearized model Eq. (B.3) with a step input $u(t) = +50.5$.

The location of the poles of the linearized model does not depend on the system states or input. So for a certain input, the linearized system may be stable, i.e., poles are on the left-hand side of the complex plane, but the actual nonlinear system could be unstable, i.e., it may have unstable dynamic poles on the right-hand side of the complex g −plane. For example, when input $u(t) = -50$, the linearized model is stable as shown in Figure B.5 but the actual nonlinear system is unstable.

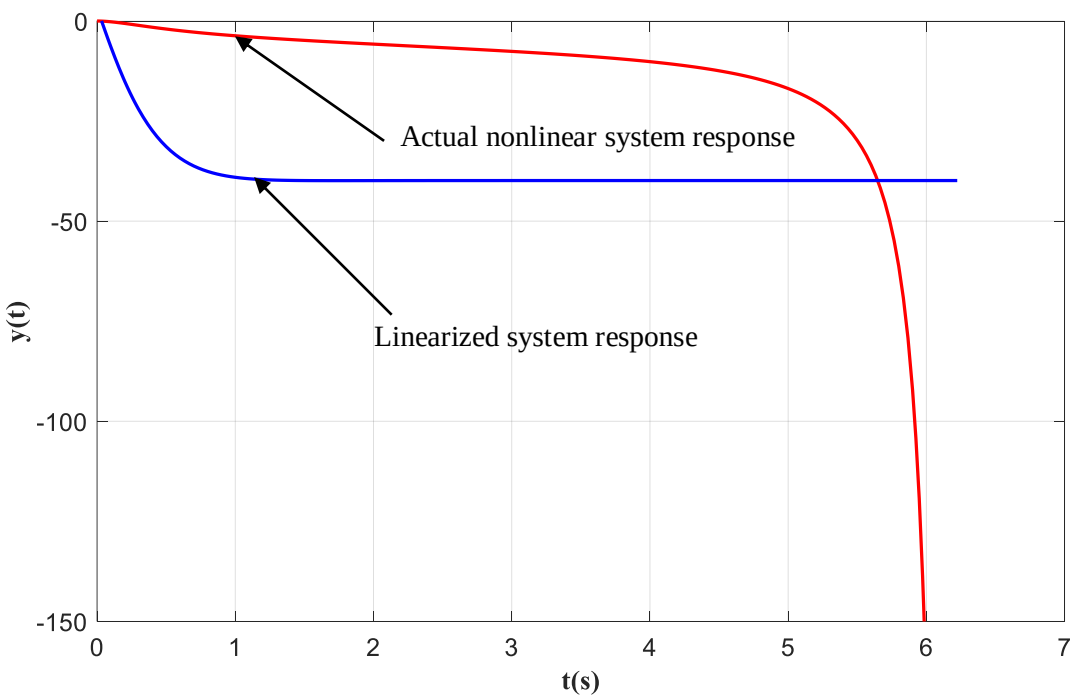

Figure B.5. The output of the nonlinear system Eq. (B.2) and its linearized model Eq. (B.3) with a step input $u(t) = -50$.

The pole locations of the linearized model and the nonlinear system for a step input $u(t) = -50$ is shown in Figure B.6. The poles of the linearized model are on the right hand side

of the complex g −plane, but the actual nonlinear system has an unstable dynamic poles as shown in Figure B.5.

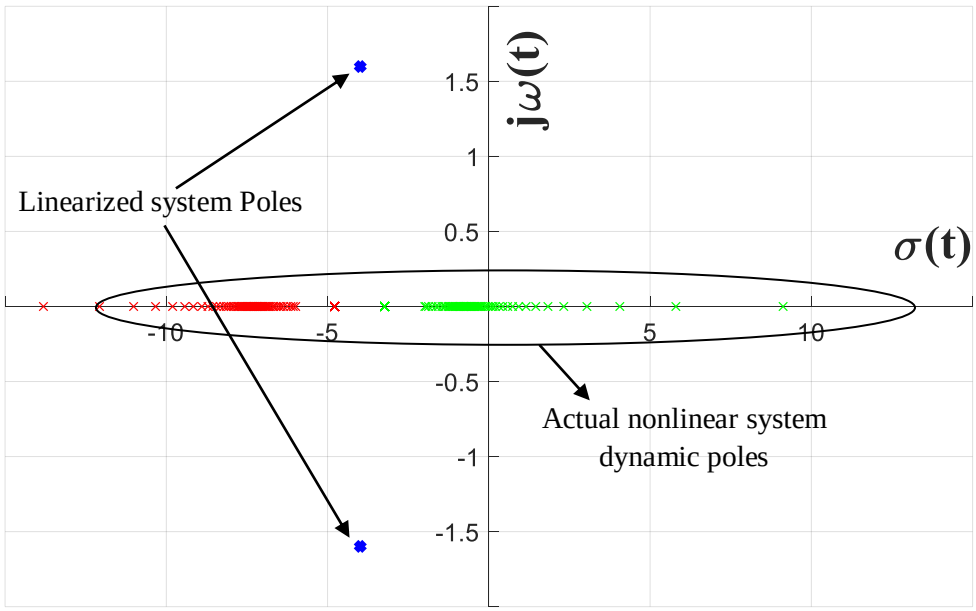

Figure B.6. The dynamic pole locations of the nonlinear system Eq. (B.2), and its linearized model Eq. (B.3) for a step input $u(t) = -50$.

From the above discussion, it is clear that linearization of a nonlinear system gives an approximate result on system performances whereas the dynamic pole motion approach gives the exact scenario of the system performances.

Appendix C
Details of the Simulink Models

The neuro-controller is a highly nonlinear error-based adaptive controller. A neuro-controller learns from the overall response and adapts its parameters to get the best overall response. For a large initial error, the overall system exhibits an under-damped and a fast transient response, while for a small error, the overall system exhibits an over-damped and a zero overshoot transient response.

The details of the Simulink models of the examples in Chapter 4 are presented here.

Example 4.1

$$\ddot{x} + 2\dot{x} + 6x = 6u(t) \tag{C.1}$$

The position feedback $K_p(e,t)$ and velocity feedback $K_v(e,t)$ of the neuro-controller are,

$$\begin{aligned} K_p(e,t) &= 40(1 + 18e^2) \\ K_v(e,t) &= 6.5\exp[-12e^2] \end{aligned} \tag{C.2}$$

The Simulink model is given in Figure C.1.

Example 4.2

$$\ddot{x} + (1 - x^2)\dot{x} + x = u(t) \tag{C.3}$$

The position feedback $K_p(e,t)$ and velocity feedback $K_v(e,t)$ of the neuro-controller is,

$$\begin{aligned} K_p(e,t) &= 24 + 150 \times e^2 \\ K_v(e,t) &= 12\exp[-40e^2] + {x_1}^2 \end{aligned} \tag{C.4}$$

The Simulink model is given in Figure C.2.

Example 4.3:

$$\begin{aligned} \dot{x_1} &= x_2 - ax_1(x_1^2 + x_2^2) \\ \dot{x_2} &= -x_1 - ax_2(x_1^2 + x_2^2) \end{aligned} \tag{C.5}$$

The position feedback $K_p(e,t)$ and the velocity feedback $K_v(e,t)$ of the neuro-controller is,

$$\begin{aligned} K_p(e,t) &= 85 + 50e^2 \\ K_v(e,t) &= 23\exp[-5e^2] \end{aligned} \tag{C.6}$$

The Simulink model is given in Figure C.3.

Example 4.4:

$$\begin{aligned} \dot{x_1} &= x_2 \\ \dot{x_2} &= -(\sin x_1)x_2 + x_3 \\ \dot{x_3} &= -(30 + {x_2}^2)x_1 - (17 + {x_1}^2)x_2 - 8x_3 + u(t) \\ y &= 5x_1 + x_2 \end{aligned} \tag{C.7}$$

The position feedback $K_p(e,t)$, the velocity feedback $K_v(e,t)$ and the acceleration feedback $K_a(e,t)$ of the neuro-controller are,

$$\begin{aligned} K_p(e,t) &= 650 + 600e^2 \\ K_v(e,t) &= 250\exp[-6e^2] \\ K_a(e,t) &= 25 + e^2 \end{aligned} \tag{C.8}$$

The Simulink model is given in Figure C.4.

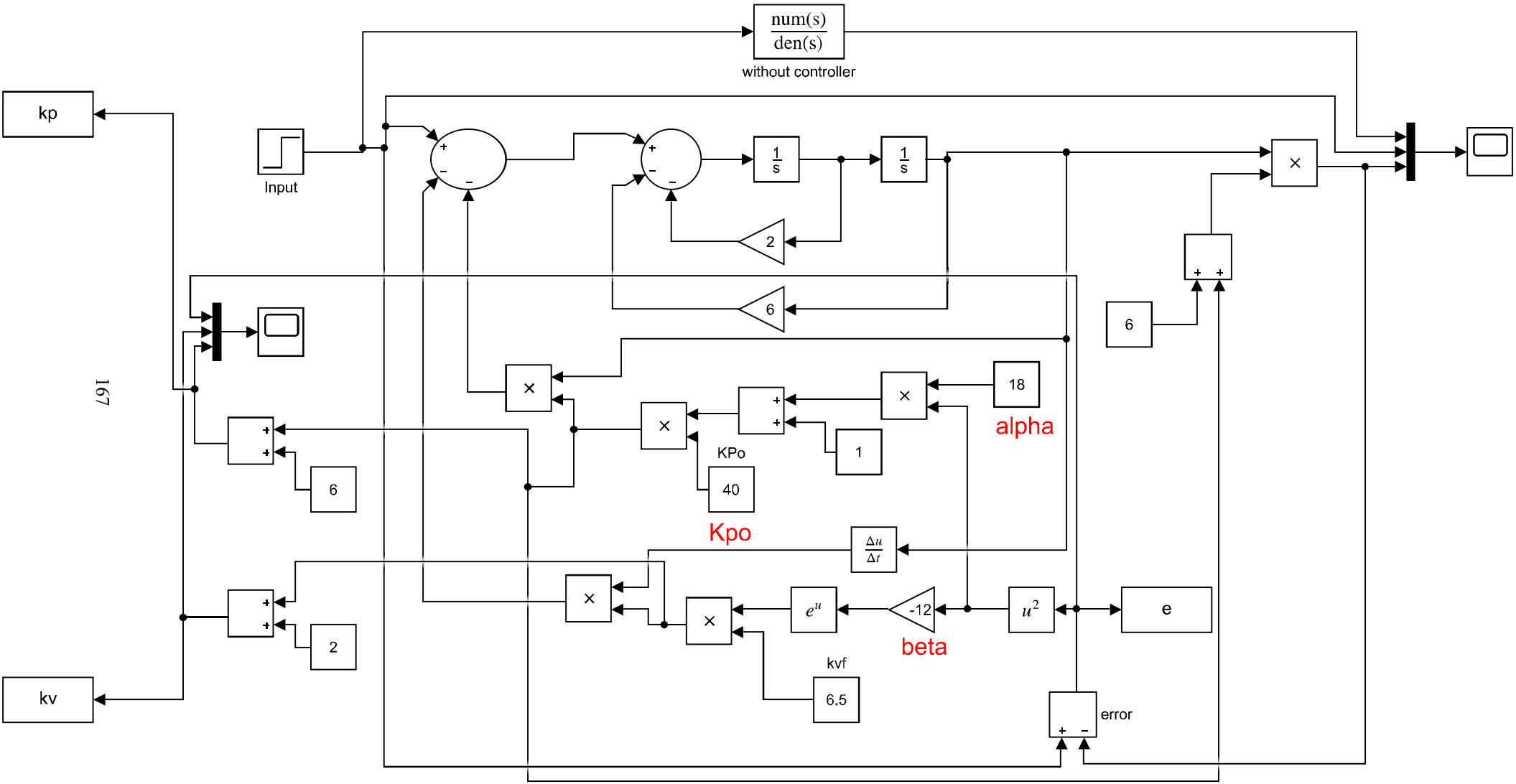

Figure C.1. Simulink model of example 4.1

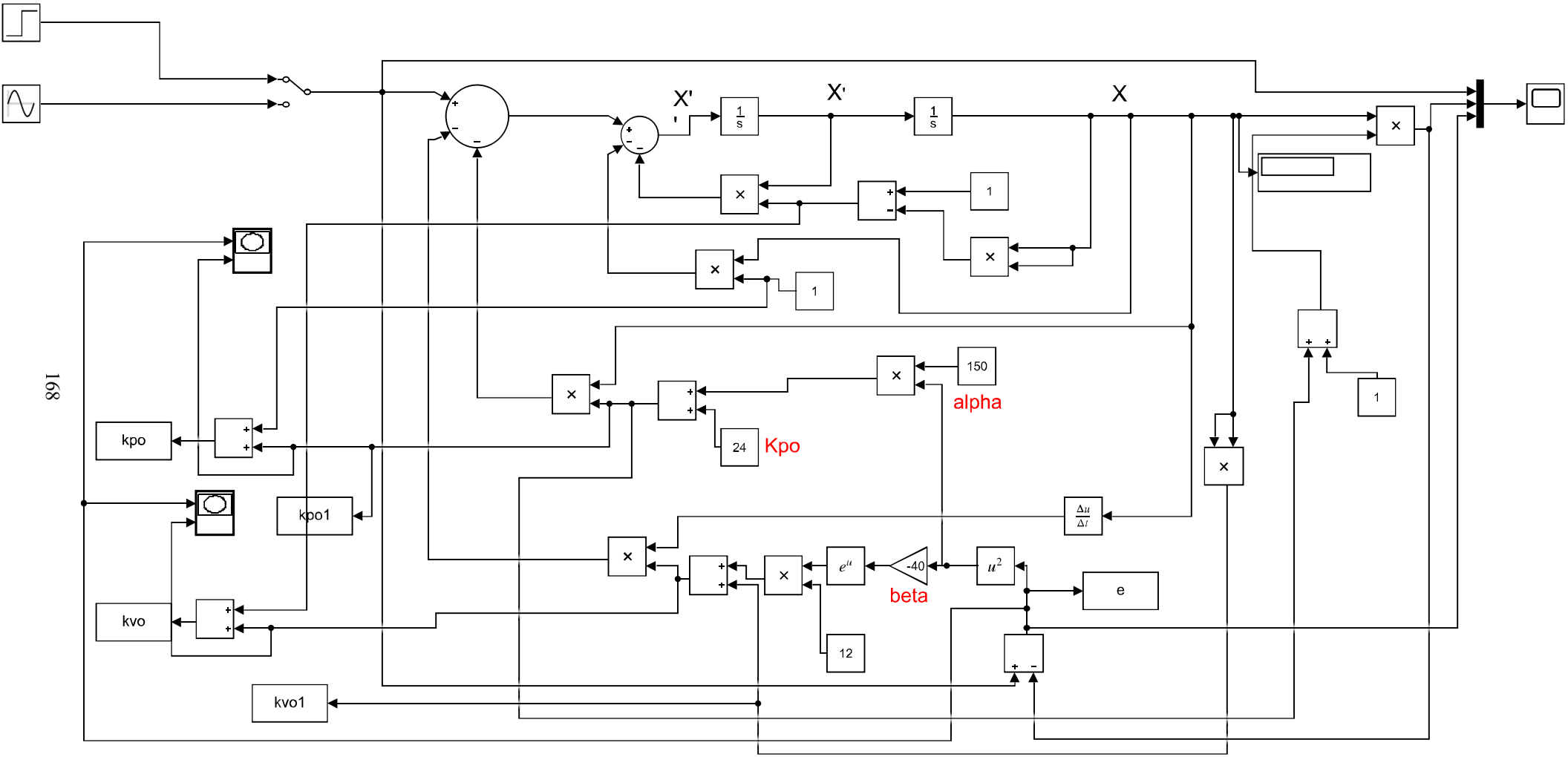

Figure C.2. Simulink model of example 4.2.

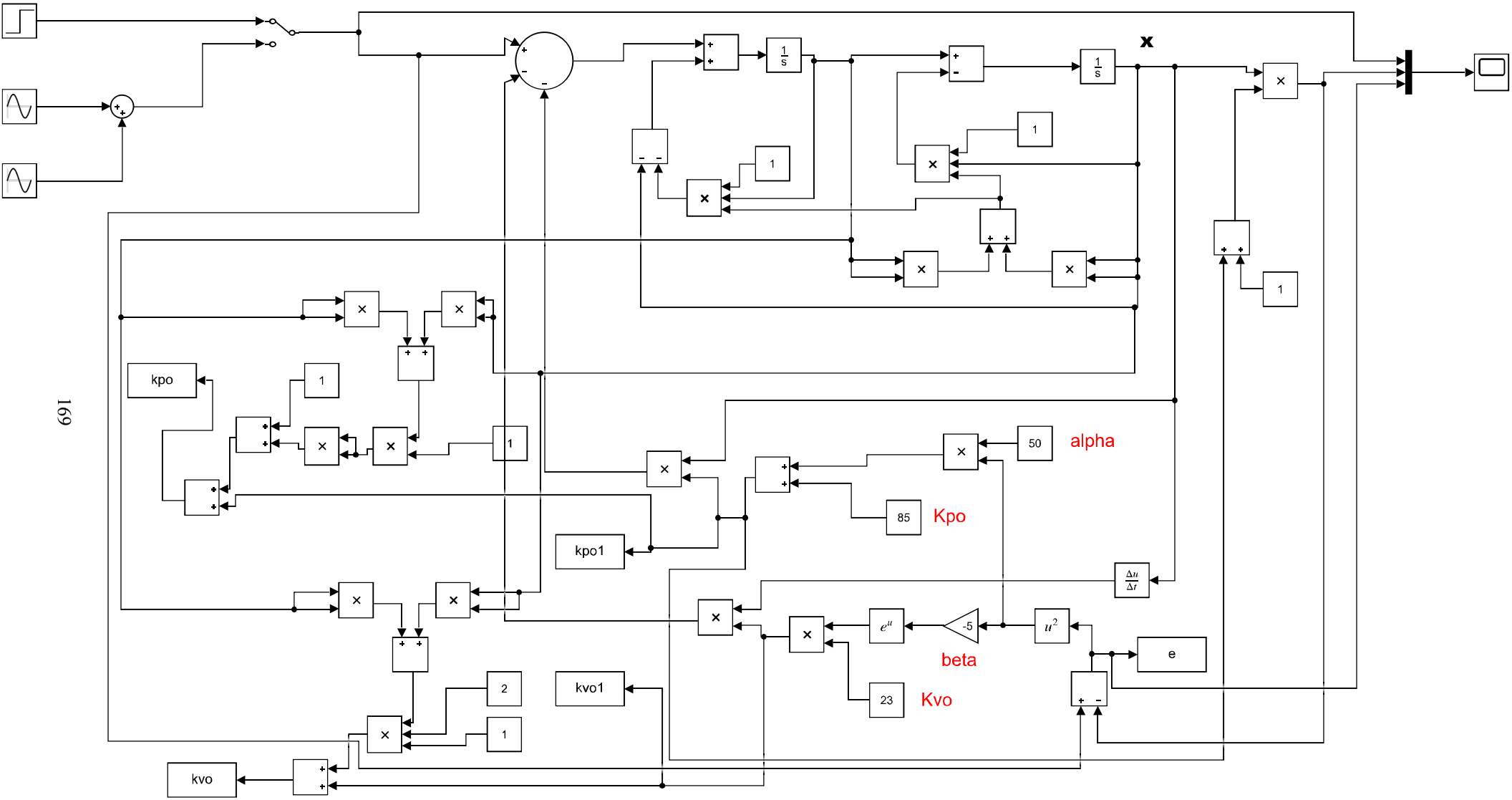

Figure C.3. Simulink model of example 4.3.

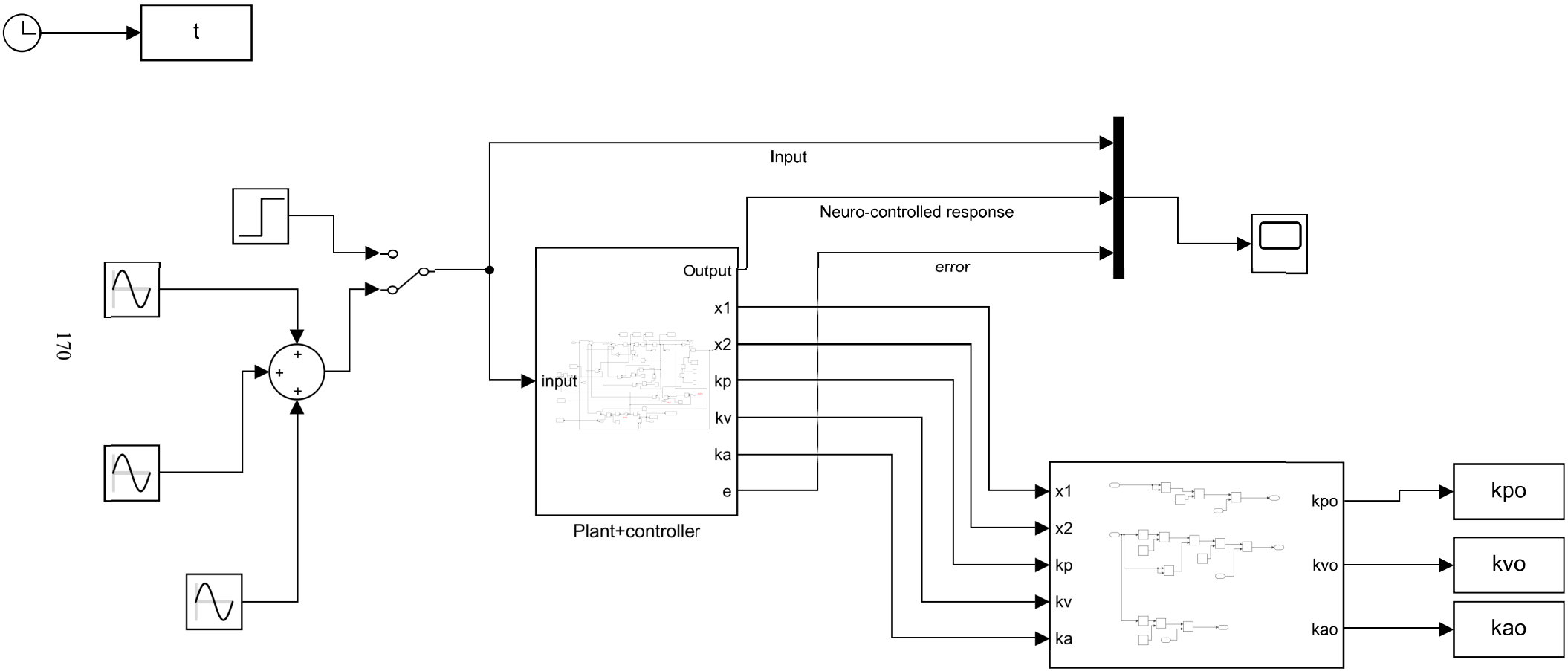

Figure C.4. Simulink model of example 4.4.

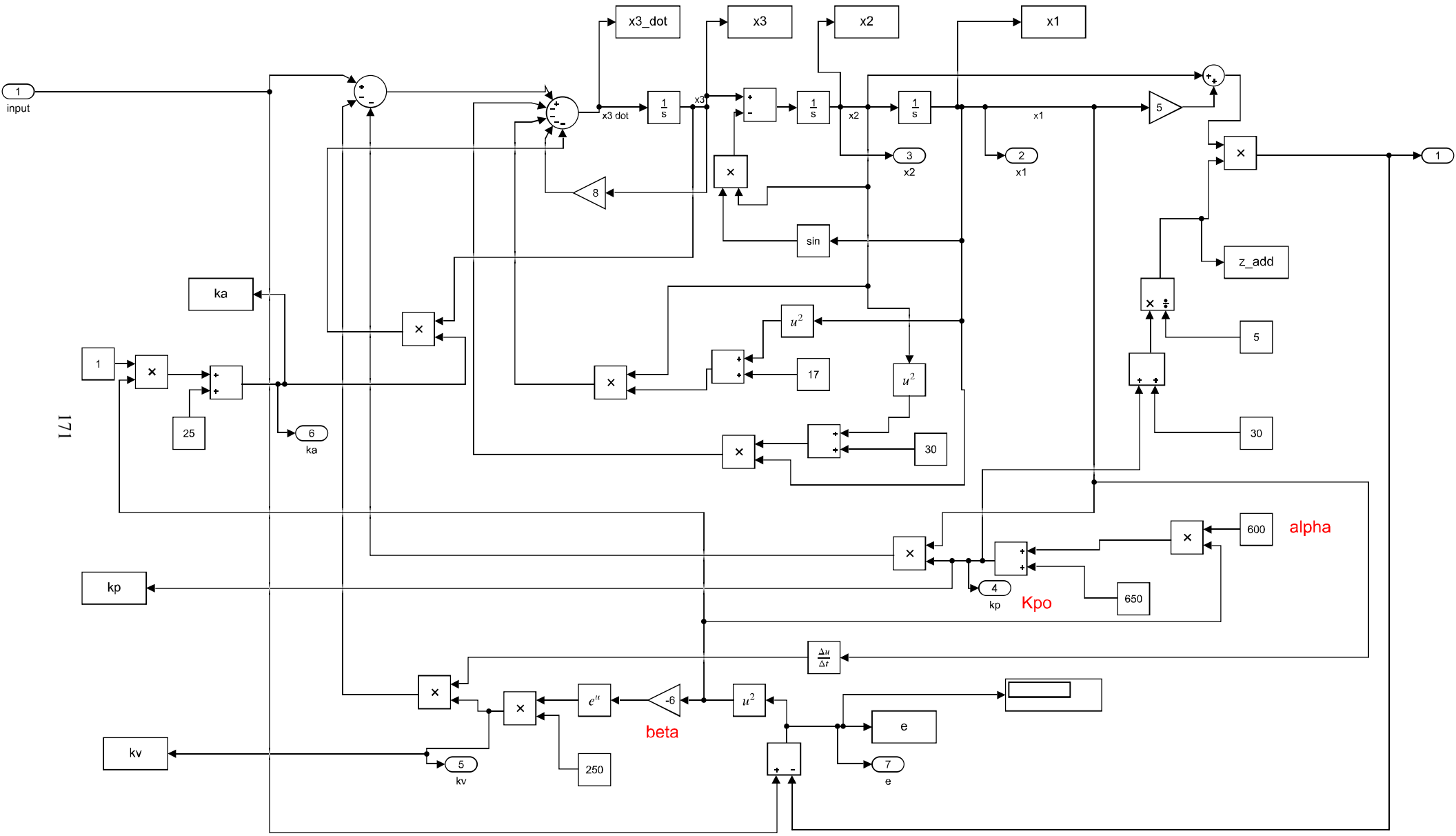

Figure C.4. Simulink model of example 4.4 (continued).

References

[1] M. M. Gupta and D. H. Rao, "Neuro-Control Systems: A Tutorial," in *Neuro-Control Systems, Theory and Applications*, New York, IEEE Press, 1994, pp. 1-43.

[2] J. Slotine and W. Li, Applied Nonlinear Control, New Jersey: Prentice-Hall, 1991.

[3] G. Chen and J. Webster, "Stability of nonlinear systems," in *Wiley Encyclopedia of Electrical and Electronics Engineering*, John Wiley & Sons, 2000, pp. 627-642.

[4] N. S. Nise, Control System Engineering, 3rd ed., New York: John Wiley & Sons, Inc., 2000.

[5] K. Ogata, Modern Control Engineering, 3rd ed., New Jersey: Prentice Hall, 1997.

[6] B. K. Sahu, M. M. Gupta and B. Subudhi, "Stability Analysis of Nonlinear Systems using Dynamic-Routh's Stability Criterion: A New Approach," in *International Conference on Advances in Computing, Communications and Informatics (ICACCI)*, Mysore, India, 2013.

[7] K. Y. Song, M. M. Gupta and N. Homma, "Design of an Error-Based Adaptive Controller for a Flexible Robot Arm Using Dynamic Pole Motion Approach," *Journal of Robotics*, vol. 2011.

[8] M. M. Gupta, "On The Design of an Error-Based Robust Neuro-Controller (Dynamic Pole Motion Control)," in *ICIICII-2015*, Wuhan, 2015.

[9] K. Y. Song, M. M. Gupta and D. Jena, "Design of an Error-Based Robust Adaptive Controller," in *Proceedings of the IEEE International Conference on Systems, Man and Cybernetics*, San Antonio, TX, USA, 2009.

[10] K. Y. Song, M. M. Gupta and W. C. Zhang, "Some New Notions in the Stability Investigations and Design of Controllers for Nonlinear Systems," in *International Conference on Industrial Electronics, Control and Robotics IECR 2010*, 2010.

[11] K. Y. Song, M. M. Gupta, D. Jena and B. Subudhi, "Design of a Robust neuro-Controller for Complex Dynamic Systems," in *Fuzzy Information Processing Society, 2009. NAFIPS 2009*, 2009.

[12] R. kalman and J. Bertram, "Control System Analysis and Design Via the "Second Method" of Lyapunov," *Journal of Basic Engineering,* pp. 371-393, June 1960.

[13] D. R. Ingwerson, "A Modified Lyapunov Method for Nonlinear Stability Analysis," *IRE Transactions on Automatic Control,* pp. 199-210, May 1961.

[14] S. H. Wu and G. M. Manke, "Popov criterion and Lagrange stability of nonlinear systems," *IEEE Transaction on Automatic Control,* vol. 12, no. 5, p. 627, 1967.

[15] L. Socha, "Frequency-domain criteria for stability of a class of nonlinear," *IEEE Transaction on Automatic Control,* vol. 20, no. 2, pp. 284-287, 1975.

[16] P. Atherton and N. Tan, "A new approach to the stability of nonlinear systems with uncertain plant parameters," in *Proceedings of the American Control Conference*, Denver, Colorado, June 4-6, 2003.

[17] S. T. Impram and N. Munro, "Stability of nonlinear systems with complex disc and norm-bounded perturbations," in *Proceedings of the American Control Conference*, Chicago, Illinois, June 2000.

[18] M. Fadali and N. Chachavalvoong, "Describing function analysis of nonlinear systems using Kharitonov approach," in *Proceedings of American Control Conference*, 1995.

[19] S. Impram and N. Munro, "Describing function analysis of nonlinear systems with parametric uncertainty," in *International Conference on Control*, 1998.

[20] N. Tan and D. Atherton, "Describing function analysis of nonlinear discrete interval systems," in *European Control Conference*, 1999.

[21] D. Swaroop and J. K. Hedrick, "On Local and Global Exponential Stability of Nonlinear

Systems," in *Proceedings of the American Control Conference*, Albuquerque, New Mexico, June 1997.

[22] X.-J. Wen, Z.-M. Wu and J.-G. Lu, "Stability Analysis of a Class of Nonlinear Fractional-Order Systems," *IEEE Transaction on Circuits and Systems-II: Express Briefs*, vol. 55, no. 11, pp. 1178-1182, November, 2008.

[23] R. Hilfer, Applications of Fractional Calculus in Physics, World Scientific, 2000.

[24] E. M. Aylward, P. A. Parrilo and J. J. E. Slotine, "Stability and robustness analysis of nonlinear systems via contraction metrics and SOS programming," *Automatica*, vol. 44, no. 6, pp. 2163-2170, 2008.

[25] P. A. Parrilo, "Semidefinite programming relaxations for semialgebraic problems," *Mathematical Programming*.

[26] H. K. Khalil, Nonlinear Systems, New York: Macmillan Publishing Company, 1992.

[27] B. C. Kuo, Automatic Control Systems, Fourth ed., NJ: Prentice-Hall Inc., 1982.